Stable Isotope Tracing of Engineered Nanoparticles

Adam John Laycock

Imperial College London

Department of Earth Sciences and Engineering

Thesis submitted for the degree of Doctor of Philosophy (Ph.D) 2014

Declaration of Originality

I declare that the content of this thesis is of my own work and any work or contributions of others is fully acknowledged and referenced.



Adam John Laycock

The copyright of this thesis rests with the author and is made available under a Creative Commons Attribution Non-Commercial No Derivatives licence. Researchers are free to copy, distribute or transmit the thesis on the condition that they attribute it, that they do not use it for commercial purposes and that they do not alter, transform or build upon it. For any reuse or redistribution, researchers must make clear to others the licence terms of this work

Acknowledgements

This thesis is the culmination of my 4 years at Imperial College and it would not have been possible without all the support that the people around me have given, academically, socially and personally.

First of all, I would like to acknowledge my supervisor, Mark. Without Mark's ideas and ambition to apply his experience and expertise to the field of environmental tracing for engineered nanoparticles, this project would never have been available for me. I would like to thank Mark for putting in so much time and effort with me and giving me the best start I could hope for in my scientific career. I will value all of our conversations, both work related and otherwise; you have provided me with a great role model for my academic career and I truly thank you.

I owe a big thanks to the entire MAGIC group. Working with such a great group of people has been a really positive experience and provided an excellent working environment. A special mention goes to Barry and Katharina; without both of you keeping the labs running and being there when you're needed most, I am sure I would not have collected all of the data presented here. I would like to thank all of the friends I have made at Imperial along the way: Luke, Flo, Claire, Fee, Martin, Henry, Alex, Ed, Annabel, Anna-Joy and others, for all the discussions, coffee breaks, beers and squash games. I hope to keep in touch and remain friends with you for years to come.

Due to the collaborative nature of the work I have performed, much of what I have achieved would not have been possible without the many colleagues and friends I have made over the last four years. A special mention goes to Éva for our monthly meetings and discussions and all the support you have given me. I would also like to acknowledge my collaborators at the Natural History Museum, Center for Ecology and Hydrology and the Facility for Environmental Nanoscience Analysis and Characterization who have made my work possible. In particular, thanks to Claus, Maria, Björn, Farhan and Agnes; without your input and support this thesis would not be what it is.

Thank you to both of my examiners, Tina van de Flierdt and Frank von der Kammer, for taking the time to read my thesis. I look forward to our discussion and to hearing your thoughts and comments.

Last but by no means least, I would like to thank my friends and family and the people who mean the most to me. A big thanks to my parents, Wendy and Trevor, who, despite not really understanding what it is I do, have fully supported me through all of my academic life. To my Nan, who sadly passed away earlier this year; I wish she was still here to see my achievement, but I know she would be very proud of me. A special mention goes to my sister, Joanne, who can always make me laugh. Alice – we have shared all of our highs and lows over the past four years and I can't imagine having achieved this without your support.

Abstract

Engineered nanoparticles (NPs) are increasingly being used in consumer products due to their novel properties. Consequently, concerns have been raised over the potential hazards that these materials may present as a result of their release into the natural environment. This has prompted numerous investigations into the environmental behavior, transport and fate of engineered NPs. Importantly the predicted environmental concentrations of these materials is often x10 to x100 lower than the natural background levels of the element. Many studies overcome this problem with the use of high dosing concentrations, however this raises concerns regarding environmental relevance.

The work presented in this thesis demonstrates how stable isotope tracing enables the accurate detection and quantification of engineered NPs in complex biological samples even when exposures are performed at low and environmentally relevant concentrations.

This thesis focuses on three of the most prominent commercially available NPs; ZnO, CeO_2 and Ag, and covers all aspects of the application of stable isotope labeling and tracing for these materials. This includes; (i) an assessment and evaluation of the technique for application with CeO_2 NPs, including the development of chemical separation and mass spectrometric methods for an environmental tracer study, (ii) the assessment of a synthesis protocol for the production of isotopically labeled Ag NPs, and (iii) two environmental tracer studies to assess the uptake and loss of Zn from ZnO NPs by an estuarine snail and earthworm.

Table of Contents

Page

List of Figures 9
List of Tables 10

Chapter 1 Introduction 11
1.1 Background 12
1.2 The status-quo 12
1.3 Stable isotope tracing 15
1.4 Thesis overview 17

Chapter 2 Development and evaluation of new techniques for stable isotope tracing of CeO_2 nanoparticles 20
Abstract 21
2.1 Introduction 22
2.2 Experimental 26
2.2.1 Samples 26
2.2.2 General procedures and reagents 28
2.2.3 Sample preparation of Ceo_2 and purified Ce samples for stable isotope analysis 28
2.2.4 Sample preparation of natural materials to investigate tracing of enriched ^{140}Ce 29
2.2.4.1 Digestion 29
2.2.4.2 Addition of ^{140}Ce spike 29
2.2.4.3 Chemical separation of Ce 30
2.2.5 Mass spectrometry 33
2.2.6 Isotope ratio modeling for samples spiked with enriched ^{140}Ce 35
2.2.7 Data reduction for isotopic tracing 36
2.3 Results and discussion 37
2.3.1 Evaluation of isotope tracing of CeO_2 nanoparticles based on inherent differences in Ce isotope composition 37
2.3.1.1 Principles 37
2.3.1.2 Precision and accuracy of Ce stable isotope data for CeO_2 and purified Ce samples 40
2.3.1.3 Isotopic variability 43
2.3.2 Tracing of stable isotope labeled CeO_2 nanoparticles 44
2.3.2.1 Principles 44
2.3.2.2 Chemical separation of Ce from complex natural samples 45
2.3.2.3 Constraints on choice of spike isotope 48
2.3.2.4 Results for natural samples spiked with an enriched ^{140}Ce spike 52

2.4 Conclusions 54
2.5 Declaration 55

Chapter 3 Synthesis and characterization of isotopically labeled silver nanoparticles for tracing studies 56
Abstract 57
3.1 Introduction 58
3.2 Experimental 62
3.2.1 Choice of isotope label 62
3.2.2 Chemicals and reagents 63
3.2.3 Synthesis 63
3.2.4 Characterization of particles 66
3.2.4.1 Dynamic light scattering (DLS) 66
3.2.4.2 Transmission electron microscopy (TEM) 66
3.2.4.3 Asymmetric flow field-flow fractionation (FlFFF) 66
3.2.4.4 Yield determination 67
3.2.4.5 Dissolution behavior 67
3.3 Results and discussion 68
3.3.1 Size characterization of particles 68
3.3.1.1 DLS analyses 68
3.3.1.2 TEM analyses 71
3.3.1.3 FlFFF analyses 72
3.3.2 Synthesis yields 74
3.3.3 Dissolution behavior 74
3.3.4 Reproducibility and reliability of synthesis method 77
3.3.5 Stability of particles 78
3.3.6 Isotope label and detection capabilities 78
3.4 Conclusions 85
3.5 Declaration 85

Chapter 4 A stable isotope tracer to determine uptake and efflux dynamics of ZnO nano- and bulk particles, and dissolved Zn to an estuarine snail 86
Abstract 87
4.1 Introduction 88
4.2 Methods 90
4.2.1 Chemicals and reagents 90
4.2.2 Experimental organisms 91
4.2.3 Preparation of isotopically enriched forms of ^{68}Zn 91
4.2.4 Characterization of ^{68}ZnO particles 92
4.2.5 Waterborne exposures 92
4.2.6 Sample preparation 93
4.2.6.1 Water samples 94
4.2.6.2 Snail samples 94

4.2.6.3 Anion chromatography 95
4.2.7 $^{68}Zn/^{66}Zn$ determination 95
4.2.8 Isotope mass balance calculations 96
4.2.9 Biodynamic modeling 98
4.2.10 Statistical analysis 99
4.3 Results and discussion 99
4.3.1 Characterization of ^{68}ZnO particles 99
4.3.2 Reactivity of ^{68}ZnO particles in experimental media 101
4.3.3 Analytical precision 103
4.3.4 Measured exposure concentrations and the influence of the shell as a binding site 105
4.3.5 Uptake and efflux dynamics of P. ulvae 107
4.4 Conclusions 110
4.5 Declaration 110

Chapter 5 Comparing earthworm uptake routes and rates for ionic Zn and ZnO nanoparticles at realistic environmental concentrations using stable isotope labeling 111
Abstract 112
5.1 Introduction 113
5.2 Methods 117
5.2.1 Materials and reagents 117
5.2.2 Synthesis and characterization of the enriched ^{68}Zn forms 118
5.2.3 Preparation of the exposure medium 119
5.2.4 Test organisms 120
5.2.5 Experimental procedure and sampling 120
5.2.6 Sample preparation 122
5.2.7 Chemical separation 123
5.2.8 Isotopic analysis and data reduction 123
5.2.9 Kinetic modeling 126
5.3 Results 126
5.3.1 Soil and pore water 126
5.3.2 Earthworms 127
5.4 Discussion 132
5.4.1 Zn behavior in soil 132
5.4.2 Uptake and accumulation 133
5.5 Conclusions 136
5.6 Declaration 136

Chapter 6 Summary 137
6.1 Thesis conclusions 138
6.2 Future work 140
6.3 Closing remarks 142

Bibliography **143**

Appendices 153

i) Synthesis and characterization of isotopically labeled silver nanoparticles for tracing studies; Student t-test populations and data 154

ii) Paper arising from the work of Chapter 3: ‘Synthesis and characterization of isotopically labeled silver nanoparticles for tracer studies’ 161

iii) Paper arising from the work of Chapter 4: ‘Stable isotope tracer to determine uptake and efflux dynamics of ZnO nano- and bulk particles and dissolved Zn to an estuarine snail’ 175

List of Figures

	Page
1.1 Isotopic compositions of natural Zn, Ag and Ce and the isotope spikes ^{68}Zn, ^{107}Ag and ^{140}Ce	16
1.2 Schematic showing how the introduction of isotopically enriched ^{68}ZnO NPs results in changes to the diagnostic $^{68}Zn/^{66}Zn$ ratio.	17
2.1 Compilation of published Ce concentrations for natural background materials and predicted environmental concentrations of CeO_2 nanoparticles	23
2.2 $\delta^{142}Ce$ values of purified Ce materials versus the isobaric correction for the presence of ^{142}Nd	42
2.3 Assessment of the ^{142}Nd correction on ^{142}Ce	42
2.4 $\delta^{142}Ce$ data for purified Ce samples	43
2.5 Recovery of Alfa Aesar Ce standard Vs $\delta^{142}Ce$ values	47
2.6 Detection sensitivities of enriched Ce isotopes	49
3.1 Contribution of enriched ^{107}Ag and the resulting $^{107}Ag/^{109}Ag$	60
3.2 TEM images and NP size distribution of Ag nanoparticles	72
3.3 FIFFF results for Ag nanoparticles	73
3.4 Dissolution behavior of Ag nanoparticles	75
4.1 Characterization of ^{68}ZnO nanoparticles	100
4.2 SEM images and XRD analysis of ^{68}ZnO bulk particles	101
4.3 DLS analysis of ^{68}ZnO nanoparticles in exposure media over 11 hours	102
4.4 Concentration of enriched ^{68}Zn Vs Natural Zn in samples	105
4.5 Enriched ^{68}Zn concentration in water samples and shell leachates	106
4.6 Enriched ^{68}Zn concentrations in soft tissue during exposure and uptake	108
4.7 Enriched ^{68}Zn concentrations in soft tissue during efflux and depuration	109
5.1 Predicted environmental concentrations of ZnO nanoparticles in soils compared to the natural Zn concentrations and those used in exposure studies	114
5.2 Enriched ^{68}Zn concentrations in soil pore waters	128
5.3 Natural Zn versus enriched ^{68}Zn concentrations in exposed earthworm tissues	129
5.4 Concentration of enriched ^{68}Zn in exposed earthworm tissue with exposure time	129
5.5 Modeled Zn tissue concentrations (from added Zn only) over 30 days	131
5.6 Proportion of dermal to total uptake of added Zn by *L. rubellus* against the concentration of Zn in pore water relative to the soil	134
6.1 Schematic of the detection of enriched ^{68}Zn with an ion microprobe	141

List of Tables

	Page
2.1 Summary of natural Ce isotope abundances, isotopic enrichment and cost of commercially available enriched Ce isotopes	24
2.2 Summary of Ce isotope data for purified Ce samples	27
2.3 Summary of results obtained for the natural samples	31
2.4 Cerium separation chemistry protocol	32
2.5 Instrumental operating parameters	33
2.6 Faraday cup arrangement with isobaric interferences	34
2.7 REE/Ce ratios of the Ce standard and sample solutions and the corresponding correction to the $^{142}Ce/^{140}Ce$ isotope ratio	41
2.8 Recovery and $\delta^{142}Ce$ values determined for standard Ce solution aliquots processed through the chemical separation	46
2.9 Summary of modeled data for the three hypothetical scenarios evaluating the detection sensitivities and quantification uncertainties for isotopically labeled CeO_2 NPs.	49
3.1 Summary of characterization results for Ag nanoparticles	64
3.2 Ag nanoparticle synthesis protocols	65
3.3 Evaluation of detection sensitivities using enriched ^{107}Ag as a tracer	81
4.1 Summary of analytical results	104
5.1 Summary of published ZnO nanoparticle soil exposures	115
5.2 Isotope abundances and atomic weights of Zn	118
5.3 Zn chemical separation protocol	123
5.4 Summary of the key exposure parameters and experimental results	127
5.5 experimental results from analysed control samples	128
5.6 Uptake and elimination rate constants	130
5.7 Bioaccumulation factors and bioconcentration factors	131

Chapter 1:

Introduction

1.1 Background

Nanoparticles (NPs) are commonly defined as materials that feature dimensions with a size of between 1 and 100 nm. Due to their size, nanomaterials (NMs) commonly have unique physical and chemical properties. Engineered NPs are specifically manufactured to take advantage of such characteristics in novel products and applications. Consequently, the known and potential benefits of engineered NMs are enormous, and a diverse range of applications have been pioneered in electronics, optics, medical technology, cosmetics, textiles, food packaging and many other fields (Woodrow Wilson Centre, 2014).

The rapidly increasing use of engineered NPs has given rise to concerns that such materials could produce a "new asbestos problem" and initiated a wider debate about the potential risks of nanoscale materials (Pacurari et al., 2010; Royal Society & Royal Academy of Engineering, 2004). This debate is informed by emerging research, which investigates the chemical reactivity, ecotoxicology and environmental cycling of engineered NPs. However, the current understanding of the toxicological properties and environmental fate of industrially produced NMs is still sketchy at best. Some toxic effects have been confirmed but more and better data are needed to carry out robust risk assessments (Ju-Nam and Lead, 2008, Handy et al., 2008a, Handy et al., 2008b).

The acquisition of such data is, however, currently hampered by analytical obstacles. A particular challenge is posed by the difficulty of distinguishing engineered NMs from the normal background levels of elements and natural NPs that are present in complex natural samples, including both geological materials (e.g., soils, sediments and marine/fresh waters) and biological tissues from plants and animals (Handy et al., 2008a, Ju-Nam and Lead, 2008, Marquis et al., 2009).

1.2 The status-quo

In-situ imaging techniques have been used to identify and quantify NP concentrations in natural samples, and these can be further coupled with methods to determine the elemental compositions of individual particles (e.g., TEM-EDX). Such

techniques are, however, only able to analyze very small volumes and many (time-consuming) individual analyses are therefore necessary to characterize larger (and more representative) bulk samples (Handy et al., 2008a, Marquis et al., 2009). Electron microscopy methods are not well suited for the quantification of NPs within complex natural samples. The detection of NPs within a natural sample is only feasible when they make up a significant contribution of the sample and far above the levels that may be realistically expected, even at high levels difficulties arise from being able to distinguish the NPs from the natural matrix and NPs. In addition to this the distribution of NPs at the nano scale will be heterogeneous and therefore a representative distribution is difficult to determine making quantification difficult.

The most straightforward means of detecting metal-based engineered NMs in bulk samples is by elemental concentration measurements. For example, the uptake of gold (Au) NPs by an organism will be associated with higher Au concentrations in tissue samples, which can be monitored with a technique such as ICP-MS (inductively coupled plasma mass spectrometry). However, this approach will only provide a sensitive means of detection if the NMs are made from elements that have very low natural background abundances – Au and Pt are good examples (Handy et al., 2008b).

For metal-based NPs, such as Ag, ZnO and CeO_2, the natural elemental background concentrations are commonly about 1-10 mg kg^{-1} but can reach %-levels. Such abundances render the detection of NMs difficult, because a large number of particles must be present in a sample to produce an anomaly in elemental concentration that exceeds both the uncertainty of the measurement and natural variations in element content. Elemental analyses by ICP-MS typically have uncertainties of about ±2% (at the 2sd confidence level) (Jarvis et al., 1992), whilst biological tissues from different organisms grown in the same environment often display variations in elemental concentration that exceed these values (e.g., ±5% to 50% were reported for Ce in plants (Wyttenbach et al., 1998). This implies, for example, that the addition/uptake of NMs is only resolvable by concentration measurements, if the Ce content of a sample is increased by at least 2%, or potentially by more than 50% (in

the case of plants). In the following, this quantity is defined as the *detection sensitivity* of a technique for NPs. Element concentration measurements hence only provide a limited detection sensitivity of about 2-50% for the tracing of engineered NMs in natural environments. When considering the variability of the absolute concentration it is important to consider the variability that is observed in the experimental system as opposed to a wider more general variability within certain samples

In experimental studies, these limitations can be overcome by conducting exposures at sufficiently high particle concentrations, but such levels typically exceed the predicted environmental concentrations (PECs) of engineered NMs by one or several orders of magnitude. For example, (Kool et al., 2011) exposed earthworms to test soils dosed with ZnO NPs at concentrations of 100 to 6400 mg kg^{-1}. This was necessary to enable the detection of the additional Zn accumulated by the organisms with concentration measurements. However, this exposure concentration is much higher than the typical background concentration of Zn in soils of 30 to 110 mg kg^{-1} (Emmett et al., 2010), and greatly exceeds the PEC of ZnO NPs in sludge treated soils of 3.2 to 32 mg kg^{-1} (Boxall et al., 2007). More recent work has demonstrated that ZnO NPs are likely to rapidly dissolve and change once they enter a natural system and are will not persist, therefore the levels that can realistically be expected in sludge treated soils is likely to be much lower than those estimated by Boxall et al., 2007.

As a consequence, the relevance of results generated in such studies has been questioned. For example, it is unclear whether the toxic effects that were reported for the exposure of plants and animals to ZnO NPs reflect uptake of dispersed NPs or unusually high (and toxic) dissolved Zn^{2+} contents from the dissolution of ZnO (Franklin et al., 2007, Wiench et al., 2009).

1.3 Stable isotope tracing

It has previously been suggested that stable isotope tracing could be used for the highly sensitive and selective detection of metal-based engineered NMs (Gulson and Wong, 2006). However, studies which (i) provide suitable procedures for the synthesis of isotopically labelled NPs, (ii) document methods for the application of labelled NPs in exposures and subsequent sample analyses, and (iii) evaluate the performance of stable isotope tracing for engineered NPs have only recently emerged (Laycock et al., 2014, Larner and Rehkämper, 2012). To a large part, this reflects the unfamiliarity of toxicologists, biologists, chemists and material scientists with the methods and instrumentation of isotopic research. The work presented in this thesis aims to bridge this gap.

The technique of stable isotope tracing of engineered NPs can be broken down into three main steps:

1) The synthesis of isotopically labeled NPs using a precursor material that is artificially enriched in a single stable isotope of the element of interest. Such enriched isotopes (also termed isotope spikes) are commercially available for all multi-isotopic elements. Zinc, for example, has five natural stable isotopes, ^{64}Zn (48.3% natural abundance), ^{66}Zn (28.0%), ^{67}Zn (4.1%) ^{68}Zn (19.0%) and ^{70}Zn (0.6%), which can be purchased with artificial enrichments of up to 99.5%. The natural isotope abundances of Zn, Ag and Ce, relative to the three isotope spikes ^{68}Zn, ^{107}Ag and ^{140}Ce, that feature in this thesis, are illustrated in Figure 1.1. The cost of enriched single isotopes ranges from about $2 to $1000 per mg, depending on the desired isotope and degree of enrichment. These costs pose a particular challenge to the preparation of labelled NPs and small-scale preparation protocols with high yields are desirable. The resulting NPs possess a distinct, non-natural isotope signature. Once synthesized, NPs are characterized in terms of their size, shape and other properties prior to use.

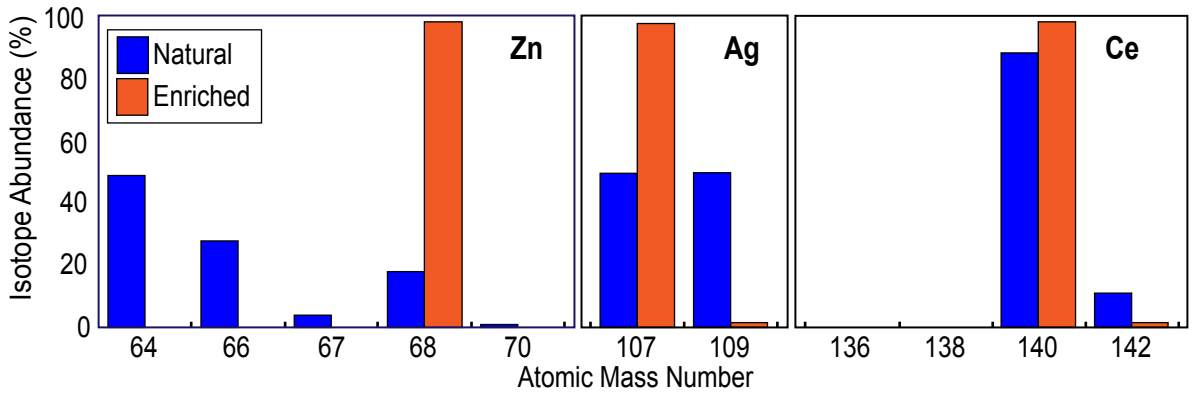


Figure 1.1 Isotopic compositions of natural Zn, Ag and Ce and the isotope spikes ^{68}Zn, ^{107}Ag and ^{140}Ce

2) The isotopically labeled NPs are subsequently employed in environmental screening and tracer studies. Importantly, such studies can be conducted at exposure levels that are within the range of PECs, and hence are directly environmentally relevant. This, in turn, implies that the elemental exposure concentrations are commonly a factor of x10 to x100 below the natural background levels, such that NP tracing by simple concentration measurements is not viable. During exposures, samples are collected at pre-determined time points for the various reservoirs/materials of the experimental system.

3) Finally, the samples are prepared for analysis by Multiple Collector Inductively Coupled Mass Spectrometry (MC-ICP-MS). To this end, the samples are dissolved and processed to separate the element of interest from the complex natural matrix. The isotopic composition of the purified elemental separates is then determined by MC-ICP-MS. The amount of an enriched isotope label in a sample is quantified by measuring a diagnostic isotope ratio. For example, if a ^{68}Zn spike is used to label ZnO NPs, the diagnostic ^{68}Zn/^{66}Zn isotope ratio of a sample can be applied for quantification. This is based on the principle that the proportion of isotope spike to natural Zn present in a sample will determine the degree to which the diagnostic ratio is perturbed from the natural value. Based on the difference between the measured diagnostic ratio for an exposed sample and the known natural background value, mass balance equations can be applied to accurately quantify the amount of isotope label present. For most elements, this method typically enables detection

sensitivities that are equivalent to less than 0.1% of the natural background concentration. A schematic of the stable isotope tracing approach for ^{68}ZnO NPs is given in Figure 1.2.

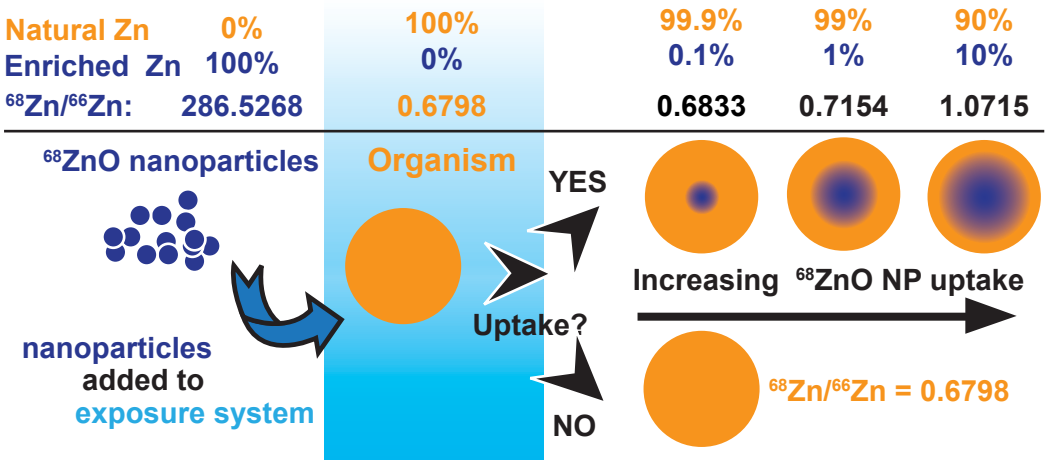


Figure 1.2 Schematic showing how the introduction of isotopically enriched ^{68}ZnO NPs results in changes to the diagnostic ^{68}Zn/^{66}Zn ratio.

1.4 Thesis Overview

The work presented here covers all aspects of the techniques which are required for stable isotope tracing of NMs, focusing on, ZnO, Ag and CeO_2 NPs.

Chapter 2 presents a full review of the use of stable isotope labeling for the tracing of CeO_2 NPs. This involves isotopic analyses of commercially available CeO_2 NPs, which demonstrate that these materials are isotopically indistinct from other sources of Ce. Therefore, an enriched isotope label is necessary to enable stable isotope tracing. The evaluation considers the various enriched Ce isotopes that are commercially available and the detection sensitivities they offer for a range of analytical scenarios. As a proof of concept, the controlled dosing of natural samples with an enriched ^{140}Ce label, followed by subsequent Ce separation and analysis, was conducted.

The use of isotopically labeled NPs requires optimized protocols for their synthesis. Due to the relatively high cost of isotopically enriched material, it is necessary for such synthesis protocols to be small-scale and reliable, offering high yields with minimal waste.

Such considerations are not a priority for most published synthesis methods and results, including synthesis yields, often go unreported. To address this issue, Chapter 3 presents a synthesis protocol, which has been adapted and evaluated for the preparation of isotopically labeled Ag NPs. Rigorous characterization of particles produced using this technique confirmed that the methods are robust and provide high yields, such that they are suitable for routine synthesis of isotopically labeled Ag NPs. Furthermore, it was shown that the labeled particles were indistinguishable, except in isotopic composition, from equivalent non-labeled particles.

Chapters 4 and 5 present and discuss the results of two exposures that apply isotopically labeled ^{68}ZnO NPs, in an aquatic and terrestrial system respectively. Crucially, these exposures were conducted at environmentally relevant NP concentrations. Biodynamic modeling was performed using the tissue concentrations of the enriched ^{68}Zn to determine the uptake and elimination rate constants of the isotope label by the exposed organisms.

Chapter 4 compares the uptake and efflux kinetics for three forms of isotopically enriched ^{68}Zn; ^{68}ZnO NPs, ^{68}ZnO bulk particles (micron sized) and dissolved ^{68}Zn, by an estuarine snail. A comparison of the bio-kinetics revealed that the behavior of the ^{68}ZnO NPs was very similar to dissolved ^{68}Zn, whereas the behavior of the bulk ^{68}ZnO particles was distinctly different. The similarity in the observations made between the dissolved ^{68}Zn and ^{68}ZnO NP exposures are most likely explained by the rapid dissolution of the NPs resulting in comparable experimental systems.

Chapter 5 assesses the dermal and oral uptake pathways of a ^{68}Zn isotope label by earthworms, when introduced as either ^{68}ZnO NPs or a dissolved ^{68}Zn form. This experiment showed that the behavior of the two ^{68}Zn forms was indistinguishable for both uptake routes. It was found that the major uptake pathway was by oral ingestion, accounting for about 95% of the total accumulation. In addition, it was primarily Zn associated with pore water that was available for dermal uptake. In comparison, published work where soil exposures with ZnO NPs and dissolved Zn were conducted using high dosing levels, found distinct differences in

the behavior between the two forms. These findings contradict the observations made here and are most likely the result of concentration dependent effects. The exposure concentration is therefore an important consideration when assessing studies for environmental risk and relevance. Furthermore, this indicates that it is unlikely that the observations made in a study conducted using high dosing levels will be representative of behavior in an equivalent experiment performed using low and predicted environmental levels.

Chapter 2:

Development and evaluation of new techniques for stable isotope tracing of CeO_2 nanoparticles

Abstract

Engineered CeO_2 nanoparticles (NPs) are becoming increasingly prevalent in consumer products and this has raised concerns about the unknown behavior and fate of such materials in the environment. Analytical limitations have hampered the detection of CeO_2 NPs in natural systems at environmentally relevant levels. This study assesses the suitability and detection sensitivity of stable isotope tracing of CeO_2 NPs in natural systems using two approaches: (i) The inherent isotope composition of commercially available CeO_2 NPs and (ii) the use of artificially enriched isotopes to synthesize and hence label CeO_2 NPs. The results demonstrate that commercially available CeO_2 NPs do not offer an isotopically distinct source of Ce that may be exploited for the purpose of stable isotope tracing. However, the technique of stable isotope labeling is promising, and can enable the detection of CeO_2 NPs at the low levels required to carry out experiments at environmentally relevant concentrations. A full evaluation for the approach of stable isotope labeling and isotopic analysis for different enriched Ce isotopes is presented. This review demonstrates that isotopically labeled CeO_2 NPs may be detected when contributing at least 19‰ and as little as 0.02‰ of the total Ce concentration, depending on the enriched isotope and analytical approach used.

2.1 Introduction

Engineered CeO_2 nanoparticles (NPs) are amongst the most extensively manufactured nanomaterials (NMs). They are widely used as a glass-polishing agent and, more recently, have been employed as an effective diesel fuel borne catalyst, significantly reducing emissions and increasing engine efficiency (Arul Mozhi Selvan et al., 2009, Cassee et al., 2011, Park et al., 2007). Despite engineered NMs being used in a wider range and larger number of consumer products, the toxicological properties and environmental fate of industrially produced NMs are still relatively poorly understood (Cassee et al., 2011, Handy et al., 2008b, Savolainen et al., 2010). This has prompted numerous studies of their predicted environmental concentrations (PECs), environmental fate and toxicity.

The environmental behavior and PECs of engineered CeO_2 NPs have been investigated using a combination of direct measurements and environmental modeling. O'Brien and Cummins (2010) modeled total PECs for Irish surface waters of ~24 ng L^{-1}. This is much higher than the concentrations of ~0.02 ng L^{-1} and ~0.4 ng L^{-1} that were estimated for UK waste-water treatment plant (WWTP) effluents and biosolids, respectively (Tiede et al., 2010). Johnson and Park (2012) modeled surface water inputs of CeO_2 NPs emanating from vehicular exhausts to calculate PECs of up to 0.02 ng L^{-1} for rivers and up to 300 ng L^{-1} for road drain water. Assuming a doubling in the market penetration of CeO_2 NPs being used as a diesel fuel additive from 2012 to 2017, and that engine filters capture 95% of ultrafine particles (Mayer, 2002), Johnson and Park (2012) estimated ceria NP concentrations of up to 16 µg kg^{-1} for soils in the direct vicinity of highways. Much higher PECs for soils were reported by Park et al. (2008) for a worst case scenario in which all diesel fueled vehicles used a CeO_2 NP additive and engine filters failed to capture NP emissions. This study estimated that after 40 years of accumulation soils would have CeO_2 NP concentrations of up to 1.12 mg kg^{-1} whilst atmospheric concentrations of up to 80 ng/m^3 were predicted.

Although there is some variability in the PECs quoted above, there is a general consensus that the expected concentrations of engineered CeO_2 NPs, or Ce derived from such NPs, are likely to be in the pg L^{-1} and µg kg^{-1} range for rivers and soils respectively

(Figure 2.1). However, for materials such as CeO_2, which have been shown to be non-degradable and will persist in the environment, then it is likely they will accumulate and increase in concentration with time. In contrast to the above PECs the natural background Ce concentrations are typically much higher (Figure 2.1). In particular, soil and sediment Ce concentrations are typically about 10-100 mg kg^{-1} (Martin and Whitfield, 1983, Othman et al., 1989), river water concentrations are normally in the range of 100-1000 ng L^{-1} (Gaillardet et al., 1997, Martin and Whitfield, 1983), whilst biological tissues generally feature 10-1000 µg kg^{-1} Ce (Chen et al., 2001, Costas et al., 2010, Lahive et al., 2014, Tjioe et al., 1983). These data (Figure 2.1) indicate that environmentally relevant exposure studies must be conducted with relatively low CeO_2 NP concentrations, in comparison to the natural Ce background levels.

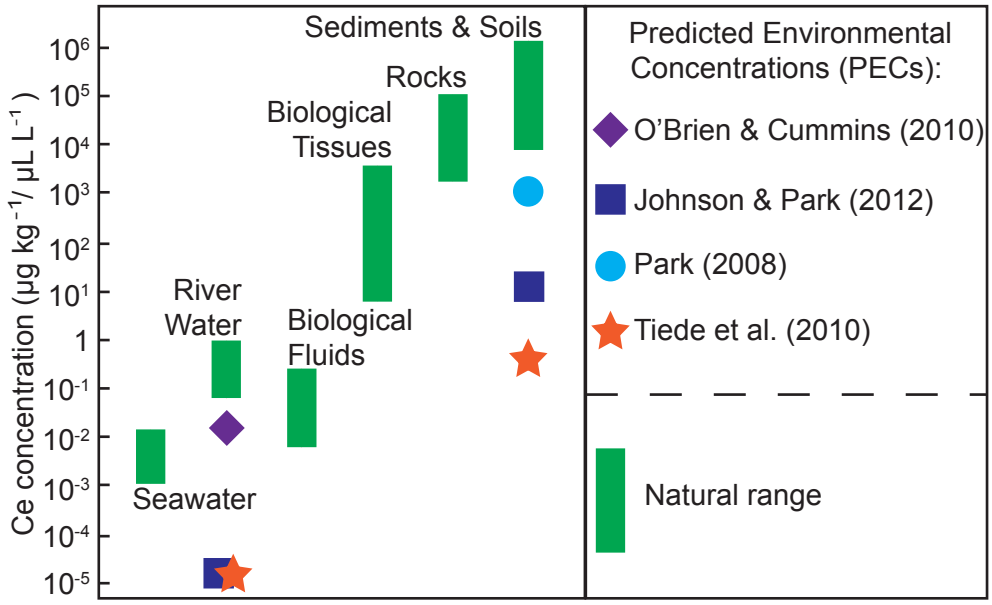


Figure 2.1 Compilation of published CeO_2 NP PECs and natural background Ce concentrations for various environments. The green bars denote the range of natural Ce concentrations compiled for seawater[a], river water[b], biological fluids[c], biological tissues[d], rocks[e], and sediments & soils[f]. The PEC data for CeO_2 NPs in river water and soils are plotted as points[g]. Data sources: [a](Donat and Bruland, 1995), [b](Gaillardet et al., 1997, Martin and Whitfield, 1983), [c](Bettinelli et al., 2002, Hollriegl et al., 2010, Inagaki and Haraguchi, 1999, Rodushkin and Odman, 2001b, Rodushkin and Odman, 2001a), [d](Chen et al., 2001, Koeberl and Bayer, 1992, Rodushkin and Axelsson, 2000), [e](Martin and Whitfield, 1983, Palme and O'Neill, 2005), [f](Gaillardet et al., 1997, Martin and Whitfield, 1983, Othman et al., 1989) [g](Johnson and Park, 2012, O'Brien and Cummins, 2010, Park et al., 2008, Tiede et al., 2010).

Conventional methods for tracing engineered NPs in bulk environmental samples are typically based on monitoring changes in the total elemental concentration that result from NP addition or uptake. Whilst such methods are well suited for tracking metals with low natural background levels (e.g., Au) they are much less sensitive when applied to elements, such as Ce, where the background concentrations are high. As a consequence, many studies commonly employ unrealistically high NP doses during exposures to achieve analytically resolvable increases in element concentration. However, the relevance of the results from studies that apply such high dosing must be carefully considered, as concentration effects may mask or induce nano-specific reactions and observations.

The distinct lack of data from environmentally relevant studies, which are carried out at or close to PECs, has lead to a drive to develop more selective and sensitive tracing methods that are capable of detecting engineered NPs in natural matrices at low levels (Handy et al., 2008a). Stable isotope tracing is one such technique, and this approach has clear advantages to alternative tracing methods. In particular, it is superior to methods that apply radiolabeling or a fluorescent marker, as such techniques involve the use of hazardous radioactive isotopes with limited half-lives or particle coatings that may be lost and/or alter chemical behavior. In addition, stable isotope tracing is highly versatile, as it can be applied to any multi-isotopic element. Hence it is applicable to Ce, which has the four stable isotopes ^{136}Ce (0.25% natural abundance), ^{138}Ce (0.19%), ^{140}Ce (88.4%) and ^{142}Ce (11.1%) (Table 2.1).

Table 2.1 Summary of natural Ce isotope abundances, isotopic enrichment and cost of commercially available enriched Ce isotopes.

	^{136}Ce	^{138}Ce	^{140}Ce	^{142}Ce
Natural isotope abundance (%)[a]	0.185	0.251	88.450	11.114
Abundance of enriched isotopes (%)[b]	30.6	41.6	99.5	93.0
Price of spike (in US $/mg)[b]	240	390	2.50	23
Cost of NPs containing 100 mg Ce, assuming 10% yield during preparation (in US $)	240 000	390 000	2 500	23 000

[a] Data from NIST literature values (Bohlke et al., 2005). [b] The isotopic enrichment and cost of the isotope spikes are from product quotes provided by Isoflex USA in March 2011.

There are two principal approaches to stable isotope tracing and the application of both methods for tracing engineered CeO_2 NPs is evaluated in this study based on analytical investigations and modeling:

First, it is conceivable that commercial CeO_2 NPs have inherent isotope compositions that are distinct from the natural background, and if large enough, such differences can be exploited for tracing purposes. This is evaluated through Ce stable isotope analyses of commercially available, high purity, Ce based materials including standard analytical solutions, salts, metals and CeO_2 NP powders. These analyses employ novel mass spectrometric techniques, which have distinct advantages compared to published methods whilst providing data of at least comparable precision.

Second, isotopic tracing of CeO_2 NPs can be achieved if the NPs are synthesized from and hence labeled with a single enriched isotope of Ce. This approach has recently been applied to CuO, ZnO and Ag NPs using the artificially enriched isotopes (>99%) ^{65}Cu, ^{68}Zn, and ^{107}Ag for their synthesis to enable detection at environmentally relevant concentrations (Khan et al., 2013, Larner et al., 2012, Laycock et al., 2014, Misra et al., 2012). In the following, a detailed evaluation of the tracing performance and cost is presented to elucidate which Ce isotopes are best used for labeling. To support this evaluation, an analytical demonstration of the extremely sensitive detection capabilities that can be achieved, even when the most cost-effective solution is employed, is provided. This validation documents the data reduction methods used and employs a novel method for the chemical separation of Ce from complex natural samples. In conjunction with the novel Ce isotope measurement techniques, the present study thus provides the full set of methods needed for the analytical investigation of samples, which are obtained from exposure studies that employ stable isotope labeled CeO_2 NPs.

2.2 Experimental

2.2.1 Samples

High-precision Ce stable isotope data were acquired for CeO_2 nano- and bulk-particles and additional samples of purified Ce based materials to identify possible differences in their isotopic composition that could be exploited for the purpose of tracing. Seven commercially available CeO_2 NP samples and three CeO_2 reference materials (of which two are also in NP form), all provided as dry powders, were analyzed in this study (Table 2.2). The reference materials (JRC NM-211, NM-212, NM-213) are available from the European Commission Joint Research Centre (JRC) whilst the commercial CeO_2 NP were sourced directly from the manufacturers.

Furthermore, three different Ce standard solutions were analyzed, whereby the Alfa Aesar solution was used as in-house Ce isotope reference material, relative to which all other Ce isotope compositions were determined. The Ce solution that was prepared by Willbold (2007) at the Bristol University (termed 'Bristol Ce' hereafter) has also been suggested as a Ce isotope reference material. Additional purified Ce based materials that were analyzed encompass two small chunks of Ce metal that were treated as distinct samples, as well as the Ce salts ammonium Ce(IV) nitrate $(NH_4)_2Ce(IV)(NO_3)_6$ and Ce(III) nitrate, $Ce(III)(NO_3)_3$ (Table 2.2).

To document the tracing capabilities that are provided when materials are labeled with an artificially enriched isotope of Ce, a selection of natural samples were doped with a known quantity of nearly pure ^{140}Ce and the resulting isotopic deviations were measured. The natural samples used were the Lufa 2.2 reference soil, the earthworm *Lumbricus rubellus* and the clam *Scrobicularia plana*.

Table 2.2 Summary of Ce isotope data for nano- and bulk-sized CeO_2 particles, including several reference materials and other purified Ce samples.

Sample type	Supplier / comments	Particle size (nm)[a]	n[b]	δ^{142}Ce (‰)[c]	± 2sd (‰)[d]	± 2se (‰)[e]
Ce Solutions:						
	Alfa Aesar; In-house δ-zero reference material			±0		
	Sigma-Aldrich		11	+0.05	0.07	0.02
	Bristol Ce solution[f]		9	+0.14	0.07	0.02
Reference materials:						
	Bulk CeO_2; JRC NM-213; Sigma-Aldrich	600 ± 400	11	+0.07	0.05	0.01
	CeO_2 NPs; JRC NM-211; Antaria	13 ± 3	15	-0.08	0.06	0.01
	CeO_2 NPs; JRC NM-212; Umicore	28 ± 10	10	+0.07	0.05	0.01
Commercial CeO_2 NPs:						
	MKnano-CeO_2-070	70	11	+0.07	0.04	0.01
	Sky Spring nano 2110 CG	10 - 30	14	+0.06	0.05	0.01
	io-li-tec NO-0029-HP	15 - 30	6	+0.03	0.02	0.01
	io-li-tec NO-0017-HP	50 - 80	6	+0.05	0.03	0.01
	Sigma-Aldrich	<25	8	+0.04	0.04	0.01
	Alfa Aesar	30	7	-0.16	0.04	0.01
	Energenics	-	11	+0.05	0.04	0.01
Ce metals (99.9% purity):						
	Piece 1; RGB Research, 99.9% purity		8	+0.11	0.06	0.02
	Piece 2; RGB Research, 99.9% purity		5	+0.12	0.05	0.02
Ce salts (99.99% purity):						
	Ammonium Ce(IV) nitrate; Sigma-Aldrich		9	+0.09	0.07	0.02
	Ce(III) nitrate; Alfa Aesar		8	+0.03	0.07	0.02

[a]Particle size as reported by supplier. [b] Number of individual analyses. [c] All isotopic data are reported relative to the in-house Alfa Aesar Specpure Ce standard solution reference material. [d] The quoted 2sd uncertainties are based on the reproducibility of n individual measurements. [e] The quoted 2se uncertainties (standard error of the mean) were calculated as 2se = 2sd/√n. [f] Bristol Ce solution from Willbold (2007)

2.2.2 General procedures and reagents

All sample preparation work was carried out in the Class 1000 clean room facility of the MAGIC Research Centre at the Department of Earth Science and Engineering, Imperial College London. Class 10 laminar flow hoods were utilized for all blank sensitive procedures. Concentrated 14.5 M HNO_3 and 6 M HCl were purified prior to use by sub-boiling distillation in quartz stills, whilst clean water of >18 MΩ cm quality was taken from a Millipore purification system. Suprapur quality 30% H_2O_2 solution (VWR) and 99.5% purity $NaBrO_3$ (Alfa Aesar) were used as purchased. The 'RE Resin' and 'LN Resin' that were employed for chromatographic purification of Ce were sourced from Eichrom Technologies and the AG 50W-X8, 200 – 400 dry mesh size cation exchange resin was purchased from Bio-Rad Laboratories. A BDH Ba Spectrosol ICP standard solution (1000 µg mL^{-1} stock solution) was used throughout. The artificially enriched ^{140}Ce (termed ^{140}Ce-E hereafter) with a purity of 99.5% was purchased as $^{140}CeO_2$ powder from Isoflex USA (Table 2.1).

2.2.3 Sample preparation of CeO_2 and purified Ce samples for stable isotope analysis

Working stock solutions with Ce concentrations of 100 µg mL^{-1} in 0.1 M HNO_3 were prepared from the CeO_2 powders and the purified Ce based materials (Table 2.2) as follows. For the three Ce standard solutions, suitable aliquots were diluted with 0.1 M HNO_3. Solutions of the two Ce metal pieces were prepared at room temperature by dissolving about 1 g of metal in 200 ml 2 M HNO_3. The resulting solutions were diluted with 2 M HNO_3 to obtain concentrated Ce solutions of 1000 µg ml^{-1}. Aliquots of these were further diluted to obtain the working stock solutions. For the $Ce(III)(NO_3)_3$ and $(NH_4)_2Ce(IV)(NO_3)_6$ salts, about 10-15 mg of material were dissolved in 4 ml 4 M HNO_3 at room temperature. The resulting solutions were evaporated to dryness and taken up in 0.1 M HNO_3.

For the CeO_2 powders (including the isotopically enriched $^{140}CeO_2$), 10-15 mg of material were weighed into 15 mL Teflon beakers, 4 mL 14.5 M HNO_3 and 1 mL 30% H_2O_2, to reduce Ce(IV) to Ce(III), were added before placing the beakers on a hotplate at 80°C. Dissolution was allowed to proceed overnight, whereupon the temperature was slowly

increased to 160°C. The beakers were again left on the hotplate overnight following which the samples were dried down. If complete digestion was not achieved before drying, the above procedure was repeated until a perfect sample solution was obtained. The samples were subsequently dried down three times with 100 µl 14.5 M HNO_3 at 100°C, before taking up in 0.1 M HNO_3.

The concentration of the ^{140}Ce-E stock solution was determined based on measurements of several (n = 8) dilute ^{140}Ce-E solutions with ^{140}Ce-E contents of about 10 to 60 ng mL^{-1}, to which Ba was added as internal standard at 160 ng mL^{-1}. Evaluation of the Ce/Ba ratios measured for the ^{140}Ce-E solutions relative to a calibration curve defined by Ce-Ba standard solutions with Ce concentrations of about 10 to 80 ng mL^{-1} and Ba concentrations of 160 ng mL^{-1}, provided the total Ce concentration for the ^{140}Ce-E stock of 11.7 ± 0.2 µg mL^{-1} (2se).

2.2.4 Sample preparation of natural materials to investigate tracing of enriched ^{140}Ce

2.2.4.1 Digestion

About 300-400 mg of dried soil, earthworm or clam tissue were weighed into microwave digestion vessels. An overnight pre-digestion was carried out at room temperature by adding 9 mL 14.5 M HNO_3 and 1 mL 30% H_2O_2. The vessels were then transferred to a Milestone EthosEZ microwave system (1200 W) where the samples were heated to 200°C over 15 minutes and maintained for a further 15 minutes. Once cooled to room temperature, samples were transferred to 15 mL Teflon vessels and evaporated to dryness before taking up in 1 M HNO_3. All sample solutions of the same type (earthworm, soil and clam) were then combined, to produce a single stock solution for each of the natural samples.

2.2.4.2 Addition of ^{140}Ce spike

For each sample type, three equal solution aliquots, equivalent to 130 mg earthworm, 570 mg clam and 30 mg soil, were taken and diluted with 1 M HNO_3 to a volume of 1 mL. An

aliquot of each sample type was allocated to one of three groups. The first was the 'non-spiked' group, where the samples were not spiked with ^{140}Ce-E, whereas the second and third group received a 'low' and 'high' dose of the ^{140}Ce-E spike solution respectively (Table 2.3). To produce the 'high-spike' group, ^{140}Ce-E was added to increase the total Ce concentration by about 0.3 to 4%, based on an initial estimate of the natural Ce content. Following analyses of the 'high-spike' aliquots, the natural Ce concentration of each sample group was determined. To produce the 'low-spike' group, the ^{140}Ce-E solution was added to the remaining aliquot to increase the total Ce concentration by about 0.1% (Table 2.3).

2.4.3. Chemical separation of Ce

For the natural samples, it was necessary to isolate Ce from the complex sample matrix prior to the isotopic analyses. This was achieved using a three-step column chromatography procedure (Table 2.4), which was adapted from the work of Rehkämper et al. (1996) and Tazoe et al. (2007). In the first step, the rare earth elements (REE) were separated as a group from the other matrix elements using shrink-fit Teflon columns packed with 240 µl RE resin. To this end, the sample solutions were loaded onto the columns and the matrix elements were eluted first using 1 M HNO_3. The REEs were then stripped from the resin with 4 M HCl (Table 2.4).

In the second step, Ce was separated from the REE fraction using 130 µl LN resin beds in Teflon columns (Table 2.4). For this, the REE fractions were dissolved in 500 µl of 10 M HNO_3 containing 20 mM $NaBrO_3$. The presence of $NaBrO_3$ is crucial, as it oxidizes Ce(III) to Ce(IV), which is subsequently retained on the LN resin. In contrast, the other REEs remain in a trivalent form and are readily eluted from the column using a 10 M HNO_3 – 20 mM $NaBrO_3$ mixture. Following this, Ce is eluted with the aid of a 6 M HCl – 20 mM H_2O_2 reagent mix. The H_2O_2 hereby acts as a reductant that converts Ce(IV) to Ce(III), and whereby the latter is no longer retained on the resin. Finally, the Ce fraction from Step 2 is passed through a 240 µl column of strongly acidic cation exchange resin (AG50W-X8) to isolate Ce from residual Na (from $NaBrO_3$) (Table 2.4).

Table 2.3 Details and results obtained for the natural samples that were processed through the column chemistry.

Sample / Aliquot	Dry Weight (mg)	Natural [Ce] (mg kg^{-1})	Total Ce (ng / nmol)	^{140}Ce-E added (ng / nmol)	Change in [Ce] (%)	Ce yield (%)[a]	Predicted δ^{142}Ce (‰)	n	Measured δ^{142}Ce ± 2sd (‰)[b]	^{142}Ce/^{140}Ce ± 2sd[c]
Soil – Lufa 2.2										
Soil non-spiked	30	24.3	730 / 5.21	–	–	59		2	–0.24 ± 0.12	0.125627 ± 0.000016
Soil low-spike	30	24.3	730 / 5.21	0.73 / 0.005	0.1	91	-1.32	1	–1.17 ± 0.10	0.125511 ± 0.000013
Soil high-spike	30	24.3	730 / 5.21	30 / 0.241	4.1	20	-42.71	2	–42.66 ± 0.17	0.120312 ± 0.000022
Earthworm – *L. rubellus*										
Earthworm non-spiked	130	3.2	420 / 3.00	–	–	83		2	–0.29 ± 0.19	0.125638 ± 0.000024
Earthworm low-spike	130	3.2	420 / 3.00	0.42 / 0.003	0.1	55	-1.37	1	–0.96 ± 0.10	0.125525 ± 0.000011
Earthworm high-spike	130	3.2	420 / 3.00	1.3 / 0.009	0.3	33	-3.63	2	–3.70 ± 0.00	0.125193 ± 0.000000
Clam – *S. plana*										
Clam non-spiked	570	0.9	500 / 3.57	–	–	35		2	–0.47 ± 0.10	0.125607 ± 0.000013
Clam low-spike	570	0.9	500 / 3.57	0.50 / 0.004	0.1	30	-1.55	1	–1.06 ± 0.09	0.125525 ± 0.000011
Clam high-spike	570	0.9	500 / 3.57	5.7 / 0.041	1.1	21	-12.64	2	–12.83 ± 0.05	0.124041 ± 0.000006

[a] Recovery of Ce from the chemical separation procedure. [b] The measured δ^{142}Ce data denote the relative deviation of the ^{142}Ce/^{140}Ce isotope ratio of a sample from the in-house Alfa Aesar standard (as measured repeatedly before and after each sample) in parts per 1000 (see text for details). The 2sd uncertainties were calculated either from the results of duplicate sample runs (if n = 2) or the precision obtained for the bracketing runs of the Alfa Aesar standard solution (if n = 1). [c] The ^{142}Ce/^{140}Ce ratios for the samples were calculated based on the measured δ^{142}Ce values, with the assumption that the in-house Alfa Aesar solution has a ^{142}Ce/^{140}Ce ratio equivalent to the reference value 0.125658, calculated from NIST literature values (Bohlke et al., 2005).

Table 2.4 Cerium separation protocol

Step 1 – RE Resin Column Length – 25 mm, Internal Ø – 3.5 mm, Volume – 240 µL	
Clean Resin	0.65 mL 4 M HCl
	1.0 mL 18 MΩ water
Condition	0.5 mL + 0.75 mL 1 M HNO_3
Load Sample	1 mL 1 M HNO_3
Wash Matrix	0.5 mL + 3.5 mL 1 M HNO_3
Elute REE	0.25 mL + 2.0 mL 4 M HCl

Step 2 – LN Resin Column Length – 26.5 mm, Internal Ø – 2.5 mm, Volume – 130 µL	
Clean Resin	3 mL 1 0 M HNO3
Condition	0.6 mL + 2.0 mL 10 M HNO_3 – 20 mM $NaBrO_3$
Load Sample	0.5 mL 10 M HNO_3 – 20 mM $NaBrO_3$
Wash Matrix	5.2 mL 10 M HNO_3 – 20 mM $NaBrO_3$
Rinse	1.6 mL 10 M HNO_3
	1 mL 18 MΩ water
Elute Ce	3 mL 6 M HCl - 20 mM H_2O_2

Step 3 – Cation Exchange Resin Column Length – 25 mm, Internal Ø – 3.5 mm, Volume – 240 µL	
Clean Resin	3 mL 6 M HCl
Condition	4 x 0.5 mL + 1mL 2 M HCl
Load Sample	3 mL 2 M HCl
Wash Matrix	3 x 0.5 mL + 3 mL 2 M HCl
Elute Ce	6 mL 6 M HCl

Aliquots of the Alfa Aesar Ce standard solution were processed through the above procedure in addition to the natural samples, in order to assess the Ce yield and evaluate any isotopic fractionation of Ce associated with separation. This is important because large laboratory-induced changes in the isotope composition of Ce can potentially limit the detection sensitivity of isotopic tracing methods.

2.2.5 Mass spectrometry

The Ce stable isotope and concentration measurements were performed with a Nu Instruments Nu Plasma HR multiple collector inductively coupled plasma mass spectrometer (MC-ICP-MS) at the Imperial College MAGIC Laboratories. The instrument is fitted with a large capacity (80 L min^{-1}) rotary pump for enhanced evacuation of the expansion chamber to improve sensitivity. A Nu Instruments DSN and a CETAC Aridus I desolvation system were employed for sample introduction, both with glass nebulizers that provided solution uptake rates of about 100 µL min^{-1}. Normal instrumental operating parameters are summarized in Table 2.5.

Table 2.5 Instrumental operating parameters

Nu Plasma MC-ICP-MS		
RF Power (W)		1300
Acceleration potential (V)		~6000
Ar coolant gas flow (L min^{-1})		13
Ar auxiliary gas flow (L min^{-1})		1
Expansion chamber vacuum (mbar)		~0.75
Analyzer vacuum (mbar)		~2 x 10^{-9}
Instrument performance		
Sensitivity for (V μg^{-1} mL^{-1}):	Ce	110 - 160
	Ba	130 - 180
Transmission efficiency (%):	Ce	0.10 - 0.14
	Ba	0.11 - 0.15

For isotopic analyses, the 100 µg mL^{-1} stock solutions of the purified Ce samples and in-house standard (Table 2.2) were diluted with 0.1 M HNO_3 to prepare measuring solutions with Ce concentrations of between 50 and 125 ng mL^{-1}. These Ce solutions were doped with a 10 µg mL^{-1} Ba stock solution to obtain Ba concentrations of 75 to 350 ng mL^{-1} and Ce/Ba ratios of between 1.5 and 3.5.

The Ce isolated from the natural samples was prepared for analysis by appropriate dilution (following an initial concentration check), to obtain Ce concentrations of 50 ng mL^{-1}, and to which Ba was added at 150 ng mL^{-1}. These sample analyses were conducted relative to a standard solution with 50 ng mL^{-1} of the Alfa Aesar Ce and 150 ng mL^{-1} Ba.

Data collection was carried out by static multiple collection with the Faraday cups of the instrument, which are fitted with 10^{11} Ω resistors. Each analysis consisted of 60 integrations of 5 seconds each, in 3 blocks of 20, where the ion beams of the atomic masses 135 (Ba), 137 (Ba), 139 (La), 140 (Ce, Nd), 141 (Pr), 142 (Ce), 143 (Nd) and 145(Nd) were monitored. Table 2.6 shows the collector arrangement that was used to measure these atomic masses, along with the natural abundances of each of the isotopes monitored. Prior to each block, baseline signals were measured for 15 seconds, whilst the ion beam was deflected in the electrostatic analyzer. Analyses of mixed Ce-Ba solutions typically yielded sensitivities of about 110 to 160 V μg^{-1} mL^{-1} for Ce and 130 to 180 V μg^{-1} L^{-1} for Ba during the course of this study, equivalent to a transmission efficiency of about 0.10 to 0.15% for both elements (Table 2.5). Each measurement was followed by a thorough (~2-3 min) washout of the sample introduction system with 0.1 M HNO_3, and this was generally sufficient to reduce the residual signal to <5 mV for ^{140}Ce.

Table 2.6 Faraday cup arrangement showing the isotopes present at each atomic mass and their corresponding natural abundances.

Collector	H5	H3	H2	H1	Ax	L2	L3
Mass	145	142	141	140	139	137	135
Element							
Ba						11.2	6.6
La					99.9		
Ce		11.1		88.5			
Pr			100				
Nd	8.3	27.2					

To determine variations in the stable isotope composition of Ce, the analyses focused on the two major Ce isotopes (Table 2.6) and the determination of $^{142}Ce/^{140}Ce$ isotope ratio. The $^{135}Ba/^{137}Ba$ isotope ratio of the admixed Ba was monitored for mass bias correction with the exponential law (Rehkämper et al., 2001), whilst the ^{145}Nd ion beam was measured for correction of the isobaric interference of ^{142}Nd on ^{142}Ce. The presence of the LREEs La and Pr was also monitored, using ^{139}La and ^{141}Pr, even though interference corrections are not necessary.

All sample measurements were bracketed with at least two analyses of the primary in-house Alfa Aesar Ce isotope reference material. Differences between the corrected $^{142}Ce/^{140}Ce$ ratios of the samples and the reference material are reported in the form of $\delta^{142}Ce$ values, which denote the relative deviation of the $^{142}Ce/^{140}Ce$ isotope ratio of a sample (R_{sam}) from the in-house Alfa Aesar standard (R_{std}) in parts per 1000:

$$\delta^{142}Ce = (((R_{sam} - R_{std}) / R_{std}) -1) \times 1000 \quad (2.1)$$

2.2.6 Isotope ratio modeling for samples spiked with enriched ^{140}Ce

The addition of ^{140}Ce-E to a natural material will produce a mixture with an intermediate $^{142}Ce/^{140}Ce$ isotope ratio. The resulting ratio of the mixture (R_{mix}) can be predicted based on the fractional molar (or atomic) abundances of ^{140}Ce and ^{142}Ce in natural Ce ($^{140}Ab_{nat}$ and $^{142}Ab_{nat}$) and ^{140}Ce-E ($^{140}Ab_{en}$ and $^{142}Ab_{en}$), if the molar amounts of natural Ce (N-Ce_{nat}) and ^{140}Ce-E (N-Ce_{en}) that are present in the mix are known:

$$R_{mix} = ((N\text{-}Ce_{nat} \times {}^{142}Ab_{nat}) + (N\text{-}Ce_{en} \times {}^{142}Ab_{en})) / ((N\text{-}Ce_{nat} \times {}^{140}Ab_{nat}) + (N\text{-}Ce_{en} \times {}^{140}Ab_{en})) \quad (2.2)$$

The predicted $\delta^{142}Ce$ values in Table 2.3 were calculated using the above relationship, based on the N-Ce_{nat} and N-Ce_{en} data, which are also listed in Table 2.3. For ^{140}Ce-E, the isotope abundances certified by the supplier (Table 2.1) were applied. The natural isotope abundances were calculated by assuming that the in-house Alfa Aesar Ce reference material ($\delta^{142}Ce = 0$) is characterized by $^{142}Ce/^{140}Ce$, $^{138}Ce/^{140}Ce$ and $^{136}Ce/^{140}Ce$ ratios equivalent to the NIST literature values (Bohlke et al., 2005). Whilst the NIST literature values are unlikely to be identical to the Alfa Aesar Ce reference material this is an appropriate approximation for a natural Ce isotope composition. These ratios were adjusted using the $\delta^{142}Ce$ values measured for the non-spiked natural sample aliquots to establish the $^{142}Ce/^{140}Ce$, $^{138}Ce/^{140}Ce$ and $^{136}Ce/^{140}Ce$ ratios ($^{142/140}R_{nat,}$ $^{138/140}R_{nat}$ and $^{136/140}R_{nat}$) of the non-

dosed natural samples. The natural molar ^{140}Ce and ^{142}Ce isotope abundances of the samples were then calculated using Equations 2.3 and 2.4:

$$^{140}Ab_{nat} = (1 + {}^{142/140}R_{nat} + {}^{138/140}R_{nat} + {}^{136/140}R_{nat})^{-1} \quad (2.3)$$

$$^{142}Ab_{nat} = {}^{142/140}R_{ref} \times {}^{140}Ab_{nat} \quad (2.4)$$

2.2.7 Data reduction for isotopic tracing

The measured $\delta^{142}Ce$ data of the samples (Table 2.3) were evaluated to quantify the amount of natural Ce and ^{140}Ce-E they contained. To achieve this, the molar fraction of ^{140}Ce-E ($fr^{140}Ce_{en}$) to total Ce in a dosed sample was calculated using mass balance:

$$fr^{140}Ce_{en} = [(^{142}Ab_{en} - (R_{meas} \times {}^{140}Ab_{en})) / ((R_{meas} \times {}^{140}Ab_{nat}) - {}^{142}Ab_{nat}) + 1]^{-1} \quad (2.5)$$

where R_{meas} is the measured $^{142}Ce/^{140}Ce$ isotope ratio of the sample. The molar abundance of ^{142}Ce in a dosed sample ($^{142}Ab_{sam}$) was then determined:

$$^{142}Ab_{sam} = (fr^{140}Ce_{en} \times {}^{142}Ab_{en}) + ((1 - fr^{140}Ce_{en}) \times {}^{142}Ab_{nat}) \quad (2.6)$$

The molar amount of ^{142}Ce in the sample ($N\text{-}^{142}Ce_{sam}$) was found based on (i) the dilution factor (D) used to prepare the measured sample aliquot, (ii) the signal intensity of ^{142}Ce in the sample solution ($^{142}Ce_{sig}$) as measured in volts (V), and (iii) the Ce signal sensitivity (Ce_{sen}), measured as V μmol^{-1} mL^{-1}. The latter was determined from analyses of a Ce-Ba standard solution with known concentrations and that was performed immediately prior to the sample analysis. Any drifts in instrumental sensitivity were hereby corrected using the admixed Ba as an internal standard. Using these parameters, molar amount of ^{142}Ce in the sample was determined as:

$$N\text{-}^{142}Ce_{sam} = (^{142}Ce_{sig} / Ce_{sen}) \times D \quad (2.7)$$

The molar amount of total Ce in the sample ($N\text{-}Ce_{sam}$) was then be found by dividing by the molar abundance of ^{142}Ce in the sample (Equation 2.6):

$$N\text{-}Ce_{sam} = N\text{-}^{142}Ce_{sam} / {}^{142}Ab_{sam} \quad (2.8)$$

The molar amounts of ^{140}Ce-E and natural Ce were determined using the results calculated from Equations 2.5 and 2.8:

$$N\text{-}Ce_{en} = N\text{-}Ce_{sam} \times fr^{140}Ce_{en} \quad (2.9)$$

$$N\text{-}Ce_{nat} = N\text{-}Ce_{sam} - (N\text{-}Ce_{sam} \times fr^{140}Ce_{en}) = N\text{-}Ce_{sam} - N\text{-}Ce_{en} \quad (2.10)$$

The mass amount of ^{140}Ce-E (M-Ce_{en}) and natural Ce (M-Ce_{nat}) was then obtained by multiplication with the atomic weight of ^{140}Ce-E ($AtWt_{en}$) and natural Ce ($AtWt_{nat}$) respectively.

$$M\text{-}Ce_{en} = N\text{-}Ce_{en} \times AtWt_{en} \quad (2.11)$$

$$M\text{-}Ce_{nat} = N\text{-}Ce_{nat} \times AtWt_{nat} \quad (2.12)$$

where the atomic weight is calculated by summing the isotope abundances multiplied by their corresponding atomic weight.

$$AtWt = \Sigma ({}^{xxx}Ab \times {}^{xxx}AtWt) \quad (2.13)$$

As the amount of ^{140}Ce-E added to each of the dosed sample aliquots was already known, the recovery of the chemical separation step could be accurately assessed and the natural Ce concentration of the samples determined (Table 2.3).

2.3 Results and discussion

2.3.1 Evaluation of isotope tracing of CeO_2 nanoparticles based on inherent differences in Ce isotope composition

2.3.1.1. Principles

Isotopic tracing of CeO_2 NPs is possible if such materials have an isotopic composition that is sufficiently distinct from the natural background (e.g., soil, water, biological tissue) in which it is to be tracked. For example, CeO_2 NPs that differ in their ^{142}Ce/^{140}Ce isotope ratio from the background value by 10‰ may be suitable for tracing. In

this case, detection and quantification of as little as 0.5 mg kg^{-1} of Ce from the NPs is already possible in a sample with a natural Ce background n of 50 mg kg^{-1}, if the isotopic measurements achieve a precision of 0.1. For Ce, isotopic variations that can be exploited for tracing may, in principle, be generated by either radioactive decay or mass dependent stable isotope variations.

The first pathway is commonly utilized for Pb, where large variations in the relative abundances of the isotopes ^{206}Pb, ^{207}Pb and ^{208}Pb are produced by decay of the radioactive parent isotopes ^{238}U, ^{235}U and ^{232}Th (Bollhofer and Rosman, 2001). Different sources of Pb differ in their isotopic composition (e.g., $^{207}Pb/^{206}Pb$ or $^{208}Pb/^{206}Pb$ ratios) because they evolved in environments with different parent-daughter (i.e., U-Th/Pb) ratios. Such radiogenic differences in isotope composition also occur for Ce due to the decay of radioactive ^{138}La to ^{138}Ce. There are number of geochemical studies that have documented variations in $^{138}Ce/^{142}Ce$ (or $^{138}Ce/^{136}Ce$) isotope ratios, which reflect this process (Tanaka and Masuda, 1982, Tazoe et al., 2007, Willbold, 2007). However, it was also shown that most geological materials (with the exception of a few rare minerals) do not exhibit radiogenic isotope variations that exceed 1‰. Primarily this is due to the long half-life ($t_{1/2} \approx 2.97 \times 10^{11}$ years) and low natural abundance of the parent isotope ^{138}La (0.09%). Whilst the small natural variations in $^{138}Ce/^{142}Ce$ can be resolved reliably (with a precision of ±0.1‰ or better), this requires the application of specialist techniques and instrumentation as well as very time-consuming measurements (Willbold, 2007). Such methods are, therefore, not suitable for routine analyses of larger sample numbers, as would be obtained from biological exposure or environmental screening studies with CeO_2 NPs.

Mass dependent differences, or fractionations, in the stable isotope composition of elements can be generated by processes of either physical (e.g., diffusion, adsorption), chemical (e.g., precipitation, redox change) or biological nature. Recent advances in mass spectrometry have allowed the resolution of such isotope effects for numerous metals, including Ca, Ba, and U, which resemble Ce due to their refractory, lithophile nature and moderate to high atomic mass number. Such studies have shown that stable isotope

fractionations are common in nature and recorded in many natural materials. Furthermore, industrial processes such as combustion or partial evaporation during smelting have been found to create distinct isotopic signatures for some metals, which have been exploited for tracing anthropogenic emissions to the environment (Shiel et al., 2010). It has also been shown that highly purified forms of some elements feature particularly large differences in their stable isotope compositions compared to the normal natural background. This is presumably due to isotopic fractionations that were generated during extraction of the element from ores and/or industrial purification (Cloquet et al., 2005).

In contrast to many other elements, stable isotope variations for Ce have received only little attention to date, with results presented in just two studies of recent origin. Nakada et al. (2013) investigated Ce stable isotope fractionation related to the oxidation of Ce(III) to Ce(IV) in a series of laboratory adsorption and precipitation experiments. Their results indicate that the degree of fractionation increases as conditions become more oxic and soluble Ce(III) is converted to insoluble Ce(IV), with the resulting Ce(IV) being isotopically lighter. Ohno and Hirata (2013) measured Ce and Nd stable isotope ratios of two igneous and three sedimentary rock reference materials and found a 1:1 correlation in the degree of fractionation for the two elements. As redox reactions are expected to produce larger isotopic effects for Ce compared to Nd, they concluded that the observed fractionations were induced without changing the oxidation state of Ce.

Whilst the findings of Ohno and Hirata (2013) are only limited to 5 samples, they reveal small but clearly resolvable natural variations in stable Ce isotope compositions. It is therefore conceivable that industrial processing and purification of Ce and the preparation of CeO_2 NPs may be associated with isotopic fractionation. If these effects are large enough they may result in a sufficiently distinct and traceable isotopic signature. The feasibility of the latter approach is tested, through Ce stable isotope analyses of various commercially available CeO_2 NPs and other samples of purified Ce based materials.

2.3.1.2. Precision and accuracy of Ce stable isotope data for CeO_2 and purified Ce samples

The isotope data obtained for the CeO_2 powders and purified Ce samples (Table 2.2) were acquired over a 9-month period that encompassed 11 separate measurement sessions and whereby a single analysis consumed approximately 50 to 100 ng of Ce. The $\delta^{142}Ce$ data collected for these samples feature 2sd reproducibilities, based on the results of 5 to 15 individual measurements, of ±0.02‰ to ±0.07‰ (Table 2.2). This performance is similar to that achieved in MC-ICP-MS stable isotope analyses for elements of similar mass when normalized to a mass difference of 1 amu (comparison of 2sd/amu results). For example, typical 2sd/amu uncertainties of ±0.01‰ to ±0.03‰ were reported for MC-ICP-MS analyses of Cd and Mo standard solutions by Abouchami et al. (2013) and Goldberg et al. (2013) respectively. Our data also compares favorably to the Ce stable isotope results of Nakada et al. (2013) and Ohno and Hirata (2013), who reported $\delta^{142}Ce$ uncertainties (2sd) of ±0.06‰ and ±0.08‰ for multiple analyses of Ce solutions. As in this study, these authors also employed MC-ICP-MS but the samples were doped with Sm, and $^{149}Sm/^{147}Sm$ was used for external normalization of the instrumental mass bias

As the analyzed samples were purified Ce materials, it is unlikely that the accuracy of the data is compromised by matrix effects and/or spectral interferences. The absence of the former is confirmed by the observation that none of the samples displayed any unusual mass bias behavior of Ba during the analyses. In addition, it was observed that the use of two different sample introduction systems and variations in the Ce, Ba concentrations and Ce/Ba ratios between sample and the bracketing standard solutions of up to 460% and 230% respectively, had no discernible effect on the $\delta^{142}Ce$ data at the quoted level of precision.

The purity of the Ce solutions was, furthermore, assessed throughout the isotopic analyses by monitoring the light REEs (LREEs) La, Pr and Nd. These elements are likely to be the most prominent contaminants, as they are difficult to separate from Ce. However, only trace amounts of the LREEs were present, with typical LREE/Ce ratios of less than 10×10^{-5} and a maximum Nd/Ce of about 50×10^{-5} for a CeO_2 powder and the two metal samples

(Table 2.7). Any Nd contamination is, however, of concern due to the isobaric interference of ^{142}Nd on ^{142}Ce, which was corrected during the analyses based on the monitoring of ^{145}Nd (Table 2.6). Table 2.7 summarizes the corrections that were applied to the δ^{142}Ce data of samples to account for the ^{142}Nd interference. The corrections are observed to be generally less than 0.2‰ but with maximum levels of up to 1.0 to 1.6‰ (Figure 2.2). The conclusion that these corrections are accurate, such that the presence of isobaric ^{142}Nd does not generate analytical artifacts is underlined by a number of observations. First, a plot of all δ^{142}Ce data versus the isobaric correction for the presence of ^{142}Nd shows no obvious correlation (Figure 2.2). Second, seven of the nine CeO_2 powders are characterized by a very narrow range of δ^{142}Ce values, even though they feature variable levels of Nd. It is highly unlikely that the isotopic homogeneity of the CeO_2 powders is a fortuitous result of an inaccurate Nd correction. Third, the two isotopically distinct CeO_2 samples are subject to only relatively small δ^{142}Ce corrections of 0.03 and 0.05‰, which implies that the negative δ^{142}Ce values are unlikely to be an artifact. In summary, these observations clearly indicate, that the applied corrections on δ^{142}Ce for the presence of isobaric ^{142}Nd were accurate even at Nd/Ce ratios of about 60 x 10^{-5}.

Table 2.7 REE/Ce ratios of measured in the Ce standard and sample solutions and the corresponding correction to the δ^{142}Ce values.

	δ^{142}Ce correction (‰)[a]	Nd/Ce (x 10^{-5})	La/Ce (x 10^{-5})	Pr/Ce (x 10^{-5})
Purified Ce materials				
Alfa Aesar Ce Solution	0.2	8.3	3.2	5.7
Other Ce solutions	0.06 – 0.3	2.4 – 12	0.3– 3.5	0.3 – 2.8
CeO_2 powders	0.03 - 1.4	1.2 - 62	0.2 - 32	0.2 – 52
Ce metals	1	44	23	1.5
Ce salts	0.03 – 0.05	1.1 – 2.2	<0.01 – 0.8	<0.01 – 4.5
Ce separated from natural samples				
Soil – Lufa 2.2	0.1 - 0.5	4.0 - 22	1.8 – 14	0.4 – 3.8
Earthworm – *L. rubellus*	0.6 - 1.6	25 - 64	21 – 55	5.4 - 15
Clam – *S. plana*	0.2 - 0.5	6.2 - 19	3.2 – 6.2	1.2 – 1.6

[a] Change in δ^{142}Ce after correction for the isobaric ^{142}Nd interference.

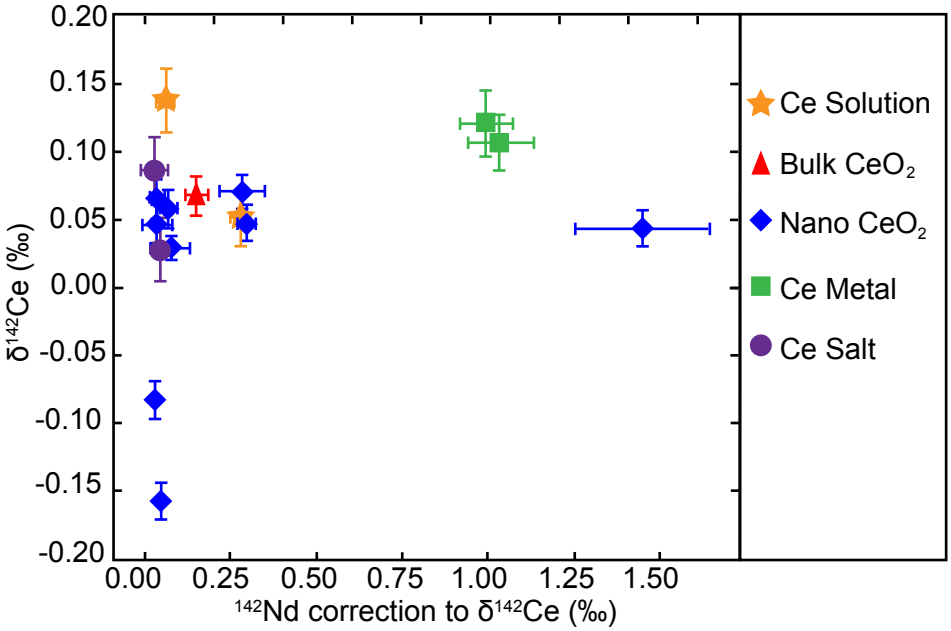


Figure 2.2 The $\delta^{142}Ce$ values of the purified Ce materials in Table 2.2 versus the isobaric correction for the presence of ^{142}Nd (Table 2.7)

To further test the robustness of and verify the correction of ^{142}Nd on ^{142}Ce by monitoring ^{145}Nd a series of Alfa Aesar standard solutions were doped with increasing amounts of a standard Nd solution. Figure 2.3 demonstrates the results of this assessment and shows that the Nd correction was suitable up to a Nd/Ce ratio of 0.01.

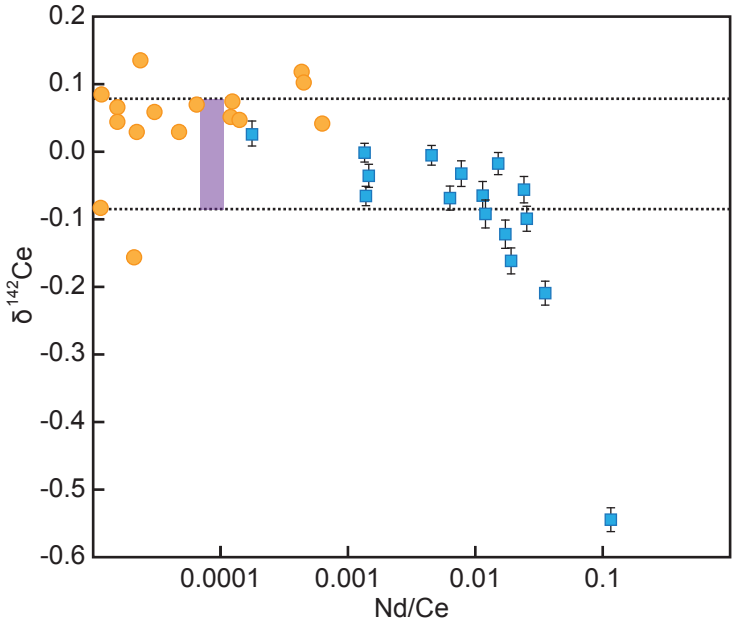


Figure 2.3 The measured $\delta^{142}Ce$ values plotted against the Nd/Ce ratio of the analyzed samples and a series of Alfa Aesaer Ce standard solutions dosed with Nd. The purple bar shows the range of non-dosed Alfa Aesar Ce standard solution measurements. The dotted lines represent the 2sd uncertainty of the Alfa Aesar Ce standard solution. Orange circles represent the measured samples. The blue squares show the Ce standard solutions dosed with varying amounts of Nd, error bars represent the internal uncertainty (2sd).

2.3.1.3. Isotopic variability

The analyzed CeO_2 NPs show a total variability in $\delta^{142}Ce$ of 0.23‰, with values of between -0.16‰ and 0.07‰. However, all but 2 of the 9 samples display a very narrow range of $\delta^{142}Ce$ values of 0.03‰ to 0.07‰, whilst the two outliers are characterized by $\delta^{142}Ce$ of –0.08‰ and –0.16‰ (Table 2.2, Figure 2.4). The CeO_2 bulk particles are essentially indistinct from most of the CeO_2 NP powders, with $\delta^{142}Ce$ = 0.07 ± 0.01‰ (2se). The remaining purified Ce samples also show only very limited variability in $\delta^{142}Ce$. The two Ce salts and the Sigma-Aldrich Ce standard solution are hereby isotopically identical, within the quoted 2se uncertainties of only 0.01 to 0.02‰, to the CeO_2 samples. The two metal samples are slightly heavier with $\delta^{142}Ce$ values of 0.11‰ and 0.12‰ (Table 2.2, Figure 2.4). This limited range in Ce isotope compositions is in accord with the Ce data published by Ohno and Hirata (2013). Even though the results of these investigations cannot be compared directly, as they are expressed relative to different $\delta^{142}Ce$ = 0 reference materials, Ohno and Hirata (2013) also found only a limited $\delta^{142}Ce$ variability of 0.14‰ for two igneous and three sedimentary rock samples (Figure 2.4).

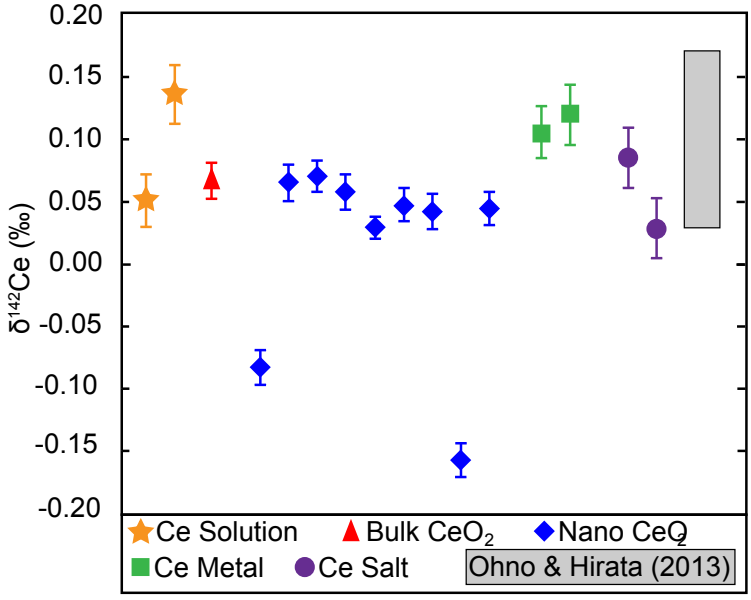


Figure 2.4 $\delta^{142}Ce$ data for the Ce samples analyzed in this study. Error bars denote the 2se uncertainties that were calculated based on multiple analyses (n = 5 to 15; Table 2.2). The grey bar denotes the range of values found by Ohno and Hirata (2013) for 5 reference rock materials. However, the position of this range in relation to our data may not be accurate, as Ohno and Hirata (2013) used a different Ce reference material to define $\delta^{142}Ce$ = 0.

In summary, the investigated Ce materials show only a limited range of isotope compositions. Even though some samples display resolvable isotopic differences, the overall variability in $\delta^{142}Ce$ of about 0.3‰ is too small to be exploitable for routine tracing purposes. This is demonstrated by a best-case scenario, which assumes that CeO_2 NPs have a $\delta^{142}Ce$ value that differs from a constant natural background by 0.3‰. In this instance, an increase in the background Ce concentration of 20%, from the addition of CeO_2 NPs, would be required to result in a change to the $\delta^{142}Ce$ value of 0.05‰. This example demonstrates that isotopic tracing methods for CeO_2 NPs which are based on inherent differences in $\delta^{142}Ce$ are of no practical value because they do not provide detection capabilities that are clearly superior to those offered by less costly and time consuming concentration measurements.

2.3.2 Tracing of stable isotope labeled CeO_2 nanoparticles

2.3.2.1. Principles

Although commercially available CeO_2 NPs are unsuitable for stable isotope tracing, the technique may still be applied, but this requires the use of NPs which are specifically prepared from and hence labeled with isotopically enriched Ce. The application of such NPs provides extremely sensitive and selective tracing capabilities, demonstrated in previous investigations with labeled CuO, ZnO and Ag NMs (Khan et al., 2013, Larner et al., 2012, Laycock et al., 2014, Misra et al., 2012). The current study presents the first evaluation of this approach for tracing CeO_2 NPs. Enriched single isotope spikes are currently sold for all four stable Ce isotopes with purities ranging from 30 to 40% for the less abundant ^{136}Ce, ^{138}Ce to more than 99% for the major ^{140}Ce isotope (Table 2.1).

In the following, modeling is presented that considers both cost and tracing sensitivity to evaluate which Ce isotopes are best employed for the preparation of labeled CeO_2 NPs. The modeling results are validated through analyses of natural samples that were spiked with ^{140}Ce-E. In addition, a novel technique was developed for the separation of Ce from complex natural samples prior to isotopic analysis. These aspects are discussed in the following sections.

2.3.2.2 Chemical separation of cerium from complex natural samples

A number of workers have published methods for the separation of Ce from geological samples to enable analyses of radiogenic differences in Ce isotope compositions. Most of these techniques employ a two-stage separation protocol, whereby the REEs are first separated as a group from other elements using either RE spec resin or TRU spec resin. Cerium is subsequently separated from the other REEs by extraction chromatography, using an inert support coated with HDEHP (di(2-ethylhexyl)orthophosphoric acid). Whilst such methods can isolate Ce at high purity, this requires the adoption of "slow" elution protocols and careful calibration of the procedure, as the REEs are eluted sequentially from the column. Ohno and Hirata (2013) applied such a chromatographic method prior to Ce stable isotope measurements and found that Ce yields from the resin needed to be >95% to avoid detectable fractionation effects, due to the preferential retention of isotopically light Ce on the stationary phase. Given these complications, such chromatographic procedures are not deemed to be well suited for routine application in isotopic tracing studies, as such work will typically involve the processing of 50 to more than 100 samples.

Alternative methods for the isolation of Ce make use of the observation that aqueous Ce^{3+} can be oxidized to Ce^{4+}, whilst the other REEs remain in the trivalent state. The stark differences in chemical properties between Ce^{4+} and the trivalent REEs can then be exploited for the isolation of Ce. This has been achieved using HDEHP, which will complex and etxract Ce^{4+} even from strongly acidic media but the trivalent REEs. Rehkämper et al. (1996) and Tazoe et al. (2007) applied this principle for the separation of Ce by liquid-liquid extraction and using extraction chromatography, respectively. In the current study, we have developed a new procedure for Ce separation, which is adapted from the above methods and summarized in Table 2.4.

The performance of the new Ce separation protocol (Table 2.4) was tested by application to three different natural materials – soil, clam and earthworm samples. Following chemical separation, the Ce fractions featured purities, as characterized by Nd/Ce, Pr/Ce and La/Ce ratios which were similar to or only marginally higher (in the case of the

earthworm samples) than those determined for commercially available pure Ce samples (Table 2.7). This demonstrates that the new method produces Ce of sufficient purity to enable precise and accurate Ce isotope measurements. Furthermore, ten individual aliquots of our in house Ce standard solution, which defines $\delta^{142}Ce = 0$, were processed through the separation procedure. Following column chemistry, the recovery of Ce was found to vary between 43% and 93%, with a mean of 71% (Table 2.8, Figure 2.5). This result is in accord with the Ce recovery from the spiked and non-spiked natural samples, which varied between 20 and 91% (Table 2.3). The reason for the variability observed in these recoveries is not clear, however the recovery of Ce from the samples was typically less than the aliquots of the Alfa Aesar Ce, this may be due to the presence of the other matrix elements. The isotope composition of the purified Ce was found to display small but resolvable variations, with $\delta^{142}Ce$ data of -0.06‰ to 0.38‰. The results show a dominance of positive $\delta^{142}Ce$ values as demonstrated by a mean +0.15 ± 0.32 (2sd; Table 2.8).

Table 2.8 Recovery and $\delta^{142}Ce$ values determined for Ce (from Alfa Aesar standard solution with $\delta^{142}Ce = 0$) processed through the column chemistry.

Aliquot	Yield (%)	$\delta^{142}Ce$ ± 2sd (‰)
1	61	0.38 ± 0.07
2	74	0.34 ± 0.06
3	43	0.29 ± 0.03
4	86	0.31 ± 0.05
5	93	0.07 ± 0.08
6	79	0.21 ± 0.06
7	58	0.00 ± 0.12
8	58	-0.02 ± 0.09
9	89	-0.02 ± 0.09
10	66	-0.06 ± 0.06
Mean	71	0.15
2sd	32	0.35

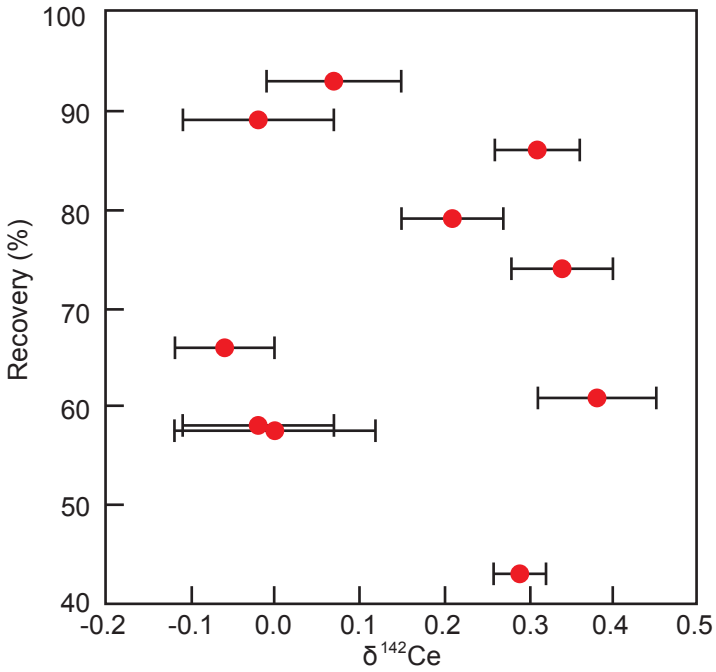


Figure 2.5 The recovery of the Alfa Aesaer Ce standard solutions after being processed through the separations procedure Vs the measured $\delta^{142}Ce$ values

The observed variable Ce yields and small but significant variations in $\delta^{142}Ce$ stand in contrast to the observations of Tazoe et al. (2007). These authors reported Ce recoveries of >98% and no isotopic fractionation for a similar separation procedure, the origin of this discrepancy is unclear. Whilst our data show no correlation between $\delta^{142}Ce$ values and yield (Figure 2.5), the observations are most readily explained by incomplete Ce recovery from the LN resin that was used for the separation procedure. The loss of Ce is hereby most likely due to the incomplete reduction of Ce^{4+}, which is strongly retained on the resin, and/or to the precipitation of insoluble CeO_2 within the resin itself. This interpretation is supported by the observation that aliquots collected immediately prior to and after the Ce elution peak exhibited only very low Ce contents. In this context, the observed isotopic effects are most likely due to isotopic fractionation between Ce^{4+} retained on the resin and aqueous Ce^{3+}, which is readily eluted. This conclusion is in accord with the finding of Nakada et al. (2013), who found that reduced Ce^{3+} is preferentially enriched in the heavier Ce isotopes relative to Ce^{4+}, resulting in positive $\delta^{142}Ce$ values, as were observed here for the Ce standard solutions (Table 2.8, Figure 2.5).

2.3.2.3 Constraints on choice of spike isotope

Key considerations when selecting an enriched Ce isotope for the preparation of isotopically labeled CeO_2 NPs are the tracing sensitivity that is required for a particular application and the cost of the spike material. In general, the best sensitivities can be achieved by employing highly enriched spike materials for isotopes that feature low natural abundances (e.g., ^{136}Ce, ^{138}Ce; Table 2.1). In such instances, even very minor additions of the enriched material to the natural Ce present in a given reservoir will produce analytically resolvable changes in Ce isotope composition. However, such isotope spikes are typically particularly expensive (e.g., ^{136}Ce, ^{138}Ce; Table 2.1). Other important factors that will determine the detection sensitivity are the precision of the isotopic data collected, which is a function of the type of mass spectrometer and data acquisition procedure used, and the elemental concentration and sample size available for analysis.

A quantitative evaluation of the impact that these factors have on the tracing sensitivity for labeled CeO_2 NPs is presented in the following. The evaluation extends to the following Ce isotope ratios: $^{136}Ce/^{140}Ce$, $^{138}Ce/^{140}Ce$ and $^{142}Ce/^{140}Ce$ (Table 2.9, Figure 2.6). Results are not shown for other possible ratios, as these would only offer inferior tracing sensitivities because they require either avoidable measurements of small Ce ion beams (e.g., $^{140}Ce/^{136}Ce$ or $^{140}Ce/^{138}Ce$ compared to $^{142}Ce/^{140}Ce$) or analyses of unfavorable (very large or small) Ce isotope ratios (e.g., $^{136}Ce/^{140}Ce$ instead of $^{136}Ce/^{142}Ce$).

Three hypothetical, but illustrative end-member scenarios are employed in the evaluation. The use of ^{140}Ce and ^{142}Ce for labeling (with enrichments of 99.5% and 93%; Table 2.1) is considered in all three scenarios, whilst the application of enriched ^{136}Ce and ^{138}Ce (with purities of 30.6% and 41.6%; Table 2.1) is considered only for Case 1 (Table 2.9). All evaluations are based on the simple inference that the addition of isotopically distinct CeO_2 NMs to a natural background, can be resolved and quantified if they induce changes in the isotope composition that exceed the uncertainty of the measurement and/or any variability in the isotope composition of the background. This threshold is designated as the *detection sensitivity* in the following. Based on this, we determined for each case, the

proportional increase in the total Ce concentration that is associated with exceeding the detection sensitivity for a given isotope label.

Table 2.9 Summary of modeled data for the three hypothetical scenarios evaluating the detection sensitivities and quantification uncertainties for isotopically labeled CeO_2 NPs.

Diagnostic isotope ratio ***(Label)***	Analytical uncertainty (‰)	Minimum increase in total [Ce] from isotope label required for detection[a]		Uncertainty in quantification of label at:	
		(‰)	(μg kg^{-1})	10 x minimum concentration ± 2sd (μg kg^{-1})	100 x minimum concentration ± 2sd (μg kg^{-1})
Case 1 – High precision instrumentation & chemical separation					
^{136}***Ce***/^{142}Ce & ^{138}***Ce***/^{142}Ce	2.5	0.02	0.8	7.6 ± 0.8	76.2 ± 0.8
^{142}Ce/^{140}***Ce***	0.8	0.7	37	369 ± 38	3691 ± 44
^{142}***Ce***/^{140}Ce	0.8	0.1	5	48 ± 5	489 ± 6
Case 2 – High precision instrumentation, chemical separation & small sample size					
^{142}Ce/^{140}***Ce***	2.5	2.3	115	1154 ± 47	11543 ± 58
^{142}***Ce***/^{140}Ce	2.5	0.3	15	153 ± 63	1532 ± 77
Case 3 – Low precision instrumentation & no chemical separation					
^{142}Ce/^{140}***Ce***	20	19	940	9401 ± 56	94013 ± 154
^{142}***Ce***/^{140}Ce	20	2.4	124	1248 ± 7	12482 ± 19

[a] Assumes that the natural Ce background has a concentration of 50 mg kg^{-1}

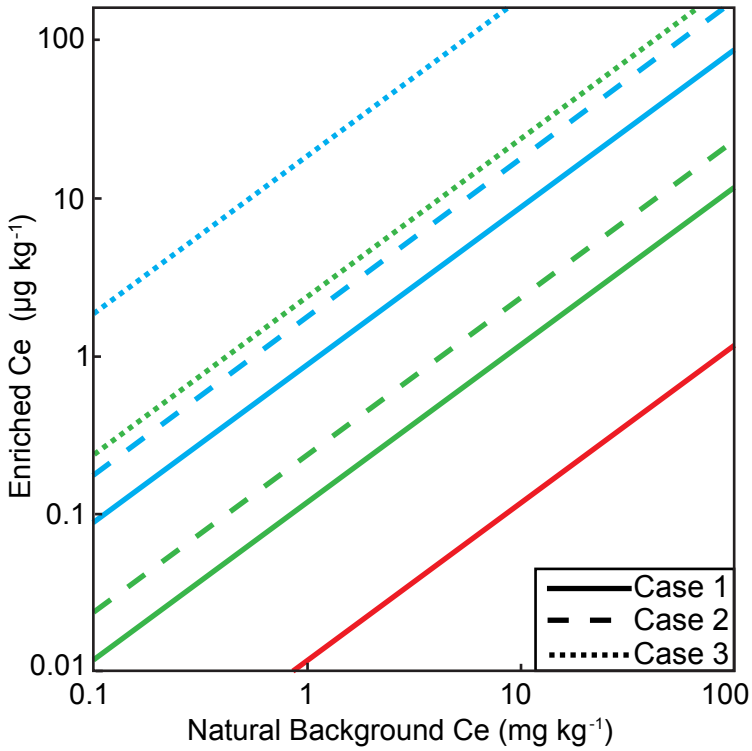


Figure 2.6 The detection sensitivities offered by the different enriched Ce isotope spikes under the three analytical scenarios presented in Case 1, 2 and 3. Where the red, green and blue lines denote the use of ^{136}Ce or ^{138}Ce, ^{142}Ce and ^{140}Ce enriched isotopes respectively.

Case 1 assumes that the methods described in this study are applied for the chemical separation and isotopic analysis of Ce and that sufficient Ce is available for optimal analysis by high precision MC-ICP-MS measurements. With these conditions, it was demonstrated that the $^{142}Ce/^{140}Ce$ isotope ratio can be determined with a precision of about ±0.5‰ or better. This takes into consideration the mass spectrometric uncertainties and possible Ce isotope fractionation during the column chemistry. In addition, an uncertainty of about ±0.3‰ is assumed to account for any potential isotopic variability of natural background Ce. Given these constraints, the addition of enriched $^{140}CeO_2$ or $^{142}CeO_2$ NPs to a sample can be detected if an isotopic effect of greater than 0.8‰ is created. This threshold corresponds to detection sensitivities of 0.7‰ and 0.1‰ when enriched ^{140}Ce and ^{142}Ce are applied as isotope label, respectively. This is equivalent to an increase in the Ce concentration of only 37 μg kg^{-1} and 5 μg kg^{-1}, respectively, from the addition of the isotopically labeled NPs, for a sample with a natural Ce background of 50 mg kg^{-1}, as would be appropriate for soils (Table 2.9, Figure 2.1 and 2.4).

A larger limiting uncertainty of 2.5‰ is assumed for Case 1, when enriched ^{136}Ce and ^{138}Ce are applied as tracer isotopes and the $^{136}Ce/^{142}Ce$ and $^{138}Ce/^{142}Ce$ ratios are measured for tracing. This accounts for the larger analytical uncertainties introduced by (i) measurements of isotopes with extremely low natural abundances, even if the sample size per analysis is increased to about 1 μg Ce; (ii) larger variability in the natural $^{136}Ce/^{142}Ce$ and $^{138}Ce/^{142}Ce$ ratios from isotopic fractionations generated during the column chemistry, due to the larger mass differences of the isotope ratios; and (iii) potential radiogenic variations in the $^{138}Ce/^{142}Ce$ ratio (Willbold, 2007, Tazoe et al., 2007). At these levels of uncertainty ^{136}Ce and ^{138}Ce enrichments offer detection sensitivities of 0.02‰ (Table 2.9, Figure 2.6). This corresponds to the addition of 0.8 μg kg^{-1} of ^{136}Ce or ^{138}Ce label to a natural background concentration of 50 mg kg^{-1} (Table 2.9, Figure 2.6).

The same analytical methods that are outlined for Case 1 are also assumed for Case 2. However, Case 2 specifically considers the larger uncertainties, which arise when only very small Ce quantities of about 1 ng are available for analysis. Based on this, it is

assumed that the Case 2 tracing sensitivities are limited by analytical uncertainties of about ±2.5‰ for the determination of $^{142}Ce/^{140}Ce$. In this scenario, detection sensitivities of 2.3‰ and 0.3‰ are achieved when ^{140}Ce or ^{142}Ce are used for labeling, respectively. Contribution of 115 µg kg^{-1} and 15 µg kg^{-1} from the enriched ^{140}Ce and ^{142}Ce isotope labels to a natural background with Ce at 50 mg kg^{-1} are, therefore, required to exceed the detection sensitivities (Table 2.9, Figure 2.6). The application of NPs labeled with ^{136}Ce or ^{138}Ce (coupled with analyses of $^{136}Ce/^{142}Ce$ and $^{138}Ce/^{142}Ce$ ratios) is not considered for Case 2. This is due to the low natural abundances of the tracer isotopes, which would render the isotopic analysis susceptible to inaccuracies, as very low signal intensities need to be monitored (Table 2.1).

In Case 3, it is assumed that the isotopic analyses are carried out using the less precise methods of quadrupole (Jarvis et al., 1992) or high resolution magnetic sector ICP-MS (Becker and Dietze, 1997), and without prior chemical separation of Ce. A number of published studies describe the acquisition of $^{140}Ce/^{142}Ce$ isotope data with such methods and report reproducibilities of about ±2% (2sd; (Jarvis et al., 1992, Li et al., 1999). This uncertainty will be the main factor that limits the tracing sensitivity of the method. Based on this threshold, detection sensitivities of 19‰ and 2.4‰ are achieved when enriched ^{140}Ce and ^{142}Ce are used as tracer isotopes. Therefore, for a typical natural soil with a Ce concentration of 50 mg kg^{-1}, the addition of 940 µg kg^{-1} and 124 µg kg^{-1} of the enriched ^{140}Ce and ^{142}Ce label would be required, to exceed the detection sensitivities (Table 2.9, Figure 2.6). The application of enriched ^{136}Ce and ^{138}Ce isotopes are not considered to be relevant for Case 3. This follows from the low natural abundances of these two isotopes (Table 2.1) and the spectral interferences that can be expected from the ubiquitous element Ba, which will render accurate and precise analyses of $^{136}Ce/^{142}Ce$ and $^{138}Ce/^{142}Ce$ ratios essentially unfeasible without chemical separation of Ce.

Overall, the best detection sensitivities are offered when enriched ^{136}Ce and ^{138}Ce are applied for labeling. These two isotopes have very low natural abundances and the enriched forms offer tracing sensitivities that exceed those that are provided by enriched

^{142}Ce and ^{140}Ce by one and two orders of magnitude, respectively (Table 2.1 and 2.9, Figure 2.6). Despite of this, their use for labeling is not likely to be practical for the majority of applications due to the very high cost of the material (Table 2.1) and the added drawback that analysis without chemical separation is not feasible. In comparison, the more abundant isotopes ^{140}Ce and ^{142}Ce provide much more cost effective options, with ^{142}Ce offering detection sensitivities an order of magnitude better compared to ^{140}Ce, but with a similar increase in cost (Table 2.1).

The summary of modeled data presented in Table 2.9 shows that the use of an enriched isotope with a low natural abundance and with more precise isotope ratio analysis the uncertainty in the quantification of the amount of label present is smaller. This is demonstrated with the two right hand columns of Table 2.9 where the uncertainty in the quantification of the isotope label is shown when 10x and 100x the minimum detection limit is added to a sample. In addition this demonstrates that with an increasing amount of label in a sample the uncertainty decreases.

The choice of which isotope label to use should be made on a case by case basis, taking into account the amount of enriched material and the detection sensitivity required, as well as the type of instrumentation that is available for the analyses. It is likely, however, that for most applications ^{140}Ce will be a very suitable choice, as it is inexpensive whilst still offering attractive tracing sensitivities, which by far surpass the performance of concentration measurements. Furthermore, application of a ^{140}Ce tracer is possible and advantageous with or without chemical separation of Ce and using a range of instrumentation.

3.2.4 Results for natural samples spiked with an enriched ^{140}Ce spike

The motivation for dosing natural samples with ^{140}Ce-E was to demonstrate that (i) the chemical separation and mass spectrometric methods described here are suitable for the tracing of a Ce isotope label and (ii) that the tracing sensitivities that were estimated in the previous chapter can indeed be achieved in an actual application.

The analyses of the non-spiked natural samples revealed slightly negative $\delta^{142}Ce$ values throughout, even though the samples were processed through the chromatographic separation procedure, which can potentially induce positive anomalies (Table 2.8). These results are not surprising, however, as a number of studies have found that biological processes tend to favor the incorporation of lighter isotopes (Beard et al., 1999, von Blanckenburg et al., 2009). These negative values are therefore most likely of biological origin and not a result of sample processing.

For the biological samples that received a high dose of ^{140}Ce-E, and where the total Ce concentrations were increased by 0.3 to 4.1%, the isotopic differences were readily resolvable, with $\delta^{142}Ce$ values of between -3.70‰ and -42.54‰ (Table 2.3). The measured and predicted values show very good agreement, with deviations of less than 0.19‰. This demonstrates excellent the accuracy of the methods, even though limited isotope fractionation may occur during the chemical separation of Ce.

The low dosed natural samples display increases in the total Ce concentration from the addition of ^{140}Ce-E, which are only marginally larger than the detection sensitivities (Table 2.3 and 2.9). Nonetheless, the measured $\delta^{142}Ce$ of the samples, of between -0.96‰ and -1.17‰, differed from the predicted values by less than 0.49‰ (Table 2.3). Notably, the measured $\delta^{142}Ce$ values are less negative than the predicted results, and this may reflect, at least in part, minor isotopic fractionation during the chromatography step.

In summary, these results demonstrate that the methods that were developed, here are well suited for employment in a stable isotope tracer study with isotopically labeled CeO_2 NPs. In particular, the chemical separation of Ce is straightforward enough to enable the high sample throughput required for environmental screening studies. Whilst limited isotope fraction can be expected during separation of Ce by column chromatography, this is not a major hindrance. In fact, our data demonstrate that the detection of ^{140}Ce-E is even possible in samples where the isotopic spike increases the natural Ce concentration by only about 0.1%. The methods presented here will thus clearly enable environmental tracer studies with CeO_2 NPs to be conducted at the PECs.

2.4 Conclusions

Our analyses have shown that commercially available CeO_2 NPs do not possess a distinct isotope signature and are therefore not suitable for the technique of stable isotope tracing. However, this approach may still be successfully applied if an enriched Ce isotope is used to produce isotopically labeled CeO_2 NPs. To synthesize such modified NPs, optimized preparation techniques are required, and these must be reliable, enable small-scale synthesis and offer high yields. Such considerations are essential when an expensive isotopically enriched pre-cursor material is used. Published synthesis methods for CeO_2 NPs are available (Goharshadi et al., 2011, Perez et al., 2008) but do not prioritize these qualities, which often go unreported in publications. Instead, published protocols typically focus on the size and shape of the NPs produced. However, synthesis methods that are optimized for the preparation of isotopically labeled NMs have already been published for ZnO, CuO and Ag NPs (Dybowska et al., 2011, Misra et al., 2012, Laycock et al., 2014), but are not yet available for CeO_2. The next step for advancing stable isotope tracing of CeO_2 NPs is, therefore, the development of a suitable synthesis protocol.

Despite the shortcomings of the Ce separation method regarding the recovery and isotope fractionation, the data and modeling presented in this work demonstrates that the sample preparation and mass spectrometric techniques that were developed during the course of this investigation are suitable for environmental screening studies, which require reliable methods and high sample throughput. In particular, the separation procedure is based on column chromatography and it applies only relatively simple and robust elution protocols, which do not require careful calibration. This means that high sample throughput can be achieved, because the straightforward methodology enables large sample numbers to be processed simultaneously. With use of a Ce double spike, which can correct for the fractionation effects that are imparted during laboratory processing, the procedure is also suitable for high precision measurements of Ce stable isotope compositions in natural samples. With further development the separation procedure may be improved to increase

the recovery and prevent isotopic fractionation by either adopting a sequential elution protocol or using an alternative to the LN resin.

The use of stable isotope labeling for CeO_2 NPs is expected to provide detection sensitivities of at least 19‰ and up to 0.02‰, depending on the isotope enrichment and analytical procedure used. In most cases, ^{140}Ce will be the most favorable isotope label as it is relatively inexpensive, whilst still offering detection sensitivities that more than sufficient to enable exposures to be performed at environmentally relevant levels. To confirm this prediction an experiment was carried out where small quantities of ^{140}Ce-E were added to natural samples, which were subsequently analyzed. These analyses confirmed that detection of ^{140}Ce-E is even possible in samples where the isotopic spike increases the natural Ce concentration by only about 0.1%.

2.5 Declaration

All the work presented in this chapter was conducted by Adam Laycock (AL) under the supervision of Mark Rehkämper (MR).

Chapter 3:

Synthesis and characterization of isotopically labeled silver nanoparticles for tracing studies

Abstract

Silver nanoparticles (AgNPs) more being used increasingly in industrial processes and consumer products, resulting in heightened emissions to the natural environment. To understand the behavior and environmental fate of AgNPs, it is paramount that they can be traced in complex natural samples from exposures at high sensitivity. The technique of stable isotope labeling is ideally suited for this purpose. To support such applications, a detailed evaluation of techniques for the preparation of stable isotope labeled AgNPs is presented, and demonstrates that isotopically modified particles are only distinguishable from particles with a natural isotope composition by their strong isotopic signature. Monodisperse suspensions of citrate-stabilized AgNPs with target sizes of 17, 20 and 30 nm were synthesized by reduction of silver nitrate solutions with sodium borohydride. The AgNP suspensions were produced using both natural Ag, which is comprised of the two stable isotopes ^{107}Ag (52%) and ^{109}Ag (48%), and Ag enriched to 99.2% in ^{107}Ag (^{107}Ag-E). Synthesis was reliably reproduced on three separate occasions in two laboratories. The AgNPs were characterized using dynamic light scattering (DLS) shortly after synthesis and after up to 12 months storage. Some of the batches were also characterized using transmission electron microscopy (TEM) and asymmetric flow field-flow fractionation (FlFFF). The particle size distributions showed good reproducibility between the laboratories and stability over the 12 months of storage. Importantly, the ^{107}Ag-E particles were indistinguishable in size and shape from particles with a natural isotope composition. The reliability, control on particle size, and high yield of about 80%, demonstrate that the synthesis technique is well suited for small-scale production of isotopically labeled AgNPs. Furthermore, isotope mass balance calculations show that the application of labeling enables tracing sensitivities for AgNPs that are at least 40 times, and possibly up to 4000 times, higher than those achievable with bulk Ag concentration measurements. This means that experiments with exposure concentrations at predicted environmental levels are possible, if the most precise isotopic measurement techniques are employed.

3.1 Introduction

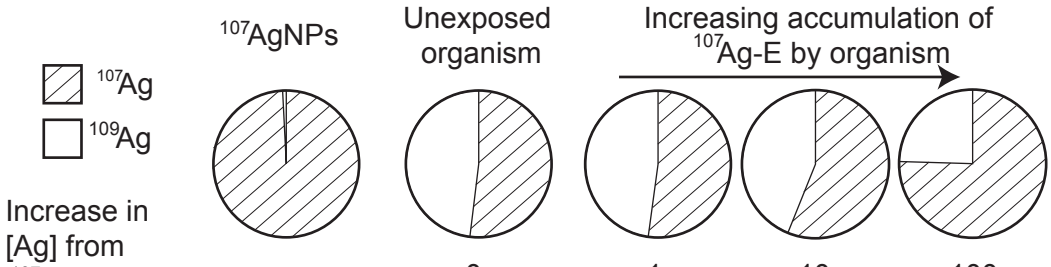
As a consequence of the ubiquitous use of Ag in the photographic and imaging industries, anthropogenic emissions of Ag and their environmental fate have been monitored for many decades (Purcell and Peters, 1998). Whilst the rise of digital photography has significantly reduced such emissions, new concerns have arisen as engineered Ag nanoparticles (AgNPs) are increasingly employed in a broad range of industrial processes and consumer products, which are subsequently emitted into the environment (Purcell and Peters, 1998, Wijnhoven et al., 2009). Whilst not comprehensive, there are currently 437 products (September 2014) listed on 'The Project for Emerging Nanotechnologies' consumer product inventory database (Woodrow Wilson Centre, 2014) that incorporate nano-silver, illustrating the diverse range of products in which this nanomaterial (NM) is used. A focus of current research and debate is whether there are (nano-) specific effects, which increase the bioavailability and toxicity of Ag when present in nanoparticulate form (Wijnhoven et al., 2009). This concern has prompted numerous studies to investigate the environmental transport, behavior, fate and ecotoxicology of engineered AgNPs.

Ideally, such studies are carried out in 'realistic' environmental conditions, whereby exposures employ NM concentrations that are similar to, or not far removed from, present or predicted values. Recently, Gottschalk et al. (2013) compiled and reviewed measured and modeled environmental concentrations of engineered NMs. Based on the reviewed data, predicted environmental levels of engineered nano-Ag are in the range of 0.1 to 100 ng L^{-1} for surface waters, 0.001 to 0.1 µg L^{-1} for effluents of waste water treatment plants, 0.001 to 1 mg kg^{-1} for biosolids, 1 to 10 µg kg^{-1} for sediments, and 0.1 to 1000 µg kg^{-1} for soils. Significantly, these levels are less than or roughly similar to, the natural Ag background concentrations of these materials. Eisler (1996) provided a summary of typical natural Ag concentrations in non-biological materials of 300 to 5000 ng L^{-1} for surface waters, 0.05 to 45 µg L^{-1} for effluents of waste water treatment plants, 225 to 960 mg kg^{-1} for sewage sludge, 1500 to 3500 µg kg^{-1} for sediments, and about 100 µg kg^{-1} for soils.

Studies that interrogate the environmental fate of AgNPs typically employ concentration measurements by ICP-MS to quantify the presence of Ag (from NPs) in exposure systems. Such analyses are straightforward but require that exposures employ AgNP concentrations that exceed 'realistic' environmental levels by several orders of magnitude. This requirement stems from (i) the comparatively high natural Ag background (see above), and (ii) the condition that unequivocal tracing of AgNPs relies on the detection of anomalies in Ag concentration that clearly exceed these background levels. For example, Shoults-Wilson et al. (2011) used AgNP concentrations of 10 to 1000 mg kg^{-1} in soil exposures of the earthworm *Eisenia fetida*, whilst Zhao and Wang (2011) applied AgNPs at 20 to 500 µg L^{-1} in a waterborne exposure of *Daphnia magna*. It is conceivable that ecotoxicity studies carried out at such high (and unrealistic) AgNP concentrations, may induce and thus identify distinct patterns of particle behavior and biological interactions that are only relevant for the high particle concentrations employed. The challenge is, therefore, to investigate whether the same effects are also observed at low but environmentally relevant NP levels.

To circumvent the limited sensitivity of concentration tracing, alternative methods for tracing NMs have been explored, particularly fluorescent coatings (Maretti et al., 2009, Xia et al., 2008) and radiolabelling (Chrastina and Schnitzer, 2010, Coutris et al., 2012, Zuykov et al., 2011), but both techniques have associated drawbacks. The application of fluorescent coatings can affect the surface chemistry of the materials and influence their behavior, such as changes to and suppression of dissolution (Lewinski et al., 2008). The coatings may furthermore dissociate from the NPs (Tenuta et al., 2011) and free ions from NP dissolution cannot be traced with this method. Radiolabelled NMs are produced by activation in a nuclear reactor (Gibson et al., 2011, Oughton et al., 2008) and the technique is therefore hindered, as specialist equipment, dedicated laboratories and licenses are required for the handling of radioactive materials. A further disadvantage is the often short half-lives of the radiolabels.

An attractive alternative method of labeling, which does not suffer from the above drawbacks, involves the application of enriched stable isotopes. The basic approach of stable isotope labeling relies on the detection of changes in a diagnostic isotope ratio, which are produced in an experimental system by the introduction of a 'contaminant' that is prepared from a highly enriched single isotope of the target element. In the case of Ag, the natural form of the element consists of nearly equal amounts of the isotopes ^{107}Ag and ^{109}Ag but highly enriched (to >99%) ^{107}Ag (^{107}Ag-E) can be purchased from a number of sources. The introduction of essentially pure ^{107}Ag into an exposure will not only increase the total Ag concentration of the system but also change the ^{107}Ag/^{109}Ag isotope ratio, such that this exceeds the natural value of ~1. The magnitude of the isotopic perturbation hereby depends on the relative contributions of ^{107}Ag-E to natural Ag (Figure 3.1). As (i) natural variations in isotope compositions are typically small for most elements and (ii) isotope ratios can be measured much more precisely than absolute concentrations, the use of enriched stable isotopes provides an extremely selective and sensitive means of elemental tracing, even in the presence of high natural background levels (Khan et al., 2013, Larner et al., 2012). Consequently, the stable isotope approach has been used successfully for several decades in the fields of medical, life and environmental sciences, when highly sensitive and precise tracing methods were required (Matwiyoff and Ott, 1973, Sridar et al., 2013).



Increase in [Ag] from ^{107}AgNPs (%)	-	0	1	10	100
^{107}Ag (%)	99.20	51.84	52.31	56.14	75.52
^{109}Ag (%)	0.80	48.16	47.69	43.86	24.48
^{107}Ag /^{109}Ag	124.0000	1.0764	1.0968	1.2802	3.0849

Figure 3.1 Demonstrates how the contribution from isotopically ^{107}Ag-E to a natural Ag background will result in a deviation in the ^{107}Ag/^{109}Ag that can be directly related to the degree of accumulation.

More recently, it has been shown that stable isotope tracing can also be applied to NMs, with pioneering studies of ZnO and CuO NPs (Misra et al., 2012, Khan et al., 2013, Larner et al., 2012, Croteau et al., 2011, Gulson et al., 2010). A unique requirement of such investigations is that the labeled NPs must be specifically prepared, from a single, highly enriched stable isotope form of the element. Particular advantages of this approach are (i) high versatility, as it can, in principle, be applied to any NP with a multi-isotopic element as main constituent; (ii) the label cannot be lost by dissociation or degradation; and (iii) the unique isotopic signature of the element remains traceable even if the speciation of the original material changes, for example by dissolution. The methodology, however, also requires that a suitable protocol for the preparation of labeled NPs is available. Whilst recipes for the synthesis of various NMs with defined sizes and properties are abundant in the literature, most of these methods are either unsuitable for the synthesis of stable isotope labeled NPs or they provide insufficient documentation for this purpose. This conclusion follows from the relatively high price of commercially available enriched stable isotopes, which typically cost about $2 to $20 per mg of metal or metal oxide. Given this non-negligible cost, methods for the preparation of isotopically labeled NMs must be optimized with a focus on small-scale synthesis, reliability and high yields. These factors, however, are generally not considered in conventional synthesis protocols, where particle size and shape are typically of higher priority.

In this study existing protocols have been examined to develop techniques for the optimized preparation of isotopically labeled AgNPs with distinct sizes. Rigorous evaluations demonstrate that the methods are suitable for routine and reliable small-scale synthesis of stable isotope labeled AgNPs at yields of ~80%. The characterization of both labeled AgNPs and control samples produced from natural Ag furthermore establishes that the labeling process does not generate distinct or unusual physico-chemical particle properties. This is essential in order to demonstrate that isotopically modified AgNPs are equivalent to AgNPs with a natural isotope composition and to validate the findings of any studies carried out using isotopically modified AgNPs, such as the recent investigation of Gigault and Hackley

(2013). These workers used asymmetric-flow field flow fractionation system coupled with on-line ICP-MS detection to show how a stable isotope label may be used to confirm the presence of Ag from an isotopically enriched source within a natural sample. While this technique offers rapid and definitive results it does not allow accurate quantification of the enriched material in a sample. This work assesses the utility of the isotope tracing approach beyond the level of simply detecting the isotope label in a sample. To this end, the results of simple model calculations are presented, which reveal the lowest levels at which isotopically labeled AgNPs can be detected and accurately quantified in relevant natural samples by stable isotope tracing, when different common mass spectrometric methods are employed for analysis.

3.2 Experimental

The AgNPs were synthesized by appropriately modified standard reduction methods (Cumberland and Lead, 2009, Römer et al., 2011). In particular, batches of particles with 3 target sizes were produced from both natural Ag and ^{107}Ag-E. Two operators carried out the AgNP synthesis on three occasions in two laboratories and the reproducibility of the methods was assessed by comprehensive characterization of the NP batches produced.

3.2.1 Choice of isotope label

When selecting an enriched stable isotope for labeling there are several key considerations, including degree of isotopic enrichment, cost of the material and the diagnostic isotope ratio that will be monitored for the purpose of tracing. A detailed discussion of these factors is provided by Larner and Rehkämper (2012). Silver has two naturally occurring stable isotopes, ^{107}Ag and ^{109}Ag, that have near equal natural abundances of 51.8% and 48.2%, respectively, and both are available at an enrichment of about 99% (Isoflex U.S.A., February 2012). As both isotopes are equally suitable for tracing, ^{107}Ag was chosen here for labeling because it was marginally cheaper than ^{109}Ag (Isoflex U.S.A., February 2012).

3.2.2 Chemicals and reagents

Powdered Ag metal enriched to 99.2% in ^{107}Ag (Isoflex U.S.A.) was converted to $^{107}AgNO_3$ by dissolution in 15.4 M HNO_3 and subsequent evaporation to dryness. Natural $AgNO_3$ (>99% purity), trisodium citrate dihydrate (>99% purity) and sodium borohydride (99.99% trace metals basis) were purchased from Sigma-Aldrich. Water of >18.2 MΩ cm quality (Millipore, UK) and quartz-distilled mineral acids were used throughout. Dilute artificial seawater (dilute-ASW) with a salinity of about 16 ‰ was produced by dissolution of 32 g of Tropic Marine Salt in 2 L purified water and used as medium for a dialysis study to assess dissolution.

3.2.3 Synthesis

The synthesis protocols used here were adapted from the methods outlined by Römer et al. (2011). Three protocols, denoted AgNP1, AgNP2, and AgNP3 (Table 3.1), were applied to produce particles with target sizes of 30, 20 and 17 nm, both with ^{107}Ag-E (denoted as 107-AgNP1, 107-AgNP2 and 107-AgNP3, respectively) and natural Ag (denoted as Nat-AgNP1, Nat-AgNP2 and Nat-AgNP3). The NP batches are further designated to indicate (i) the date of synthesis, either May or October 2012 (May12 or Oct12), and (ii) the laboratory in which synthesis was conducted, either at the Facility for Environmental Nanoscience Analysis and Characterization (FENAC) at the University of Birmingham or the MAGIC (Mass Spectrometry and Isotope Geochemistry at Imperial College) Laboratories at Imperial College London, (F and IC respectively). For example, the non-labeled AgNPs with a 20 nm target size prepared at FENAC in October 2012 are identified as Nat-AgNP2-Oct12-F (Table 3.1).

For synthesis, 100 mL aqueous solutions of 0.25 mM sodium citrate and 0.30 mM silver nitrate were cooled to 4°C, combined in a conical flask and vigorously stirred. To the AgNP1 and AgNP2 batches, 6 mL aqueous $NaBH_4$ was added at a concentration of 10 and 1 mM, respectively, whilst nothing was added to the AgNP3 batch at this stage. For all

Table 3.1 Summary of characterization data obtained for batches of ^{107}AgNPs and natural AgNPs prepared on three different occasions using the three synthesis protocols. Results are shown for both pristine particles and after up to 12 months of storage

	Freshly Prepared Particles									Particles after Storage		
		DLS		TEM		FIFFF					DLS	
Particle Batch[a]	Yield (%)	Diameter[b] (nm)	PDI[c]	Diameter[d] (nm)	CV[e]	d_n[f] (nm)	d_w[g] (nm)	PD[h]	FWHM[i] (nm)	Storage[j] (Months)	Diameter[d] (nm)	PDI[e]
AgNP1 protocol – target particle size 30 nm												
Nat-AgNP1-May12-F	91	41.6	0.25			36	49	1.3	24	12	41.5	0.25
107-AgNP1-May12-F	64	29.3	0.22			27	31	1.2	26	12	29.7	0.20
Nat-AgNP1-May12-IC	14	35.5	0.26							12	35.3	0.23
107-AgNP1-May12-IC		31.2	0.16									
Nat-AgNP1-Oct12-F	79	26.5	0.13	22.3 ± 6.7	0.30					6	26.8	0.11
107-AgNP1-Oct12-F	98	31.2	0.18	28.2 ± 8.3	0.29					6	33.7	0.22
AgNP2 protocol – target particle size 20 nm												
Nat-AgNP2-May12-F	87	20.7	0.33			18	21	1.2	18	12	19.7	0.25
107-AgNP2-May12-F	83	16.7	0.25			17	22	1.3	17	12	14.6	0.34
Nat-AgNP2-May12-IC	61	17.2	0.28							8	16.8	0.35
107-AgNP2-May12-IC	61	16.3	0.27							12	17.5	0.18
Nat-AgNP2-Oct12-F	63	22.6	0.15	19.5 ± 5.7	0.29					6	22.9	0.10
107-AgNP2-Oct12-F	78	23.9	0.20	20.1 ± 6.3	0.31					6	24.1	0.18
AgNP3 protocol – target particle size 17 nm												
Nat-AgNP3-May12-F		17.1	0.20			16	18	1.1	11			
107-AgNP3-May12-F		24.3	0.24									
Nat-AgNP3-May12-IC	77	18.2	0.23							12	16.8	0.31
107-AgNP3-May12-IC	31	20.6	0.29							12	24.1	0.21
Nat-AgNP3-Oct12-F	80	17.2	0.25	18.0 ± 5.2	0.29					6	32.5	0.52
107-AgNP3-Oct12-F	76	28.1	0.44	16.3 ± 4.8	0.29					6	26.1	0.39

TEM - Transmission Electron Microscopy, CV – Coefficient of Variance, DLS - Dynamic light scattering, FIFFF – Asymmetric Flow Field Flow Fractionation, [a] Each particle batch was designated depending on (i) whether the batch was labeled or non-labeled (107-AgNP or Nat-AgNP), (ii) which synthesis protocol was used for the production (1, 2 or 3; see Table 3.2), (iii) whether the particles were made in May or October 2012 (May12 or Oct12) and (iv) the laboratory in which the synthesis was carried out, either at FENAC, University of Birmingham (F) or the MAGIC Laboratory, Imperial College London (IC). [b] The hydrodynamic diameter was calculated as the average of individual DLS measurements. [c] Polydispersity index.[d] The average TEM diameter ± 1sd is calculated from analyses of 234 -337 individual particles. [e] CV = Standard deviation/TEM diameter. [f] The number average hydrodynamic diameter. [g] The weighted average hydrodynamic diameter. [h] Polydispersity (d_n/d_f). [i] Full width at half maximum. [j] Particle storage was in the dark at 4°C.

protocols, the mixtures were then boiled for 90 minutes, after which the AgNP1 and AgNP2 mixtures were removed from the heat. For the AgNP3 batches, 6 mL of 10 mM aqueous $NaBH_4$ solution were added to the mixture after 90 minutes of boiling, followed by boiling for a further 10 minutes. All solutions were thereafter allowed to cool overnight in the dark at room temperature. A summary of the synthesis protocols is given in Table 3.2.

Table 3.2 Summary of AgNP synthesis protocols

Step	Synthesis protocol		
	AgNP1	AgNP2	AgNP3
Mix Na-citrate[1] & Ag-nitrate[2] solutions then stir for	10 min	10 min	10 min
Add 6 mL $NaBH_4$[3] solution	10 mM	1 mM	-
Boil mixture	90 min	90 min	90 min
Add 6 mL $NaBH_4$[3] solution	-	-	10 mM
Continue to boil	-	-	10 min
Allow to cool in the dark	RT[4]	RT[4]	RT[4]

[1] 100 mL of 0.30 mM Na-citrate solution in >18.2 MΩ cm water. [2] 100mL of 0.25 mM Ag-nitrate solution in >18.2 MΩ cm water. [3] Aliquot, with appropriate dilution, of 100mL of 10mM $NaBH_4$ stock solution in >18.2 MΩ cm water. [4] RT = Room temperature.

The particle suspensions were filtered through 0.1 μm pore-size cellulose acetate filters to remove any larger (non-nano) particulates. Non-reacted reagents were thereafter removed by either diafiltration or dialysis. In the diafiltration method, the volume of the suspensions was reduced to ~20 mL without drying, by forcing through a 1 kDa (~1 nm) molecular weight cut-off (MWCO) regenerated cellulose ultrafiltration membrane (Amicon, Millipore) using a nitrogen gas pressurized and stirred filtration cell. The suspension volume was then re-adjusted back to ~200 mL using 0.15 mM sodium citrate solution and this process was repeated three times. For the dialysis method, the suspensions were transferred to 1 kDa MWCO dialysis bags (Spectra/Por) followed by dialysis against 5 L of 0.15 mM sodium citrate solution for 72 hours. The AgNP suspensions in aqueous Na-citrate from all protocols and filtration methods were thereafter stored in the dark at 4°C.

3.2.4 *Characterization of particles*

3.2.4.1 Dynamic light scattering (DLS)

The hydrodynamic diameter (average size) and polydispersity index (PDI) of the AgNPs were determined at 25°C using a Zetasizer Nano ZS ZEN3600 (Malvern Instruments Ltd. Malvern, UK) operating with a He-Ne laser at a wavelength of 633 nm and measuring back-scattered light at 173° relative to the incident beam. Each sample was analyzed at least 5 consecutive times within 24 hours of filtering. Some samples were analyzed after up to 12 months storage to give an indication of particle stability.

3.2.4.2 Transmission electron microscopy (TEM)

For TEM analyses, the AgNPs from 10 mL of the stock suspensions were deposited onto 300 mesh Formvar/carbon coated Cu-grids by ultracentrifugation (Beckman L-75) at 30,000 rpm for 60 minutes. Grids were then rinsed by immersing in 18 MΩ water for a few seconds and dried overnight. The TEM micrographs were obtained from 3 to 5 different areas on each grid, at a magnification of 30,000x, 100,000x and 300,000x. The diameters of at least 200 particles in each sample were then determined on the micrographs with 300,000x magnification using the computer software Digital Micrograph (Gatan Inc.).

3.2.4.3 Asymmetric flow field-flow fractionation (FlFFF)

The hydrodynamic diameter distributions of selected AgNP batches (Table 3.1), were determined within one week of preparation by FlFFF, using an AF2000 instrument (Postnova Analytics) following the method of Römer et al. (2011) and Baalousha and Lead (2012). The FlFFF channel featured a 1 kDa regenerated cellulose ultrafiltration membrane (Postnova Analytics) with a 0.01 M $NaNO_3$ carrier solution. The AgNPs were fractionated with cross-flow and detector flow both set to 1 mL min^{-1}, and their elution from the FlFFF channel was monitored by UV-absorbance measurements at 254 nm (Postnova Analytics). The FlFFF channel thickness was calibrated by analyzing polystyrene latex standards with known diffusion coefficients under the same flow conditions as the AgNPs, and the diffusion

coefficient distributions of the AgNPs were thereafter calculated using FIFFF theory (Litzen, 1993). The hydrodynamic diameter distributions were calculated from diffusion coefficients with the Stokes-Einstein equation.

3.2.4.4 Yield determination

To assess synthesis yields, 10 µl aliquots of 24 particle suspensions were dissolved in concentrated HNO_3 and refluxed on a hotplate at 80°C for 48 hours to ensure complete dissolution. The resulting solutions were evaporated to dryness and re-dissolved in 0.1 M HNO_3. Aliquots of these stock solutions were then used to prepared more dilute 0.1 M HNO_3 'measuring' solutions that featured Ag concentrations of about 20 ng mL^{-1} and that were doped with Pd as an internal standard, also at 20 ng mL^{-1}. The technique of internal standardization, as opposed to an isotope dilution protocol, was applied for quantification because the former produces sufficiently accurate and precise data (about ± 1 to 2%) and its application is very straightforward for analyses of both labeled and unlabeled materials.

For quantification, the samples were analyzed relative to a standard solution with Ag and Pd abundances of 20 ng mL^{-1} in the same acid matrix, using a Nu Plasma multiple collector ICP-MS (MC-ICP-MS) instrument at the Imperial College MAGIC Laboratories. In these analyses the total Ag (^{107}Ag + ^{109}Ag) signal intensities obtained for samples were compared to the standard solution and ^{105}Pd was monitored to correct for any drifts in instrumental sensitivity. The measurements provided the total Ag concentrations of the solutions and the yields of the synthesis methods were then calculated based on (i) the dilutions factors used for the preparation of the measuring solutions and (ii) the total mass of Ag used for particle preparation.

3.2.4.5 Dissolution behavior

The dissolution of the AgNPs was assessed by equilibrium dialysis. To this end, a PE container was filled with 500 mL of a suspension of 107-AgNP2-Oct-F in dilute-ASW, at a concentration of 0.9 mg L^{-1} Ag and 3.9 mg L^{-1} sodium citrate. Dilute-ASW was chosen as

used for the dissolution experiments as it is a common media used in aquatic exposure studies. Two dialysis bags (1kDa MWCO) were filled with 25 mL of dilute-ASW and immersed in the container. The container was thereafter kept in the dark to avoid Ag photodecomposition and stirred continuously. Sample aliquots of 0.5 mL were taken from both the inside and outside of the dialysis bags on 14 occasions over a period of 27 days. A control experiment to assess how dissolved Ag behaves during dialysis was carried out under the same conditions with 1 mg L^{-1} Ag from an aqueous solution of $AgNO_3$. The background Ag concentrations for both experiments were assessed from representative samples of dilute-ASW. Following completion of the experiments, the Ag concentrations of sample aliquots were determined at FENAC by graphite furnace atomic absorption spectrometry (GFAAS, Perkin Elmer AAS600).

3.3 Results and discussion

All information gathered from the characterization of the 18 batches of AgNPs that were prepared during the study is summarized in Table 3.1 and discussed in the following.

3.3.1 Size characterization of particles

3.3.1.1 DLS analyses

The average hydrodynamic diameter measured by DLS on the freshly made particles deviates by less than ± 20% from the target size, with the exception of three batches (Nat-AgNP1-May12-F, 107-AgNP3-May12-F, and 107-AgNP3-Oct12-F), where the average diameter was 40 to 70% larger than the target size (Table 3.1).

In the following, we present and discuss the results of a statistical evaluation that interrogates whether isotopic labeling or other factors (e.g., date or laboratory of synthesis) had a significant impact on the size of the prepared AgNPs. In order to incorporate all particle suspensions in this evaluation, including batches with different target sizes, we adopted the following procedure:

(i) All particle suspensions were split into one of three groups depending on their target particle size (17, 20 and 30nm). For each individual batch, the proportional difference from the mean size (PDMS) of the group was calculated. This was achieved by finding the mean particle size (MS), as determined by DLS, for each group. The particle size determined for an individual suspension (SamS) was then subtracted from the mean value, to calculate the absolute difference between the individual and mean particle sizes. The proportional difference was then determined by dividing the absolute difference by the mean particle size (Equation 3.1, Table 3.1, Appendices).

$$PDMS = (MS - SamS) / MS \quad (3.1)$$

This normalization procedure was validated by t-tests that, where possible, were carried out using both measured absolute size data and the calculated relative size differences. Specifically, this was possible when the DLS sizes of Nat-AgNPs were compared with 107-AgNPs for each of the three target sizes (30 nm, 20 nm, 17 nm; Table 3.1) Notably, these three t-tests yielded exactly identical results when they were conducted with both the absolute and the normalized size data (appendices). This result validates the application of the normalized particles size data (obtained as detailed above) in further t-tests.

(ii) The PDMSs calculated for each individual particle suspension were pooled in different manners to produce populations that were evaluated using a Student's t-test. These tests evaluated whether there are significant and systematic differences in size that can be assigned to a specific factor (appendices).

Based on two-tailed t-tests for populations of unequal variance, there was no significant difference at the 95% confidence level ($p = 0.05$) when the PDMSs were grouped into the following populations; (i) Nat-AgNPs and labeled 107-AgNPs ($p = 0.57$), (ii) synthesis at the FENAC and Imperial College laboratories ($p = 0.18$), (iii) synthesis date (e.g., May12-F, May12-IC and Oct12-F; $p = 0.27$ to 0.73), (iv) NP preparation by operators AL and

BS (particle synthesis in May and October 2012 respectively; $p = 0.45$), and (v) freshly prepared and aged particles after 6-12 months storage ($p = 0.98$). These results were obtained with the omission of batches 107-AgNP1-May12-F and 107-AgNP3-Oct12-F, which have particularly anomalous sizes of 41.6 nm (target size 30 nm) and 28.1 nm (target size 17 nm), respectively. These unusually large deviations from the target size may reflect experimental problems during synthesis. However, very similar results are produced when these data are included in the above t-test evaluations. A detailed summary of the t-test data and calculated p-values is presented in the appendices.

Notably, the average particle diameters of the suspensions after storage deviated by less than 3.5 nm from the average diameters that were measured directly after preparation. The only exception is sample Nat-AgNP3-Oct-F, where the average diameter increased by about 90% (15.3 nm; Table 3.1). The PDIs determined by DLS were less than 0.45 for all AgNP suspensions and less than 0.3 for 16 of the 18 batches, indicating that the particle size distributions were fairly monodisperse (Table 3.1). A t-test demonstrated that there was no significant difference between the PDIs of (i) Nat-AgNPs and 107-AgNPs ($p = 0.59$) and (ii) pristine particles and particles after storage ($p = 0.65$) (appendices).

Whilst the t-tests discussed above indicate that there are no statistically significant differences in particles size and PDI that can be assigned to a single factor. The data of Table 3.1 nonetheless demonstrate small but resolvable differences in particle size for NP batches prepared with the same protocol. Given the results of the t-tests, these disparities most likely reflect ‘normal’ batch-to-batch variations that occur, if syntheses are carried out on different days, in different laboratories and by different operators. These results hence provide an indication of the particle size variability that can be expected if different scientists apply the protocols of Table 3.2 in their own laboratories. In contrast, Römer et al. (2011) previously demonstrated that, using similar protocols for the preparation of AgNPs, repeated synthesis by the same operator, in the same laboratory with the same equipment and reagents, can routinely provide particle batches with highly reproducible sizes. In summary, these results thus demonstrate that despite small batch-to-batch variations in particles size

that reflect slight differences in experimental conditions, the protocols summarized in Table 3.2 are suitable for the robust and reliable synthesis of AgNPs in different laboratories.

3.3.1.2 TEM analyses

The freshly prepared AgNP batches synthesized in October 2012 (Table 3.1) were imaged by TEM and evaluated by measuring the longest axis of discrete particles rather than their aggregates (Table 3.1, Figure 3.2). The TEM micrographs show that the particles were spherical in shape and had a consistent size distribution, with the standard deviation of all batches being 40 to 45% of the average particle diameter, equivalent to coefficients of variance (standard deviation/average diameter) of 0.29-0.31 (Baalousha and Lead, 2013) (Table 3.1). It is likely that the aggregation of particles seen in the micrographs occurred during drying of the samples on the TEM grids and is not due to the fusion of particles during synthesis. This conclusion is supported by the predominance of discrete particles in suspension, as indicated by the DLS results.

The average diameters determined from the TEM micrographs were typically 10 to 15% (about 3 - 4 nm) smaller than the average hydrodynamic diameters determined by DLS. This is a well-known phenomenon, which reflects that larger particles scatter proportionally more light, such that the average DLS particle diameters are biased towards larger values (Baalousha and Lead, 2012). The exceptions to this are samples Nat-AgNP3-Oct12-F and 107-AgNP3-Oct12-F. The Nat-AgNP3-Oct12-F particle batch shows an average TEM particle size that is very close to that determined by DLS, whereas there is a large discrepancy between the DLS (28.1 nm) and TEM (16.3 nm) size data for 107-AgNP3-Oct12-F. These observations are likely a consequence of the polydispersity of the respective samples. In particular, the particle size distribution histogram of Nat-AgNP3-Oct12-F shows a narrow size distribution (Figure 3.2), suggesting it is highly monodisperse and therefore the DLS analysis shows very little size bias. In contrast, 107-AgNP3-Oct12-F is the most polydisperse sample (PDI = 0.44), and this may reflect a small number of larger particles in the suspension that heavily bias the DLS measurement.

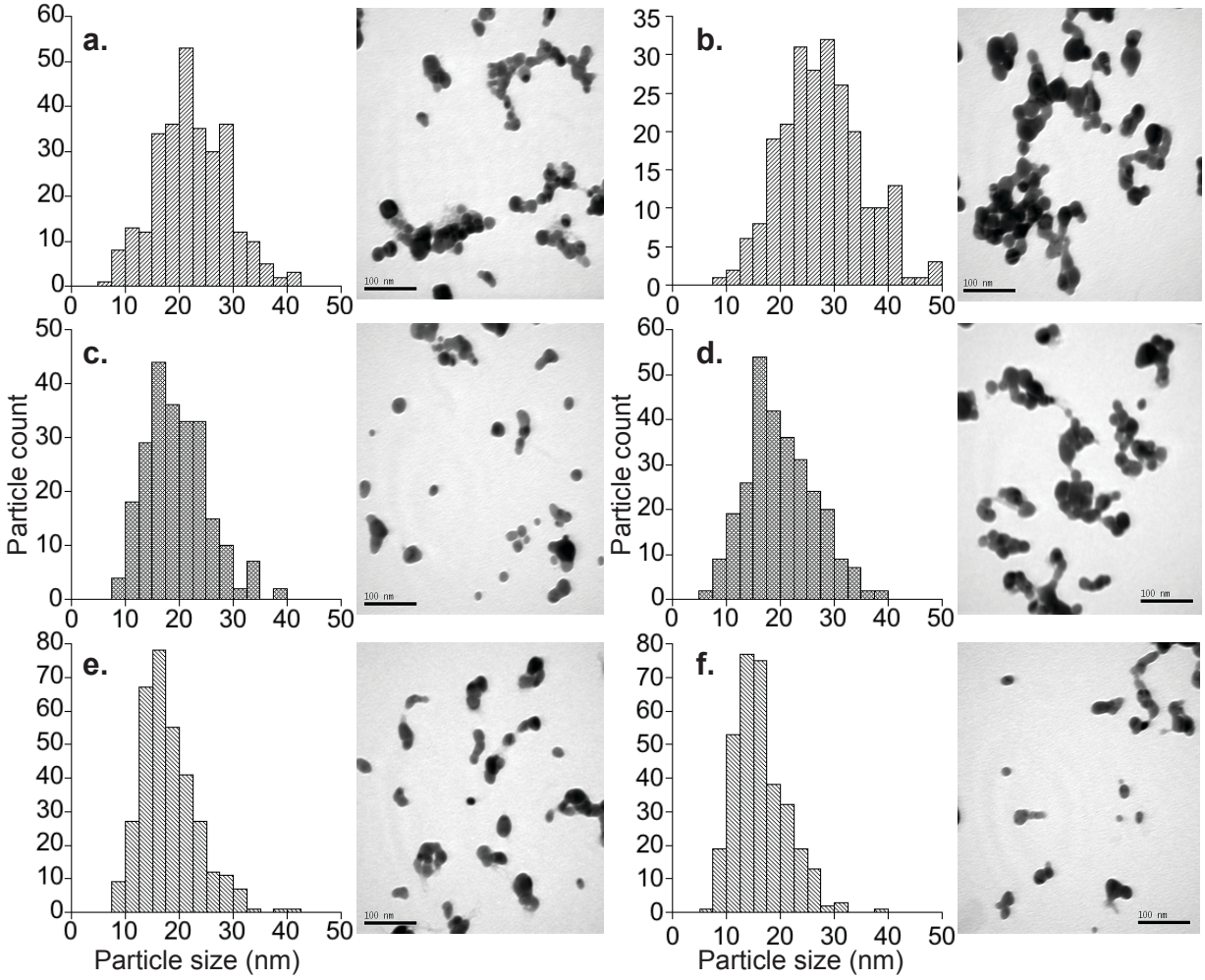


Figure 3.2 TEM images and measured particle size distributions for particles batches synthesized in October 2012. all images are at a magnification of 300 000x; scale bars are 0.1 µm. (a) Nat-AgNP1-Oct12-F average particle size = 22.3 ± 6.7 nm (1sd) n = 290; (b) 107-AgNP1-Oct12-F average particle size = 28.2 ± 8.3 nm (1sd) n = 236; (c) Nat-AgNP2-Oct12-F average particle size = 19.5 ± 5.7 nm (1sd) n = 234; (d) 107-AgNP2-Oct12-F average particle size = 20.1 ± 6.3 nm (1sd) n = 283; (e) Nat-AgNP3-Oct12-F average particle size = 18.0 ± 5.3 nm (1sd) n = 337; (f) 107-AgNP3-Oct12-F average particle size = 16.3 ± 4.8 nm (1sd) n = 333.

3.3.1.3 FIFFF analyses

The FIFFF analysis (Baalousha and Lead, 2007, Baalousha et al., 2008) of selected AgNP samples provided full width at half maximum (FWHM) data for particle batches Nat-AgNP1-May12-F (24 nm), 107-AgNP1-May12-F (26 nm), Nat-AgNP2-May12-F (18 nm), 107AgNP2-May12-F (17 nm) and Nat-AgNP3-May12-F (11nm) (Figure 3.3, Table 3.1). In addition, the FIFFF data were used to determine the number average hydrodynamic

diameters (d_n), mass average hydrodynamic diameters (d_w) and polydispersity (PD) using Equations 3.2, 3.3 and 3.4, respectively, with results given in Table 3.1.

$$d_n = \Sigma_i C_i X_i / \Sigma_i C_i \quad (3.2)$$

$$d_w = \Sigma_i C_i X_i^2 / \Sigma_i C_i X_i \quad (3.3)$$

$$PD = d_w / d_n \quad (3.4)$$

Here, C_i is the UV-absorbance signal at a given hydrodynamic diameter, X_i. The d_n values were typically slightly smaller (up to 13%) whilst d_w was slightly larger (up to 32%) compared to the particle size determined by DLS. The d_n values for 107-AgNP2-May12-F (17 nm) and Nat-AgNP2-May12-F (18 nm) was only slightly larger than for Nat-AgNP3-May12-F (16 nm). The two former samples also showed a higher PD value than Nat-AgNP3-May12-F, with size distributions tailing towards larger diameters (Figure 3.3). As a consequence, there is a slightly lager difference in d_w values between 107-AgNP2-May12-F (22 nm) and Nat-AgNP2-May12-F (21 nm) versus Nat-AgNP3-May12-F (18 nm).

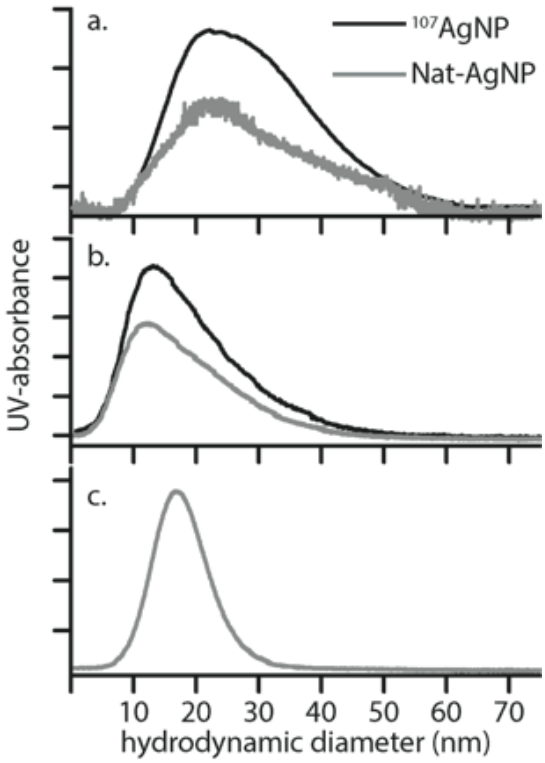


Figure 3.3 Hydrodynamic diameter distributions determined by FIFFF for selected AgNP batches. (a): 107-AgNP1-May12-F and Nat-AgNP1-May12-F, (b) 107-AgNP2-May12-F, Nat-AgNP2-May12-F and (c) Nat-AgNP3-May12-F.

3.3.2 Synthesis yields

Reliable small-scale synthesis techniques with high yields are required for the production of isotopically labeled NPs, due to the expense of using enriched stable isotopes (e.g., about $3.50 per mg for ^{107}Ag purchased from Isoflex USA in February 2012). The total Ag concentrations of 24 different particle suspensions, encompassing 16 batches of labeled ^{107}AgNPs and 8 batches of non-labeled AgNPs, were determined to assess the yield of the synthesis protocols (Table 3.1). Typically the yields were between 60% and 98%, with an average of 78% ± 23% (1sd). Considering that only small amounts of ^{107}Ag are required for a single synthesis (~2.7 mg) and due to the excellent yields achieved here, the preparation of ^{107}AgNPs is quite affordable, with a cost of approximately $4 to $5 per mg.

3.3.3 Dissolution behavior

The results of the dialysis experiments are shown in Figure 3.4. The particle stock suspension was added directly to the dilute-ASW without prior treatment or washing to remove excess sodium citrate. Although this effect was not investigated, the presence of sodium citrate at the expected concentration of ~4 mg L^{-1} is not anticipated to have a significant influence on the dissolution behavior. The Ag contents measured on the outside of the dialysis bags represent the total Ag concentration of the dilute-ASW, encompassing both particulate and dissolved forms of Ag. In contrast, the Ag measured inside the bags has crossed a 1kDa MWCO dialysis membrane and therefore reflects the dissolved component only. The experimental setup therefore ensures that identical Ag concentrations for the dialysis bags and the container are only achieved, when all Ag in the latter reservoir is in dissolved form.

The dialysis control experiment, where 1.00 mg L^{-1} of aqueous Ag was introduced into the containers, can be used to assess the behavior of dissolved Ag in the absence of AgNPs. At the beginning of the control experiment, the Ag concentrations inside the dialysis bags increased rapidly and reached the same level (of about 0.8-1.1 mg L^{-1}) as on the outside after 8 hours, demonstrating the time required for equilibrium to establish over the

dialysis membrane (Figure 3.4a). During the remaining 27 days of the experiment, the Ag concentrations inside and outside the dialysis bags were always essentially identical, and this shows that the setup functioned well to provide a reliable monitor of dissolved Ag contents on the outside of the dialysis bags. However, the Ag concentration outside the bags decreased during most of the experiment to a value of about 0.4 mg L^{-1} after 22 days. This indicates that dissolved Ag was lost, presumably as a result of adsorption onto the container walls and the dialysis membrane. The small final increase in dissolved Ag concentration that is seen at day 27, is likely due to desorption of the Ag from the surfaces of the container and dialysis bags

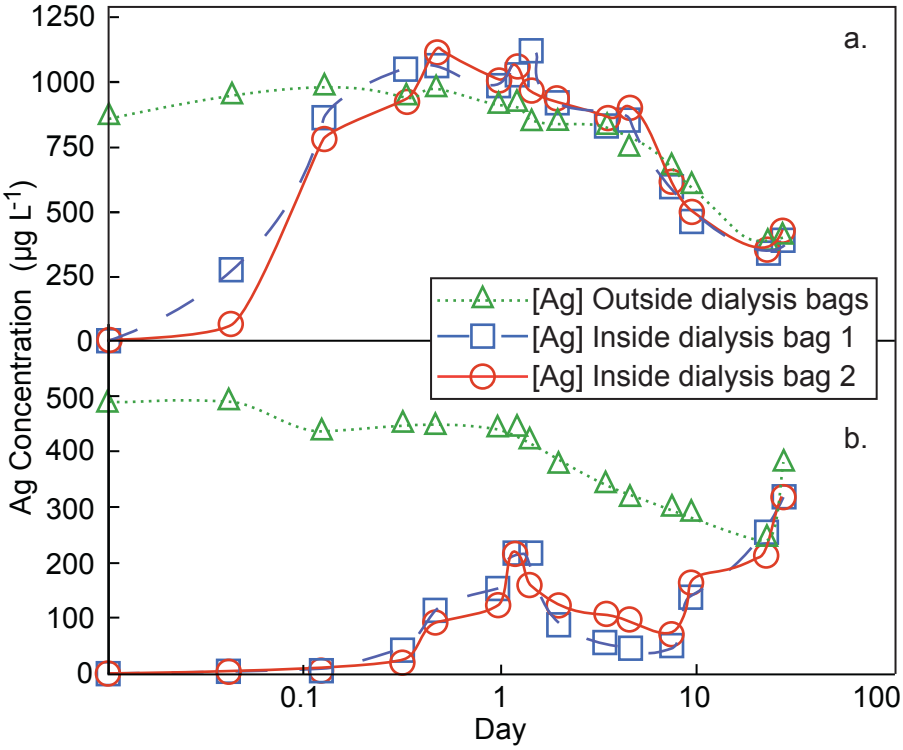


Figure 3.4 Results for AgNP dissolution behavior in dilute-ASW, assessed by dialysis. (a) Control experiment, whereby aqueous $AgNO_3$ solution is added to the dilute-ASW outside of the dialysis bags to a concentration of 1 mg L^{-1}. (b) Experiment where ^{107}AgNPs, from particle batch 107-AgNP2-Oct12-F, were added to the dilute-ASW outside of the dialysis bags to a concentration of 0.9 mg L^{-1}.

In the dialysis experiment of sample 107-AgNP2-Oct12-F, the Ag concentration outside the bags immediately after NP addition was 0.5 mg L^{-1}, a recovery of only 56% (Figure 3.4b). The container was furthermore black in color after the addition of the ^{107}AgNPs,

which indicates that AgNP adsorption to container surfaces was responsible for the loss of Ag. During the experiment, the Ag concentration outside of the bags generally decreased until day 22. For the same time period, the Ag contents inside both dialysis bags initially showed an increase over the first 28 hours, followed by a decrease until day 8, with increasing concentrations observed thereafter (Figure 3.4b). On day 22, the Ag concentrations outside and within both dialysis bags were identical and all three concentrations rose continuously during the final time period to day 27. This final increase in concentration is similar to that seen in the control experiment, which suggests that it is also most likely caused by desorption of Ag from surfaces that are in contact with the dilute-ASW.

Due to the adsorptive losses of both dissolved and nanoparticulate Ag during dialysis, it is difficult to quantify the dissolution behavior of the AgNPs. It may be assumed, however, that the dissolution of AgNPs will be similar, regardless of whether they are in suspension or adsorbed to container walls. With this assumption, this data can be applied to derive some general conclusions about the dissolution behavior of AgNPs. In particular, after an initial 8-hour equilibration time, the control experiment with dissolved Ag exhibited nearly identical Ag concentrations inside and outside of the dialysis bags (Figure 3.4a). During the same time period, the dialysis experiment with NP sample 107-AgNP2-Oct12-F showed low Ag concentrations inside the dialysis bags (0.02-0.04 mg L^{-1}), which correspond to only 2-5% of the ^{107}AgNP concentration that was initially added to the container (Figure 3.4b). These observations indicate that the ^{107}AgNP suspension in dilute-ASW produced only a very small fraction of dissolved Ag during the first few hours of the experiment. Over the following 27 days of the ^{107}AgNP dialysis experiment, the Ag concentrations inside the dialysis bags displayed an overall increase, demonstrating extensive ^{107}AgNP dissolution (Figure 3.4b). This conclusion is supported by the observation that very similar Ag concentrations were observed for the inside and outside of the dialysis bags on day 27, with a final Ag concentrations of 0.32 mg L^{-1} for both bags (Figure 3.4b). As some dissolved Ag was probably lost to adsorption onto the container walls, the value of 0.32 mg L^{-1} can be taken to represent a tentative minimum estimate for the solubility of the ^{107}AgNPs in dilute-ASW.

Given the adsorption problems encountered here with the dialysis technique, future AgNP dissolution studies should consider using alternative methods, such as ultrafiltration or single particle ICP-MS, to obtain improved constraints on the dissolution behavior of AgNPs.

3.3.4 Reproducibility and reliability of synthesis method

The three synthesis protocols produced fairly monodisperse AgNP suspensions throughout, but suspensions prepared with the same protocol display small but significant batch-to-batch variations in size, regardless of the isotopic composition of the AgNPs (Table 3.1). A detailed evaluation of the results (Table 3.1) demonstrates, however, that the protocols for particle target sizes of 30 nm (AgNP1), 20 nm (AgNP2) and 17 nm (AgNP3) still offer acceptable control on particle size. Protocol AgNP1 produced the largest particles (26.5 – 31.2 nm, average = 30.7 ± 2.9 nm; 1sd, n = 5), whilst the particles from protocols AgNP2 (16.3 – 23.9 nm, average = 19.6 nm ± 3.0 nm; 1sd, n = 6) and AgNP3 (17.1 – 24.3 nm, average = 19.5 ± 2.7 nm; 1sd, n = 5) were smaller but similar. These quoted averages were calculated from all DLS data obtained for freshly prepared particles (Table 3.1), excluding the two most obvious outliers (Nat-AgNP1-May12-F and 107-AgNP3-Oct12-F), but very similar results are obtained when the complete dataset is considered (appendices).

These findings demonstrate that the methods provide a robust means of obtaining small batches of isotopically labeled AgNPs with diameters that closely match desired target sizes. However, due to the observed batch-to-batch variations in size, particle characterization will need to be carried out for applications, which require that particles diameters are known to a high degree of accuracy. Although only three synthesis protocols were utilized here, it is likely that the experimental conditions can be adjusted to target larger and smaller particle sizes. For example, slightly modified versions of the synthesis methods applied here were used in previous studies to produce AgNPs with diameters as small as 11.5 nm (Tejamaya et al., 2012) and 7.2 nm (Römer et al., 2011) when measured by TEM.

3.3.5 Stability of particles

The particle suspensions in aqueous Na-citrate solutions were stored in the dark at 4°C to help prevent ageing. To assess the stability of the particle suspensions under these conditions, a selection of particle batches were characterized by DLS periodically during 12 months of storage (Table 3.1). Batch Nat-AgNP3-Oct12-F showed the most significant signs of ageing, as after 6 months storage the average particle size and PDI increased from 17.2 to 32.5 nm and 0.25 to 0.52, respectively. Whilst this is the type of change that would be expected as a result of particle aggregation, it was shown by Römer et al. (2011) that small citrate-capped Ag NPs generally have a greater stability and exhibit less agglomeration than larger particles. This indicates that the aggregation determined for sample Nat-AgNP3-Oct12-F may be an atypical result. All other particle batches exhibited no significant signs of ageing with all samples less than a 15% change in the average DLS particle size (Table 3.1). In addition, the PDI data also display only minor changes, indicating that the particle suspensions remained fairly monodisperse. The size and PDI results, furthermore, reveal no difference in aging behavior between natural and isotopically labeled AgNPs (Table 3.1). Any changes that might occur to the stock suspensions, such as agglomeration, may influence the particle behavior, but would have no effect on the isotope label or tracing capabilities.

3.3.6 Isotope label and detection capabilities

The motivation for synthesizing AgNPs from ^{107}Ag-E is to produce a material with a distinct non-natural isotope signature, which can be used in experiments and exposures, so that changes induced in the ^{107}Ag/^{109}Ag isotope ratio of relevant samples (e.g. biological materials, soil or water) can be used to trace and quantify the presence of the labeled material (Croteau et al., 2011, Gulson et al., 2010, Khan et al., 2013, Larner et al., 2012, Larner and Rehkämper, 2012) (Figure 3.1). The contribution of ^{107}Ag-E to a sample is only detectable when the deviation induced in the ^{107}Ag/^{109}Ag ratio of the sample clearly exceeds

(i) the precision of the isotopic measurement or (ii) any natural variations in the isotope composition of Ag. These factors are discussed below.

Isotopic analyses of Ag are generally carried out using ICP-MS instrumentation, as measurements by thermal ionization mass spectrometry (TIMS) are significantly more cumbersome (Chen and Wasserburg, 1990). Using standard quadrupole ICP-MS (Q-ICP-MS) instruments, $^{107}Ag/^{109}Ag$ ratios can typically be measured with a precision of about 1 to 5% (2sd). Improved data with a precision of ±0.2 to 1% (2sd) can be obtained with Q-ICP-MS at optimal analytical conditions (including separation of Ag from matrix elements) or by the application of single collector sector field ICP-MS (SF-ICP-MS) (Heumann et al., 1998). Even more precise isotopic measurements are possible by multiple collector ICP-MS (MC-ICP-MS), which can achieve uncertainties of better than ±0.02% (2sd) for $^{107}Ag/^{109}Ag$ on purified solutions of Ag (Schönbächler et al., 2007, Woodland et al., 2005).

Studies to investigate natural stable isotope fractionation of Ag are extremely limited in number and scope, with a primary focus on Ag ores (which are straightforward to analyze) and a few igneous rocks (Chugaev and Chernyshev, 2012, Hauri et al., 2000, Woodland et al., 2002). Data are also available from an archeological study on the provenance of coins (Desaulty et al., 2011) and an investigation into natural isotope fractionation based on a limited number of environmental samples (Luo et al., 2010). These analyses revealed only minor differences of about ±0.05% in the $^{107}Ag/^{109}Ag$ ratios of the samples, relative to the NIST SRM 978a Ag isotope standard. Such small variations are only resolvable using MC-ICP-MS and hence have no impact on the sensitivity that can be achieved for the detection of isotopically labeled AgNPs by Q-ICP-MS and SF-ICP-MS. Given the published results, it is furthermore unlikely that samples, such as soils or sediments, from a single location will exhibit geological Ag isotope fractionations that exceed ±0.02% and hence impact the AgNP detection sensitivity of MC-ICP-MS. However, there are currently no studies that investigate whether changes in Ag isotope composition are generated by biological uptake and processing of this element. Based on data acquired for other elements, such Zn (Arnold et al., 2010) and Cd (Ripperger et al., 2007), it is conceivable that biotic reactions may induce

Ag isotope effects in the range of 0.02% to 0.05% and such fractionations may be preserved in biological tissue and fluids, water samples or soils and sediments. It is unlikely, however, that biological isotope effects will normally exceed 0.1% to 0.2% and hence no serious impact on the detection sensitivity of MC-ICP-MS for isotopically labeled AgNPs is expected. Nonetheless, it will be important for future work to carefully characterize possible biological Ag isotope fractionations. If natural Ag isotope variations of ≥0.05% are found to be common and deemed to be obstructive, this problem can be readily circumvented by analyses of appropriate control samples. Such measurements can characterize the natural Ag isotope composition and variability of the background, and this permits appropriate corrections and/or uncertainties to be applied to the isotopic data collected for exposed samples.

Ecotoxicology studies typically generate and require analyses for a large number of samples (more than 100), making it important to consider the balance between optimal data quality and high sample throughput. Whilst MC-ICP-MS can provide unrivalled precision for the determination of $^{107}Ag/^{109}Ag$, such analyses are also particularly laborious, because Ag must be separated from any sample matrix prior to analysis. In contrast, quadrupole and sector field ICP-MS can be employed for direct $^{107}Ag/^{109}Ag$ measurements without chemical separation. As sample preparation is much more straightforward, the latter instruments can achieve significantly higher sample throughput but at the cost of somewhat poorer precision for the data, which ultimately limits the tracing capabilities.

In the following the tracing sensitivities that can be achieved using ^{107}Ag-E (and thus $^{107}AgNPs$) are discussed for two hypothetical cases with relevance to ecotoxicology, and where the end member methods of Q-ICP-MS and MC-ICP-MS are evaluated for detection (Table 3.3). Case 1 involves analyses of 5 mg dry weight samples of biological tissue, as might be obtained from invertebrates following exposures, with a realistic Ag background of 100 ng g^{-1} (Eisler, 1996). Case 2 is for a 5 mL water sample (a realistic volume for removal and analysis from a laboratory exposure) that features a Ag background concentration of 200 ng L^{-1}, as would be appropriate for river, lake and estuarine waters (Eisler, 1996). Based on the concentrations quoted above, the Case 1 and 2 samples would contain only 0.5 ng

and 1 ng of Ag, respectively (Table 3.3), and these small amounts will limit the precision of the isotopic analyses by ICP-MS. Based on literature data and test measurements conducted at Imperial College (for MC-ICP-MS), it is estimated that the diagnostic $^{107}Ag/^{109}Ag$ isotope ratio can be determined in these samples with a precision of about ±5% for Q-ICP-MS and ± 0.05% for MC-ICP-MS (an intermediate precision is expected for SF-ICP-MS).

The precision of mass spectrometric measurements is defined here as the 2sd

Table 3.3 Summary of data for the hypothetical cases that evaluate the detection sensitivities and quantification uncertainties achievable for tracing of ^{107}Ag-E in environmental samples

	Case 1	**Case 2**
Sample	5 mg biological tissue	5 mL water
Background Ag concentration	100 ng g^{-1}	200 ng L^{-1}
Total natural Ag content of sample	0.5 ng	1 ng
Analysis by Q-ICP-MS, precision ±5% (2sd)		
Minimum concentration change detectable by $^{107}Ag/^{109}Ag$ analysis*	2.6 ng g^{-1}	5.2 ng L^{-1}
Uncertainty in quantification of ^{107}Ag-E at:		
10x minimum concentration	126 ± 3.12 ng g^{-1}	252 ± 6.24 ng L^{-1}
100x minimum concentration	360 ± 4.37 ng g^{-1}	720 ± 8.76 ng L^{-1}
Analysis by MC-ICP-MS, precision ±0.05% (2sd)		
Minimum concentration change detectable by $^{107}Ag/^{109}Ag$ analysis*	0.026 ng g^{-1}	0.052 ng L^{-1}
Uncertainty in quantification of ^{107}Ag-E at:		
10x minimum concentration	100.26 ± 0.026 ng g^{-1}	200.52 ± 0.053 ng L^{-1}
100x minimum concentration	102.6 ± 0.027 ng g^{-1}	205.2 ± 0.055 ng L^{-1}

* smallest increase in the Ag concentration from the addition of ^{107}Ag-E, which is resolvable by measurement of the $^{107}Ag/^{109}Ag$ isotope ratio using a given technique.

calculated from replicate isotope analyses of samples or a standard reference material. The analytical precision is a key factor because it determines the smallest change in the $^{107}Ag/^{109}Ag$ isotope ratio (ΔR_{res}), as induced by addition of the ^{107}Ag tracer, which is analytically resolvable as a deviation from the natural $^{107}Ag/^{109}Ag$ (R_{nat}) ratio, such that ΔR_{res} = 2sd.

The addition of an ^{107}Ag-E tracer to a natural sample will increase the $^{107}Ag/^{109}Ag$ ratio of the system. In the following the R_{res} is defined as the $^{107}Ag/^{109}Ag$ isotope ratio, which

is associated with the smallest addition of ^{107}Ag-E tracer that is resolvable by measurement. R_{res} is therefore given by:

$$R_{res} = R_{nat} + \Delta R_{res} \quad (3.5)$$

Isotope mass balance can then be used to calculate the minimum molar amount of ^{107}Ag-E (N_{res}-Ag_{en}), from labeled ^{107}AgNPs, that must be added to a given molar amount of natural Ag (N-Ag_{nat}) in a system, to increase the ^{107}Ag/^{109}Ag ratio from R_{nat} to R_{res}:

$$N_{res}\text{-}Ag_{en} = N\text{-}Ag_{nat} \times ((R_{res} \times {}^{109}Ab_{nat}) - {}^{107}Ab_{nat}) / ({}^{107}Ab_{en} - (R_{res} \times {}^{109}Ab_{en})) \quad (3.6)$$

Where the fractional (molar) isotope abundances of ^{107}Ag and ^{109}Ag in the ^{107}Ag-E ($^{107}Ab_{en}$ and $^{109}Ab_{en}$) and natural Ag ($^{107}Ab_{nat}$ and $^{109}Ab_{nat}$) are 99.2%, 0.8% and 51.8%, 48.2%, respectively. Equation 3.6 can be readily revised to determine the minimum molar concentration [N_{res}-Ag_{en}] of ^{107}Ag-E that must be added to obtain R_{res} – this requires only that N-Ag_{nat} is substituted with the molar concentration of natural Ag, [N-Ag_{nat}]. Given that the atomic weights of natural Ag and ^{107}Ag-E differ by less than 1%, Equation 3.6 also provides a sufficiently accurate approximation for calculation of the minimum masses and mass concentrations of ^{107}Ag-E, which must be added to the system, to achieve a detectable change in the final ^{107}Ag/^{109}Ag ratio.

The molar fraction of ^{107}Ag-E to total Ag (fr_{en}) present in the sample is given by:

$$fr_{en} = N\text{-}Ag_{en} / (N\text{-}Ag_{nat} + N\text{-}Ag_{en}) \quad (3.7)$$

Where N-Ag_{en} is the molar amount of ^{107}Ag-E. Equation 3.7 can be recast such that the final ^{107}Ag/^{109}Ag isotope ratio of an exposed sample (R_{sam}) is used to quantify the molar fraction of ^{107}Ag-E:

$$fr_{en} = [({}^{107}Ab_{en} - (R_{sam} \times {}^{109}Ab_{en})) / ((R_{sam} \times {}^{109}Ab_{nat}) - {}^{107}Ab_{nat}) + 1]^{-1} \quad (3.8)$$

The fractional molar abundance of ^{109}Ag in the exposed sample ($^{109}Ab_{sam}$) is then:

$$^{109}Ab_{sam} = (fr_{en} \times {}^{109}Ab_{en}) + ((1 - fr_{en}) \times {}^{109}Ab_{nat}) \quad (3.9)$$

The molar abundance of total Ag (N-Ag) and ^{107}Ag-E in the sample can be determined by first quantifying the molar amount of ^{109}Ag (N-^{109}Ag) in the sample. This can be readily achieved using standard ICP-MS techniques, where a solution prepared from a known aliquot of the sample is analyzed, such that N-^{109}Ag can be determined relative to a suitable calibration curve. Following this, N-Ag and N-Ag_{en} can be calculated from:

$$N\text{-}Ag = (N\text{-}^{109}Ag / {}^{109}Ab_{sam}) \quad (3.10)$$

$$N\text{-}Ag_{en} = (N\text{-}^{109}Ag / {}^{109}Ab_{sam}) \times fr_{en} \quad (3.11)$$

The mass and mass concentration of ^{107}Ag-E (M-Ag_{en} and [M-Ag_{en}] respectively) in the sample can then be obtained as:

$$M\text{-}Ag_{en} = N\text{-}Ag_{en} \times AtW_{en} \quad (3.12)$$

$$[M\text{-}Ag_{en}] = (N\text{-}Ag_{en} \times AtW_{en}) / M \quad (3.13)$$

Where M is the sample mass. The atomic weight of the ^{107}Ag-E, AtW_{en}, can be determined from:

$$AtW_{en} = ({}^{107}Ab_{en} \times {}^{107}AtW) + ({}^{109}Ab_{en} \times {}^{109}AtW) \quad (3.14)$$

Where ^{107}AtW and ^{109}AtW are the known atomic weights of ^{107}Ag and ^{109}Ag. Calculations analogous to those performed in Equations 3.12 to 3.14 can be used to derive the total mass of Ag (M-Ag) and the Ag mass concentration [M-Ag] in the sample.

The results of these calculations for Cases 1 and 2 are given in Table 3.3. In detail, they indicate that isotopic tracing with Q-ICP-MS requires that the addition of ^{107}Ag-E raises the total Ag concentration by at least 2.6%, to 102.6 ng g^{-1} for the tissue (Case 1) and 205 ng L^{-1} for the water sample (Case 2; Table 3.3). With MC-ICP-MS, measurements of the ^{107}Ag/^{109}Ag ratio are about 100-fold more precise and consequently the tracing sensitivity is

also improved by two orders of magnitude. In this scenario the Ag sample concentration only needs to increase by 0.026%, from the addition of ^{107}Ag-E, to generate analytically resolvable differences in the ^{107}Ag/^{109}Ag isotope ratio. For the tissue and water samples, this means that increases in the Ag concentration to 100.026 ng g^{-1} (from 100 ng g^{-1}) and 200.05 g L^{-1} (from 200 g L^{-1}), respectively, are already traceable by isotopic analyses. Evaluation of the detection sensitivity for a given isotope label, analytical approach and natural background concentration in this manner, enables appropriate experimental plans and dosing levels to be prepared.

The uncertainties of the isotope ratio analyses can be propagated through the above equations to assess the impact that this will have on the calculated mass of enriched tracer material present in a sample or its mass concentration. Importantly, the uncertainties do not scale in a linear manner and depend on the isotopic enrichment of the tracer and the proportion of ^{107}Ag-E to natural Ag in the sample. To demonstrate this, the uncertainties for [M-Ag_{en}] in Cases 1 and 2 (Table 3.3) were calculated for the addition of ^{107}Ag-E tracer at levels, which exceed the smallest detectable molar concentration N_{res}-Ag_{en} by a factor of 10x and 100x.

The results of these calculations are promising because they indicate that despite the unfavorable natural isotope composition of Ag, stable isotope labeling of Ag can provide detection sensitivities and uncertainties of quantification that are far better than those achievable by concentration tracing. Considering that the latter methodology can only provide unequivocal results if the concentration anomalies generated by elemental uptake exceed the natural background levels by at least a factor of 2 (but preferably more), the application of stable isotope labeling enhances the tracing sensitivity by at least a factor of 40 (using Q-ICP-MS for detection) and possibly by up to a factor of ~4000 (with use of MC-ICP-MS). Furthermore, with the superior precision of MC-ICP-MS for isotopic analyses, the tracing sensitivities are likely to be sufficiently high, to enable experiments to be carried out at low and environmentally relevant exposure concentrations.

3.4 Conclusions

In this study, published methods were assessed for the small-scale synthesis of citrate-capped AgNPs from both natural Ag and ^{107}Ag-E. Three different synthesis protocols were used on three occasions and in two laboratories to obtain AgNPs with target sizes of 17, 20 and 30 nm. All particles batches produced were thoroughly characterized and the results demonstrate that the new procedures provide reproducible, monodisperse particle suspensions at high yields of ~80% and with a long-term stability of up to 12 months. Whilst the measurements revealed small but significant batch-to-batch variations in size, the particles were generally found to have diameters that closely matched the desired target sizes. Detailed statistical tests furthermore argue against systematic differences in size between AgNPs prepared from ^{107}Ag-E versus natural Ag. In summary, these results show that the new methods are ideally suited for the small-scale preparation of isotopically labeled AgNPs. Simple isotope mass balance calculations furthermore demonstrate that application of stable isotope labeling can increase the detection sensitivity of AgNPs in environmental samples by at least a factor of 40 and possibly by up to 4000x, in comparison to commonly employed bulk Ag concentration measurements. Use of the most precise isotopic measurement techniques should therefore, permit environmentally realistic exposure scenarios.

3.5 Declaration

This work was conceived and designed by Mark Rehkämper (MR) and Adam Laycock (AL). MR supervised the aspects of work that were performed at Imperial College while Eva Valsami-Jones (EV) and Jamie Lead (JL) supervised the work conducted at FENAC, University of Birmingham. Isabella Römer (IR) introduced the Ag NP synthesis technique to AL and Bjorn Stölpe (BS). The synthesis and characterization of the Ag NP suspensions was performed by AL and BS. BS also conducted the dissolution study with advice from Agnieszka Dybowska (AD). AL performed the isotope modeling presented in this chapter.

Chapter 4:

A stable isotope tracer to determine uptake and efflux dynamics of ZnO nano- and bulk particles and dissolved Zn to an estuarine snail

Abstract

Zinc oxide nanoparticles (ZnO NPs) are amongst the most commercialized engineered nanomaterials. Their biological impact in aquatic organisms has been associated to dissolution, but there is also evidence of nano-specific effects. In this study the waterborne uptake and efflux kinetics of isotopically labeled ^{68}ZnO NPs (7.8 ± 1.2 nm), in comparison to aqueous ^{68}Zn and ^{68}ZnO bulk particles (up to 2 μm), were determined for the estuarine snail *Peringia ulvae* following a 7 d exposure (nominal enriched ^{68}Zn concentration of 20 μg L^{-1}) and 28 d depuration. Detection of the ^{68}Zn label was achieved by high precision multiple-collector ICP-MS (MC-ICP-MS). Previous characterization in artificial estuarine water revealed that the NPs underwent initial aggregation, and solubilized up to 60% within 1-2 days. Bulk and aqueous forms were significantly more bioavailable than ^{68}ZnO NPs ($p<0.05$), but after correcting for dissolution, aqueous (0.074 L^{-1} g^{-1} d^{-1}) and NP (0.070 L^{-1} g^{-1} d^{-1}) uptake rate constants were highly comparable. The rate constant of loss for ^{68}Zn aqueous (0.012 ± 0.005 d^{-1}) and ^{68}ZnO NPs (0.012 ± 0.007 d^{-1}) were identical. These results strongly suggest that in this exposure scenario the bioaccumulation of Zn from ZnO NPs is primarily dependent upon solubility.

4.1 Introduction

Zinc oxide nanoparticles (ZnO NPs) are used in a number of commercial applications, including sunscreens, coatings and paint (Osmond and Mccall, 2010). Some are therefore expected to be released into the environment, particularly the aquatic environment. The biological impact of ZnO NPs is often attributed to their solubility and the release of labile Zn. ZnO NPs were shown to exhibit rapid dissolution kinetics in freshwater, resulting in a ZnO NP exposure being equally as toxic to algae (*Pseudokirchneriella subcapitata*) as dissolved $ZnCl_2$ (Franklin et al., 2007). However, complete dissolution is not always the case and rarely is uptake by the organism and quantification of dissolution in the medium considered in the same study. This is perhaps why the presence of soluble Zn^{2+} within a ZnO NP exposure did not fully account for the adverse toxic effects induced in zebrafish embryos (Zhu et al., 2009) or growth and survivorship inhibition in the amphipod *Corophium volutator* (Fabrega et al., 2011). This would indicate that the particles themselves exert a nano-specific effect that is distinct from the aqueous Zn.

The aim of the present study was to determine if dissolution alone accounts for the bioavailability of Zn when ZnO NPs are dispersed in estuarine water and presented to the snail *Peringia ulvae* (Gastropoda; Hydrobiidae), a key estuarine species (Shipp and Grant, 2006). The bioavailability and *in vivo* fate of Zn from ZnO NPs were assessed using the principles of biodynamic modeling (Luoma and Rainbow, 2005). Specifically by quantifying the rates of influx (uptake) and efflux of Zn into and from the organism to provide a better understanding of the accumulation of Zn from ZnO NPs. This is important as accumulation of a contaminant is generally regarded as a prerequisite to adverse biological effects (Tessier and Turner, 1995). For comparison uptake and efflux rates were also determined following exposures to aqueous Zn and ZnO bulk particles. If the bioavailability of Zn from the ZnO NP is dependent on solubility, then the uptake rate of Zn in a ZnO NP versus an aqueous Zn exposure should be comparable if only the dissolved concentrations are considered. Moreover, loss dynamics would be identical regardless of the original form of Zn (i.e. aqueous vs. nano).

Dissolution and aggregation were quantified in stock solution freshwater and the artificial estuarine water, which were also used as the exposure media. The behavior of NPs in artificial waters may not necessarily reflect their behavior in natural waters, this is largely owing to the absence of organic matter (Keller et al., 2010). In addition a number of other factors have also been shown to influence the solubility of ZnO in aqueous systems. Miao et al. (2010) found that ZnO NP dissolution increased with decreases in pH and particle surface area, and that dissolution was accelerated in seawater, which is relevant to the present study conducted in water with 17 practical salinity units (psu). As dissolution is a function of concentration, solubility is particularly relevant when working at environmentally realistic Zn concentrations (Franklin et al., 2007). Total Zn concentrations within aquatic environments vary with anthropogenic activity and natural geology. Dissolved Zn concentrations in the natural estuarine environments can be as high as 5 μg L^{-1} (Luoma and Rainbow, 2008) and may reach 50 μg L^{-1} in contaminated hotspots (Wood et al., 2011). In comparison, predicted environmental releases of ZnO NPs in European and U.S. surface water ranged from 1-10 ng L^{-1}, and up to 430 ng L^{-1} in treated wastewater (Gottschalk et al., 2009). In biological samples, a soft tissue concentration of 34.5 μg g^{-1} was estimated to fulfill metabolic Zn requirements (White and Rainbow, 1985), whilst the measured Zn tissue burden of the field collected *P. ulvae* used in this study was 148 ± 31 μg g^{-1} (mean value ± S.D., n = 30). Thus to differentiate Zn accumulated by organisms above their natural background it becomes necessary to use a label if exposures conducted at environmentally relevant levels are desired (Dybowska et al., 2011). Enriched stable isotopes have been suggested as one such label that may be used to trace engineered NPs containing multi-isotopic elements (Croteau et al., 2011, Gulson and Wong, 2006).

The three forms of Zn (aqueous, nano and bulk) investigated in this study were prepared using Zn composed of, and hence labeled with, >99% of the stable isotope ^{68}Zn. In comparison natural Zn has a ^{68}Zn isotope abundance of ~19%, and Zn isotope compositions display only limited natural variability. For example, the $^{68}Zn/^{66}Zn$ ratio varies by only ~0.25% in natural biological samples (Larner and Rehkämper, 2012). These labeled Zn materials,

therefore, possess a distinct and non-natural isotope signature. Once the ^{68}Zn label is introduced into the experimental system it is possible to trace it by measuring the diagnostic ^{68}Zn/^{66}Zn isotope ratio in the various components of the system. Deviations from the natural ^{68}Zn/^{66}Zn isotope ratio indicate the presence of the isotopically enriched ^{68}Zn-E. The magnitude of this perturbation can be used to quantify the relative and absolute amount of ^{68}Zn-E.

Whilst distinct isotopes, and compounds made thereof, display very slight differences in their physical and chemical properties, these differences are not of consequence in tracer studies with enriched isotopes. It is therefore valid to assume that particles synthesized from ^{68}Zn-E display the same environmental behavior as equivalent particles with a natural Zn isotope composition (Dybowska et al., 2011), this makes them ideal for the purpose of tracing. Enriched stable isotopes are also advantageous over other forms of labeling, such as fluorescent dyes or radioactive isotopes (Misra et al., 2012), as they are not beset with problems where the label may be lost as a result of dissociation or radioactive decay. In the present study, stable isotope labeling is used in conjunction with multiple collector inductively coupled plasma mass spectrometry (MC-ICP-MS). Very small changes in isotope ratio are analytically resolvable using this approach and therefore it offers very low levels of detection for isotopically labeled materials. Isotopically enriched particles are just recently being utilized in ecotoxicological studies (Croteau et al., 2011, Larner et al., 2012, Misra et al., 2012), but there remains a far greater potential for their use.

4.2 Methods

4.2.1 Chemicals and reagents

Isotopically enriched ^{68}Zn was purchased from Isoflex USA (CA, USA) as dry powders in the form of ^{68}ZnO bulk particles and ^{68}Zn metal, the latter was used to prepare the aqueous and NP forms. For this study, a single 100 L batch of artificial estuarine water (17 psu) was prepared from Tropic Marin Sea Salt (Dr Biener GmbH, Germany). Concentrated, 14.5 M HNO_3 and 6 M HCl were purified prior to use by sub-boiling distillation

in a quartz still, and water of >18 MΩ cm quality (Millipore, UK) and 30% Suprapur H_2O_2 (VWR International Ltd, UK) were used throughout.

4.2.2 Experimental organisms

P. ulvae were collected from the Blackwater Estuary, Essex, UK (51˚46'05"N 00˚50'13"E) at low tide and maintained in the laboratory in synthetic estuarine water at 10 ± 1˚C with an approximate 16 h light: 8 h dark. Two days before the start of the exposures, adult snails (>2 mm) were randomly assigned into 90 groups of 25 individuals. Food (*Chlorella vulgaris*) was withheld during this period. *C. vulgaris* was cultured in 3N-BBM+V medium (Culture Collection of Algae and Protozoa, Scottish Marine Institute, UK) also under 16 h light: 8 h dark cycles.

4.2.3 Preparation of isotopically enriched forms of ^{68}Zn

The ^{68}ZnO NPs were synthesized by forced hydrolysis in diethylene glycol (DEG) as outlined by Dybowska et al. (2011). This was achieved by dissolving the ^{68}Zn-E metal in acetic acid by refluxing for 72 hours at 90°C, before evaporating to dryness at 80°C to leave an ^{68}Zn-E acetate precursor material. The precursor (100 mg) was then added to 50 mL DEG which was placed in an oil bath at 60°C for 70 hours, after which the temperature was raised to 180°C. When the mixture temperature stabilized, it was stirred (200 rpm) and 100 µL 18 MΩ water was added to force hydrolysis and precipitate ^{68}ZnO NPs. The ^{68}Zn-E concentration of the NP stock suspension was measured as 743 mg L^{-1} using ICP-OES.

Stock suspensions of the ^{68}ZnO bulk particles in DEG and aqueous ^{68}Zn in 18 MΩ water were also prepared at 743 mg L^{-1} ^{68}Zn-E. The latter was prepared by dissolving ^{68}Zn-E metal powder in 6M HCl. This solution was evaporated to produce $^{68}ZnCl_2$, which was dissolved in 18 MΩ water.

4.2.4 Characterization of ^{68}ZnO particles

To determine particle size, shape and size distribution the ^{68}ZnO NPs and ^{68}ZnO bulk particles were imaged using TEM (Hitachi 7100, 100kV) and SEM (Ultra plus FESEM, Carl Zeiss), respectively. The crystal structure of both the NP and bulk forms was verified by X-ray diffraction (XRD, Enraf Nonius) and compared to a ZnO standard (ICDD [36-1451]). A Zetasizer Nano ZS (Malvern Instruments Ltd) was used to determine the primary particle size, polydispersity and zeta potential of the stock ^{68}ZnO NP and bulk particle DEG suspensions. Analysis of 1:10 (v/v) dilutions of the ^{68}ZnO NP stock suspensions with 17 psu water was also carried out by DLS over 11 h at 30 min intervals and was performed at 10°C to reflect experimental conditions.

4.2.5 Waterborne exposures

A number of precautions were made to eliminate the risk of background Zn entering the exposure system. Plastic laboratory-ware was used in preference to glass as the latter has been shown to leach Zn to a greater extent (Kay, 2004). All plastic-ware was soaked in 1 M HCl and thoroughly rinsed in 18 MΩ water before use. Exposure chambers (50 mL plastic beakers) were pre-soaked at 20 µg L^{-1} ^{68}Zn-E, added as aqueous ^{68}Zn, ^{68}ZnO NPs or ^{68}ZnO bulk particles, for 72 h to saturate surface binding sites. At the start of the exposure (i.e. t = 0 d) 3 of the 90 groups of snails were sampled for baseline measurements, *C. vulgaris* (both the stock culture and in 25 mL 17 psu water as presented to the snails for food during efflux) and the 17 psu water were taken for background determinations of the ^{68}Zn/^{66}Zn isotope ratio. The 100 L batch of exposure media was also sampled at the end of the experiment.

The remaining 87 groups of snails were randomly divided amongst the controls and exposures to aqueous ^{68}Zn, ^{68}ZnO NPs or ^{68}ZnO bulk particles. For each form of ^{68}Zn-E, 27 groups of snails were exposed to 20 µg L^{-1} ^{68}Zn-E and the 6 remaining groups were used as controls (no added ^{68}Zn-E). The 743 mg L^{-1} stocks of each ^{68}Zn-E form were diluted with 18 MΩ water to produce intermediate stocks with 20 mg L^{-1} ^{68}Zn-E. DEG was added to the

aqueous ^{68}Zn intermediate stock to match the DEG concentration in the NP and bulk particle intermediate stocks. Each group of snails was placed in a pre-soaked exposure chamber with 25 mL 17 psu water and 25 µL of the corresponding intermediate stock solution to achieve the ^{68}Zn-E exposure concentration of 20 µg L^{-1}. Samples of the exposure solutions were taken to verify the concentration. To minimize potential particle aging and dissolution the exposures were renewed each day for 7 days from freshly prepared intermediate stock solution. At each renewal, snails were removed from the exposure chamber and both the chamber and snails washed thoroughly with 18 MΩ water. Separate plastic-ware was used for each treatment and controls to prevent cross-contamination of the isotope label between treatments. Snails and exposure water from each treatment were sampled on days 1, 4 and 7, with control snails also sampled on day 7. Snails were not fed during the exposure phase of this study.

On day 7 of the exposure, the remaining 57 groups of snails (18 for each ^{68}Zn-E treatment and 3 controls) were rinsed thoroughly in 17 psu water and transferred to new acid-washed plastic beakers containing 25 mL of 17 psu water to investigate the efflux rate of the different ^{68}Zn-E forms. During this depuration phase, snails and water were sampled on days 1, 2, 4, 7, 14 and 28. The renewal of clean water was made at these time points, with an additional water change and sampling of water only on day 21. During efflux snails were fed with *C. vulgaris,* which was added to the water at the time of renewal. Post-exposure snails sacrificed by freezing and stored at -20°C as groups of 25 individuals.

4.2.6 Sample preparation

Samples obtained from the exposures were prepared for isotopic analysis within Class 10 laminar flowhoods (MAGIC laboratory class 1000 clean room facility, Imperial College), and were subsequently analyzed by MC-ICP-MS (MAGIC laboratory) to determine the diagnostic ^{68}Zn/^{66}Zn isotope ratio. These analyses require a pure Zn solution, necessitating the isolation of Zn from the matrix elements present in samples. The sample

matrix was purified by anion exchange chromatography. Full details of all sample treatment follow:

4.2.6.1 Water samples

The 25 mL water samples were collected in acid cleaned 50 mL Falcon tubes and stored in a freezer at -20°C. For preparation, the samples were defrosted at room temperature and a homogenous 5 mL aliquot was taken. These fractions were transferred to acid cleaned pre-weighed 7 mL Teflon vials, which were then re-weighed and the sample weight recorded. The water was then acidified with 1 mL 6 M HCl resulting in a 6 mL 1 M HCl sample solution. The acidified samples were then refluxed overnight on a hotplate at 80°C to ensure homogenization and dissolution of any particulate material.

4.2.6.2 Snail samples

The groups of 25 *P. ulvae* were defrosted at room temperature before the soft tissue was dissected from the shell for analysis, as described by Khan et al. (2012). Each group of snails were left overnight in 10 mL 0.06 M HCl at room temperature. This served 2 purposes: (i) to leach Zn from the surface of the shells and (ii) to soften the operculum opening and the attachment of the collumellar muscles to the shell of the snails. The soft tissue and shell leachate solution were then transferred to acid cleaned pre-weighed Teflon vials and placed on a hotplate at 60°C and 120°C, respectively, until dry. The dry tissue weight was recorded before adding 1 mL 14.5 M HNO_3 and returning to a hotplate at 80°C overnight. The tissue samples were transferred to microwave digestion vessels where a further 3 mL 14.5 M HNO_3 and 3 mL H_2O_2 was added and left overnight at room temperature. The vessels were then transferred to a CEM MARS5 microwave unit (1200W) where digestion was achieved by increasing the temperature to 200°C over 15 minutes and maintaining the temperature at 200°C before being allowed to cool to room temperature. The resulting sample solutions were transferred to 15 mL Teflon vials and the acid matrix converted to HCl. Finally both the soft tissue digestions and shell leachates were dissolved in 6 mL 1 M HCl.

4.2.6.3 Anion chromatography

The sample solutions in 1 M HCl were processed through a one-step anion exchange column chemistry, as described in Arnold et al. (2010). This procedure serves to efficiently isolate Zn from the sample matrix with an essentially quantitative yield. Pre-cleaned columns, with resin beds that had internal diameters of 3.5 mm and a volume of 240 µL, were filled with Bio-Rad AG MP-1 100-200 mesh anion exchange resin. The resin was cleaned and conditioned successively with 16 mL 0.1 M HNO3, 0.5 mL 18 MΩ H_2O and 4 aliquots of 0.5 mL 1 M HCl. The sample solutions (6 mL 1 M HCl) were then loaded onto the columns and matrix elements were eluted with 8 mL 1 M HCl. Finally, Zn was stripped from the resin using 6 mL 0.01 M HCl.

To verify the recovery of Zn from these biological sample matrices, the above procedure was performed with representative unexposed biological samples and the matrix elements were collected at the '8 mL 1 M HCl' elution step. Following this, the matrix was doped with an equivalent (and known) amount of the in-house 'London Zn' standard solution of natural Zn (Arnold et al., 2010). The separation chemistry was then performed as described above, and the concentration of the recovered Zn was determined by MC-ICP-MS. These measurements demonstrated a near 100% recovery of Zn from the column (99 ± 8%, n = 2) thereby precluding that the results are biased by isotope fractionation during the column chemistry.

4.2.7 $^{68}Zn/^{66}Zn$ determination

The purified Zn solutions were dried and subsequently taken up in 0.1 M HNO_3 for isotopic analysis with a Nu Instruments Nu Plasma HR MC-ICP-MS instrument. A DSN desolvator system (Nu Instruments) and glass nebulizers with solution flow rates of ~100-120 µL min^{-1} was used for sample introduction. The sample analyses were conducted as three blocks of twenty 5s integrations. Ion beams were measured using static multiple collection with Faraday cups, equipped with 10^{11} Ω resistors, on atomic masses 62 (Ni), 63 (Cu), 64 (Ni, Zn), 65 (Cu), 66 (Zn), 67 (Zn), and 68 (Zn). The electronic baseline was

measured for 15s prior to each block by deflecting the ion beam in the electrostatic analyzer. Instrumental sensitivities of about 120 V ppm^{-1} were routinely achieved for Zn and Cu. The ^{62}Ni ion beam was used to correct for the isobaric interference on ^{64}Zn. The sample measurements were carried out relative to analyses of a solution of pure natural Zn (London Zn; in the same acid matrix) which was used as an in-house standard reference value. The samples and standard solutions were prepared at Zn concentrations of 50 ng mL^{-1} and were doped with equal amounts of a pure ICP Romil Cu solution to Cu concentrations of 50 ng mL^{-1}. The addition of Cu enables accurate correction of the raw measured Zn isotope ratios for instrumental mass bias by external normalization relative to the $^{65}Cu/^{63}Cu$ ratio, which is also monitored during the analyses (Rehkämper et al., 2001). The magnitude of any deviation in the Zn isotope composition of a sample from natural Zn can then be used to quantify the amount of ^{68}Zn-E in the sample.

4.2.8 Isotope mass balance calculations

The diagnostic $^{68}Zn/^{66}Zn$ isotope ratio measured for samples is an expression of the molar amounts of natural Zn ($N\text{-}Zn_{nat}$) and ^{68}Zn-E ($N\text{-}Zn_{en}$) and their isotopic compositions. The measured $^{68}Zn/^{66}Zn$ (R_{meas}) of a sample can therefore be expressed as:

$$R_{meas} = ((N\text{-}Zn_{nat} \times {}^{68}Ab_{nat}) + (N\text{-}Zn_{en} \times {}^{68}Ab_{en})) / ((N\text{-}Zn_{nat} \times {}^{66}Ab_{nat}) + (N\text{-}Zn_{en} \times {}^{66}Ab_{en})) \quad (4.1)$$

Where $^{xx}Ab_{nat}$ and $^{xx}Ab_{en}$ denote the molar abundance of the ^{xx}Zn isotope in natural Zn and ^{68}Zn-E respectively. The fractional molar abundances of natural Zn isotopes were determined from analyses of the London Zn standard solution measurements that bracketed the samples analyses. Whereas the certified fractional molar abundances, provided by Isoflex, of 0.9878 (^{68}Zn) and 0.0033 (^{66}Zn) were used for the ^{68}Zn-E. Equation 4.1 may be recast to calculate the molar fraction of ^{68}Zn-E ($fr^{68}Zn_{en}$) to natural Zn in the sample:

$$fr^{68}Zn_{en} = [(({}^{68}Ab_{en} - (R_{meas} \times {}^{66}Ab_{en})) / ((R_{meas} \times {}^{66}Ab_{nat}) - {}^{68}Ab_{nat}))+1]^{-1} \quad (4.2)$$

The molar proportion of ^{68}Zn-E to total Zn was then used to determine the fractional molar abundance of each Zn isotope in the sample. For example the molar abundance of ^{68}Zn in a sample ($^{68}Ab_{sam}$) is found by:

$$^{68}Ab_{sam} = (fr^{68}Zn_{en} \times {}^{68}Ab_{en}) + ((1 - fr^{68}Zn_{en}) \times {}^{68}Ab_{nat}) \quad (4.3)$$

The molar amount of total Zn in a sample ($N\text{-}Zn_{sam}$) was calculated by dividing the molar amount of a ^{66}Zn ($N\text{-}^{66}Zn_{sam}$) by the molar abundance of ^{66}Zn ($^{66}Ab_{sam}$) in the sample.

$$N\text{-}Zn_{sam} = N\text{-}^{66}Zn_{sam} / {}^{66}Ab_{sam} \quad (4.4)$$

Where the molar amount of ^{66}Zn in the measured sample solution was found by dividing the measured ^{66}Zn signal intensity of the sample by the Zn signal sensitivity as determined by analysis of the London-Zn standard solution, with a known isotopic composition and concentration, immediately prior to the sample analysis. The molar amounts of ^{68}Zn-E and natural Zn are then found by multiplying the results from Equations 4.2 and 4.4:

$$N\text{-}Zn_{en} = N\text{-}Zn_{sam} \times fr^{68}Zn_{en} \quad (4.5)$$

$$N\text{-}Zn_{nat} = N\text{-}Zn_{sam} - N\text{-}Zn_{en} = N\text{-}Zn_{sam} \times (1 - fr^{68}Zn_{en}) \quad (4.6)$$

The mass amounts of ^{68}Zn-E ($M\text{-}Zn_{en}$) and natural Zn ($M\text{-}Zn_{nat}$) were then determined by multiplying with the atomic weight of the ^{68}Zn-E ($AtWt_{en}$) and natural Zn ($AtWt_{nat}$) respectively:

$$M\text{-}Zn_{en} = N\text{-}Zn_{en} \times AtWt_{en} \quad (4.7)$$

$$M\text{-}Zn_{nat} = N\text{-}Zn_{nat} \times AtWt_{nat} \quad (4.8)$$

Where the atomic weight can be found from the sum of the stable Zn isotope abundances (^{xx}Ab) multiplied by their corresponding atomic mass (^{xx}AtWt):

$$AtWt = \Sigma\ {}^{xx}Ab \times {}^{xx}AtWt \quad (4.9)$$

The mass concentration of ^{68}Zn-E in a sample can then be determined by dividing the mass from Equation 4.7 by the original weight or volume of the sample.

4.2.9 Biodynamic modeling

The biodynamic modeling used here quantifies the singular processes of uptake and loss to reconstruct bioaccumulation from the balance of these unidirectional fluxes (Luoma and Rainbow, 2005). This study presents uptake and loss rate constants calculated from a 7 day exposure and subsequent 28 day depuration of *P. ulvae* exposed to three forms of ^{68}Zn-E.

First the efflux rate constants were calculated from the change in ^{68}Zn-E body burden during the 28 d depuration period following exposure as follows:

$$[^{68}\text{Zn-E}]_{snail} = [^{68}\text{Zn-E}]^{0}_{snail}\, e^{-kt} \quad (4.10)$$

where $[^{68}\text{Zn-E}]_{snail}$ is the measured ^{68}Zn-E concentration in the snail tissue (μg g^{-1} (dry weight)) at a given time point during the efflux period, $[^{68}\text{Zn-E}]^{0}_{snail}$ is the ^{68}Zn-E concentration (μg g^{-1} (dry weight)) at the start of the efflux period (i.e. t = 0 d of depuration), k is the rate constant of loss (d^{-1}), and t is depuration time (d). The slope formed by the points of $[^{68}\text{Zn-E}]_{snail}$ and $[^{68}\text{Zn-E}]^{0}_{snail}$ represents the rate constant for loss (k_e in d^{-1}).

To calculate the unidirectional rate of ^{68}Zn-E influx (or uptake, U, in μg ^{68}Zn-E g^{-1} dry tissue weight d^{-1}) for the exposure of *P. ulvae* to 20 μg L^{-1} ^{68}Zn-E, the measured ^{68}Zn-E concentration in the snail tissue, which reflects the accumulated concentration from exposure (i.e. a balance of uptake and loss), was corrected using the k_e to account for physiological loss during exposure time.

$$U = [^{68}\text{Zn-E}]_{snail} / 1-(k_e \times t) \quad (4.11)$$

The uptake rate constant (k_u in g^{-1} L^{-1} d^{-1}) was calculated from the influx rate divided by the measured ^{68}Zn-E exposure concentration ($[^{68}\text{Zn-E}]$) (Wang and Ke, 2002).

$$k_u = U / [^{68}\text{Zn-E}]_{exp} \quad (4.12)$$

4.2.10 Statistical analysis

Significant differences ($p \leq 0.05$) between uptake and efflux rates of snails exposed to different ^{68}Zn forms were determined by analysis of covariance (ANCOVA) with post-hoc Tukey's Test. Analyses were performed using STATISTICA software (StatSoft Ltd, Tulsa, OK, USA).

4.3 Results and discussion

4.3.1 Characterization of ^{68}ZnO particles

TEM analysis showed the ^{68}ZnO NPs to be spherical and homogeneous in size and shape, with a diameter of 7.8 ± 1.2 nm (n=100, Figure 4.1 A-C). The crystal structure was verified as being ZnO by XRD analysis (Figure 4.1D). DLS analysis of the ^{68}ZnO NP stock diluted in 18 MΩ water (1:10) revealed a mean hydrodynamic diameter of 38.4 ± 0.7 nm (Figure 4.1E). These characteristics are consistent with those reported in other studies using NPs synthesized with the same method. For example the ^{67}ZnO NPs utilized by Buffet et al. (2012) were determined to be <10 nm by TEM imaging and ~40 nm in deionized water by DLS measurements. Similarly synthesized ^{68}ZnO NPs used by Larner et al. (2012) had a hydrodynamic diameter of 33.0 ± 0.1 nm when suspended in deionized water and measured by DLS and a primary particle size of <10 nm was found from TEM images. The discrepancy between particle size and hydrodynamic diameter is likely the result of the hydration sphere around the primary particles in solution and in the presence of DEG. The zeta potential of the ^{68}ZnO NPs in this study was +20.3 ± 0.8 mV and the PDI (polydispersity index) was 0.175, which also compares favorably with those previously reported (zeta potential +17.2 ± 0.5 mV and PDI of 0.375 by Larner et al. (2012)). The consistency of these comparisons demonstrates that the forced hydrolysis synthesis protocol (Dybowska et al., 2011) produces highly comparable batches of particles. The reproducibility of the synthesis enables meaningful comparisons between ecotoxicological studies, and in particular allows the effect of specific variables to be tested, such as NP behavior in different environmental conditions (e.g. salinity) and amongst different species.

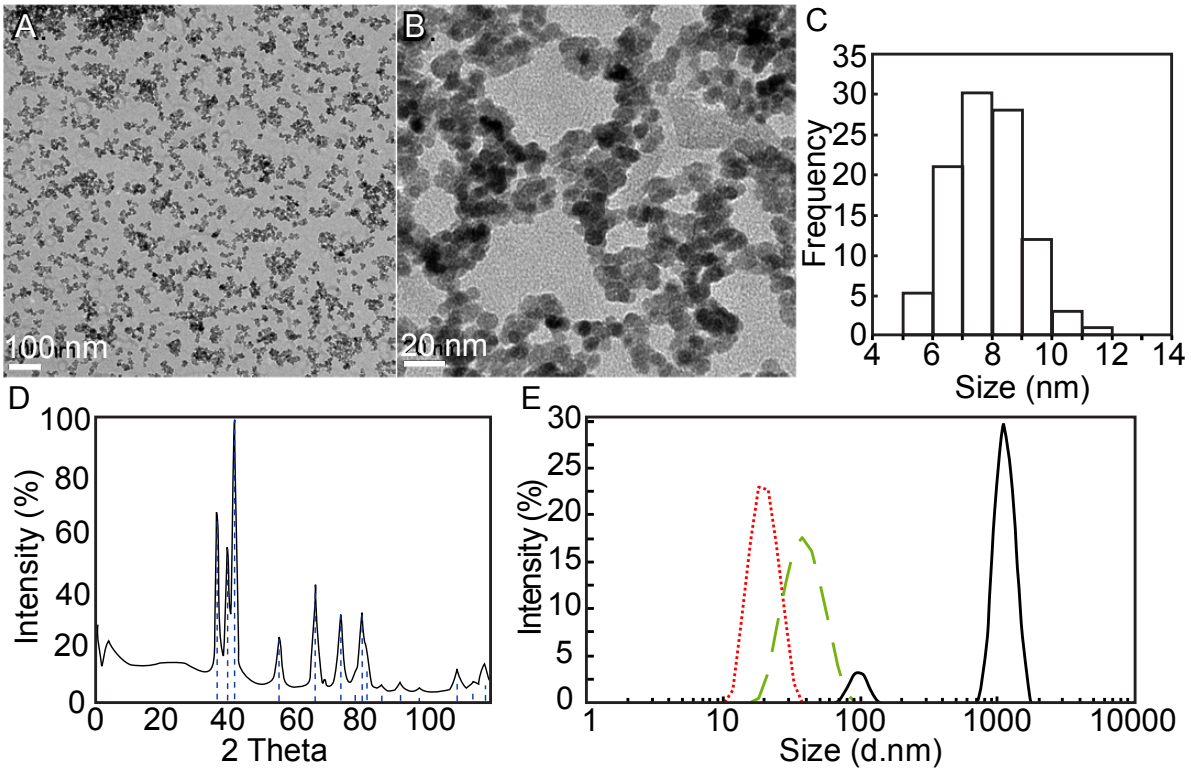


Figure 4.1 Characterization of ^{68}ZnO NPs after synthesis. Particles imaged by TEM (A and B) were determined to have an average size of 7.8 ± 1.2 nm (n = 100) with a size distribution close to the mean (C). The XRD pattern of the synthesized NPs (solid black line, is shown against the peak positions marked of the ZnO standard (ICDD [36-1451], dashed blue lines) which confirms the ZnO crystal structure (D). The hydrodynamic diameter size distribution of the ^{68}ZnO NPs expressed by intensity (%) in DEG (dotted red line), DI water (dashed green line) and after 3 hours in 17 psu water (solid black line) was measured by DLS (E).

The SEM images shows that the ^{68}ZnO bulk particles are highly heterogeneous, with single particles and aggregates varying in shape and size from a few hundred nm to over 2 µm (Figure 4.2 A and B). The commercially available ^{68}ZnO bulk particles had an identical crystal structure to the ZnO standard (Figure 4.2C). DLS analysis of the bulk particle stock, diluted in 18 MΩ water (1:10), also indicated heterogeneity with a hydrodynamic diameter of 556 ± 53 nm, a relatively high PDI of 0.563 and a surface charge of -23.8 ± 0.23 mV. Although DLS is recognized as being unsuitable for highly heterogeneous suspensions and where particles may sediment, it provides a useful comparison of the polydispersity and surface charge of the bulk particles in relation to the NP form.

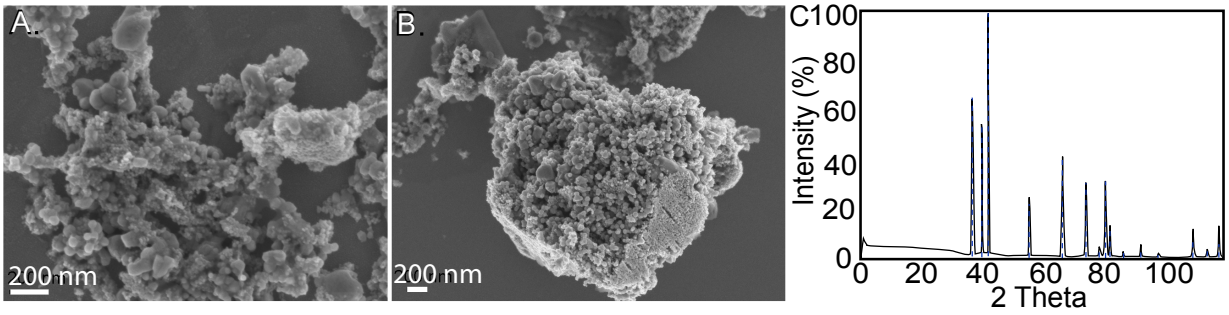


Figure 4.2 SEM images (A and B) and XRD (C) for ^{68}ZnO bulk particles purchased from Isoflex USA (CA, USA). The primary particles purchased as a powder were suspended in 18 MΩ water and presented a mean size 556 ± 53 nm, but a relatively high polydispersity index (see text). The XRD pattern of the bulk particles (solid black line) is shown with the peak positions marked for that of the ZnO standard ICDD [36-1451] (dashed blue line).

4.3.2 Reactivity of ^{68}ZnO particles in experimental media

Seven hours after dispersion of the ^{68}ZnO NPs in estuarine water (at 1:10 (v/v) dilution) DLS analysis could no longer detect particles in suspension, presumably owing to dissolution and/or aggregation and sedimentation (Figure 4.3). In determining the bioavailability of ^{68}ZnO NP and bulk particles to the estuarine amphipod *Corophium volutator*, the solubility and aggregation of both forms was assessed in artificial seawater (25 psu, Tropic Marin Sea Salt) by Larner et al. (2012). The ^{68}ZnO NPs used in that study were synthesized with the same protocol and facilities and, as described, the characterization of the primary particles was highly comparable. The ^{68}ZnO bulk particles used in both studies were from the same commercially sourced batch. Thus the environmental characterizations previously performed by Larner et al. (2012) are applicable to the present exposure scenario.

Equilibrium dialysis experiments conducted by these workers with the ^{68}ZnO NPs in artificial seawater demonstrated both fast initial aggregation of the NPs and release of aqueous ^{68}Zn into the medium. The former is confirmed by the DLS measurements in 17 psu water, which show that the ^{68}ZnO NPs typically form aggregates of 2-4 μm in size that are not present in dilutions with 18 MΩ water (Figure 4.1E). The dissolution of the ^{68}ZnO NPs was found to occur primarily within 24 hours with subsequent dissolution being less

pronounced and near-equilibrium attained after 48 hours. At equilibrium, 60% of the particles had dissolved. This is in agreement with other studies that reported partial to complete dissolution of ZnO NPs (Franklin et al., 2007, Li et al., 2011, Miller et al., 2010, Peng et al., 2011). Of the 48 ecotoxicology studies reviewed (Ma et al., 2013), more than half demonstrated that partial dissolution of ZnO NPs contributed to the toxicity of the exposure.

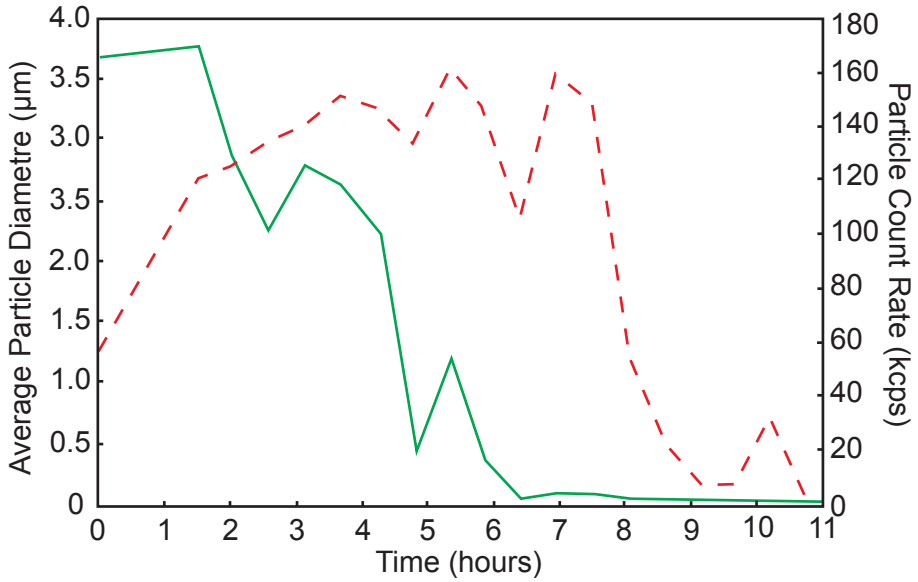


Figure 4.3 DLS measurements of the ^{68}ZnO NPs in 17 psu exposure media, 1:10 (v/v) dilution, at 10°C taken every 30 minutes over 11 hours showing the average particle size (red dashed line) and particle count rate (green solid line). Once in the exposure media the ^{68}ZnO NPs appear to aggregate rapidly with an increase in average aggregate size from about 1µm to 3.5µm over the first 4 hours. Conversely there is a decrease in the particle count rate most likely due to settling and dissolution resulting in the number of particle in suspension declining. After 7 hours the particle number in suspension is insufficient for reliable analysis.

The environmental stability of NPs is heavily influenced by pH, particle size and surface area, although other factors (e.g. solution concentration and temperature) are also important (Borm et al., 2006, Miao et al., 2010). Thus seawater which is slightly alkaline (pH range 7.4-8), has high ionic strength, and high concentrations of anions (Cl^- and SO_4^{2-}) that can serve as binding ligands, will promote aggregation of NPs to relatively small clusters, which readily dissolve (Miao et al., 2010, Peng et al., 2011).

Dissolution kinetics vary amongst studies, likely resulting from the exact nature of the NPs used, concentrations and variations in experimental set-ups, but there is some consensus that ZnO NPs do dissolve, at least partially. Peng et al. (2011) predicted that

similarly synthesized ZnO NPs without surfactants (for example this study, Buffet et al. (2012) and Larner et al. (2012)) would form similarly sized aggregates in spite of differences in concentrations and morphologies. Such aggregates will display a similar external surface, which is directly related to the diffusion efficiency of the solute (aqueous Zn), and hence comparable dissolution kinetics are expected for particles that have similar characteristics (Borm et al., 2006, Peng et al., 2011).

In comparison, Larner et al. (2012) found that the ^{68}ZnO bulk particles did not reach equilibrium during dissolution studies (148 h) and <2% dissolution was observed. Again, high ionic strength media promotes aggregation and in the case of the larger bulk aggregates, result in rapid sedimentation. Such that the larger bulk aggregates would exhibit much lower rate of solubility than the smaller ^{68}ZnO NPs aggregates (Fabrega et al., 2011) and the fate of the ^{68}ZnO bulk particles would be to settle out from solution as aggregates whilst remaining largely insoluble.

4.3.3 Analytical precision

The control samples of water, snail tissue and diatoms showed a total (natural) variability of ~0.1% for the diagnostic ^{68}Zn/^{66}Zn isotope ratio (~0.663). A recent data compilation indicates that the total observed variability for ^{68}Zn/^{66}Zn in natural biological samples is ~0.25% (Larner and Rehkämper, 2012). In comparison, samples obtained from the exposure to ^{68}Zn-E in the present study were found to deviate from the natural ^{68}Zn/^{66}Zn ratio by at least 2% and up to more than 800%, Table 4.1 presents a summary of the analyses and calculated ^{68}Zn-E concentrations of the exposed samples. This demonstrates that natural isotopic variations have only a negligible impact on the isotopic data obtained for the exposed samples.

The use of MC-ICP-MS allows the rapid and routine determination of the ^{68}Zn/^{66}Zn isotope ratio to a precision of better than 0.05% in a single analysis consuming ~30 ng Zn. As the isotopic composition of both natural and ^{68}Zn-E are known Equation 4.2 can be used to quantify the amount of ^{68}Zn-E required to alter the natural isotope ratio by 0.15%, thereby

Table 4.1 Summary of analytical results and calculated concentrations obtained from the MC-ICP-MS analysis of experimental samples

	Aqueous ^{68}Zn exposure system				Bulk ^{68}ZnO exposure system				^{68}ZnO nanoparticle exposure system			
Sample	n	^{68}Zn /^{66}Zn ratio	Total [Zn]	[^{68}Zn-E]	n	^{68}Zn /^{66}Zn ratio	Total [Zn]	[^{68}Zn-E]	n	^{68}Zn /^{66}Zn ratio	Total [Zn]	[^{68}Zn-E]
Tissue			µg g^{-1}	µg g^{-1}			µg g^{-1}	µg g^{-1}			µg g^{-1}	µg g^{-1}
d1 exp	3	0.721 ± 0.011	95 ± 23	1.6 ± 0.3	3	0.698 ± 0.038	109 ± 14	1.1 ± 0.5	3	0.690 ± 0.007	126 ± 39	1.0 ± 0.3
d4 exp	1	0.847	147	7.5	1	0.902	132	8.6	1	0.745	119	2.8
d7 exp	3	0.996 ± 0.018	108 ± 24	9.6 ± 2.5	3	1.063 ± 0.031	121 ± 39	12.8 ± 5.0	3	0.807 ± 0.027	114 ± 27	4.6 ± 1.4
d1 ef	1	0.967	107	8.8	1	1.173	111	14.4	1	0.816	123	5.3
d2 ef	1	0.921	133	9.4	1	1.110	133	15.4	1	0.799	162	6.3
d4 ef	2	0.979 ± 0.050	109 ± 36	9.4 ± 4.4	1	1.001	155	14.0	1	0.791	151	5.5
d7 ef	1	0.858	149	8.1	1	1.095	101	11.4	1	0.806	119	4.8
d14 ef	1	0.867	155	8.7	1	1.341	101	16.7	1	0.827	116	5.3
d28 ef	2	0.932 ± 0.023	100 ± 1	7.3 ± 0.6	3	1.059 ± 0.229	118 ± 41	12.1 ± 6.1	3	0.814 ± 0.006	88 ± 38	3.7 ±1.6
Water			ng mL^{-1}	ng mL^{-1}			ng mL^{-1}	ng mL^{-1}			ng mL^{-1}	ng mL^{-1}
d1 exp	1	2.238	15.6	4.93	2	1.23 ± 0.14	21.7 ± 9.8	2.88 ± 0.80	2	1.221 ± 0.140	18.7 ± 0.7	2.5 ± 0.3
d4 exp	1	4.868	15.4	8.56	2	1.72 ± 0.02	14.4 ± 0.5	3.35 ± 0.11	2	2.283 ± 0.166	13.0 ± 2.1	4.1 ± 0.2
d7 exp	2	6.160 ± 0.162	15.9 ± 3.5	9.83 ± 2.04	2	1.70 ± 0.14	20.6 ± 4.2	4.68 ± 0.57	2	2.532 ± 0.505	18.3 ± 0.2	5.8 ± 0.3
d1 ef	2	2.114 ± 0.370	25.2 ± 7.2	7.28 ± 0.79	2	1.65 ± 0.15	30.0 ± 14.9	6.52 ± 2.55	1	1.576	21.7	4.6
d2 ef	1	2.036	15.4	4.44	2	1.40 ± 0.15	16.3 ± 0.6	2.91 ± 1.14	1	1.140	17.9	2.2
d4 ef	1	1.926	9.8	2.66	1	1.56	15.5	3.24	1	1.092	17.2	1.9
d7 ef	2	1.473 ± 0.164	16.0 ± 1.6	3.03 ± 0.20	1	1.29	15.6	2.40	1	0.945	20.0	1.5
d14 ef	1	1.324	15.7	2.55	2	1.87 ± 0.26	13.7 ± 1.0	3.55 ± 0.32	1	0.909	12.3	0.8
d21 ef	1	1.843	7.2	1.86	1	1.68	10.7	2.45	1	1.170	7.3	0.9
d28 ef	1	1.379	8.0	1.39	1	1.21	10.3	1.42	1	1.042	7.2	0.7
Shell Leachate[a]			ng mL^{-1}	ng mL^{-1}			ng mL^{-1}	ng mL^{-1}			ng mL^{-1}	ng mL^{-1}
d4 exp	1	2.248	80.4	25.56	1	1.076	81.9	8.84	1	1.3120	82.5	13.20
d1 ef	1	2.405	74.9	25.37	1	1.432	96.9	17.82	1	1.3300	96.6	15.80
d4 ef	1	1.713	79.7	18.77	1	1.025	114.5	10.98	1	1.1440	104.6	12.92
d14 ef	1	1.586	95.5	20.35	1	1.283	103.1	15.85	1	1.1500	87.6	10.93

Tissue, water and shell sample concentrations are shown for each of the treatment groups (aqueous ^{68}Zn, ^{68}ZnO NPs and ^{68}ZnO bulk particles). The analyzed control samples showed a natural ^{68}Zn/^{66}Zn ratio of 0.663. The n value denoted the number of individual analyses at that time-point, where triplicate groups were analyzed the data is presented as mean values ± 1sd. For tissue samples each n represents a pool of 25 individual snail sort tissues. The time point notation 'd' represents the number of days of exposure (exp) and efflux (ef) the samples have undergone. [a] The shell leachate concentrations are given as the amount of Zn per mL of the exposure media i.e. 25 mL.

exceeding the natural background variability and precision of the analysis. Such a perturbation of the $^{68}Zn/^{66}Zn$ isotope ratio can already be achieved by an increase of only 0.03% in the total Zn concentration from the addition of ^{68}Zn-E. The strength of this method is demonstrated when considering the contribution of ^{68}Zn-E in the samples was at least 2% to >60% of the total Zn, resulting in deviations in the isotope ratio 2-3 orders of magnitude above the required 0.15% (Figure 4.4). This demonstrates that the approach of stable isotope labeling offers high enough to enable detection even when exposures are conducted at low and environmentally realistic exposure concentrations

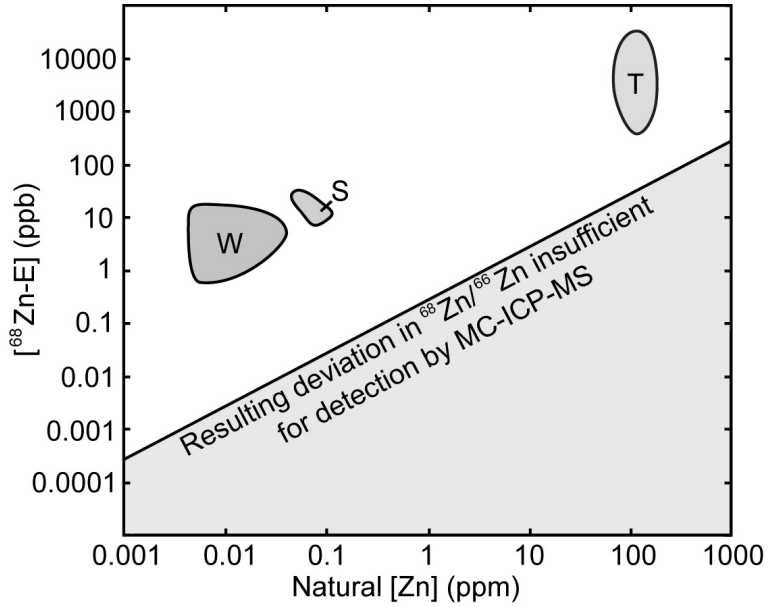


Figure 4.4 The use of high precision MC-ICP-MS in conjunction with stable isotope labelling offers tracing sensitivities orders of magnitude below traditional techniques. The plotted regions encompass data spread of the water (W, n = 70), shell leachate (S, n = 12) and tissue (T, n = 45) samples analyzed. Although the form of ^{68}Zn-E (aqueous, nano and bulk) differed between samples, analyses of water, shell leachate and water overlapped in terms of proportion of ^{68}Zn-E vs. natural Zn. The shaded region of the graph shows the level at which the contribution of Zn from an enriched source does not perturb the $^{68}Zn/^{66}Zn$ isotope ratio sufficiently to be distinguishable by MC-ICP-MS.

4.3.4 Measured exposure concentrations and the influence of the shell as a binding site

The waterborne exposure concentrations were verified by measuring the ^{68}Zn-E concentration of freshly prepared media prior to exposure (Day 0). These were found to be 20.1 ± 0.3, 16.2 ± 0.9 and 23.6 ± 6.3 µg L^{-1} for aqueous ^{68}Zn, ^{68}ZnO NP and ^{68}ZnO bulk exposures, respectively (n = 3, Figure 4.5). For each form this compared favorably with the nominal ^{68}Zn-E concentration of 20 µg L^{-1}. The ^{68}ZnO NP concentration was lower than

expected possibly due to heterogeneity in the prepared media. Waterborne ^{68}Zn-E concentrations decreased in all treatments following 24 h exposure, but rose steadily during the 7 d exposure period. After moving the snails to clean medium for efflux, ^{68}Zn-E concentrations in the water were not immediately reduced, but rather a steady decline was observed. Analysis of the shell leachate revealed that ^{68}Zn-E was recovered from the shell surface following exposures to each ^{68}Zn-E form (Figure 4.5). Shell leachate concentrations, represented as µg of ^{68}Zn-E L^{-1} of efflux water, remained relatively consistent during the analyzed time points of both the exposure and efflux stage; with ^{68}Zn-E concentrations of approximately 20-25, 10-15 and 7-20 µ g L^{-1} for aqueous ^{68}Zn, ^{68}ZnO NP and ^{68}ZnO bulk exposures, respectively (n = 4). During the 7 day exposure period, and particularly within the first 24 h, it is likely that the shell provided binding sites for Zn and reduced the amount bioavailable ^{68}Zn-E concentration within the water. The shells of marine gastropods have been shown to accumulate (primarily by sorption) substantial concentrations of Zn during 30 h waterborne exposures, where up to 77% of the total Zn body burden was found on the shell (Wang and Ke, 2002). The low concentrations of ^{68}Zn-E in the water samples analyzed from the efflux period likely result from the adsorption of ^{68}Zn-E to the shell's outer surface, rather than any significant elimination of accumulated ^{68}Zn-E by the snail. As discussed in the next section, the ^{68}Zn-E accumulated from all forms was eliminated extremely slowly.

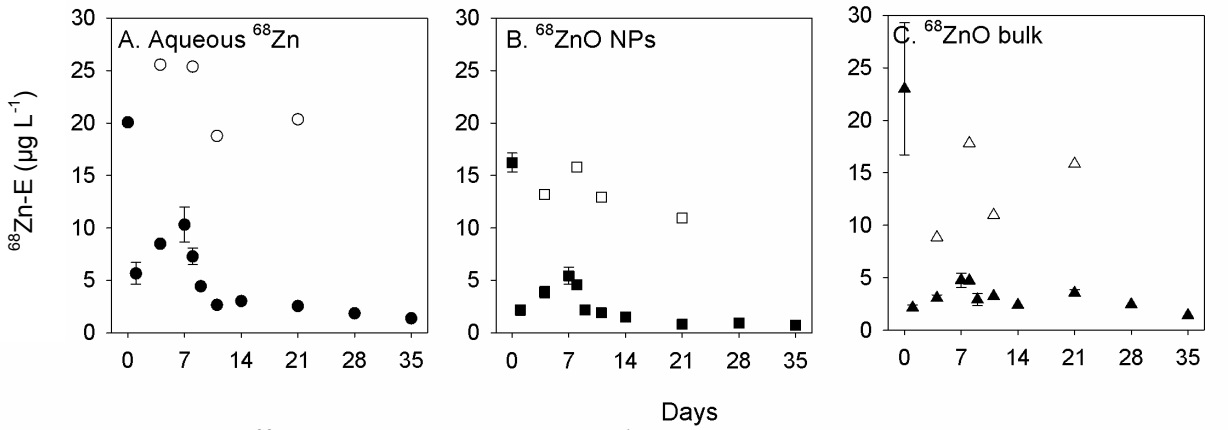


Figure 4.5 Total ^{68}Zn-E concentrations (µg L^{-1}, error bars where present are the standard deviation of duplicate or triplicate samples, else each symbol represents a single measure) in water samples (black symbols) and *P. ulvae* shell leachate (open symbols) for aqueous ^{68}Zn (A, circles), ^{68}ZnO NP (B, squares) and ^{68}ZnO bulk (C, triangles) treatments over the 35 d of the study, where the first 7 days were the exposure period followed by 28 d depuration. The day 0 point is the measured starting ^{68}Zn-E concentration in the exposure, nominally 20 µg L^{-1}.

4.3.5 Uptake and efflux dynamics of P. ulvae

All three forms of ^{68}Zn-E were available for uptake by *P. ulvae* during waterborne exposures at 20 µg L^{-1}. Unidirectional influx rates determined from the efflux-corrected tissue burdens revealed that ^{68}Zn-E presented as ^{68}ZnO NPs was the least available form, with an influx rate approximately 2-fold lower than that of aqueous ^{68}Zn, whilst ^{68}ZnO bulk particles were the most bioavailable (Figure 4.6). Analysis of covariance (ANCOVA) with a post-hoc Tukey's test demonstrated that the uptake rate for ^{68}ZnO NPs was significantly different to both aqueous ^{68}Zn and ^{68}ZnO bulk particle forms. The relatively high rate of influx following ^{68}ZnO bulk particle exposure is likely related to rapid agglomeration and limited dissolution within the estuarine water as discussed. The sedimentation of the bulk particle aggregates would render them unavailable for waterborne uptake, but highly available for ingestion. *P. ulvae* primarily feeds on particulate organic detritus and inorganic sediments by grazing over the sediment surface. Thus rather than a waterborne exposure, the uptake of the ^{68}ZnO bulk particles was presumably achieved primarily through diet. A similar finding was reported previously, where *C. volutator* was proposed to have fed on sedimented ZnO bulk particles leading to a reduction in growth that was not consistent with aqueous Zn exposures (Fabrega et al., 2011). The relative importance of the dietary exposure route, in comparison to a waterborne route, has been established in the literature for a number of metals and different aquatic species (Casado-Martinez et al., 2009, Griscom et al., 2002, Luoma et al., 1992). In addition the efficiency of Zn assimilation from ZnO NP aggregates mixed with diatom food was 86% in studies with the snail *Lymnaea stagnalis* and ingestion was likely to be the dominant uptake pathway (Croteau et al., 2011).

The uptake rates shown in Figure 4.6 were divided by the measured ^{68}Zn-E exposure concentrations to provide the uptake rate constants (k_u, Equation 4.12) for each form. Uptake rate constants of 0.042 L^{-1} g^{-1} d^{-1}, 0.074 L^{-1} g^{-1} d^{-1} and 0.085 L^{-1} g^{-1} d^{-1} were calculated for the ^{68}ZnO NP, aqueous ^{68}Zn and ^{68}ZnO bulk particle forms respectively. This would suggest that the bulk particles were more bioavailable than aqueous ^{68}Zn, which is more bioavailable than the ^{68}ZnO NPs. Larner et al. (2012) demonstrated that comparable

batches of ^{68}ZnO NPs were shown to undergo 60% dissolution (by weight) in estuarine water in 1-2 days. Thus, for the measured ^{68}Zn-E concentration of 16.2 ± 0.9 µg L^{-1} in the ^{68}ZnO NP exposure, it may be assumed that approximately 9.7 µg L^{-1} would be present as aqueous Zn. If this concentration is used to determine the uptake rate constant of the ^{68}Zn-E from the NP, a value of 0.070 L^{-1} g^{-1} d^{-1} is calculated, which is almost identical to the value derived from the aqueous ^{68}Zn exposures of 0.074 L^{-1} g^{-1} d^{-1}. This strongly suggests that the bioavailability of ^{68}Zn-E in NP from is linked to solubility and ZnO NPs do not deliver Zn to the snail until they have undergone, at least partial, dissolution.

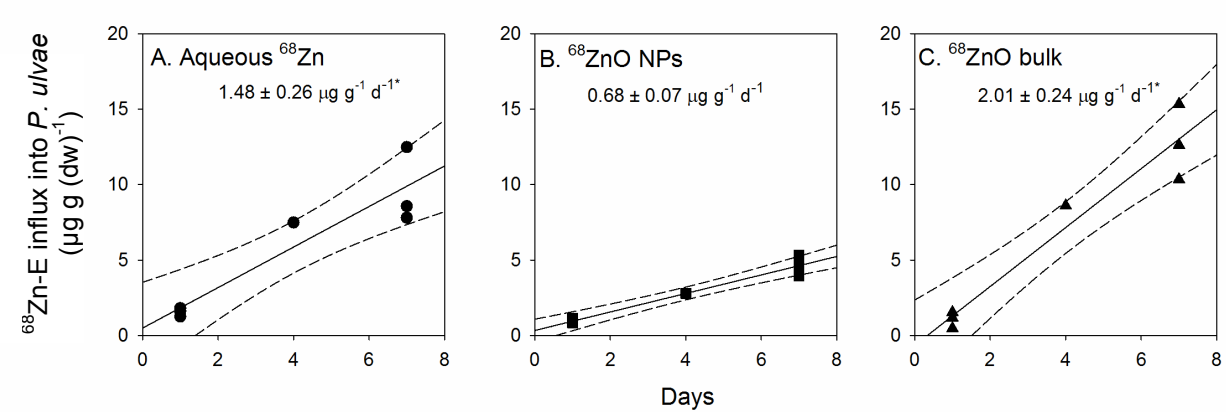


Figure 4.6 Unidirectional influx (i.e. uptake corrected for efflux) of aqueous ^{68}Zn (A, closed circles), ^{68}ZnO NPs (B, closed squares) and ^{68}ZnO bulk (C, closed triangles) into *P. ulvae* soft tissue during 7 d exposure to ^{68}Zn-E at nominal concentrations of 20 µg L^{-1}. Each symbol represents one pooled sample of 25 individual snails. The linear regression (solid line) presented with 95% confidence limits (dashed lines). The influx rates are shown for each form ± sd.

The ^{68}Zn-E accumulated from all sources was lost extremely slowly by *P. ulvae* during a 28 d depuration period. For all forms, efflux appeared to fit a one-component loss model, and there were no statistical differences between the efflux rate constants of each form (Figure 4.7, $p<0.05$, ANCOVA). However, the efflux rate constants (Equation 4.10*)* for ^{68}Zn-E accumulated following exposure to aqueous ^{68}Zn and ^{68}ZnO NPs were identical, with values of 0.012 ± 0.005 and 0.012 ± 0.007 d^{-1}, respectively, and are three-fold higher than that of ^{68}ZnO bulk particles at 0.004 ± 0.005 d^{-1}. Effectively, ^{68}Zn-E accumulated via aqueous and NP exposures were eliminated at a rate of 1.2% d^{-1}, whereas ^{68}Zn-E accumulated via the bulk exposure was lost at a slower rate of 0.4% d^{-1}. There are very few studies on the

efflux of Zn from saltwater gastropods and fewer still that involve NPs and bulk particles. However, those studies that have reported efflux rate constants show that elimination of ingested Zn generally occurs slowly. For *Babylonia formasae habei*, *Nassarius teretiusculus* and *Rapana venosa* the Zn efflux rate constants were 0.0057, 0.0138 and 0.0105 d^{-1}, respectively (Onat and Topcuoglu, 1999, Wang and Ke, 2002). Although these values were determined following dietary exposures, it has been demonstrated that neither exposure route (diet or water) nor form (ZnO NP or dissolved Zn) significantly altered the efflux rate constant in *Lymnaea stagnalis*, which remained at approximately 0.08 d^{-1} (Croteau et al., 2011). The consistency of the *L. stagnalis* loss rate constants between NP and dissolved forms, particularly following the ingestion of the NP would suggest Zn from the ZnO NP undergoes a similar physiological fate as Zn taken up as the dissolved form (Croteau et al., 2011).

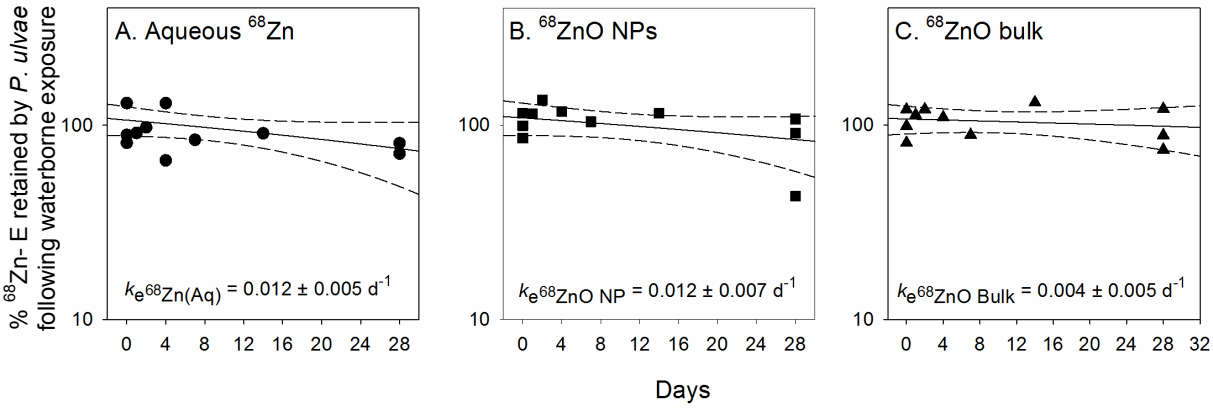


Figure 4.7 Proportional loss of ^{68}Zn-E from *P. ulvae* soft tissue over time following waterborne exposure to aqueous ^{68}Zn (A, closed circles), ^{68}ZnO NPs (B, closed squares) and ^{68}ZnO bulk (C, closed triangles). Each symbol (pooled sample of 25 individual snails) represents the ^{68}Zn-E concentration as a percentage of the of the total tissue concentration at day 0. For each form loss is described linearly (solid line) and is presented with 95% confidence limits (dashed lines). Efflux rate constants (k_e, ± sd) are presented for each form.

The identical uptake (when NP dissolution is accounted for) and loss rates constants of ^{68}Zn-E for *P. ulvae* exposed to aqueous and NP forms provides compelling evidence that ^{68}Zn-E from the ^{68}ZnO NP is both entering and eliminated from the snail as the aqueous form after the NPs have already undergone dissolution in the estuarine environment. Thus, the bioavailability of Zn from ZnO NPs when exposed via dispersion in water is primarily

dependent upon their solubility. However, when particulate Zn forms are large enough to be ingested, uptake is accentuated even beyond that of exposure to aqueous Zn. This study adds to the growing body of work which demonstrates that at environmentally realistic concentrations the environmental availability and toxicological impact of ZnO NPs is linked to their solubility when presented dispersed in estuarine water and that Zn can be delivered via larger aggregates with a higher efficiency probably via ingestion.

4.4 Conclusions

These results strongly suggest that solubility of ZnO NPs in exposure media is a key parameter that determines the availability of the Zn constituent. The ability to conduct environmentally relevant exposures, especially for a metal as abundant as Zn, was made possible by employing stable isotope tracing combined with high-precision mass spectrometry. This methodology enabled the highly sensitive detection of newly accumulated Zn even in the presence of high and variable backgrounds concentrations. This methodology is highly applicable in determining the bioavailability of metal containing NPs when the constituent metal is multi-isotopic.

4.5 Declaration

This work was designed and conceived by Adam Laycock (AL), Mark Rehkämper (MR) and Farhan Khan (FK). The isotopically labeled materials were synthesized and prepared by AL. Agnieszka Dybowska (AD) performed the characterization of the ZnO materials. The exposures were conducted by AL and FK. All sample preparation, analysis and data reduction was carried out by AL. Subsequent modeling and data interpretation was performed by AL and FK. MR supervised all aspects of work covered a Imperial College while Eva Valsami-Jones (EV) was the senior supervisor overseeing work conducted at the Natural History Museum.

Chapter 5:

Comparing earthworm uptake routes and rates for ionic Zn and ZnO nanoparticles at realistic environmental concentrations using stable isotope labeling

Abstract

The environmental behavior and toxicity of ZnO nanoparticles (NPs) has received much attention in recent years due to their novel properties and incorporation into consumer products. Previous studies have found differences in the uptake of Zn from soil by organisms when the element is introduced in dissolved and ZnO NP forms. Such work, however, was generally conducted at exposure levels that by far exceeded the predicted environmental concentrations (PECs) of ZnO NPs. This was necessary to circumvent detection problems, which are posed by the high Zn background concentrations of soils and biological tissues. To carry out an exposure at environmentally relevant conditions, we here employed Zn that was isotopically enriched to 99.5% in ^{68}Zn, to prepare isotopically labeled ^{68}ZnO NPs and a dissolved phase of ^{68}Zn. These materials were employed in an exposure to accurately assess and compare the uptake and elimination rate constants of the two Zn forms at relevant PECs by the earthworm *Lumbricus rubellus*. The standard test soil LUFA-Speyer 2.2 was dosed with isotopically enriched ^{68}Zn (^{68}Zn-E) to a concentration of 5 mg kg^{-1}. Sealed (dermal only uptake) and unsealed earthworms (dermal and oral uptake) were then introduced into the test soils and exposed for up to 72 hours to assess the uptake kinetics. Following the exposures, the Zn isotope compositions of the samples were analyzed by multiple collector inductively coupled plasma mass spectrometry. This enabled the detection of ^{68}Zn-E in earthworm tissue after only 4 hours of dermal exposure, when the uptake of ^{68}Zn-E had increased the total Zn tissue concentration by only 0.03‰. While unsealed worms took up ^{68}Zn-E much faster than sealed worms, the calculated uptake rate constants for the soils dosed with the two forms of Zn are identical within error for the two sets of worms. Furthermore, the elimination rate constants are identical within error for all worms and Zn treatments. This demonstrates that the major Zn uptake route of the earthworms is through ingestion. It also indicates that at realistic exposure concentrations there is no distinguishable difference between the uptake of Zn introduced as ZnO NPs and dissolved Zn by the earthworm *L. rubellus*.

5.1 Introduction

The novel properties exhibited by engineered nanoparticles (NPs) have resulted in these materials becoming increasingly prevalent in consumer products. Zinc oxide (ZnO) NPs, for example, have found use in sunscreens, cosmetics and paints due to their UV absorbance properties (Woodrow Wilson Centre, 2014, Auffan et al., 2009). The increased manufacture and use of engineered NPs will inevitably lead to a corresponding increase in their release into natural environments (Luoma, 2008). Engineered NPs are likely to end up in water treatment plants and be removed as part of the water treatment sludge, therefore in places where such sludge is applied to agricultural land it is expected that soils will be a major sink. Gottschalk et al. (2009) modeled predicted environmental concentrations (PECs) for ZnO NPs in European sewage treatment plant sludge of 17.1 mg kg^{-1}, resulting in annual fluxes of 3.25 μg kg^{-1} to sludge treated soils. Furthermore, PECs of 2.2 to 22 mg kg^{-1} and 3.2 to 32 mg kg^{-1} were modeled by Boxall (2007) for sewage treatment sludge and for sludge treated soils, respectively, assuming between 10% and 100% market penetration for ZnO NPs in sunscreens (Figure 5.1). These PECs are most likely to be over estimates as more recent work has demonstrated that once ZnO NPs enter natural systems they will be subject to rapid dissolution and changes and are therefore unlikely to persist (Bian et al., 2011). In comparison to these PECs natural Zn concentrations a typically much higher, a USGS survey determined Zn concentrations of between 10 and 113 mg kg^{-1} for 38 rural organic rich soils, away from sources of pollution and fertilizer use (Smith et al., 2005). A comparable UK countryside survey found a similar range of Zn abundances of 36 to 109 mg kg^{-1} (Emmett et al., 2010) (Figure 5.1). Taken together, these data imply that the concentrations of ZnO NPs in sewage treated soils are unlikely to exceed the natural Zn background levels and are likely to be significantly lower, by a factor of x10 or more (Figure 5.1). Despite of this, the unknown behavior and interactions of these materials in the environment has prompted studies to determine if NPs pose a risk.

Traditional methods for tracing and quantifying the presence of metal and metal oxide NPs in bulk natural samples commonly rely on elemental concentration

measurements. Such methods assume that an increase in the elemental concentration for an exposed organism or reservoir relative to a control is due to uptake of the element from the introduced material (Hooper et al., 2011, Hu et al., 2010). This approach can be readily applied when the natural background concentration of the element is low and constant in relevant samples. However, for ubiquitous elements that are found at high and variable concentrations, such as Zn, any uncertainties are magnified. For exposures with ZnO NPs, this necessitates that high doses are employed, such that uptake generated final Zn concentrations, which ideally exceed the natural background values by a factor of about x10 to x100. In this case, the variability of the Zn background can be neglected and uptake can be accurately quantified.

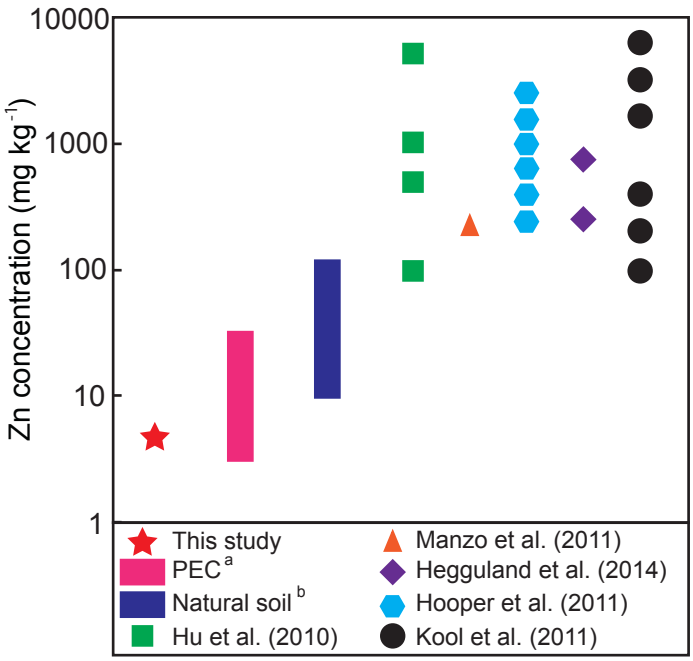


Figure 5.1 The exposure concentrations of Zn used in this study compared to previous studies and the ranges of the PECs for ZnO NPs in soils. [a] (Boxall, 2007) and natural soil Zn concentrations [b] (Emmett et al., 2010, Smith et al., 2005)

Data for published soil exposures with ZnO NPs are summarized in Table 5.1. All of these studies, with the exception of Hu et al. (2010), carried out comparable exposures with both ZnO NP and dissolved Zn. Three of the five studies (Heggelund et al., 2014, Hooper et al., 2011, Kool et al., 2011) concluded that the toxicity of dissolved Zn is greater, even though higher Zn body burdens were observed in the ZnO NP exposures (Hooper et al.,

2011). Based on this, it was suggested that the release of Zn ions from the dissolution of ZnO NPs was responsible for the observed toxic effects. This is supported by previous work, which showed that ZnO NPs are highly soluble in water (Bian et al., 2011). Although the role of dissolution is likely to be important, the interactions of ZnO NPs are expected to be more complex in soils as opposed to aquatic environments. For example, the fraction of ZnO NPs that dissolved in soil porewater was shown to increase slowly from <0.5% to <10% of total Zn during 12 months of soil aging (Kool et al., 2011). This slow increase in concentration may be a result of the pore water surrounding the NPs becoming saturated and limiting further dissolution as a result of the high dosing levels.

Table 5.1. Summary of published soil exposure studies

Author	Test organisms	Exposure concentration (mg kg^{-1})	Length of study	NP specific toxicity?
Hegguland et al., 2014	Eisenia fetida	238 – 2500	28 days	Yes
Hooper et al., 2011	Eisenia veneta	250 & 750	21 days	No
Hu et al., 2010	Eisenia fetida	100 – 5000	7 days	Yes
Kool et al., 2011	Folosomia candida	100 - 6400	28 days	No
Manzo et al., 2011	Lapidum sativum Vicia faba Heterocyipris incongruens Folosomia candida	230	8 days	Yes

Other investigations, however, obtained evidence for 'nano-specific' effects. For example, Manzo et al. (2011) found that ZnO NPs exert a higher toxic effect than dissolved Zn for some species. This finding is in agreement with the results of Hu et al. (2010), who propose that the production of reactive oxygen species (ROS), induced by the high surface area of NPs, can generate NP specific toxicity. Ma et al. (2011) also conclude that ZnO NPs induce toxicity via production of ROS as a result of exposure to UV radiation from sunlight. This effect is, however, not seen under artificial light and organisms that live in soil may not be affected due to the shallow penetration depth of UV radiation into soils (Gong et al., 2001).

Hooper et al. (2011) suggested that conservative risk assessments for ZnO NPs may be conducted if it is assumed that all Zn from the NPs are available in dissolved form. However, if nano-specific toxicity exists, as concluded by Hu et al. (2010) and Manzo et al. (2011), this may not be appropriate. All studies listed in Table 5.1 used exposure concentrations in the range of 100 to 6400 mg kg^{-1}. Clearly, these exposure levels by far exceed the PECs and, in most cases, also the natural Zn background contents of soils (Figure 5.1). Care must therefore be taken when considering the environmental relevance of these studies. In the case of Heggelund et al. (2014) and Kool et al. (2011), the spiking of soils with high Zn concentrations was shown to influence the soil chemistry and significantly change soil pH. At these conditions, the behavior of the ZnO NPs is unlikely to be representative of equivalent scenarios conducted at PECs.

Although biological uptake and accumulation of ZnO NPs in earthworms has been identified (Hooper et al., 2011, Hu et al., 2010), the kinetics have not been accurately assessed. Rather, effect levels are often reported to demonstrate the relative toxicity of ZnO NPs compared to dissolved Zn and/or larger ZnO particles (Heggelund et al., 2014, Kool et al., 2011, Manzo et al., 2011). The toxicity of metals in soil is not directly correlated to the total concentration alone, but also to the bioavailability. The latter is highly dependent on the elemental form and soil properties, which will also influence the uptake pathway by an organism. It is, therefore, important to investigate the bioavailability and kinetics of ZnO NPs at environmentally realistic concentrations and to constrain the route through which they enter the body. This information can then be used to evaluate if they pose any novel risks when present in soils. While toxicity studies such as those presented in Table 5.1 may be best performed and require high dosing concentrations, it is desirable to perform uptake studies to assess the biokinetics at environmentally realistic concentrations which may not place an organism under stress.

In this study, we compare the dietary and dermal uptake of Zn from soil by the earthworm *Lumbricus rubellus*. The Zn is hereby introduced to the soil in the form of ZnO NPs and dissolved $ZnCl_2$. Zinc is expected to enter earthworms via two main pathways – (i)

dermal uptake by direct contact with soil pore water, whereby it was shown that considerable exchange of water occurs across the body wall (Laverack, 1963), and (ii) dietary uptake of Zn and NPs adsorbed to soil particles, from the earthworm's burrowing behavior and digestion of organic soil constituents. Importantly, this was investigated at an environmentally relevant Zn exposure concentration of 5 mg kg^{-1} (Figure 5.1). By introducing the ZnO NPs at these low levels it is expected that they will undergo rapid dissolution that will not be restricted by saturated pore waters, as was likely the case of Kool et al., 2011. This will result in a similar exposure scenario to the soil dosed with dissolved Zn and therefore comparable uptake should be observed. The tracing and quantification of Zn at these low levels was made possible by the use of stable isotope labeling in conjunction with high precision isotope ratio analysis by multiple collector inductively coupled plasma mass spectrometry (MC-ICP-MS) (Larner and Rehkämper, 2012). This technique was previously successfully applied to aquatic exposures, such as in Chapter 4, where it enabled accurate quantification, even at low exposure concentrations (Khan et al., 2013, Larner et al., 2012). This is the first study to apply this approach to soils and terrestrial organisms.

5.2 Methods

5.2.1 Materials and reagents

The well characterized, Loamy sand standard test soil LUFA-Speyer 2.2 (Sp 2121, Germany, 2009), with a $pHCaCl_2$ of 5.5, a total organic carbon content of 2.09%, a cation exchange capacity of 10.0 meq/100 g and a water-holding capacity (WHC) of 46.5%, was used as the exposure medium. The soil was oven-dried at 60°C overnight prior to use, to eliminate undesired soil fauna.

Zinc that is artificially enriched in the ^{68}Zn isotope (^{68}Zn-E) from the natural abundance of 18.8% to 99.5% (Table 5.2), was purchased as a metal powder from Isoflex USA (USA) and used for the preparation of ^{68}ZnO NPs and $^{68}ZnCl_2$ salt. AnalaR grade concentrated 14.5 M HNO_3 and 6 M HCl were purified prior to dilution and/or use by sub-boiling distillation in a quartz still. Trace element grade Optima 28 M HF was purchased from

Fisher Scientific. Miilli-Q water of >18 MΩ cm quality (Millipore, UK) and 30% Suprapur H_2O_2 (VWR UK) were used throughout.

Table 5.2 Summary of isotope abundances and atomic weights of natural Zn and ^{68}Zn-E

Isotope	Atomic Mass[a] (g mol^{-1})	Isotope Abundances Natural Zn[a] (%)	^{68}Zn-E[a] (%)
^{64}Zn	63.9291	49.14	0.31
^{66}Zn	65.9260	27.78	0.33
^{67}Zn	66.9271	4.04	0.56
^{68}Zn	67.9248	18.43	98.78
^{70}Zn	69.9253	0.61	0.02
Atomic weight (g mol^{-1})[c]		65.3783	67.9007

[a] Atomic weights and natural Zn isotope abundances from NIST literature values (Audi et al., 2003, Bohlke et al., 2005) [b] Isotope abundances of ^{68}Zn-E provided by Isoflex [c]Multiplying the abundance of each isotope with its atomic mass and summing the results will give the atomic weight of a sample.

5.2.2 Synthesis and characterization enriched ^{68}Zn forms

A stock solution of dissolved ^{68}Zn-E was prepared by first dissolving a weighed amount of the ^{68}Zn-E metal in 6 M HCl. Subsequent evaporation to dryness left $^{68}ZnCl_2$ salt, which was taken up in water to produce a $^{68}Zn^{2+}$ stock solution with a Zn concentration of 743 mg L^{-1}.

The ^{68}ZnO NPs were synthesized by forced hydrolysis of Zn acetate in diethylene glycol (DEG), following the method of Dybowska et al. (2011). The ^{68}ZnO NPs that were applied in this study are from the same synthesis batch as those used by Khan et al. (2013) (Chapter 4), where full details of the preparation and characterization can be found. Briefly, ^{68}Zn-E acetate precursor material was first prepared from the ^{68}Zn-E metal. The acetate was dissolved in DEG, gently heated before water was added to force hydrolysis and the precipitation of ^{68}ZnO NPs. This reaction produced a ^{68}ZnO NP stock suspension with a Zn concentration of 743 mg L^{-1}. A vortexer was used to ensure homogenous distribution of the ^{68}ZnO NP in the DEG stock suspension before this was employed in the soil exposure.

The ^{68}ZnO NPs were analyzed by X-Ray Diffraction (XRD) to confirm the crystal structure by comparison with the ZnO standard ICDD [36-1451]. Based on TEM image analysis the particles were characterized as round and homogenous in nature with an average primary size of 7.8 ± 1.2 nm (n = 100). Dynamic Lights Scattering (DLS) analyses provided an average hydrodynamic diameter of 38.4 ± 0.7 nm. The hydrodynamic diameter determined by DLS is significantly larger than the TEM image analysis as the ZnO particles typically occurred as small aggregates when in the suspension. These results are consistent with previous studies, which also found that ZnO NPs can have primary particle sizes of <10nm when imaged by TEM and hydrodynamic diameters of ~40 nm when analyzed by DLS, following dilution in water (Buffet et al., 2012, Larner et al., 2012).

5.2.3 Preparation of the exposure medium

Eight replicate soil samples with 600 g dry weight each were prepared, three for treatment with ^{68}ZnO NPs and dissolved ^{68}Zn, respectively, and two control samples. The replicate ^{68}ZnO and dissolved ^{68}Zn soils were dosed individually by spreading out on a tray and adding 4.04 mL of the corresponding ^{68}Zn-E stock suspension/solution, such that ^{68}Zn-E was added at a concentration of 5 mg kg^{-1}. This is equivalent to the PEC, modeled by Boxall (2007), for sewage treated soils, assuming a 16% market penetration for ZnO NPs in sunscreens. To match the DEG concentration of the ^{68}ZnO NP spiked soils, 4.04 mL of DEG was added to the soils spiked with dissolved ^{68}Zn and one of the control samples. All but one of the soils hence had a final DEG concentration of 7.5 g kg^{-1}. A homogenous distribution of ^{68}Zn-E and DEG was achieved by thorough mixing with a spatula followed by the addition of water to achieve a moisture content of 27% (w/w), corresponding to 50% of the maximum WHC. The soils were then left to equilibrate for two days prior to the introduction of the earthworms.

The levels of DEG in the spiked soils are not expected to induce adverse effects in the exposed earthworms, however there is a lack of published data to confirm this. A report on the effects of ethylene glycol, which has a very similar molecular structure to DEG, was

shown to result in 25% mortality of the earthworm *Eisenia* fetida when exposed at a concentration of 20 mg kg^{-1} (Canadian environmental quality guidelines report, 1999). To investigate whether the presence of DEG at 7.5 g kg^{-1} had an observable effect on the behavior and mortality of *L. rubellus,* a separate one-week trial experiment was carried out prior to the main set of exposures.

5.2.4 Test organisms

The test organism used in this study was the earthworm *Lumbricus rubellus* and all specimens were reared in a laboratory culture at the Centre for Ecology and Hydrology (Wallingford, UK). Worms were kept in moist soil and fed with horse manure free of any pharmaceuticals. Two days prior to exposure, adult worms with developed clitellum and wet weights ranging from 1.08 to 2.25 g were transferred to clean Lufa 2.2 soil for acclimatization and kept in the dark at 50% of WHC, and a temperature of 12-14°C.

After 2 days acclimatization, 90 earthworms were rinsed with distilled water and blotted dry on filter paper, placed in petri dishes lined with moist filter paper and allowed to void their guts for a further 2 days. Six control earthworms were selected at this stage, which were used to confirm the natural Zn isotope composition of unexposed acclimatized earthworms. The remaining 84 acclimatized earthworms were split into 2 groups of 42. One of the groups was prevented from oral ingestion so that only dermal uptake through the body wall was possible. This was achieved by sealing the mouth parts with medical hystacryl glue (Braun aesculap, Germany) using the method described by Vijver et al. (2003). This involved removing mucus from the mouth region of the earthworms, before dipping into the glue. Earthworms were kept separate until the glue had dried, and then introduced into the test soil.

5.2.5 Experimental procedure and sampling

All soils were sampled once they had acclimatized prior to introduction of the earthworms. Samples of ~2 g were collected, whereby smaller aliquots were removed and

then combined to ensure representative sampling. The samples were oven dried at 60°C prior to preparation for Zn isotope analysis. Soil pore water was collected both prior to and following completion of the exposure period. To this end, ~30 g soil from each treatment were placed in 50 mL Falcon tubes. The tubes were centrifuged for 90 minutes at 4000 g before pipetting the pore water from the top of the tube. The pore water samples were then frozen for storage.

The uptake experiments were conducted in two stages over a period of six days, whereby earthworms were sampled after 4, 8, 24, 36, 48 and 72 hours. For the first exposure set, three sealed and unsealed earthworms, with a mean wet weight of 1.62 ± 0.21 g (1sd; range = 1.15 to 2.02 g), were added to each of the eight soil replicates described above. One sealed and unsealed earthworm were removed from the test soils dosed with ^{68}Zn-E after 4, 8 and 24 hours of exposure. Once the first exposure set had been completed, a second batch of three sealed and three unsealed earthworms, with a mean wet weight of 1.40 ± 0.25 g (1sd; range = 1.11 to 2.21 g) were added back into each test soils. For the second exposure set, one sealed and one unsealed earthworm were removed from each container at 36, 48 and 72 hours. The earthworms exposed to the control soils were removed after 72 hours.

The exposure soils were reused in this manner to most effectively use the amount of ^{68}ZnO NPs available, and the chosen procedure enabled a doubling of sampling time points. The 24 hour delay prior to the second exposure set is unlikely to have affected the properties of the soil, the test organisms or the ^{68}Zn-E compounds. No impact on the final results is, therefore, expected. Throughout the 6 day exposure, the behavior and appearance of the earthworms was recorded. After sampling, the earthworms were rinsed with water, blotted dry on filter paper and weighed. Subsequently, the unsealed earthworms were placed in petri dishes lined with a piece of moist filter paper and allowed to void their gut for 48 hours, with the filter paper being changed after 24 hours. For *L. rubellus*, egestion for 48 hours has been shown to be sufficient for depuration (Arnold and Hodson, 2007). The earthworms were then snap frozen, freeze-dried for 2 days and the dried tissue weighed.

5.2.6 Sample preparation

Sample preparation and chemical separation of Zn was carried out at the Imperial College MAGIC Laboratories in an ISO 6 clean room equipped with ISO 3 laminar flowhoods. The samples of earthworm, soil and pore water were prepared for microwave digestion in the following manner. Soil aliquots of 250 mg were weighed into 15 mL Teflon vials, 4 mL 14.5 M HNO_3 and 1 mL 28 M HF were added before placing on a hot plate at 90°C. The temperature was then raised to 190°C and the samples were left to reflux overnight, before evaporation to dryness. Water samples were thawed and centrifuged in 50 mL Falcon tubes at 10,000 rpm for 10 minutes to ensure removal of any remaining soil detritus. A 5 mL aliquot was then transferred to a clean 15 mL Teflon vial and evaporated to dryness. The dry soil and water samples were then taken up in 3 mL 14.5 M HNO_3, which were then transferred to individual TFM microwave digestion vessels. The whole dried and weighed earthworm samples were transferred directly to microwave digestion vessels without any pre-treatment. To these vessels 14.5 M HNO_3 was added to result in a final volume of 9 mL, to this 1 mL H_2O_2 was added, before leaving to stand at room temperature overnight.

The microwave vessels were transferred to an Ethos EZ microwave system (Analytix Ltd) (1200 W) where digestion was achieved by heating the samples to 200°C over 15 minutes and maintaining at this temperature for a further 15 minutes. Following digestion, the solutions were transferred to 15 mL Teflon vials, evaporated to dryness and re-dissolved in 1 mL 1 M HNO_3. All samples were then inspected to ensure that no digestion residues were present. For a few earthworm samples, small silica grains were observed in the solution, presumably because a small amount of soil had remained within the earthworms gut even after 48 hours of depuration. These samples were centrifuged at 13,000 rpm for 10 minutes in 1.5 mL centrifuge tubes and the clear solutions then decanted into clean Teflon vials.

Once clear solutions in 1 mL 1 M HNO_3 had been established for all samples, aliquots of 10 µl (1%), 200 µl (20%) and 1 mL (100%) were taken from the earthworm, soil

and pore water samples, respectively. The aliquots were transferred to clean Teflon vials, dried down with HCl to convert to chloride form and then taken up in 6 mL 1 M HCl, for chemical separation of Zn from matrix elements.

5.2.7 Chemical separation

Precise isotope ratio determination by MC-ICP-MS requires pure Zn sample solutions in order to avoid matrix effects and isobaric interferences (Rehkämper et al., 2004). To achieve this, the 1 M HCl sample solutions were processed through a one step anion exchange column chemistry procedure, as outlined by Arnold et al. (2010), in Chapter 4, and summarized in Table 5.3. The separation procedure was assessed by processing aliquots of the in-house 'London Zn' isotope reference solution (Arnold et al., 2010, Larner and Rehkämper, 2012). These experiments confirmed that near 100% recovery was achieved and analyses yielded Zn isotope compositions that were identical, within uncertainty, to analyses of unprocessed and untreated 'London Zn'.

Table 5.3 Zn chemical separation protocol

MP1 Resin Column Length – 25 mm, Internal Ø – 3.5 mm, Volume – 240 µl	
Clean Resin	16 mL 0.1 M HNO_3
	0.5 mL 18 MΩ water
Condition	4 x 0.5 mL 1 M HCl
Load Sample	6 mL 1 M HCl
Wash Matrix	3 x 1 mL + 5 mL 1 M HCl
Elute Zn	6 mL 0.01 M HCl

5.2.8 Isotopic analysis and data reduction

Once pure Zn samples were obtained, measuring solutions of samples and the London Zn reference material (Arnold et al., 2010) were prepared to a Zn concentration of 50 ng mL^{-1} in 0.1 M HNO_3. Care was taken to ensure that working solutions analyzed in the same measurement session were prepared using the same batch of acid and doped with equal amounts of a Romil Cu solution to 50 ng mL^{-1}.

The isotopic analyses were conducted at the Imperial College MAGIC Laboratories with a Nu Plasma HR MC-ICP-MS using methods outlined by (Larner and Rehkämper, 2012) and in Chapter 4. The measured $^{68}Zn/^{66}Zn$ ratios were hereby corrected for instrumental mass bias by external normalization relative to the admixed Cu (Larner and Rehkämper, 2012, Rehkämper et al., 2001). Each analysis consumed <1 mL of solution, equating to <50 ng Zn.

In an exposed sample, the diagnostic $^{68}Zn/^{66}Zn$ ratio (R_{meas}) is a function of the proportion of ^{68}Zn-E that is present relative to the natural Zn background, and the degree of isotopic enrichment (for the ^{68}Zn-E). If the isotope compositions of the enriched and the natural endmember are known (Table 5.2), the proportion of ^{68}Zn-E to total Zn (fr_{en}) in a sample can be calculated as:

$$fr_{en} = (({}^{68}Ab_{en} - (R_{meas} \times {}^{66}Ab_{en})) / ((R_{meas} \times {}^{66}Ab_{nat}) - {}^{68}Ab_{nat}) + 1)^{-1} \quad (5.1)$$

Here, 'Ab' with a prefix of '^{68}' or '^{66}' refers to the relative (molar) abundance of the corresponding isotope in ^{68}Zn-E or natural Zn, as identified by the suffix '$_{en}$' or '$_{nat}$', respectively. From the proportion of ^{68}Zn-E to total Zn, the abundance of each isotope of Zn In a sample can be calculated. For example, the isotopic abundance of ^{66}Zn in a sample ($^{66}Ab_{sam}$) can be determined by:

$$^{66}Ab_{sam} = (fr_{en} \times {}^{66}Ab_{en}) + ((1 - fr_{en}) \times {}^{66}Ab_{nat}) \quad (5.2)$$

In this study, the molar amount of ^{66}Zn for each sample (N-$^{66}Zn_{sam}$) was determined by comparing the measured ^{66}Zn ion beam intensity to a suitable calibration curve, whereby admixed Cu was used as internal standard. The total molar amount of Zn in the sample (N-Zn_{sam}) was then calculated by dividing the molar amount of ^{66}Zn in the sample by the isotopic abundance of ^{66}Zn (as determined with Equation 5.2):

$$N\text{-}Zn_{sam} = N\text{-}{}^{66}Zn_{sam} / {}^{66}Ab_{sam} \quad (5.3)$$

The molar amounts of ^{68}Zn-E (N-Zn$_{en}$) and natural Zn (N-Zn$_{nat}$) were derived from fr$_{en}$, the proportion of ^{68}Zn-E in the sample (Equation 5.1).

$$N\text{-}Zn_{en} = N\text{-}Zn_{sam} \times fr_{en} \quad (5.4)$$

$$N\text{-}Zn_{nat} = N\text{-}Zn_{sam} - (N\text{-}Zn_{sam} \times fr_{en}) = N\text{-}Zn_{sam} - N\text{-}Zn_{en} \quad (5.5)$$

The mass amounts of ^{68}Zn-E (M-Zn$_{en}$) and natural Zn (M-Zn$_{nat}$) in the sample were be determined by multiplying the molar amount by the corresponding atomic weight of enriched ^{68}Zn (AtWt$_{en}$) or natural Zn (AtWt$_{nat}$) (Table 5.2).

$$M\text{-}Zn_{en} = N\text{-}Zn_{en} \times AtWt_{en} \quad (5.6)$$

$$M\text{-}Zn_{nat} = N\text{-}Zn_{nat} \times AtWt_{nat} \quad (5.7)$$

In order to detect and quantify the presence of ^{68}Zn-E in a sample, the isotopic analysis must identify an analytically resolvable deviation from the natural ^{68}Zn/^{66}Zn ratio. The smallest clearly resolvable isotopic deviation in ^{68}Zn/^{66}Zn is thereby determined by both the precision of the analytical technique and the level of natural isotopic variability. The former is best defined by the between-run (external) precision of standard solution analyses, which typically featured a repeatability of better than ±0.10‰ (2sd). The latter is constrained by the data obtained for the control earthworm specimens, which provided a mean value with an uncertainty of ±0.13‰ (2sd, n = 8). Based on error propagation, a deviation in ^{68}Zn/^{66}Zn (between sample and natural value) of only 0.16‰ is therefore analytically resolvable at the 2sd level. This is equivalent to an increase in the total Zn concentration of a sample, from the addition of ^{68}Zn-E, of only 0.03‰. For example, the control samples had natural Zn concentrations of between 400 and 800 mg kg^{-1} for the earthworms, 15 mg kg^{-1} for soil and 10 µg L^{-1} for soil pore water. To create an analytically resolvable deviation in these samples, the addition of 0.01 to 0.02 mg kg^{-1}, 0.5 µg kg^{-1} and 0.3 ng L^{-1} of ^{68}Zn-E is therefore required, respectively.

5.2.9 Kinetic Modeling

The rate constants for Zn uptake (k_1, $g_{soil}\ g_{worm}^{-1}\ h^{-1}$) and elimination ($k_2$, h^{-1}) were estimated by applying a one-compartment first order kinetic model to the data for the 72 hour uptake phase (Janssen et al., 1991):

$$[^{68}Zn\text{-}E]_{worm} = (k_1/k_2)^* [^{68}Zn\text{-}E]_{soil} *(1- e^{-k2*t}) \quad (5.8)$$

Here $[^{68}Zn\text{-}E]_{worm}$ is the concentrations of ^{68}Zn-E in the earthworm tissue at a given time t (in hours), and $[^{68}Zn\text{-}E]_{soil}$ is the measured ^{68}Zn-E concentration of the dry soil. At the start of the exposure (t = 0 hr) C_{worm} = 0, as the earthworms contain only natural Zn. Significant differences between uptake and elimination rates for sealed and unsealed earthworms were compared using a generalized likelihood ratio test (Sokal and Rohlf, 1995). All analyses were run in the software package SPSS.

5.3 Results

5.3.1 Soil and pore water

The soill samples dosed with ^{68}ZnO NP and dissolved ^{68}Zn had measured dry weight ^{68}Zn-E concentrations of 3.38 ± 0.84 mg kg^{-1} (1sd, n = 4) and 3.44 ± 0.94 mg kg^{-1} (1sd, n = 4), respectively (Table 5.4). These concentrations are identical, within uncertainty, and show a recovery of >70% with respect to the ^{68}Zn-E exposure concentration of 5 mg kg^{-1}. The pore water samples that were collected after 2 days of acclimatization from soils spiked with ^{68}ZnO NPs and dissolved ^{68}Zn, had ^{68}Zn-E concentrations of 57.8 ± 14.5 µg L^{-1} (1sd, n = 4) and 51.9 ± 7.6 µg L^{-1} (1sd, n = 4), respectively. At the end of the 6 day experiment, the concentrations had increased to 96.5 ± 6.3 µg L^{-1} (1sd, n = 5) and 120 ± 6 µg L^{-1} (1sd, n = 4) for the ^{68}ZnO NP and the dissolved ^{68}Zn exposure, respectively (Table 5.4, Figure 5.2). The control samples, as would be expected, all show $^{68}Zn/^{66}Zn$ isotope ratios that are within the expected natural variability and natural Zn concentrations that are comparable to the exposed samples (Table 5.5)

Table 5.4 Summary of key exposure parameters and experimental results obtained in this study

		^{68}ZnO NP exposure				**Dissolved ^{68}Zn exposure**		
	n	^{68}Zn /^{66}Zn ratio	Total [Zn]	[^{68}Zn-E]	n	^{68}Zn /^{66}Zn ratio	Total [Zn]	[^{68}Zn-E]
Unsealed Earthworm Tissue			mg kg^{-1}	mg kg^{-1}			mg kg^{-1}	mg kg^{-1}
4 hr	2	0.6642 ± 0.008	786 ± 25	0.23 ± 0.12	2	0.6684 ± 0.0039	525 ± 164	0.69 ± 0.39
8 hr	1	0.6646	936	0.44	1	0.6727	363	1.03
24 hr	1	0.6715	889	2.19	1	0.6705	733	1.59
36 hr	2	0.6870 ± 0.0214	753 ± 658	3.22 ± 0.10	2	0.6877 ± 0.0090	614 ± 119	4.29 ± 0.66
48 hr	3	0.6775 ± 0.078	1201 ± 489	4.45 ± 0.71	3	0.6830 ± 0.0092	778 ± 351	4.00 ± 0.69
72 hr	3	0.6977 ± 0.0065	577 ± 195	5.58 ± 0.93	2	0.6931 ± 0.0152	855 ± 329	6.33 ± 0.32
Sealed Earthworm Tissue			mg kg^{-1}	mg kg^{-1}			mg kg^{-1}	mg kg^{-1}
4 hr	2	0.6633 ± 0.0000	610 ± 83	0.03 ± 0.02	2	0.6633 ± 0.0000	611 ± 351	0.04 ± 0.04
8 hr	1	0.6633	506	0.04	1	0.6638	312	0.07
24 hr	1	0.6633	1235	0.09	1	0.6641	589	0.18
36 hr	1	0.6643	372	0.13	1	0.6640	713	0.19
48 hr	1	0.6646	504	0.23	1	0.6637	1106	0.21
72 hr	2	0.6642 ± 0.0003	818 ± 243	0.22 ± 0.05	2	0.6642 ± 0.0002	937 ± 457	0.29 ± 0.12
Soil			mg kg^{-1}	mg kg^{-1}			mg kg^{-1}	mg kg^{-1}
0 hr	4	1.5776 ± 0.1534	15.9 ± 2.6	3.38 ± 0.84	4	1.4300 ± 0.1901	15.9 ± 2.6	3.44 ± 0.94
Pore Water			µg L^{-1}	µg L^{-1}			µg L^{-1}	µg L^{-1}
0 hr	4	13.9966 ± 3.5378	72.0 ± 14.5	57.8 ± 14.5	4	13.2652 ± 1.7515	65.5 ± 8.1	51.9 ± 7.6
72 hr	5	13.1583 ± 0.2552	122 ± 8	96.5 ± 6.3	4	14.1575 ± 1.8955	149 ± 6	119 ± 6

n = number of individual samples analyzed; where multiple individuals were analyzed the data in the table are given as averages ± 1sd.

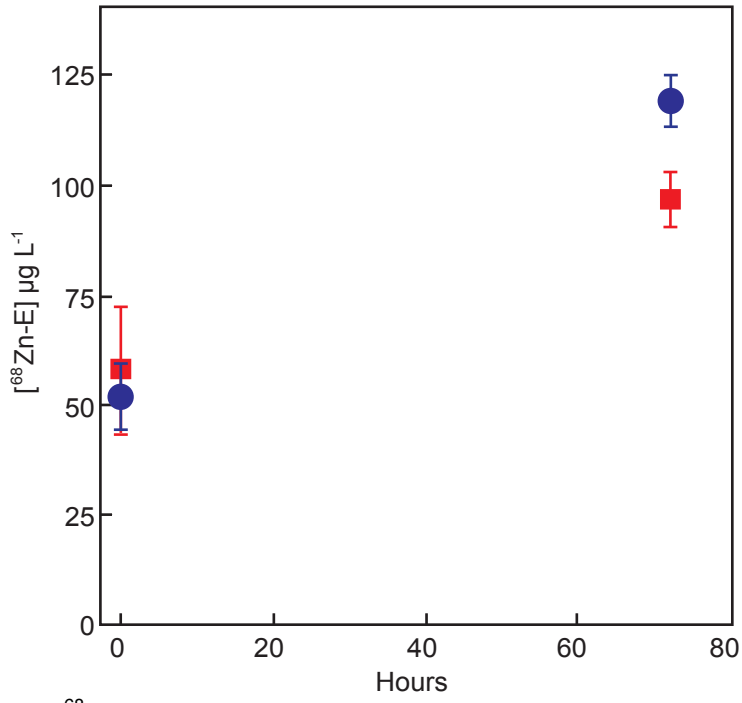


Figure 5.2 Enriched ^{68}Zn concentrations in soil pore waters of the soils dosed with ^{68}ZnO NPs (red squares) and dissolved ^{68}Zn (blue circles).

Table 5.5 experimental results from analyzed control samples.

Sample type	n	^{68}Zn/^{66}Zn ratio (±1sd)	Total [Zn] (±1sd)
Earthworm	8	0.6631 ± 0.0001	708 ± 306 mg kg^{-1}
Soil	2	0.6632 ± 0.0000	13.6 ± 2.9 mg kg^{-1}
Pore water	1	0.6635	10 µg L^{-1}

n = number of individual whole earthworms analyzed

5.3.2 Earthworms

There was no mortality of earthworms over the exposure period. Furthermore, the behavior and appearance of earthworms in the ^{68}Zn-E and DEG dosed soils did not differ from those observed in the non-dosed control samples, both for the 7 day pre-trial and the main exposure.

Detection of ^{68}Zn-E in the earthworm tissues was achieved for all exposed organisms, and, accurate quantification of ^{68}Zn-E was possible even after only 4 hours of dermal exposure, when the contribution of ^{68}Zn-E to total Zn was as little as 0.03‰. Figure 5.2 demonstrates that the majority of exposed earthworms had ^{68}Zn-E concentrations that were orders of magnitude above the minimum detection levels discussed in section 5.2.8. In general, the samples exposed for longer periods of time displayed higher levels of ^{68}Zn-E (Table 5.4, Figure 5.4).

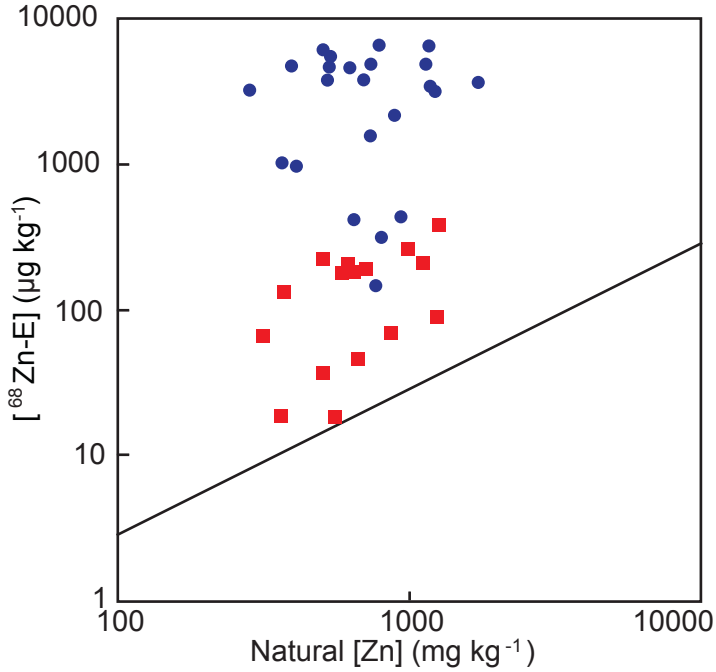


Figure 5.3 The concentration of natural Zn and ^{68}Zn-E in the samples analyzed. Where blue circles and red squares represent exposed unsealed and sealed earthworms, respectively. The black line represents the smallest amount of ^{68}Zn-E that is analytically resolvable by change in the ^{68}Zn/^{66}Zn isotope ratio, when measured by MC-ICP-MS

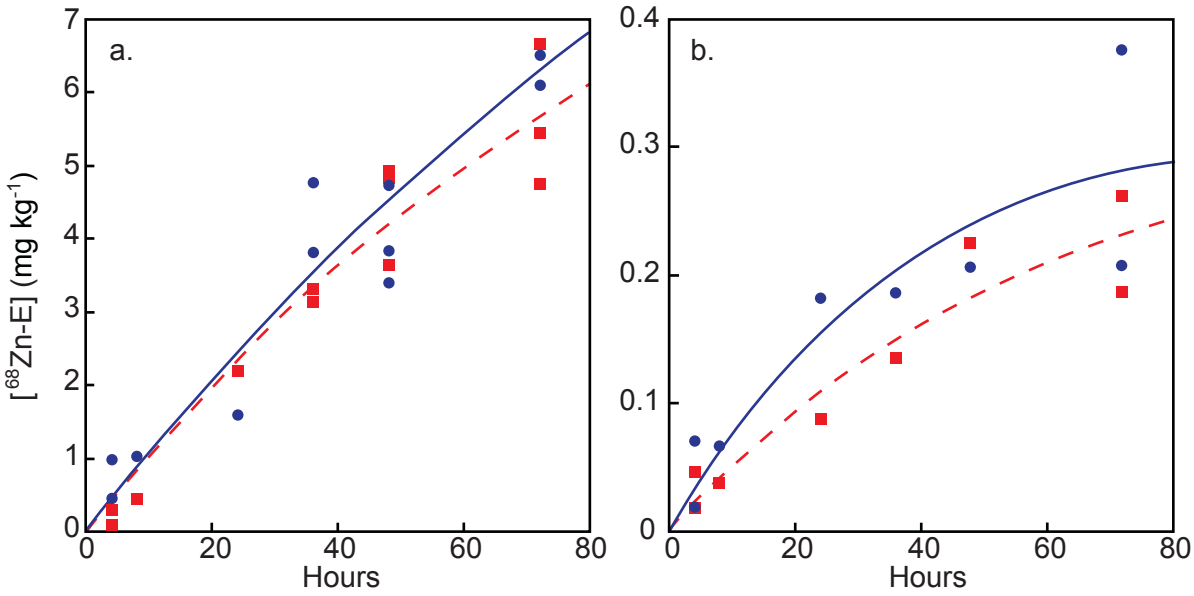


Figure 5.4 ^{68}Zn-E concentrations in earthworms exposed to ^{68}ZnO NPs (red squares and dashed line) and dissolved ^{68}Zn (blue circles and solid line). a) Unsealed earthworms (dermal and oral uptake). b) Sealed earthworms (dermal uptake only). The best fit lines were calculated using the modeled results and the uptake and elimination rate constants given in Table 5.7

The uptake and elimination rate constants were calculated from the isotopic data (Table 5.4), using a one-compartment model (Equation 5.8). For the unsealed earthworms (oral and dermal uptake) exposed to ^{68}ZnO NPs, uptake (k_1) and elimination (k_2) rate constants of 0.032 ± 0.005 g_{soil} g_{worm}^{-1} h^{-1} and 0.009 ± 0.006 h^{-1} were calculated (all uncertainties are ± 1sd). Comparable rate constants were found for the unsealed earthworms exposed to dissolved ^{68}Zn, with results of k_1 = 0.031 ± 0.006 g_{soil} g_{worm}^{-1} h^{-1} and k_2 = 0.006 ± 0.007 h^{-1}. Much lower uptake but similar elimination rate constants were determined for the exposures with sealed earthworms (dermal uptake only). These provided results of k_1 = 0.0016 ± 0.0004 g_{soil} g_{worm}^{-1} h^{-1} and k_2 = 0.016 ± 0.011 h^{-1} for the ^{68}ZnO NP exposures and of k_1 = 0.0025 ± 0.0009 g_{soil} g_{worm}^{-1} h^{-1} and k_2 = 0.026 ± 0.017 h^{-1} for the dissolved ^{68}Zn exposures (Table 5.6). The generalized likelihood ratio test demonstrated that there was no significant difference between the uptake and elimination rate constants calculated for the two forms of ^{68}Zn-E and for exposures with both the unsealed and sealed worm specimens.

Table 5.6 Calculated uptake (k_1) and elimination (k_2) rate constants

^{68}ZnO NP exposure			Dissolved ^{68}Zn exposure		
k_1, (g_{soil} g_{worm}^{-1} h^{-1})[a]	k_2, (h^{-1})[a]	R^2	k_1, (g_{soil} g_{worm}^{-1} h^{-1})[a]	k_2, (h^{-1})[a]	R^2
Unsealed Earthworm					
0.032 ± 0.005	0.009 ± 0.006	0.946	0.031 ± 0.006	0.006 ± 0.007	0.919
Sealed Earthworm					
0.0016 ± 0.0004	0.016 ± 0.011	0.917	0.0025 ± 0.0009	0.026 ± 0.017	0.843

[a] Uptake and elimination rates errors are ± 1sd.

The ^{68}Zn-E concentrations of earthworm tissue were modeled for an exposure period of 30 days for both ^{68}Zn-E forms using the calculated rate constants (Table 5.6, Figure 5.5). The results for dermal only uptake indicate that steady state ^{68}Zn tissue concentrations of ~0.3 mg kg^{-1} are reached after approximately 1 week in exposures to both ZnO NP and dissolved Zn. A longer period of 2 to 3 weeks is required until a dynamic equilibrium is achieved for the exposures with dermal and dietary accumulation. In this case, the modeling suggests steady state ^{68}Zn tissue concentrations of ~11.5 mg kg^{-1} and ~16.5 mg kg^{-1} for the ^{68}ZnO NP and dissolved ^{68}Zn exposures, respectively (Figure 5.5).

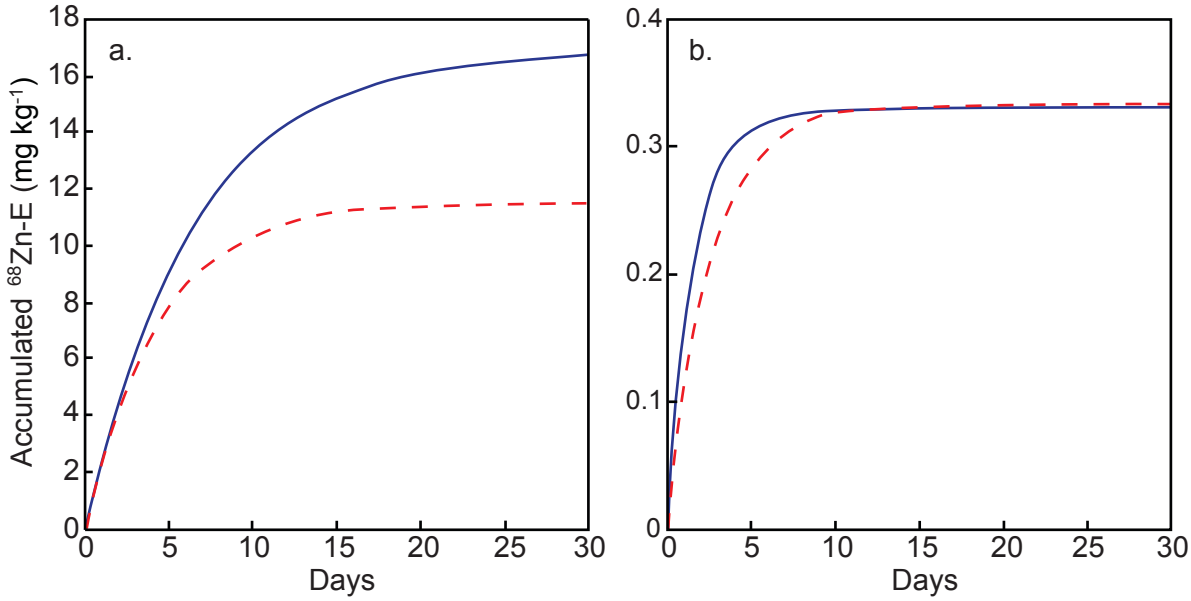


Figure 5.5 Modeled ^{68}Zn concentrations from uptake of ^{68}Zn introduced as ^{68}ZnO NPs (red dashed line) and dissolved ^{68}Zn (solid blue line) over a period of 30 days using the uptake and elimination rate constants calculated from the 72 hour exposure in a) Unsealed earthworms (dermal and oral uptake) b) Sealed earthworms (dermal uptake only)

The modeled tissue concentrations were subsequently applied to calculate bioaccumulation factors (BAFs) and bioconcentration factors (BCFs). To this end, the inferred ^{68}Zn-E tissue burden from the modeling was divided by the concentration of ^{68}Zn-E in the soil and the pore water (as measured after 72 hr of exposure), respectively (Table 5.7). These calculations provided BAFs of 0.10 for sealed earthworms exposed to either form of Zn, and 3.40 and 4.86 for unsealed earthworms when exposed to ZnO NPs and dissolved Zn, respectively. Furthermore, BCFs of 3.5 and 2.8 were calculated for the sealed earthworms, and of 119.1 and 139.4 for the unsealed earthworms, following exposure to ZnO NPs and dissolved Zn respectively (Table 5.7).

Table 5.7 Bioaccumulation factors (BAFs) and bioconcentration factors (BCFs) calculated from the modeled ^{68}Zn concentration data of Fig. 5.4 (see text for details).

	ZnO NPs		Dissolved Zn	
	BAF	BCF	BAF	BCF
Dermal uptake	0.10	3.5	0.10	2.8
Dermal & oral uptake	3.40	119.1	4.86	139.4
Hegguelund et al., 2014 [a]	0.48	77.7	0.39	31.2

[a] Average BAFs and BCFs from 'medium pH soil'

5.4 Discussion

5.4.1 Zn Behavior in Soil

After the 2 day acclimatization period, the ^{68}Zn-E concentrations in the two exposure systems (dissolved ^{68}Zn and ^{68}ZnO NP dosing) were identical within error in the case of both soils and pore waters (Table 5.4, Figure 5.2). This suggests a comparable partitioning behavior for the two forms of Zn, with similar amounts binding to the available soil surfaces and entering the pore water phase. After the 6-day exposure period, the ^{68}Zn-E concentration of the pore water had increased for both treatments, whereby the endpoint concentration was ~24% higher when dissolved ^{68}Zn was added (Table 5.4). This supports the suggestion that the NPs underwent rapid dissolution during the acclimatization period and that the two forms of Zn display similar behavior and partitioning within the soils when present at environmentally relevant concentrations.

These results can be compared to the study of Heggelund et al. (2014), where soils were dosed with ZnO NPs and $ZnCl_2$ at much higher Zn concentrations of 238 mg kg^{-1} to 2500 mg kg^{-1}. After acclimatization for 10 days, these workers found that soils treated with $ZnCl_2$ had pore water Zn concentrations that were 20-50 fold higher compared to equivalent soils dosed with ZnO NPs. The largest differences were hereby seen at high levels of Zn addition. This suggests that the difference in Zn partitioning observed by Heggelund et al. (2014) is (i) a consequence of the high Zn dosing levels that were employed, and (ii) not characteristic of the Zn behavior observed at the lower, environmentally relevant, concentrations used here.

It was, furthermore, observed in previous studies, that the treatment of soils with high concentrations of ZnO NPs or dissolved Zn can both increase or decrease the soil pH (Heggelund et al., 2014, Kool et al., 2011). Such changes in pH will have an impact on soil properties, hence making it difficult to assess the relevance of any effects and toxicity, which are induced by the ZnO NPs. In contrast, the low Zn dosing levels employed in this study, are not expected to have any impact on the soil chemistry.

5.4.2 Zn Uptake and accumulation

In this study, the uptake of the two ^{68}Zn-E forms by the earthworm *L. rubellus* yielded essentially indistinguishable results. However, accumulation of ^{68}Zn-E in the unsealed worms leads to ^{68}Zn-E tissue concentrations that are about a factor of x20 higher than in sealed specimens (Figure 5.4, Table 5.4). This demonstrates that ^{68}Zn-E from ZnO NPs is bioavailable and that oral ingestion constitutes the major uptake pathway, whilst uptake through the body plays a minor but significant role (~5% of total uptake). Further investigation of the kinetics revealed that the uptake rate constants for ^{68}Zn-E by *L. rubellus* are also an order of magnitude higher for the unsealed than sealed worms, but are identical within error for the two forms of ^{68}Zn-E. In contrast, the elimination rate constants are indistinguishable regardless of ^{68}Zn-E form and uptake pathway (Table 5.6).

The similarity observed in the tissue accumulation and uptake kinetics for the two ^{68}Zn-E forms is presumably related to the low dosing concentrations that were employed. In particular, the dissolution of ^{68}ZnO NPs over the 2 day acclimatization period is likely to have produced exposure conditions similar to those established in soils treated with dissolved ^{68}Zn, this is supported by the similarity of the ^{68}Zn-E concentrations in the soil pore waters (Figure 5.2). In contrast dissolution may be limited when higher concentrations of ZnO NPs are employed, due to the pore water surrounding the NPs approaching or achieving saturation. The findings of Heggelund et al. (2014) and Hooper et al. (2011) are relevant in this context, as they reported higher Zn tissue concentrations for earthworms exposed to ZnO NPs as opposed to dissolved Zn, when high dosing levels were employed. This observation was attributed to direct internalization of ZnO NPs by the organisms, which may deliver nano-specific toxicity. However, in this study exposures to the two ^{68}Zn-E forms yielded identical internal ^{68}Zn-E concentrations. This suggests that there is a fundamental difference in the Zn uptake pathways that are relevant when ZnO NPs are present at high and low levels in soils. In particular, this may reflect more rapid and/or complete dissolution of the NPs within the soil at low concentrations, such that discrete particles are not available

for uptake by organisms, whereas in the high concentration exposures NPs were observed to be taken up directly.

Vijver et al. (2003) also assessed the dermal uptake pathway of metals by the earthworm *L. rubellus*. These workers found that dermal uptake accounted for 21% and 30% of total Zn uptake in exposures with two contaminated field soils that had Zn concentrations of 732 mg kg^{-1} and 2092 mg kg^{-1}, respectively. Further understanding of the dermal uptake route can be gained by combining the data of Vijver et al. (2003) with the results of the current study. In particular, this combined dataset reveals a positive correlation between the proportion of Zn uptake via the dermal route and the Zn concentration of the pore water relative to the soil (Figure 5.6). This correlation may indicate that it is Zn associated with the pore water, which is primarily available for dermal uptake. Furthermore, the BCFs of 3.5 and 2.8 that were determined here for the sealed earthworms are similar to the BAFs for the unsealed specimens (Table 5.7). This also supports the conclusion that it is primarily Zn associated with pore water, which is available for dermal uptake by the earthworms.

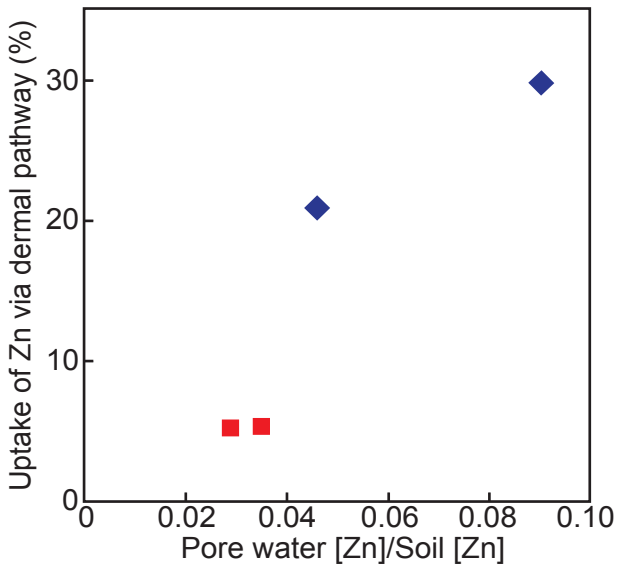


Figure 5.6 The proportion of dermal to total uptake of Zn vs the Zn concentration of porewater relative to soil. The red squares and blue diamonds represent data from this study and Vijver et al. (2003) respectively.

Heggelund et al. (2014) also reported BAFs and BCFs based on exposures that were conducted at the EC_{50} concentrations of ZnO NPs and $ZnCl_2$, using the total Zn concentrations determined for earthworm tissue, soils and pore water. These results cannot be directly compared to the data reported here, as our study focuses solely on the mass balance of the added ^{68}Zn-E, whilst the natural Zn background is ignored. The values calculated as part of this study are arguably more relevant as only the added ^{68}Zn-E is considered and this was dosed at low, environmentally relevant concentrations. The BAFs of 0.48 and 0.39 that were reported by Heggelund et al. (2014) for exposures with ZnO NP and dissolved Zn, respectively, are much lower than our results of 3.40 and 4.86 for equivalent experiments (Table 5.7). Heggelund et al. (2014) interpret BAFs of <1 as the earthworms being under stress at the high Zn concentrations and attempting to regulate metal uptake. This would suggest that the values of >1 observed here indicate that the earthworms were scavenging and retaining metals from the environment and not in a state of regulating excess Zn. However this difference is likely to be at least partly due to BAFs being calculated using added Zn only as opposed to total Zn, and the low concentrations used in this study.

The indistinguishable bioavailability and accumulation of Zn from ZnO NPs and dissolved Zn found in this study reinforces the study of Hooper et al. (2011), who suggested that risk assessments can assume that the Zn introduced by ZnO NPs is available in ionic form. However, our data does not unequivocally demonstrate in which form the ^{68}Zn-E enters earthworm tissue when ^{68}ZnO NPs are present. If ^{68}ZnO NPs, or specific forms of ^{68}Zn which are derived from the NPs, are internalized, this could possibly lead to nano-specific effects, which may only be evident in chronic or repeated exposures. Further work is hence necessary, which investigates (i) the chemical transformation experienced by different forms of Zn in relevant natural environments and (ii) in which forms Zn is available to and taken up by.

5.5 Conclusions

The results of this study clearly demonstrate the advantages of using an enriched stable isotope label for tracing purposes. Here, it has enabled a detailed characterization of the uptake of Zn from ZnO NPs and dissolved $ZnCl_2$ by earthworms, when these were employed at an environmentally relevant exposure concentration of 5 mg kg^{-1} in soil. The level of sensitivity provided by the methods was sufficient to allow quantification of even very small fluxes, such as the dermal Zn uptake by earthworms after only four hours of exposure.

The major pathway for uptake of Zn into earthworm tissue was by oral ingestion, with dermal uptake accounting for ~5% of the total accumulation. In addition, it is primarily Zn associated with pore water, which is available for dermal uptake. Importantly, the results of this study demonstrate that the behavior and bioavailability of ZnO NPs, when introduced at an environmentally relevant concentration, are indistinguishable from dissolved Zn, regardless of the uptake pathway. Some of the results presented in this study do not correlate well with similar exposure studies where higher exposure concentrations were used. This is an important finding, which indicates that concentration dependent effects must be taken into consideration in such investigations.

5.6 Declaration

The work presented in this chapter was designed and conceived by Adam Laycock (AL) and Mark Rehkämper (MR) from Imperial College and Claus Svendsen (CS) and Maria Diez-Ortiz (MD) from The Centre for Ecology and Hydrology. AL synthesized and prepared the isotopically labeled material. MD conducted the soil exposures with earthworms and collected the relevant samples. All sample preparation, isotopic analysis, data reduction and biodynamic modeling was carried out by AL. MR supervised the aspects of work performed by AL at Imperial College while CS supervised the work performed by MD at the Centre for Ecology and Hydrology.

Chapter 6:

Summary

6.1 Thesis summary and conclusions

The aim of this thesis was to develop the technique of stable isotope tracing for engineered nanoparticles (NPs). The primary motivation was to achieve detection capabilities that are sufficiently sensitive, such that these materials can be quantified in complex natural samples, even when exposures are conducted at predicted environmental concentrations. Prior to performing such exposures, it is important to (i) carefully evaluate the detection capabilities that are achievable for a specific isotope, isotope enrichment and analytical procedure, and (ii) identify an appropriate technique to produce the desired isotopically labeled NPs. These considerations were examined in Chapters 2 and 3 for CeO_2 and Ag NPs, respectively.

In Chapter 2, commercially available CeO_2 NPs were found to display only a limited variability of less than 0.25‰ in the $^{142}Ce/^{140}Ce$ isotope ratio and were also isotopically indistinct from other commercial sources of Ce. Thus, these materials do not possess a sufficiently unique and hence traceable isotopic signature. However, the use of stable isotopes offers a powerful tool for the detection and tracing of engineered CeO_2 NPs, if the particles are synthesized from material that is artificially enriched in a single stable Ce isotope. The best results, in terms of detection and quantification, are offered when enriched isotopes with low natural abundances are used, and when sample analysis is conducted with high precision instrumentation. Under such conditions, it was found that an increase of 0.02‰ in the total Ce concentration from the addition of an enriched ^{136}Ce or ^{138}Ce isotope label, would be sufficient for their detection. However, the high cost associated with enriched isotopes that have a low natural abundance means that the more affordable ^{140}Ce isotope label is likely to be favorable for most applications. The detection of an enriched ^{140}Ce isotope label is still already possible when the Ce concentration is increased by only 0.7‰, with the cost being approximately x100 lower than the enriched ^{136}Ce or ^{138}Ce isotopes.

Also presented in Chapter 2 are optimized methods for the preparation and analysis by multiple collector ICP-MS of samples generated from environmental screening studies.

These methods are validated through the controlled dosing of natural samples with an enriched ^{140}Ce isotope spike.

To apply stable isotope labeling to NPs it is first necessary to have specifically optimized synthesis protocols. Such protocols will ideally be small-scale and reliable, whilst providing high yields. These factors will influence the final cost of the isotopically labeled NPs and therefore may determine whether a study is financially feasible. Methods for the synthesis of isotopically labeled Ag NPs are presented in Chapter 3. The labeled NPs are shown to be indistinguishable from equivalent NPs, prepared using natural Ag. The Ag isotope system is relatively simple, with only two naturally occurring stable isotopes of near equal abundance. As such, either of the enriched Ag stable isotopes can be detected when they increase the total Ag concentration of a sample by as little as 0.3‰.

The two exposures conducted with isotopically labeled ^{68}ZnO NPs, described in Chapters 4 and 5, were informed by an evaluation of the detection capabilities offered by an enriched ^{68}Zn isotope label (Larner and Rehkämper, 2012). Chapter 4 explores the uptake and efflux of enriched ^{68}Zn by the estuarine snail *Peringia ulvae*, when introduced as either ^{68}ZnO NPs, dissolved ^{68}Zn or ^{68}ZnO bulk-particles. It was concluded that the ^{68}ZnO NPs most likely underwent rapid dissolution in the artificial seawater exposure media resulting in behavior that was comparable to the dissolved ^{68}Zn and differed from the ^{68}ZnO bulk-particle exposures.

Chapter 5 presents the results for an exposure of the earthworm *Lumbricus rubellus* to ^{68}ZnO NPs and dissolved ^{68}Zn in soils. The sealing of the mouthparts of selected earthworms, to prevent ingestion, allowed dermal and dietary uptake routes to be assessed separately. This study found that the partitioning behavior of the two Zn forms were indistinguishable in the soil. Both sealed and unsealed earthworms furthermore yielded uptake and elimination rate constants for the ^{68}Zn isotope label that were identical, within error, for both ^{68}Zn forms. In addition the observations suggest that is enriched ^{68}Zn associated with the pore water that was available for uptake via the dermal route.

Importantly, this study was conducted at environmentally relevant levels and highlighted how studies performed using high and excessive dosing may be subject to concentration effects.

6.2 Future work

The approach of stable isotope labeling provides immense potential for studying the behavior and environmental fate of engineered NPs at low and environmentally relevant concentrations. The methodology, therefore, offers the opportunity to test or validate the findings of studies that have been performed at higher dosing levels. By comparing the observations made in the high dosing studies with work conducted at low and environmentally relevant levels it should be possible to determine if the high concentrations mask or induce nano-specific effects.

There are currently published protocols for the synthesis of isotopically labeled ZnO, CuO and Ag NPs (Dybowska et al., 2011, Laycock et al., 2014, Misra et al., 2012). However, the approach of stable isotope labeling may be applied to any engineered NP which features a multi-isotopic element as the major constituent. It is therefore expected that methods for the preparation of other isotopically labeled NPs will become available in the future.

An exciting possibility offered by stable isotopes is that multiple enriched isotopes can be employed in a single experiment or exposure. This would allow a single exposure system to be treated with several enriched isotopes simultaneously. This could be approached in one of two ways. First, exposures could be performed using several types of isotopically labeled NPs, for example ^{107}Ag and ^{68}ZnO NPs. Second, for elements with three or more isotopes, multiple forms of the same element can be labeled with different enriched isotopes, for example aqueous ^{66}Zn and ^{68}ZnO NPs. Experiments that employ multiple enriched isotopes offer important benefits. In particular, the approach can dramatically reduce the number of samples produced, and therefore increase sample throughput whilst decreasing the cost of sample analysis. Furthermore, dosing of the same exposure system with different forms of the same element with distinct labels of two (or more) different NPs

would allow direct comparisons to be made and reduce uncertainties that may arise from natural variability or individual behavior.

A limitation of the current work is that the form of an isotopically enriched label in a sample cannot be unequivocally determined. It would be beneficial to be able to monitor the changes that NPs undergo once introduced to an exposure system and identify the form in which an isotope label is available to an organism. One way in which this may be achievable would be to conduct isotopic mapping of an exposed sample using an ion microprobe. For example, if an exposed tissue is analyzed and the enriched isotope label is found in discrete locations as opposed to being homogeneously dispersed, then this would be indicative of the direct uptake of NPs, which could then deliver nano-specific effects (Figure 6.1).

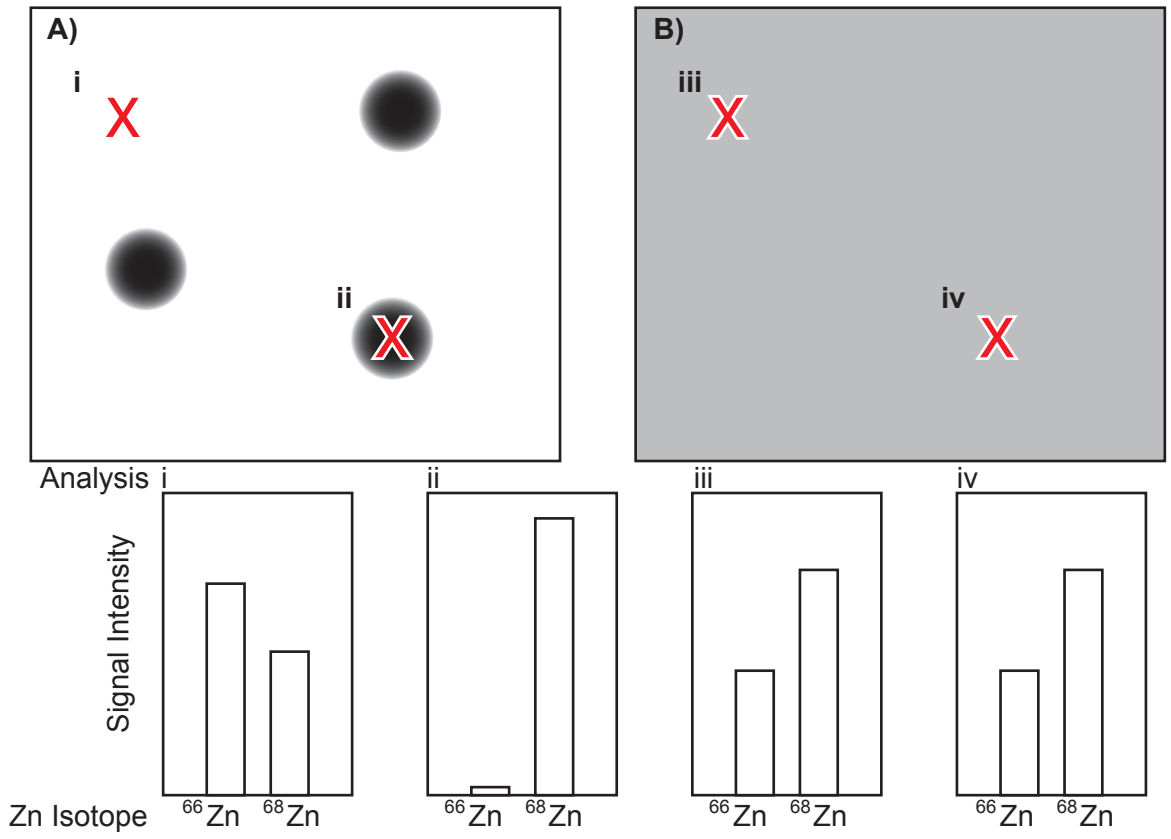


Figure 6.1 Two samples exposed to isotopically labeled ^{68}ZnO NPs. Black regions contain only enriched ^{68}Zn, white areas are natural Zn only, and grey fields are a mixture of these. A) A sample containing discrete ^{68}ZnO NPs. B) A sample where the ^{68}Zn from the ^{68}ZnO NPs has become evenly distributed throughout and NPs are no longer evident.

Such analyses may be achievable using a NanoSIMS instrument, which can offer a resolution of up to ~50nm and detection limits in the ppb range. However, this approach would also offer distinct disadvantages. For example such analysis would focus on small samples, such as a cross section of an individual organism, this raises two issues i) If the analyzed sample is representative of not just the individual but also of the exposed organisms ii) In order to locate and identify a single NP within an organism the individual must contain a high number of particles and therefore high dosing is likely to be required, which would raise the question of environmental relevance and representative behavior.

6.3 Closing remarks

This thesis has covered all aspects of stable isotope labeling and tracing for engineered NPs, from the evaluation and modeling of the detection sensitivities of isotopically labeled CeO_2 NPs, the development of an appropriate synthesis protocol for isotopically labeled Ag NPs, and the application of ^{68}ZnO NPs in environmental tracer studies. The most important advantage of stable isotope labeling is the unparalleled detection capabilities that the approach offers. The ability to detect and quantify these materials at environmentally relevant levels is essential in order to understand the behavior, transport and fate of engineered NPs. The technique of stable isotope labeling and tracing therefore has much more to offer, and it is likely that studies that employ these methods and materials will make important contributions to this field of research.

The nature of this work has necessitated the collaboration of workers from the fields of isotopic analysis, ecotoxicity, and material science. Only through a combined effort will the required facilities and knowledge be brought together to accomplish such research.

Bibliography

ABOUCHAMI, W., GALER, S. J. G., HORNER, T. J., REHKAMPER, M., WOMBACHER, F., XUE, Z. C., LAMBELET, M., GAULT-RINGOLD, M., STIRLING, C. H., SCHONBACHLER, M., SHIEL, A. E., WEIS, D. & HOLDSHIP, P. F. 2013. A Common Reference Material for Cadmium Isotope Studies - NIST SRM 3108. *Geostandards and Geoanalytical Research,* 37**,** 5-17.

ARNOLD, R. E. & HODSON, M. E. 2007. Effect of time and mode of depuration on tissue copper concentrations of the earthworms Eisenia andrei, Lumbricus rubellus and Lumbricus terrestris. *Environmental Pollution,* 148**,** 21-30.

ARNOLD, T., SCHÖNBÄCHLER, M., REHKÄMPER, M., DONG, S., ZHAO, F. J., KIRK, G. J., COLES, B. J. & WEISS, D. J. 2010. Measurement of zinc stable isotope ratios in biogeochemical matrices by double-spike MC-ICPMS and determination of the isotope ratio pool available for plants from soil. *Anal Bioanal Chem,* 398**,** 3115-25.

ARUL MOZHI SELVAN, V., ANAND, R. B. & UDAYAKUMAR, M. 2009. Effects of Cerium Oxide Nanoparticle Addition in Diesel and Diesel-Biodiesel-Ethanol Blends on the performance and emission characteristics of a C1 Engine. *ARPN Journal of Engineering and Applied Sciences,* 4, 1819-6608.

AUDI, G., WAPSTRA, A. & THIBAULT, C. 2003. The AME2003 atomic mass evaluation:(II). Tables, graphs and references. *Nuclear Physics A,* 729**,** 337-676.

AUFFAN, M., ROSE, J., BOTTERO, J. Y., LOWRY, G. V., JOLIVET, J. P. & WIESNER, M. R. 2009. Towards a definition of inorganic nanoparticles from an environmental, health and safety perspective. *Nature Nanotechnology,* 4**,** 634-641.

BAALOUSHA, M. & LEAD, J. R. 2007. Characterization of natural aquatic colloids (< 5 nm) by flow-field flow fractionation and atomic force microscopy. *Environmental Science & Technology,* 41**,** 1111-1117.

BAALOUSHA, M. & LEAD, J. R. 2012. Rationalizing Nanomaterial Sizes Measured by Atomic Force Microscopy, Flow Field-Flow Fractionation, and Dynamic Light Scattering: Sample Preparation, Polydispersity, and Particle Structure. *Environmental Science & Technology,* 46**,** 6134-6142.

BAALOUSHA, M. & LEAD, J. R. 2013. Nanoparticle dispersity in toxicology. *Nature Nanotechnology,* 8**,** 308-309.

BAALOUSHA, M., MANCIULEA, A., CUMBERLAND, S., KENDALL, K. & LEAD, J. R. 2008. Aggregation and surface properties of iron oxide nanoparticles: Influence of pH and natural organic matter. *Environmental Toxicology and Chemistry,* 27**,** 1875-1882.

BEARD, B. L., JOHNSON, C. M., COX, L., SUN, H., NEALSON, K. H. & AGUILAR, C. 1999. Iron isotope biosignatures. *Science,* 285**,** 1889-1892.

BECKER, J. S. & DIETZE, H. J. 1997. Double-focusing sector field inductively coupled plasma mass spectrometry for highly sensitive multi-element and isotopic analysis - Invited lecture. *Journal of Analytical Atomic Spectrometry,* 12**,** 881-889.

BETTINELLI, M., SPEZIA, S., TERNI, C., RONCHI, A., BALDUCCI, C. & MINOIA, C. 2002. Determination of rare earth elements in urine by electrothermal vaporization inductively coupled plasma mass spectrometry. *Rapid Communications in Mass Spectrometry,* 16**,** 579-584.

BIAN, S. W., MUDUNKOTUWA, I. A., RUPASINGHE, T. & GRASSIAN, V. H. 2011. Aggregation and Dissolution of 4 nm ZnO Nanoparticles in Aqueous Environments: Influence of pH, Ionic Strength, Size, and Adsorption of Humic Acid. *Langmuir,* 27**,** 6059-6068.

BOHLKE, J. K., DE LAETER, J. R., DE BIEVRE, P., HIDAKA, H., PEISER, H. S., ROSMAN, K. J. R. & TAYLOR, P. D. P. 2005. Isotopic compositions of the elements, 2001. *Journal of Physical and Chemical Reference Data,* 34**,** 57-67.

BOLLHOFER, A. & ROSMAN, K. J. R. 2001. Isotopic source signatures for atmospheric lead: The Northern Hemisphere. *Geochimica Et Cosmochimica Acta,* 65**,** 1727-1740.

BORM, P., KLAESSIG, F. C., LANDRY, T. D., MOUDGIL, B., PAULUHN, J., THOMAS, K., TROTTIER, R. & WOOD, S. 2006. Research strategies for safety evaluation of nanomaterials, Part V: Role of dissolution in biological fate and effects of nanoscale particles. *Toxicological Sciences,* 90**,** 23-32.

BOXALL, A. C., Q; SINCLAIR, C; JONES, A; AITKEN, R; JEFFERSON, B; WATTS, C 2007. Current and future predicted environmental exposure to engineered nanoparticles.

BOXALL, A., CHAUDHRY, Q., SINCLAIR, C., JONES, A., AITKEN, R., JEFFERSON, B. & WATTS, C. 2007. Current and future predicted environmental exposure to engineered nanoparticles. *Central Science Laboratory, Department of the Environment and Rural Affairs, London, UK*, 89.

BUFFET, P. E., AMIARD-TRIQUET, C., DYBOWSKA, A., RISSO-DE FAVERNEY, C., GUIBBOLINI, M., VALSAMI-JONES, E. & MOUNEYRAC, C. 2012. Fate of isotopically labeled zinc oxide nanoparticles in sediment and effects on two endobenthic species, the clam Scrobicularia plana and the ragworm Hediste diversicolor. *Ecotoxicology and Environmental Safety,* 84, 191-198.

CANADIAN COUNCIL OF MINISTERS OF THE ENVIRONMENT 1999. Canadian soil quality guidelines for the protection of environmental and human health: Ethylene glycol. *Canadian environmental quality guidelines, 1999, Canadian Council of Ministers of the Environment.* Winnipeg.

CASADO-MARTINEZ, M. C., SMITH, B. D., DELVALLS, T. A. & RAINBOW, P. S. 2009. Pathways of trace metal uptake in the lugworm Arenicola marina. *Aquatic Toxicology,* 92, 9-17.

CASSEE, F. R., VAN BALEN, E. C., SINGH, C., GREEN, D., MUIJSER, H., WEINSTEIN, J. & DREHER, K. 2011. Exposure, Health and Ecological Effects Review of Engineered Nanoscale Cerium and Cerium Oxide Associated with its Use as a Fuel Additive. *Critical Reviews in Toxicology,* 41, 213-229.

CHEN, C. Y., ZHANG, P. Q. & CHAI, Z. F. 2001. Distribution of some rare earth elements and their binding species with proteins in human liver studied by instrumental neutron activation analysis combined with biochemical techniques. *Analytica Chimica Acta,* 439, 19-27.

CHEN, J. H. & WASSERBURG, G. J. 1990. The Isotopic Composition of Ag in Meteorites and the Presence of Pd-107 in Protoplanets. *Geochimica Et Cosmochimica Acta,* 54, 1729-1743.

CHRASTINA, A. & SCHNITZER, J. E. 2010. Iodine-125 radiolabeling of silver nanoparticles for in vivo SPECT imaging. *International Journal of Nanomedicine,* 5, 653-659.

CHUGAEV, A. V. & CHERNYSHEV, I. V. 2012. High-noble measurement of Ag-107/Ag-109 in native silver and gold by multicollector inductively coupled plasma mass spectrometry (MC-ICP-MS). *Geochemistry International,* 50, 899-910.

CLOQUET, C., ROUXEL, O., CARIGNAN, J. & LIBOUREL, G. 2005. Natural cadmium isotopic variations in eight geological reference materials (NIST SRM 2711, BCR 176, GSS-1, GXR-1, GXR-2, GSD-12, Nod-P-1, Nod-A-1) and anthropogenic samples, measured by MC-ICP-MS. *Geostandards and Geoanalytical Research,* 29, 95-106.

COSTAS, M., LAVILLA, I., GIL, S., PENA, F., DE LA CALLE, I., CABALEIRO, N. & BENDICHO, C. 2010. Evaluation of ultrasound-assisted extraction as sample pre-treatment for quantitative determination of rare earth elements in marine biological tissues by inductively coupled plasma-mass spectrometry. *Analytica Chimica Acta,* 679, 49-55.

COUTRIS, C., JONER, E. J. & OUGHTON, D. H. 2012. Aging and soil organic matter content affect the fate of silver nanoparticles in soil. *Science of the Total Environment,* 420, 327-333.

CROTEAU, M. N., DYBOWSKA, A. D., LUOMA, S. N. & VALSAMI-JONES, E. 2011. A novel approach reveals that zinc oxide nanoparticles are bioavailable and toxic after dietary exposures. *Nanotoxicology,* 5, 79-90.

CUMBERLAND, S. A. & LEAD, J. R. 2009. Particle size distributions of silver nanoparticles at environmentally relevant conditions. *Journal of Chromatography A,* 1216, 9099-9105.

DESAULTY, A. M., TELOUK, P., ALBALAT, E. & ALBAREDE, F. 2011. Isotopic Ag-Cu-Pb record of silver circulation through 16th-18th century Spain. *Proceedings of the National Academy of Sciences of the United States of America,* 108**,** 9002-9007.

DONAT, J. R. & BRULAND, K. W. 1995. Trace elements in the oceans. *In:* SALBU, B. & STEINNES, E. *Trace Elements in Natural Waters.* CRC Press. 247-281

DYBOWSKA, A. D., CROTEAU, M. N., MISRA, S. K., BERHANU, D., LUOMA, S. N., CHRISTIAN, P., O'BRIEN, P. & VALSAMI-JONES, E. 2011. Synthesis of isotopically modified ZnO nanoparticles and their potential as nanotoxicity tracers. *Environmental Pollution,* 159**,** 266-273.

EISLER, R. 1996. Silver hazards to fish, wildlife and invertebrates: A synoptic review. *In:* SERVICE, N. B. *Contaminat Hazards Reviews Report 32.* U.S. Department of the Interior.

EMMETT, B., REYNOLDS, B., CHAMBERLAIN, P., ROWE, E., SPURGEON, D., BRITTAIN, S., FROGBROOK, Z., HUGHES, S., LAWLOR, A. & POSKITT, J. 2010. Countryside survey: soils report from 2007.

FABREGA, J., LUOMA, S. N., TYLER, C. R., GALLOWAY, T. S. & LEAD, J. R. 2011. Silver nanoparticles: Behaviour and effects in the aquatic environment. *Environment International,* 37**,** 517-531.

FRANKLIN, N. M., ROGERS, N. J., APTE, S. C., BATLEY, G. E., GADD, G. E. & CASEY, P. S. 2007. Comparative toxicity of nanoparticulate ZnO, bulk ZnO, and ZnCl2 to a freshwater microalga (Pseudokirchneriella subcapitata): The importance of particle solubility. *Environmental Science & Technology,* 41**,** 8484-8490.

GAILLARDET, J., DUPRE, B., ALLEGRE, C. J. & NEGREL, P. 1997. Chemical and physical denudation in the Amazon River basin. *Chemical Geology,* 142**,** 141-173.

GIBSON, N., HOLZWARTH, U., ABBAS, K., SIMONELLI, F., KOZEMPEL, J., CYDZIK, I., COTOGNO, G., BULGHERONI, A., GILLILAND, D., PONTI, J., FRANCHINI, F., MARMORATO, P., STAMM, H., KREYLING, W., WENK, A., SEMMLER-BEHNKE, M., BUONO, S., MACIOCCO, L. & BURGIO, N. 2011. Radiolabelling of engineered nanoparticles for in vitro and in vivo tracing applications using cyclotron accelerators. *Archives of Toxicology,* 85**,** 751-773.

GIGAULT, J. & HACKLEY, V. A. 2013. Differentiation and characterization of isotopically modified silver nanoparticles in aqueous media using asymmetric-flow field flow fractionation coupled to optical detection and mass spectrometry. *Analytica Chimica Acta,* 763**,** 57-66.

GOHARSHADI, E. K., SAMIEE, S. & NANCARROW, P. 2011. Fabrication of cerium oxide nanoparticles: Characterization and optical properties. *Journal of Colloid and Interface Science,* 356**,** 473-480.

GOLDBERG, T., GORDON, G., IZON, G., ARCHER, C., PEARCE, C. R., MCMANUS, J., ANBAR, A. D. & REHKAMPER, M. 2013. Resolution of inter-laboratory discrepancies in Mo isotope data: an intercalibration. *Journal of Analytical Atomic Spectrometry,* 28**,** 724-735.

GONG, A., YE, C. M., WANG, X. J., LEI, Z. F. & LIU, J. M. 2001. Dynamics and mechanism of ultraviolet photolysis of atrazine on soil surface. *Pest Management Science,* 57**,** 380-385.

GOTTSCHALK, F., SONDERER, T., SCHOLZ, R. W. & NOWACK, B. 2009. Modeled Environmental Concentrations of Engineered Nanomaterials (TiO2, ZnO, Ag, CNT, Fullerenes) for Different Regions. *Environmental Science & Technology,* 43**,** 9216-9222.

GOTTSCHALK, F., SUN, T. & NOWACK, B. 2013. Environmental concentrations of engineered nanomaterials: Review of modeling and analytical studies. *Environmental pollution,* 181**,** 287-300.

GRISCOM, S. B., FISHER, N. S. & LUOMA, S. N. 2002. Kinetic modeling of Ag, Cd and Co bioaccumulation in the clam Macoma balthica: quantifying dietary and dissolved sources. *Marine Ecology Progress Series,* 240**,** 127-141.

GULSON, B. L. & WONG, H. 2006. Stable isotope tracing–a way forward for nanotechnology. *Environ. Health Perspect.,* 114**,** 1486-1488.

GULSON, B., MCCALL, M., KORSCH, M., GOMEZ, L., CASEY, P., OYTAM, Y., TAYLOR, A., MCCULLOCH, M., TROTTER, J., KINSLEY, L. & GREENOAK, G. 2010. Small Amounts of Zinc from Zinc Oxide Particles in Sunscreens Applied Outdoors Are Absorbed through Human Skin. *Toxicological Sciences,* 118**,** 140-149.

HANDY, R. D., KAMMER, F. V. D., LEAD, J. R., HASSELLÖV, M., OWEN, R. & CRANE, M. 2008a. The ecotoxicology and chemistry of manufactured nanoparticles. *Ecotoxicol.,* 17**,** 287-314.

HANDY, R. D., OWEN, R. & VALSAMI-JONES, E. 2008a. The ecotoxicology of nanoparticles and nanomaterials: current status, knowledge gaps, challenges, and future needs. *Ecotoxicology,* 17**,** 315-325.

HAURI, E., CARLSON, R. & BAUER, J. 2000. The timing of core formation and volatile depletion in solar system objects from high-precision 107Pd-107Ag isotope systematics. *31st Lunar and Planetary Science Conference.* Houstan, Texas.

HEGGELUND, L. R., DIEZ-ORTIZ, M., LOFTS, S., LAHIVE, E., JURKSCHAT, K., WOJNAROWICZ, J., CEDERGREEN, N., SPURGEON, D. & SVENDSEN, C. 2014. Soil pH effects on the comparative toxicity of dissolved zinc, non-nano and nano ZnO to the earthworm Eisenia fetida. *Nanotoxicology,* 8**,** 559-572.

HEUMANN, K. G., GALLUS, S. M., RADLINGER, G. & VOGL, J. 1998. Precision and accuracy in isotope ratio measurements by plasma source mass spectrometry. *Journal of Analytical Atomic Spectrometry,* 13**,** 1001-1008.

HOLLRIEGL, V., GONZALEZ-ESTECHA, M., TRASOBARES, E. M., GIUSSANI, A., OEH, U., HERRAIZ, M. A. & MICHALKE, B. 2010. Measurement of cerium in human breast milk and blood samples. *Journal of Trace Elements in Medicine and Biology,* 24**,** 193-199.

HOOPER, H. L., JURKSCHAT, K., MORGAN, A. J., BAILEY, J., LAWLOR, A. J., SPURGEON, D. J. & SVENDSEN, C. 2011. Comparative chronic toxicity of nanoparticulate and ionic zinc to the earthworm Eisenia veneta in a soil matrix. *Environment International,* 37**,** 1111-1117.

HU, C. W., LI, M., CUI, Y. B., LI, D. S., CHEN, J. & YANG, L. Y. 2010. Toxicological effects of TiO2 and ZnO nanoparticles in soil on earthworm Eisenia fetida. *Soil Biology & Biochemistry,* 42**,** 586-591.

INAGAKI, K. & HARAGUCHI, H. 1999. Determination of rare earth elements in human blood serum by inductively coupled plasma mass spectrometry after chelating resin preconcentration. *Analyst,* 125**,** 191-196.

JANSSEN, M. P. M., BRUINS, A., DEVRIES, T. H. & VANSTRAALEN, N. M. 1991. Comparison of Cadmium Kinetics in 4 Soil Arthropod Species. *Archives of Environmental Contamination and Toxicology,* 20**,** 305-312.

JARVIS, K. E., GRAY, A. L. & HOUK, R. S. 1992. *Handbook of inductively coupled plasma mass spectrometry*, Blackie, London.

JOHNSON, A. C. & PARK, B. 2012. Predicting contamination by the fuel additive cerium oxide engineered nanoparticles within the United Kingdom and the associated risks. *Environmental Toxicology and Chemistry,* 31**,** 2582-2587.

JU-NAM, Y. & LEAD, J. R. 2008. Manufactured nanoparticles: An overview of their chemistry, interactions and potential environmental implications. *Science of the Total Environment,* 400**,** 396-414.

KAY, A. R. 2004. Detecting and minimizing zinc contamination in physiological solutions. *BMC physiology,* 4**,** 4.

KELLER, A. A., WANG, H. T., ZHOU, D. X., LENIHAN, H. S., CHERR, G., CARDINALE, B. J., MILLER, R. & JI, Z. X. 2010. Stability and Aggregation of Metal Oxide Nanoparticles in Natural Aqueous Matrices. *Environmental Science & Technology,* 44**,** 1962-1967.

KHAN, F. R., LAYCOCK, A., DYBOWSKA, A., LARNER, F., SMITH, B. D., RAINBOW, P. S., LUOMA, S. N., REHKAMPER, M. & VALSAMI-JONES, E. 2013. Stable Isotope Tracer To Determine Uptake and Efflux Dynamics of ZnO Nano- and Bulk Particles and Dissolved Zn to an Estuarine Snail. *Environmental Science & Technology,* 47**,** 8532-8539.

KHAN, F. R., MISRA, S. K., GARCIA-ALONSO, J., SMITH, B. D., STREKOPYTOV, S., RAINBOW, P. S., LUOMA, S. N. & VALSAMI-JONES, E. 2012. Bioaccumulation Dynamics and Modeling in an Estuarine Invertebrate Following Aqueous Exposure to Nanosized and Dissolved Silver. *Environmental Science & Technology,* 46**,** 7621-7628.

KOEBERL, C. & BAYER, P. M. 1992. Concentrations of Rare-Earth Elements in Human Brain-Tissue and Kidney-Stones Determined by Neutron-Activation Analysis. *Journal of Alloys and Compounds,* 180**,** 63-70.

KOOL, P. L., ORTIZ, M. D. & VAN GESTE, C. A. M. 2011. Chronic toxicity of ZnO nanoparticles, non-nano ZnO and ZnCl2 to Folsomia candida (Collembola) in relation to bioavailability in soil. *Environmental Pollution,* 159**,** 2713-2719.

LAHIVE, E., JURKSCHAT, K., SHAW, B., HANDY, R., SPURGEON, D. & SVENDSEN, C. 2014. Toxicity of cerium oxide nanoparticles to the earthworm Eisenia fetida: subtle effects. *Environmental Chemistry,* 11, 268-278.

LARNER, F. & REHKÄMPER, M. 2012. Evaluation of stable isotope tracing for ZnO nanomaterials - new constraints from high precision isotope analyses and modeling. *Environmental Science & Technology,* 46**,** 4149-58.

LARNER, F., DOGRA, Y., DYBOWSKA, A., FABREGA, J., STOLPE, B., BRIDGESTOCK, L. J., GOODHEAD, R., WEISS, D. J., MOGER, J., LEAD, J. R., VALSAMI-JONES, E., TYLER, C. R., GALLOWAY, T. S. & REHKÄMPER, M. 2012. Tracing Bioavailability of ZnO Nanoparticles Using Stable Isotope Labeling. *Environmental Science & Technology,* 46**,** 12137-12145.

LAVERACK, M. S. 1963. *The physiology of earthworms,* Oxford, Pergamon Press.

LAYCOCK, A., STOLPE, B., RÖMER, I., DYBOWSKA, A., VALSAMI-JONES, E., LEAD, J. R. & REHKÄMPER, M. 2014. Synthesis and characterization of isotopically labeled silver nanoparticles for tracing studies. *Environmental Science: Nano,* 1**,** 271-283.

LEWINSKI, N., COLVIN, V. & DREZEK, R. 2008. Cytotoxicity of nanoparticles. *Small,* 4**,** 26-49.

LI, B., SUN, Y. L. & YIN, M. 1999. Determination of cerium, neodymium and samarium in biological materials at low levels by isotope dilution inductively coupled plasma mass spectrometry. *Journal of Analytical Atomic Spectrometry,* 14**,** 1843-1848.

LI, M. H., POKHREL, S., JIN, X., MADLER, L., DAMOISEAUX, R. & HOEK, E. M. V. 2011. Stability, Bioavailability, and Bacterial Toxicity of ZnO and Iron-Doped ZnO Nanoparticles in Aquatic Media. *Environmental Science & Technology,* 45**,** 755-761.

LITZEN, A. 1993. Separation Speed, Retention, and Dispersion in Asymmetrical Flow Field-Flow Fractionation as Functions of Channel Dimensions and Flow-Rates. *Analytical Chemistry,* 65**,** 461-470.

LUO, Y., DABEK-ZLOTORZYNSKA, E., CELO, V., MUIR, D. C. G. & YANG, L. 2010. Accurate and Precise Determination of Silver Isotope Fractionation in Environmental Samples by Multicollector-ICPMS. *Analytical Chemistry,* 82**,** 3922-3928.

LUOMA, S. N. & RAINBOW, P. S. 2005. Why is metal bioaccumulation so variable? Biodynamics as a unifying concept. *Environmental Science & Technology,* 39**,** 1921-1931.

LUOMA, S. N. & RAINBOW, P. S. 2008. *Metal contamination in aquatic environments : science and lateral management,* Cambridge, Cambridge University Press.

LUOMA, S. N. 2008. Silver nanotechnologies and the environment. *Woodrow Wilson International Center for Scholars. Washington, DC, USA***,** 72.

LUOMA, S. N., JOHNS, C., FISHER, N. S., STEINBERG, N. A., OREMLAND, R. S. & REINFELDER, J. R. 1992. Determination of Selenium Bioavailability to a Benthic Bivalve from Particulate and Solute Pathways. *Environmental Science & Technology,* 26**,** 485-491.

MA, H. B., WILLIAMS, P. L. & DIAMOND, S. A. 2013. Ecotoxicity of manufactured ZnO nanoparticles - A review. *Environmental Pollution,* 172**,** 76-85.

MA, H., KABENGI, N. J., BERTSCH, P. M., UNRINE, J. M., GLENN, T. C. & WILLIAMS, P. L. 2011. Comparative phototoxicity of nanoparticulate and bulk ZnO to a free-living nematode Caenorhabditis elegans: The importance of illumination mode and primary particle size. *Environmental Pollution,* 159**,** 1473-1480.

MANZO, S., ROCCO, A., CAROTENUTO, R., PICIONE, F. D., MIGLIETTA, M. L., RAMETTA, G. & DI FRANCIA, G. 2011. Investigation of ZnO nanoparticles' ecotoxicological effects towards different soil organisms. *Environmental Science and Pollution Research,* 18**,** 756-763.

MARETTI, L., BILLONE, P. S., LIU, Y. & SCAIANO, J. C. 2009. Facile Photochemical Synthesis and Characterization of Highly Fluorescent Silver Nanoparticles. *Journal of the American Chemical Society,* 131**,** 13972-13980.

MARQUIS, B. J., LOVE, S. A., BRAUN, K. L. & HAYNES, C. L. 2009. Analytical methods to assess nanoparticle toxicity. *Analyst,* 134**,** 425-439.

MARTIN, J. M. & WHITFIELD, M. 1983. *The significance of the river input of chemical elements to the ocean,* New York, Plenum Press.

MATWIYOFF, N. A. & OTT, D. G. 1973. Stable isotope tracers in the life sciences and medicine. *Science (New York, N Y),* 181**,** 1125-33.

MAYER, A. Definition, measurement and filtration of ultrafine solid particles emitted by diesel engines. Proceedings of the 19th ATW-EMPA Symposium, 2002.

MIAO, A. J., ZHANG, X. Y., LUO, Z. P., CHEN, C. S., CHIN, W. C., SANTSCHI, P. H. & QUIGG, A. 2010. Zinc Oxide Engineered Nanoparticles Dissolution and Toxicity to Marine Phytoplankton. *Environmental Toxicology and Chemistry,* 29**,** 2814-2822.

MILLER, R. J., LENIHAN, H. S., MULLER, E. B., TSENG, N., HANNA, S. K. & KELLER, A. A. 2010. Impacts of Metal Oxide Nanoparticles on Marine Phytoplankton. *Environmental Science & Technology,* 44**,** 7329-7334.

MISRA, S. K., DYBOWSKA, A., BERHANU, D., CROTEAU, M. N., LUOMA, S. N., BOCCACCINI, A. R. & VALSAMI-JONES, E. 2012. Isotopically Modified Nanoparticles for Enhanced Detection in Bioaccumulation Studies. *Environmental Science & Technology,* 46**,** 1216-1222.

NAKADA, R., TAKAHASHI, Y. & TANIMIZU, M. 2013. Isotopic and speciation study on cerium during its solid-water distribution with implication for Ce stable isotope as a paleo-redox proxy. *Geochimica Et Cosmochimica Acta,* 103**,** 49-62.

O'BRIEN, N. & CUMMINS, E. 2010. Nano-Scale Pollutants: Fate in Irish Surface and Drinking Water Regulatory Systems. *Human and Ecological Risk Assessment,* 16**,** 847-872.

OHNO, T. & HIRATA, T. 2013. Determination of Mass-Dependent Isotopic Fractionation of Cerium and Neodymium in Geochemical Samples by MC-ICPMS. *Analytical Sciences,* 29**,** 47-53.

ONAT, B. & TOPCUOGLU, S. 1999. A laboratory study of Zn and Cs-134 depuration by the sea snail (Rapana venosa). *Journal of Environmental Radioactivity,* 46**,** 201-206.

OSMOND, M. J. & MCCALL, M. J. 2010. Zinc oxide nanoparticles in modern sunscreens: An analysis of potential exposure and hazard. *Nanotoxicology,* 4**,** 15-41.

OTHMAN, B. D., WHITE, W. M. & PATCHETT, J. 1989. The Geochemistry of Marine-Sediments, Island-Arc Magma Genesis, and Crust Mantle Recycling. *Earth and Planetary Science Letters,* 94**,** 1-21.

OUGHTON, D. H., HERTEL-AAS, T., PELLICER, E., MENDOZA, E. & JONER, E. J. 2008. Neutron activation of engineered nanoparticles as a tool for tracing their environmental fate and uptake in organisms. *Environmental Toxicology and Chemistry,* 27**,** 1883-1887.

PACURARI, M., CASTRANOVA, V. & VALLYATHAN, V. 2010. Single-and multi-wall carbon nanotubes versus asbestos: are the carbon nanotubes a new health risk to humans? *Journal of Toxicology and Environmental Health, Part A,* 73**,** 378-395.

PALME, H. & O'NEILL, H. S. C. 2005. Cosmochemical estimates of mantle composition. *In:* CARLSON, R. W. *The Mantle and Core.* Amsterdam: Elsevier. *Treatise on geochemistry*, *2*, 1-38.

PARK, B., DONALDSON, K., DUFFIN, R., TRAN, L., KELLY, F., MUDWAY, I., MORIN, J. P., GUEST, R., JENKINSON, P., SAMARAS, Z., GIANNOULI, M., KOURIDIS, H. & MARTIN, P. 2008. Hazard and risk assessment of a nanoparticulate cerium oxide-based diesel fuel additive - A case study. *Inhalation Toxicology,* 20**,** 547-566.

PARK, B., MARTIN, P., HARRIS, C., GUEST, R., WHITTINGHAM, A., JENKINSON, P. & HANDLEY, J. 2007. Initial in vitro screening approach to investigate the potential health and environmental hazards of Envirox trade mark - a nanoparticulate cerium oxide diesel fuel additive. *Part Fibre Toxicol,* 4**,** 12.

PENG, X. H., PALMA, S., FISHER, N. S. & WONG, S. S. 2011. Effect of morphology of ZnO nanostructures on their toxicity to marine algae. *Aquatic Toxicology,* 102**,** 186-196.

PEREZ, J. M., ASATI, A., NATH, S. & KAITTANIS, C. 2008. Synthesis of biocompatible dextran-coated nanoceria with pH-dependent antioxidant properties. *Small,* 4**,** 552-556.

PURCELL, T. W. & PETERS, J. J. 1998. Sources of silver in the environment. *Environmental Toxicology and Chemistry,* 17**,** 539-546.

REHKÄMPER, M., GÄRTNER, M., GALER, S. J. G. & GOLDSTEIN, S. L. 1996. Separation of Ce from other rare-earth elements with application to Sm-Nd and La-Ce chronometry. *Chemical Geology,* 129**,** 201-208.

REHKÄMPER, M., SCHÖNBÄCHLER, M. & STIRLING, C. H. 2001. Multiple collector ICP-MS: Introduction to instrumentation, measurement techniques and analytical capabilities. *Geostandards Newsletter - the Journal of Geostandards and Geoanalysis,* 25**,** 23-40.

REHKÄMPER, M., WOMBACHER, F. & AGGARWAL, J. K. 2004. *Handbook of Stable Isotope Analytical Techniques*.

RIPPERGER, S., REHKÄMPER, M., PORCELLI, D. & HALLIDAY, A. N. 2007. Cadmium isotope fractionation in seawater - A signature of biological activity. *Earth and Planetary Science Letters,* 261**,** 670-684.

RODUSHKIN, I. & AXELSSON, M. D. 2000. Application of double focusing sector field ICP-MS for multielemental characterization of human hair and nails. Part II. A study of the inhabitants of northern Sweden. *Science of the Total Environment,* 262**,** 21-36.

RODUSHKIN, I. & ODMAN, F. 2001a. Application of inductively coupled plasma sector field mass spectrometry for elemental analysis of urine. *Journal of Trace Elements in Medicine and Biology,* 14**,** 241-247.

RODUSHKIN, I. & ODMAN, F. 2001b. Assessment of the contamination from devices used for sampling and storage of whole blood and serum for element analysis. *Journal of Trace Elements in Medicine and Biology,* 15**,** 40-45.

RÖMER, I., WHITE, T. A., BAALOUSHA, M., CHIPMAN, K., VIANT, M. R. & LEAD, J. R. 2011. Aggregation and dispersion of silver nanoparticles in exposure media for aquatic toxicity tests. *Journal of Chromatography A,* 1218**,** 4226-4233.

ROYAL SOCIETY & ROYAL ACADEMY OF ENGINEERING 2004. Nanoscience and nanotechnologies: opportunities and uncertainties. London: Royal Society & Royal Academy of Engineering.

SAVOLAINEN, K., PYLKKANEN, L., NORPPA, H., FALCK, G., LINDBERG, H., TUOMI, T., VIPPOLA, M., ALENIUS, H., HAMERI, K., KOIVISTO, J., BROUWER, D., MARK, D., BARD, D., BERGES, M., JANKOWSKA, E., POSNIAK, M., FARMER, P., SINGH, R., KROMBACH, F., BIHARI, P., KASPER, G. & SEIPENBUSCH, M. 2010. Nanotechnologies, engineered nanomaterials and occupational health and safety - A review. *Safety Science,* 48**,** 957-963.

SCHÖNBÄCHLER, M., CARLSON, R. W., HORAN, M. E., MOCK, T. D. & HAURI, E. H. 2007. High precision Ag isotope measurements in geologic materials by multiple-collector ICPMS: An evaluation of dry versus wet plasma. *International Journal of Mass Spectrometry,* 261**,** 183-191.

SHIEL, A. E., WEIS, D. & ORIANS, K. J. 2010. Evaluation of zinc, cadmium and lead isotope fractionation during smelting and refining. *Science of the Total Environment,* 408**,** 2357-2368.

SHIPP, E. & GRANT, A. 2006. Hydrobia ulvae feeding rates: A novel way to assess sediment toxicity. *Environmental Toxicology and Chemistry,* 25**,** 3246-3252.

SHOULTS-WILSON, W. A., REINSCH, B. C., TSYUSKO, O. V., BERTSCH, P. M., LOWRY, G. V. & UNRINE, J. M. 2011. Role of Particle Size and Soil Type in Toxicity of Silver Nanoparticles to Earthworms. *Soil Science Society of America Journal,* 75**,** 365-377.

SMITH, D. B., CANNON, W. F., WOODRUFF, L. G., GARRETT, R. G., KLASSEN, R., KILBURN, J. E., HORTON, J. D., KING, H. D., GOLDHABER, M. B. & MORRISON, J. M. 2005. *Major-and trace-element concentrations in soils from two continental-scale transects of the United States and Canada*, US Department of the Interior, US Geological Survey.

SOKAL, R. R. & ROHLF, F. J. 1995. *Biometry : the principles and practice of statistics in biological research,* New York ; Oxford, Freeman.

SRIDAR, C., HANNA, I. & HOLLENBERG, P. F. 2013. Quantitation of UGT1A1 in human liver microsomes using stable isotope-labelled peptides and mass spectrometry based proteomic approaches. *Xenobiotica; the fate of foreign compounds in biological systems,* 43**,** 336-45.

TANAKA, T. & MASUDA, A. 1982. The La-Ce Geochronometer - a New Dating Method. *Nature,* 300**,** 515-518.

TAZOE, H., OBATA, H. & GAMO, T. 2007. Determination of cerium isotope ratios in geochemical samples using oxidative extraction technique with chelating resin. *Journal of Analytical Atomic Spectrometry,* 22**,** 616-622.

TEJAMAYA, M., RÖMER, I., MERRIFIELD, R. C. & LEAD, J. R. 2012. Stability of Citrate, PVP, and PEG Coated Silver Nanoparticles in Ecotoxicology Media. *Environmental Science & Technology,* 46**,** 7011-7017.

TENUTA, T., MONOPOLI, M. P., KIM, J., SALVATI, A., DAWSON, K. A., SANDIN, P. & LYNCH, I. 2011. Elution of Labile Fluorescent Dye from Nanoparticles during Biological Use. *Plos One,* 6, e25556.

TESSIER, A. & TURNER, D. R. 1995. *Metal speciation and bioavailability in aquatic systems,* New York, USA, J. Wiley.

TIEDE, K., WESTERHOFF, P., HANSEN, S. F., FERN, G. J., HANKIN, S. M., AITKEN, R. J., CHAUDHRY, Q. & BOXALL, A. 2010. Review of the Risks Posed to Drinking Water by Man-made Nanoparticles. FERA, UK.

TJIOE, P. S., VOLKERS, K. J., KROON, J. J. & DEGOEIJ, J. J. M. 1983. Distribution Patterns of Rare-Earth Elements in Biological-Materials Evaluated by Radiochemical Neutron-Activation Analysis. *Journal of Radioanalytical Chemistry,* 80**,** 129-139.

VIJVER, M. G., VINK, J. P. M., MIERMANS, C. J. H. & VAN GESTEL, C. A. M. 2003. Oral sealing using glue: a new method to distinguish between intestinal and dermal uptake of metals in earthworms. *Soil Biology & Biochemistry,* 35**,** 125-132.

VON BLANCKENBURG, F., VON WIREN, N., GUELKE, M., WEISS, D. J. & BULLEN, T. D. 2009. Fractionation of Metal Stable Isotopes by Higher Plants. *Elements,* 5**,** 375-380.

WANG, W. X. & KE, C. H. 2002. Dominance of dietary intake of cadmium and zinc by two marine predatory gastropods. *Aquatic Toxicology,* 56**,** 153-165.

WHITE, S. L. & RAINBOW, P. S. 1985. On the Metabolic Requirements for Copper and Zinc in Mollusks and Crustaceans. *Marine Environmental Research,* 16**,** 215-229.

WIENCH, K., WOHLLEBEN, W., HISGEN, V., RADKE, K., SALINAS, E., ZOK, S. & LANDSIEDEL, R. 2009. Acute and chronic effects of nano- and non-nano-scale TiO2 and ZnO particles on mobility and reproduction of the freshwater invertebrate Daphnia magna. *Chemosphere,* 76**,** 1356-1365.

WIJNHOVEN, S. W. P., PEIJNENBURG, W. J. G. M., HERBERTS, C. A., HAGENS, W. I., OOMEN, A. G., HEUGENS, E. H. W., ROSZEK, B., BISSCHOPS, J., GOSENS, I., VAN DE MEENT, D., DEKKERS, S., DE JONG, W. H., VAN ZIJVERDEN, M., SIPS, A. J. A. M. & GEERTSMA, R. E. 2009. Nano-silver - a review of available data and knowledge gaps in human and environmental risk assessment. *Nanotoxicology,* 3**,** 109-138.

WILLBOLD, M. 2007. Determination of Ce isotopes by TIMS and MC-ICPMS and initiation of a new, homogeneous Ce isotopic reference material. *Journal of Analytical Atomic Spectrometry,* 22**,** 1364-1372.

WOOD, C. M., FARRELL, A. P. & BRAUNER, C. J. 2011. *Fish Physiology: Homeostasis and Toxicology of Essential Metals: Homeostasis and Toxicology of Essential Metals*, Academic Press.

WOODLAND, S. J., REHKÄMPER, M., HALLIDAY, A. N., LEE, D. C., HATTENDORF, B. & GUNTHER, D. 2005. Accurate measurement of silver isotopic compositions in geological materials including low Pd/Ag meteorites. *Geochimica Et Cosmochimica Acta,* 69**,** 2153-2163.

WOODLAND, S. J., REHKÄMPER, M., LEE, D. C. & HALLIDAY, A. N. 2002. High precision MC-ICPMS measurement of Ag isotopic ratios. *Geochimica Et Cosmochimica Acta,* 66**,** A847-A847.

WOODROW WILSON INTERNATIONAL CENTER, 2014. *The Nanotechnology Consumer Products Inventory* [Online]. Woodrow Wilson International Center for Scholars Available from: http://www.nanotechproject.org/cpi [Accessed September 2014].

WYTTENBACH, A., TOBLER, L., SCHLEPPI, P. & FURRER, V. 1998. Variation of the rare earth element concentrations in the soil, soil extract and in individual plants from the same site. *Journal of radioanalytical and nuclear chemistry,* 231**,** 101b-106.

XIA, T., KOVOCHICH, M., LIONG, M., MADLER, L., GILBERT, B., SHI, H. B., YEH, J. I., ZINK, J. I. & NEL, A. E. 2008. Comparison of the Mechanism of Toxicity of Zinc Oxide and Cerium Oxide Nanoparticles Based on Dissolution and Oxidative Stress Properties. *Acs Nano,* 2**,** 2121-2134.

ZHAO, C. M. & WANG, W. X. 2011. Comparison of Acute and Chronic Toxicity of Silver Nanoparticles and Silver Nitrate to Daphnia Magna. *Environmental Toxicology and Chemistry,* 30**,** 885-892.

ZHU, X. S., WANG, J. X., ZHANG, X. Z., CHANG, Y. & CHEN, Y. S. 2009. The impact of ZnO nanoparticle aggregates on the embryonic development of zebrafish (Danio rerio). *Nanotechnology,* 20, 195103.

ZUYKOV, M., PELLETIER, E. & DEMERS, S. 2011. Colloidal complexed silver and silver nanoparticles in extrapallial fluid of Mytilus edulis. *Marine Environmental Research,* 71**,** 17-21.

Appendices

Appendices i)

Synthesis and characterization of isotopically labeled silver nanoparticles for tracing studies

Student t-test

populations and data

Particles sizes and Proportional difference from the mean (PDMS) determined by DLS

*** Best data = the two largest outliers were removed prior to statistical evaluation**

PDMS = (MS - SamS) / MS

MS = Mean particle size for all particles with the same target size

SamS = Measured particle size of sample

Pristine Particles:

Particle Batch	All Data Diameter (nm)	PDMS	PDI	Best Data Diameter (nm)	PDMS
AgNP1 - 30nm					
Nat-AgNP1-May12-F	41.6	0.28	0.25		
107-AgNP1-May12-F	29.3	-0.10	0.22	29.3	-0.05
Nat-AgNP1-May12-IC	35.5	0.09	0.26	35.5	0.15
107-AgNP1-May12-IC	31.2	-0.04	0.16	31.2	0.01
Nat-AgNP1-Oct12-F	26.5	-0.19	0.13	26.5	-0.14
107-AgNP1-Oct12-F	31.2	-0.04	0.18	31.2	0.01
Average	**32.6**			**30.7**	
SD	**4.9**			**2.9**	
AgNP2 - 20nm					
Nat-AgNP2-May12-F	20.7	0.06	0.33	20.7	0.02
107-AgNP2-May12-F	16.7	-0.15	0.25	16.7	-0.17
Nat-AgNP2-May12-IC	17.2	-0.12	0.28	17.2	-0.15
107-AgNP2-May12-IC	16.3	-0.17	0.27		
Nat-AgNP2-Oct12-F	22.6	0.16	0.15	22.6	0.12
107-AgNP2-Oct12-F	23.9	0.22	0.20	23.9	0.18
Average	**19.6**			**20.2**	
SD	**3.0**			**2.9**	
AgNP3 - 17nm					
Nat-AgNP3-May12-F	17.1	-0.18	0.20	17.1	-0.12
107-AgNP3-May12-F	24.3	0.16	0.24	24.3	0.25
Nat-AgNP3-May12-IC	18.2	-0.13	0.23	18.2	-0.07
107-AgNP3-May12-IC	20.6	-0.02	0.29	20.6	0.06
Nat-AgNP3-Oct12-F	17.2	-0.18	0.25	17.2	-0.12
107-AgNP3-Oct12-F	28.1	0.34	0.44		
Average	**20.9**			**19.5**	
SD	**4.1**			**2.7**	

Aged Particles

Particle Batch	Storage (months)	All Data Diameter (nm)	All Data PDMS	All Data PDI	Best Data Diameter (nm)	Best Data PDMS
AgNP1 - 30nm						
Nat-AgNP1-May12-F	12	41.5	0.24	0.25		
107-AgNP1-May12-F	12	29.7	-0.11	0.20	29.7	-0.05
Nat-AgNP1-May12-IC	12	35.3	0.06	0.23	35.3	0.13
107-AgNP1-May12-IC						
Nat-AgNP1-Oct12-F	6	26.8	-0.20	0.11	26.8	-0.15
107-AgNP1-Oct12-F	6	33.7	0.01	0.22	33.7	0.07
Average		33.4			**31.4**	
SD		5.6			**3.3**	
AgNP2 - 20nm						
Nat-AgNP2-May12-F	12	19.7	0.02	0.25	19.7	0.02
107-AgNP2-May12-F	12	14.6	-0.24	0.34	14.6	-0.24
Nat-AgNP2-May12-IC	8	16.8	-0.13	0.35	16.8	-0.13
107-AgNP2-May12-IC	12	17.5	-0.09	0.18	17.5	-0.09
Nat-AgNP2-Oct12-F	6	22.9	0.19	0.10	22.9	0.19
107-AgNP2-Oct12-F	6	24.1	0.25	0.18	24.1	0.25
Average		**19.3**			**19.3**	
SD		**3.4**			**3.4**	
AgNP3 - 17nm						
Nat-AgNP3-May12-F						
107-AgNP3-May12-F						
Nat-AgNP3-May12-IC	12	16.8	-0.32	0.31	16.8	-0.14
107-AgNP3-May12-IC	12	24.1	-0.03	0.21	24.1	0.24
Nat-AgNP3-Oct12-F	6	32.5	0.31	0.52	32.5	0.67
107-AgNP3-Oct12-F	6	26.1	0.05	0.39		
Average		**24.9**			**24.5**	
SD		**5.6**			**6.4**	

Nat AgNPs vs. 107AgNPs for AgNP1, 2 & 3
Using particle size

	All Data	Best Data
AgNP1		
Nat-May12-F	41.6	
Nat-May12-IC	35.5	35.5
Nat-Oct12-F	26.5	26.5
Average	34.5	31.0
SD	6.2	4.5
107-May12-F	29.3	29.3
107-May12-IC	31.2	31.2
107-Oct12-F	31.2	31.2
Average	30.6	30.6
SD	0.9	0.9
t-test p-value	**0.46**	**0.94**

	All Data
AgNP2	
Nat-May12-F	20.7
Nat-May12-IC	17.2
Nat-Oct12-F	22.6
Average	20.2
SD	2.2
107-May12-F	16.7
107-May12-IC	16.3
107-Oct12-F	23.9
Average	19.0
SD	3.5
t-test p-value	**0.71**

	All Data	Best Data
AgNP3		
Nat-May12-F	17.1	17.1
Nat-May12-IC	18.2	18.2
Nat-Oct12-F	17.2	17.2
Average	17.5	17.5
SD	0.5	0.5
107-May12-F	24.3	24.3
107-May12-IC	20.6	20.6
107-Oct12-F	28.1	
Average	24.3	22.5
SD	3.1	1.9
t-test p-value	**0.08**	**0.22**

Nat AgNPs vs. 107AgNPs for AgNP1, 2 & 3
Using proportional difference from the mean

	All Data	Best Data
AgNP1		
Nat-May12-F	0.28	
Nat-May12-IC	0.09	0.15
Nat-Oct12-F	-0.19	-0.14
Average	0.06	0.01
SD	0.19	0.15
107-May12-F	-0.10	-0.05
107-May12-IC	-0.04	0.01
107-Oct12-F	-0.04	0.01
Average	-0.06	-0.01
SD	0.03	0.03
t-test p-value	**0.46**	**0.94**

	All Data
AgNP2	
Nat-May12-F	0.06
Nat-May12-IC	-0.12
Nat-Oct12-F	0.16
Average	0.03
SD	0.11
107-May12-F	-0.15
107-May12-IC	-0.17
107-Oct12-F	0.22
Average	-0.03
SD	0.18
t-test p-value	**0.71**

	All Data	Best Data
AgNP3		
Nat-May12-F	-0.18	-0.12
Nat-May12-IC	-0.13	-0.07
Nat-Oct12-F	-0.18	-0.12
Average	-0.16	-0.10
SD	0.02	0.03
107-May12-F	0.16	0.25
107-May12-IC	-0.02	0.06
107-Oct12-F	0.34	
Average	0.16	0.15
SD	0.15	0.09
t-test p-value	**0.08**	**0.22**

Nat Ag vs. 107AgNPs for each synthesis ocassion
Using proportional difference from the mean

	All Data	Best Data
May12-F		
AgNP1	0.28	
AgNP2	0.06	0.02
AgNP3	-0.18	-0.12
Average	0.05	-0.05
SD	0.19	0.07
107AgNP1	-0.10	-0.05
107AgNP2	-0.15	-0.17
107AgNP3	0.16	0.25
Average	-0.03	0.01
SD	0.14	0.18
t-test p-value	**0.66**	**0.72**

	All Data	Best Data
May12-IC		
AgNP1	0.09	0.15
AgNP2	-0.12	-0.15
AgNP3	-0.13	-0.07
Average	-0.05	-0.02
SD	0.10	0.13
107AgNP1	-0.04	0.01
107AgNP2	-0.17	0.00
107AgNP3	-0.02	0.06
Average	-0.07	0.02
SD	0.07	0.02
t-test p-value	**0.82**	**0.68**

	All Data	Best Data
Oct12-F		
AgNP1	-0.19	-0.14
AgNP2	0.16	0.12
AgNP3	-0.18	-0.12
Average	-0.07	-0.05
SD	0.16	0.12
107AgNP1	-0.04	0.01
107AgNP2	0.22	0.18
107AgNP3	0.34	
Average	0.17	0.10
SD	0.16	0.08
t-test p-value	**0.20**	**0.32**

Nat AgNPs vs. 107AgNPs for all factors
Using proportional difference from the mean

	All Data	Best Data
Nat Ag		
NatAgNP1-May12-F	0.28	
NatAgNP1-May12-IC	0.09	0.15
NatAgNP1-Oct12-F	-0.19	-0.14
NatAgNP2-May12-F	0.06	0.02
NatAgNP2-May12-IC	-0.12	-0.15
NatAgNP2-Oct12-F	0.16	0.12
NatAgNP3-May12-F	-0.18	-0.12
NatAgNP3-May12-IC	-0.13	-0.07
NatAgNP3-Oct12-F	-0.18	-0.12
Average	-0.02	-0.04
SD	0.16	0.11
107 Ag		
107AgNP1-May12-F	-0.10	-0.05
107AgNP1-May12-IC	-0.04	0.01
107AgNP1-Oct12-F	-0.04	0.01
107AgNP2-May12-F	-0.15	-0.17
107AgNP2-May12-IC	-0.17	0.00
107AgNP2-Oct12-F	0.22	0.18
107AgNP3-May12-F	0.16	0.25
107AgNP3-May12-IC	-0.02	0.06
107AgNP3-Oct12-F	0.34	
Average	0.02	0.04
SD	0.17	0.12
t-test p-value	**0.57**	**0.26**

Synthesis at FENAC vs. Imperial
Using proportional difference from the mean

	All Data	Best Data
FENAC		
NatAgNP1-May12	0.28	
NatAgNP2-May12	0.06	0.02
NatAgNP3-May12	-0.18	-0.12
NatAgNP1-Oct12	-0.19	-0.14
NatAgNP2-Oct12	0.16	0.12
NatAgNP3-Oct12	-0.18	-0.12
107AgNP1-May12	-0.10	-0.05
107AgNP2-May12	-0.15	-0.17
107AgNP3-May12	0.16	0.25
107AgNP1-Oct12	-0.04	0.01
107AgNP2-Oct12	0.22	0.18
107AgNP3-Oct12	0.34	
Average	0.03	-0.05
SD	0.19	0.07
Imperial		
NatAgNP1-May12	0.09	0.15
NatAgNP2-May12	-0.12	-0.15
NatAgNP3-May12	-0.13	-0.07
107AgNP1-May12	-0.04	0.01
107AgNP2-May12	-0.17	0.00
107AgNP3-May12	-0.02	0.06
Average	-0.06	0.00
SD	0.09	0.09
t-test p-value	**0.18**	**0.96**

Synthesis by AL vs. BS
Using proportional difference from the mean

	All Data	Best Data
AL		
NatAgNP1-May12-F	0.28	
NatAgNP2-May12-F	0.06	0.02
NatAgNP3-May12-F	-0.18	-0.12
107AgNP1-May12-F	-0.10	-0.05
107AgNP2-May12-F	-0.15	-0.17
107AgNP3-May12-F	0.16	0.25
NatAgNP1-May12-IC	0.09	0.15
NatAgNP2-May12-IC	-0.12	-0.15
NatAgNP3-May12-IC	-0.13	-0.07
107AgNP1-May12-IC	-0.04	0.01
107AgNP2-May12-IC	-0.17	0.00
107AgNP3-May12-IC	-0.02	0.06
Average	-0.03	-0.05
SD	0.14	0.07
BS		
NatAgNP1-Oct12	-0.19	-0.14
NatAgNP2-Oct12	0.16	0.12
NatAgNP3-Oct12	-0.18	-0.12
107AgNP1-Oct12	-0.04	0.01
107AgNP2-Oct12	0.22	0.18
107AgNP3-Oct12	0.34	
Average	0.05	0.01
SD	0.20	0.13
t-test p-value	**0.45**	**0.76**

NatAg Vs 107Ag for all factors Using PDIs

	All Data
Nat Ag	
NatAgNP1-May12-F	0.25
NatAgNP1-May12-IC	0.26
NatAgNP1-Oct12-F	0.13
NatAgNP2-May12-F	0.33
NatAgNP2-May12-IC	0.28
NatAgNP2-Oct12-F	0.15
NatAgNP3-May12-F	0.20
NatAgNP3-May12-IC	0.23
NatAgNP3-Oct12-F	0.25
Average	0.23
SD	0.06
107Ag	
107AgNP1-May12-F	0.22
107AgNP1-May12-IC	0.16
107AgNP1-Oct12-F	0.18
107AgNP2-May12-F	0.25
107AgNP2-May12-IC	0.27
107AgNP2-Oct12-F	0.20
107AgNP3-May12-F	0.24
107AgNP3-May12-IC	0.29
107AgNP3-Oct12-F	0.44
Average	0.25
SD	0.08
t-test p-value	**0.59**

Pristine Vs Aged Using PDIs

	All Data
Pristine	
Nat-AgNP1-May12-F	0.25
107-AgNP1-May12-F	0.22
Nat-AgNP1-May12-IC	0.26
107-AgNP1-May12-IC	0.16
Nat-AgNP1-Oct12-F	0.13
107-AgNP1-Oct12-F	0.18
Nat-AgNP2-May12-F	0.33
107-AgNP2-May12-F	0.25
Nat-AgNP2-May12-IC	0.28
107-AgNP2-May12-IC	0.27
Nat-AgNP2-Oct12-F	0.15
107-AgNP2-Oct12-F	0.20
Nat-AgNP3-May12-F	0.20
107-AgNP3-May12-F	0.24
Nat-AgNP3-May12-IC	0.23
107-AgNP3-May12-IC	0.29
Nat-AgNP3-Oct12-F	0.25
107-AgNP3-Oct12-F	0.44
Average	0.24
SD	0.07
Aged	
Nat-AgNP1-May12-F	0.25
107-AgNP1-May12-F	0.20
Nat-AgNP1-May12-IC	0.23
Nat-AgNP1-Oct12-F	0.11
107-AgNP1-Oct12-F	0.22
Nat-AgNP2-May12-F	0.25
107-AgNP2-May12-F	0.34
Nat-AgNP2-May12-IC	0.35
107-AgNP2-May12-IC	0.18
Nat-AgNP2-Oct12-F	0.10
107-AgNP2-Oct12-F	0.18
Nat-AgNP3-May12-IC	0.31
107-AgNP3-May12-IC	0.21
Nat-AgNP3-Oct12-F	0.52
107-AgNP3-Oct12-F	0.39
Average	0.27
SD	0.12
t-test p-value	**0.65**

Appendices ii)

Paper arising from the work of Chapter 3:

‘Synthesis and characterization of isotopically labeled silver nanoparticles for tracer studies’

Environmental Science Nano

ROYAL SOCIETY OF CHEMISTRY

PAPER

View Article Online
View Journal

Synthesis and characterization of isotopically labeled silver nanoparticles for tracing studies†

Cite this: DOI: 10.1039/c3en00100h

Adam Laycock,*[ab] Björn Stolpe,[c] Isabella Römer,[c] Agnieszka Dybowska,[b] Eugenia Valsami-Jones,[bc] Jamie R. Lead[cd] and Mark Rehkämper[ab]

Published on 27 March 2014. Downloaded on 27/04/2014 23:45:40.

Received 3rd December 2013,
Accepted 26th March 2014

DOI: 10.1039/c3en00100h

rsc.li/es-nano

Silver nanoparticles (AgNPs) are ever more being used in industrial processes and consumer products, resulting in increasing emissions to the natural environment. To understand the behavior and environmental fate of AgNPs, it is paramount that they can be traced in complex natural samples from exposures at high sensitivity. The technique of stable isotope labeling is ideally suited for this purpose. To support such applications, we present a detailed evaluation of techniques for the preparation of stable isotope labeled AgNPs and demonstrate that isotopically modified particles are only distinguishable from particles with a natural isotope composition by their strong isotopic signature. Monodisperse suspensions of citrate-stabilized AgNPs with target sizes of 17, 20 and 30 nm were synthesized by reduction of silver nitrate solutions with sodium borohydride. The AgNP suspensions were produced using both natural Ag, which is comprised of the two stable isotopes ^{107}Ag (52%) and ^{109}Ag (48%), and Ag enriched to 99.2% in ^{107}Ag. Synthesis was reliably reproduced on three separate occasions in two laboratories. The AgNPs were characterized using dynamic light scattering (DLS) shortly after synthesis and after up to 12 months storage. Some of the batches were also characterized using transmission electron microscopy (TEM) and asymmetric flow field-flow fractionation (FlFFF). The particle size distributions showed good reproducibility between the laboratories and stability over 12 months of storage. Importantly, the ^{107}Ag-enriched particles were indistinguishable in size and shape from particles with a natural isotope composition. The reliability, control on particle size, and high yield of about 80%, demonstrate that the synthesis technique is well suited for small-scale production of isotopically labeled AgNPs. Isotope mass balance calculations furthermore show that the application of labeling enables tracing sensitivities for AgNPs that are at least 40 times, and possibly up to 4000 times, higher than those achievable with bulk Ag concentration measurements and experiments with exposure concentrations that approach predicted environmental levels are possible, if the most precise isotopic measurement techniques are employed.

Nano impact

The application of isotopically labeled nanoparticles enables the accurate and precise tracing of these materials in exposure experiments, even when carried out at low and environmentally relevant concentrations. However, isotopically labeled nanoparticles are not commercially available and published synthesis techniques tend to be unsuitable for use with an isotopically enriched pre-cursor material. This is the first study to provide protocols specifically optimized for the small-scale, high yield synthesis of isotopically labeled silver nanoparticles with defined sizes. The synthesis techniques are rigorously assessed and shown to be fit for purpose. Apart from their isotope composition the silver nanoparticles produced using both a 'natural' and an isotopically enriched precursor are shown to be indistinguishable. In addition the nanoparticle suspensions are shown to be stable after 12 months storage. A comprehensive evaluation of the nanoparticles produced here demonstrates the detection capabilities possible when these materials are employed in environmental tracer studies. Detailed equations are also presented to show how the quantification of an enriched isotope label can be achieved from the isotope ratio of a sample.

[a] Department of Earth Science & Engineering, Imperial College London, South Kensington, London SW7 2AZ, England, UK. E-mail: a.laycock10@imperial.ac.uk; Tel: +44 (0)20 7594 7140
[b] Department of Earth Sciences, Natural History Museum, Cromwell Road, London SW7 5BD, England, UK
[c] School of Geography, Earth and Environmental Sciences, University of Birmingham, Edgbaston, Birmingham, B15 2TT, England, UK
[d] Center for Environmental Nanoscience and Risk, Department of Environmental Health Sciences, Arnold School of Public Health, University of South Carolina, Columbia, SC 29208, USA

† Electronic supplementary information (ESI) available. See DOI: 10.1039/c3en00100h

Published on 27 March 2014. Downloaded on 27/04/2014 23:45:40.

1. Introduction

As a consequence of the ubiquitous use of Ag in the photography and imaging industries, anthropogenic emissions of Ag and their environmental fate have been monitored for many decades.[1] Whilst the rise of digital photography has significantly reduced such emissions, new concerns have arisen as engineered Ag nanoparticles (AgNPs) are increasingly employed in a broad range of industrial processes and consumer products and emitted into the environment.[1,2] Whilst not comprehensive, there are currently 390 products (November 2013) listed on the Woodrow Wilson Database[3] that incorporate nano-silver, demonstrating the diverse range of products in which this nanomaterial is found. A focus of current research and debate is whether there are (nano-) specific effects, which increase the bioavailability and toxicity of Ag when present in nanoparticulate form.[2] This concern has prompted numerous studies to investigate the environmental transport, behavior, fate and ecotoxicology of engineered AgNPs.

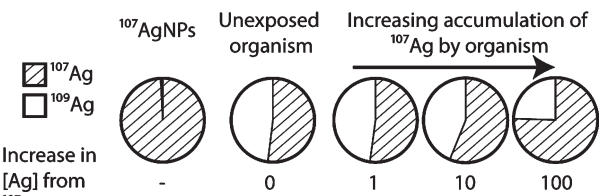
Ideally, such studies are carried out at 'realistic' environmental conditions, whereby exposures employ NM (nanomaterial) concentrations that are similar to or not far removed from present or predicted values. Recently, Gottschalk, *et al.*[4] compiled and reviewed measured and modeled environmental concentrations of engineered NMs. Based on the reviewed data, predicted environmental levels of engineered nano-Ag are in the range of 0.1 to 100 ng L^{-1} for surface waters, 1 to 100 ng L^{-1} for effluents of waste water treatment plants, 1 to 1000 μg kg^{-1} for biosolids, 1 to 10 μg kg^{-1} for sediments, and 0.1 to 1000 μg kg^{-1} for soils. Significantly, these levels are roughly similar to the natural Ag background concentrations of these materials.[5]

Studies that interrogate the environmental fate of AgNPs typically employ concentration measurements by ICP-MS to quantify the presence of Ag (from NPs) in exposure systems. Such analyses are straightforward but require that exposures employ AgNP concentrations that exceed 'realistic' environmental levels by several orders of magnitude. This requirement follows from (i) the comparatively high natural Ag background (see above), and (ii) the condition that unequivocal tracing of AgNPs relies on the detection of anomalies in Ag concentration that clearly exceed these background levels. For example, Shoults-Wilson, *et al.*[6] used AgNP concentrations of 10 to 1000 mg kg^{-1} in soil exposures of the earthworm *Eisenia fetida*, whilst Zhao and Wang[7] applied AgNPs at 20 to 500 μg L^{-1} in a waterborne exposure of *Daphnia magna*. It is conceivable that ecotoxicity studies, which are carried out at such high (and unrealistic) AgNP concentrations, may induce and thus identify distinct patterns of particle behavior and biological interactions that are only relevant for the high particle concentrations that are employed. The challenge is, therefore, to investigate whether the same effects are also observed at low but environmentally relevant NP levels.

To circumvent the limited sensitivity of concentration tracing, alternative NM tracing methods have been explored, particularly fluorescent coatings[8,9] and radiolabeling,[10–12] but both techniques have associated drawbacks. The application of fluorescent coatings can affect the surface chemistry of the materials and influence their behavior, such as changes to and suppression of dissolution.[13] The coatings may furthermore dissociate from the NPs[14] and free ions from NP dissolution cannot be traced with this method. Radiolabeled nanomaterials are produced by activation in a nuclear reactor[15,16] and the technique is therefore hindered, as specialist equipment, dedicated laboratories and licenses are required for the handling of radioactive materials. A further disadvantage is the often short half-lives of the radiolabels.

An attractive alternative method of labeling, which does not suffer from the above drawbacks, involves the application of enriched stable isotopes. The basic approach of stable isotope labeling relies on the detection of changes in a diagnostic isotope ratio, which are produced in an experimental system by the introduction of a 'contaminant' that is prepared from a highly enriched single isotope of the target element. In the case of Ag, the natural form of the element consists of nearly equal amounts of the isotopes ^{107}Ag and ^{109}Ag but highly enriched (to >99%) ^{107}Ag can be purchased from a number of sources. The introduction of essentially pure ^{107}Ag into an exposure will not only increase the total Ag concentration of the system but also change the $^{107}Ag/^{109}Ag$ isotope ratio, such that this exceeds the natural value of ~1. The magnitude of the isotopic perturbation hereby depends on the relative contributions of enriched ^{107}Ag to natural Ag (Fig. 1). As (i) natural variations in isotope compositions are typically small for most elements and (ii) isotope ratios can be measured much more precisely than absolute concentrations, the use of enriched stable isotopes provides an extremely selective and sensitive means of elemental tracing, even in the presence of high natural background levels.[17,18] Consequently, the stable isotope approach has been used successfully for several decades in the fields of medical, life and environmental sciences, when highly sensitive and precise tracing methods were required.[19,20]

More recently, it has been shown that stable isotope tracing can also be applied to nanomaterials, with pioneering studies of ZnO and CuO NPs.[17,18,21–23] A unique requirement of such investigations is that the labeled NPs must be specifically prepared, from a single, highly enriched stable isotope



Increase in [Ag] from ^{107}AgNPs (%)	-	0	1	10	100
^{107}Ag (%)	99.20	51.84	52.31	56.14	75.52
^{109}Ag (%)	0.80	48.16	47.69	43.86	24.48
^{107}Ag/^{109}Ag	124.0000	1.0764	1.0968	1.2802	3.0849

Fig. 1 Demonstrates how the contribution from isotopically enriched ^{107}Ag to a natural Ag background will result in a deviation in the $^{107}Ag/^{109}Ag$ that can be directly related to the degree of accumulation.

 This journal is © The Royal Society of Chemistry 2014

Published on 27 March 2014. Downloaded on 27/04/2014 23:45:40.

form of the element. Particular advantages of this approach are (i) high versatility, as it can, in principle, be applied to any NP with a multi-isotopic element as the main constituent; (ii) the label cannot be lost by dissociation or degradation; and (iii) the unique isotopic signature of the element remains traceable even if the speciation of the original material changes, for example by dissolution. The methodology, however, also requires that a suitable protocol for the preparation of labeled NPs is available. Whilst recipes for the synthesis of various NMs with defined sizes and properties are abundant in the literature, most of these methods are either unsuitable for the synthesis of stable isotope labeled NPs or they provide insufficient documentation for this purpose. This conclusion follows from the relatively high price of commercially available enriched stable isotopes, which typically cost about $2 to $20 per mg of metal or metal oxide. Given this non-negligible cost, methods for the preparation of isotopically labeled NMs must be optimized with a focus on small-scale synthesis, reliability and high yields. These factors, however, are generally not considered in conventional synthesis protocols, where particle size and shape are typically of higher priority.

In this study, we have examined existing protocols to develop techniques for the optimized preparation of isotopically labeled AgNPs with distinct sizes. Rigorous evaluations demonstrate that the methods are suitable for routine and reliable small-scale synthesis of stable isotope labeled AgNPs at yields of ~80%. The characterization of both labeled AgNPs and control samples produced from natural Ag furthermore unequivocally establishes that the labeling process does not generate distinct or unusual physico-chemical particle properties. This is essential in order to demonstrate that isotopically modified AgNPs are equivalent to AgNPs with a natural isotope composition and to validate the findings of any studies carried out using isotopically modified AgNPs, such as the recent investigation of Gigault and Hackley.[24] These workers[24] used asymmetric-flow field flow fractionation system coupled with on-line ICP-MS detection to show how a stable isotope label may be used to confirm the presence of Ag from an isotopically enriched source within a natural sample. While this technique offers rapid and definitive results it does not allow accurate quantification of the enriched material in a sample. Our study assesses the utility of the isotope tracing approach beyond the level of simply detecting the isotope label in a sample. To this end, we present the results of simple model calculations, which reveal the lowest levels at which isotopically labeled AgNPs can be detected and accurately quantified in relevant natural samples by stable isotope tracing, when different common mass spectrometric methods are employed for analysis.

2. Experimental

The AgNPs were synthesized by appropriately modified standard reduction methods.[25,26] In particular, batches of particles with 3 target sizes were produced from both natural Ag and enriched ^{107}Ag. Two operators carried out the AgNP synthesis on three occasions in two laboratories and the reproducibility of the methods was assessed by comprehensive characterization of all NP batches produced.

2.1 Choice of isotope label

When selecting an enriched stable isotope for labeling there are several key considerations, including degree of isotopic enrichment, cost of the material and the diagnostic isotope ratio that will be monitored for the purpose of tracing. A detailed discussion of these factors is provided by Larner and Rehkämper.[27] Silver has two naturally occurring stable isotopes, ^{107}Ag and ^{109}Ag, that have near equal natural abundances of 51.8% and 48.2%, respectively, and both are available at an enrichment of about 99% (Isoflex U.S.A., February 2012). As both isotopes are equally suitable for tracing, ^{107}Ag was chosen here for labeling because it was marginally cheaper than ^{109}Ag (Isoflex U.S.A., February 2012).

2.2 Chemicals and reagents

Powdered Ag metal enriched to 99.2% in ^{107}Ag (Isoflex U.S.A.) was converted to $^{107}AgNO_3$ by dissolution in 15.4 M HNO_3 and subsequent evaporation to dryness. Natural $AgNO_3$ (>99% purity), trisodium citrate dihydrate (>99% purity) and sodium borohydride (99.99% trace metals basis) were purchased from Sigma-Aldrich. Water of >18.2 MΩ cm quality (Millipore, UK) and quartz-distilled mineral acids were used throughout. Dilute artificial seawater (dilute-ASW) with a salinity of about 16 PSU was produced by dissolution of 32 g of Tropic Marin Salt in 2 L purified water and used as medium for a dialysis study to assess dissolution.

2.3 Synthesis

The synthesis protocols used here were adapted from the methods outlined by Römer, *et al.*[26] Three protocols, denoted AgNP1, AgNP2, and AgNP3 (Table 1), were applied to produce particles with target sizes of 30, 20 and 17 nm, both with enriched ^{107}Ag (denoted as 107-AgNP1, 107-AgNP2 and 107-AgNP3, respectively) and natural Ag (denoted as Nat-AgNP1, Nat-AgNP2 and Nat-AgNP3). The NP batches are further designated to indicate (i) the date of synthesis, either May or October 2012 (May12 or Oct12), and (ii) the laboratory in which synthesis was conducted, either at the Facility for Environmental Nanoscience Analysis and Characterization (FENAC) at the University of Birmingham or the MAGIC (Mass Spectrometry and Isotope Geochemistry at Imperial College) Laboratories at Imperial College London, (F and IC respectively). For example, the non-labeled AgNPs with a 20 nm target size prepared at FENAC in October 2012 are identified as Nat-AgNP2-Oct12-F (Table 1).

For synthesis, 100 mL aqueous solutions of 0.25 mM sodium citrate and 0.30 mM silver nitrate were cooled to 4 °C, combined in a conical flask and vigorously stirred. To the AgNP1 and AgNP2 batches, 6 mL aqueous $NaBH_4$ was added

Published on 27 March 2014. Downloaded on 27/04/2014 23:45:40.

Table 1 Summary of characterization data obtained for batches of ^{107}AgNPs and natural AgNPs prepared on three different occasions using the three synthesis protocols. Results are shown for both pristine particles and after up to 12 months of storage

Freshly prepared particles										Particles after storage		
	DLS			TEM		FIFFF				DLS		
Particle batch[a]	Yield (%)	Diameter[b] (nm)	PDI[c]	Diameter[d] (nm)	CV[e]	d_n[f] (nm)	d_w[g] (nm)	PD[h]	FWHM[i] (nm)	Storage[j] (months)	Diameter[b] (nm)	PDI[c]
AgNP1 protocol – target particle size 30 nm												
Nat-AgNP1-May12-F	91	41.6	0.25			36	49	1.3	24	12	41.5	0.25
107-AgNP1-May12-F	64	29.3	0.22			27	31	1.2	26	12	29.7	0.20
Nat-AgNP1-May12-IC	14	35.5	0.26							12	35.3	0.23
107-AgNP1-May12-IC		31.2	0.16									
Nat-AgNP1-Oct12-F	79	26.5	0.13	22.3 ± 6.7	0.30					6	26.8	0.11
107-AgNP1-Oct12-F	98	31.2	0.18	28.2 ± 8.3	0.29					6	33.7	0.22
AgNP2 protocol – target particle size 20 nm												
Nat-AgNP2-May12-F	87	20.7	0.33			18	21	1.2	18	12	19.7	0.25
107-AgNP2-May12-F	83	16.7	0.25			17	22	1.3	17	12	14.6	0.34
Nat-AgNP2-May12-IC	61	17.2	0.28							8	16.8	0.35
107-AgNP2-May12-IC	61	16.3	0.27							12	17.5	0.18
Nat-AgNP2-Oct12-F	63	22.6	0.15	19.5 ± 5.7	0.29					6	22.9	0.10
107-AgNP2-Oct12-F	78	23.9	0.20	20.1 ± 6.3	0.31					6	24.1	0.18
AgNP3 protocol – target particle size 17 nm												
Nat-AgNP3-May12-F		17.1	0.20			16	18	1.1	11			
107-AgNP3-May12-F		24.3	0.24									
Nat-AgNP3-May12-IC	77	18.2	0.23							12	16.8	0.31
107-AgNP3-May12-IC	31	20.6	0.29							12	24.1	0.21
Nat-AgNP3-Oct12-F	80	17.2	0.25	18.0 ± 5.2	0.29					6	32.5	0.52
107-AgNP3-Oct12-F	76	28.1	0.44	16.3 ± 4.8	0.29					6	26.1	0.39

DLS – Dynamic light scattering, TEM – Transmission electron microscopy, FIFFF – Asymmetric Flow Field Flow Fractionation.[a] Each particle batch was designated depending on (i) whether the batch was labeled or non-labeled (107-AgNP or Nat-AgNP), (ii) which synthesis protocol was used for the production (1, 2 or 3; see Table 2), (iii) whether the particles were made in May or October 2012 (May12 or Oct12) and (iv) the laboratory in which the synthesis was carried out, either at FENAC, University of Birmingham (F) or the MAGIC Laboratory, Imperial College London (IC). [b] The hydrodynamic diameter was calculated as the average of individual DLS measurements. [c] Polydispersity index. [d] The average TEM diameter ±1sd is calculated from analyses of 234–337 individual particles. [e] Coefficient of variance = Standard deviation/TEM diameter. [f] The number average hydrodynamic diameter. [g] The weighted average hydrodynamic diameter. [h] Polydispersity (d_n/d_f). [i] Full width at half maximum. [j] Particle storage was in the dark at 4 °C.

at a concentration of 10 and 1 mM, respectively, whilst nothing was added to the AgNP3 batch at this stage. For all protocols, the mixtures were then boiled for 90 minutes, after which the AgNP1 and AgNP2 mixtures were removed from the heat. For the AgNP3 batches, 6 mL of 10 mM aqueous $NaBH_4$ solution were added to the mixture after 90 minutes of boiling, followed by boiling for a further 10 minutes. All solutions were thereafter allowed to cool overnight in the dark at room temperature. A summary of the synthesis protocols is given in Table 2.

The particle suspensions were filtered through 0.1 μm pore-size cellulose acetate filters to remove any larger (non-nano) particulates. Non-reacted reagents were thereafter removed by either diafiltration or dialysis. In the diafiltration method, the volume of the suspensions was reduced to ~20 mL without drying, by forcing through a 1 kDa (~1 nm) molecular weight

Table 2 Summary of AgNP synthesis protocols

	Synthesis protocol		
Step	AgNP1	AgNP2	AgNP3
Mix Na-citrate[a] & Ag-nitrate[b] solutions then stir for	10 min	10 min	10 min
Add 6 mL $NaBH_4$[c] solution	10 mM	1 mM	—
Boil mixture	90 min	90 min	90 min
Add 6 mL $NaBH_4$[c] solution	—	—	10 mM
Continue to boil	—	—	10 min
Allow to cool in the dark	RT[d]	RT[d]	RT[d]

[a] 100 mL of 0.30 mM Na-citrate solution in >18.2 MΩ cm water. [b] 100 mL of 0.25 mM Ag-nitrate solution in >18.2 MΩ cm water. [c] Aliquot, with appropriate dilution, of 100 mL of 10 mM $NaBH_4$ stock solution in >18.2 MΩ cm water. [d] RT = room temperature.

 This journal is © The Royal Society of Chemistry 2014

Published on 27 March 2014. Downloaded on 27/04/2014 23:45:40.

cut-off (MWCO) regenerated cellulose ultrafiltration membrane (Amicon, Millipore) using a nitrogen gas pressurized and stirred filtration cell. The suspension volume was then re-adjusted back to ~200 mL using 0.15 mM sodium citrate solution and this process was repeated three times. For the dialysis method, the suspensions were transferred to 1 kDa MWCO dialysis bags (Spectra/Por) followed by dialysis against 5 L of 0.15 mM sodium citrate solution for 72 hours. The AgNP suspensions in aqueous Na-citrate from all protocols and filtration methods were thereafter stored in the dark at 4 °C.

2.4 Characterization of particle size

2.4.1 Dynamic light scattering (DLS). The hydrodynamic diameter (average size) and polydispersity index (PDI) of the AgNPs were determined at 25 °C using a Zetasizer Nano ZS ZEN3600 (Malvern Instruments Ltd. Malvern, UK) operating with a He–Ne laser at a wavelength of 633 nm and measuring back-scattered light at 173° relative to the incident beam. Each sample was analyzed at least 5 consecutive times within 24 hours of filtering. Some samples were analyzed after up to 12 months storage to give an indication of particle stability.

2.4.2 Transmission electron microscopy (TEM). For TEM analyses, the AgNPs from 10 mL of the stock suspensions were deposited onto 300 mesh Formvar/carbon coated Cu-grids by ultracentrifugation (Beckman L-75) at 30 000 rpm for 60 minutes. Grids were then rinsed by immersing in 18 MΩ water for a few seconds and dried overnight. The TEM micrographs were obtained from 3 to 5 different areas on each grid, at a magnification of 30 000×, 100 000× and 300 000×. The diameters of at least 200 particles in each sample were then determined on the micrographs with 300 000× magnification using the computer software Digital Micrograph (Gatan Inc.).

2.4.3 Asymmetric flow field-flow fractionation (FlFFF). The hydrodynamic diameter distributions of selected AgNP batches (Table 1), were determined within one week of preparation by FlFFF, using an AF2000 instrument (Postnova Analytics) following the method of Römer, *et al.*[26] and Baalousha and Lead.[28] The FlFFF channel featured a 1 kDa regenerated cellulose ultrafiltration membrane (Postnova Analytics) and 0.01 M $NaNO_3$ was used as a carrier solution. The AgNPs were fractionated with cross-flow and detector flow both set to 1 mL min^{-1}, and their elution from the FlFFF channel was monitored by UV-absorbance measurements at 254 nm (Postnova Analytics). The FlFFF channel thickness was calibrated by analyzing polystyrene latex standards with known diffusion coefficients under the same flow conditions as the AgNPs, and the diffusion coefficient distributions of the AgNPs were thereafter calculated using FlFFF theory.[29] The hydrodynamic diameter distributions were calculated from diffusion coefficients with the Stokes–Einstein equation.

2.4.4 Yield determination. To assess synthesis yields, 10 μl aliquots of 24 particle suspensions were dissolved in concentrated HNO_3 and refluxed on a hotplate at 80 °C for 48 hours to ensure complete dissolution. The resulting solutions were evaporated to dryness and re-dissolved in 0.1 M HNO_3. Aliquots of these stock solutions were then used to prepared more dilute 0.1 M HNO_3 'measuring' solutions that featured Ag concentrations of about 20 ng mL^{-1} and that were doped with Pd as an internal standard, also at 20 ng mL^{-1}. The technique of internal standardization, as opposed to an isotope dilution protocol, was applied for quantification because the former produces sufficiently accurate and precise data (about ±1 to 2%) and its application is very straightforward for analyses of both labeled and unlabeled materials.

For quantification, the samples were analyzed relative to a standard solution with Ag and Pd abundances of 20 ng mL^{-1} in the same acid matrix, using a Nu Plasma multiple collector ICP-MS (MC-ICP-MS) instrument at the Imperial College MAGIC Laboratories. In these analyses the total Ag (^{107}Ag + ^{109}Ag) signal intensities obtained for samples were compared to the standard solution and ^{105}Pd was monitored to correct for any drifts in instrumental sensitivity. The measurements provided the total Ag concentrations of the solutions and the yields of the synthesis methods were then calculated based on (i) the dilutions factors used for the preparation of the measuring solutions and (ii) the total mass of Ag used for particle preparation.

2.4.5 Dissolution behavior. The dissolution of the AgNPs was assessed by equilibrium dialysis. To this end, a PE container was filled with 500 mL of a suspension of 107-AgNP2-Oct-F in dilute-ASW, at a concentration of 0.9 mg L^{-1} Ag and 3.9 mg L^{-1} sodium citrate. Two dialysis bags (1 kDa MWCO) were filled with 25 mL of dilute-ASW and immersed in the container. The container was thereafter kept in the dark to avoid Ag photodecomposition and stirred continuously. Sample aliquots of 0.5 mL were taken from both the inside and outside of the dialysis bags on 14 occasions over a period of 27 days. A control experiment to assess how dissolved Ag behaves during dialysis was carried out under the same conditions with 1 mg L^{-1} Ag from an aqueous solution of $AgNO_3$. The background Ag concentrations for both experiments were assessed from representative samples of dilute-ASW. Following completion of the experiments, the Ag concentrations of sample aliquots were determined at FENAC by graphite furnace atomic absorption spectrometry (GFAAS, Perkin Elmer AAS600).

3. Results & discussion

All information gathered from the characterization of the 18 batches of AgNPs that were prepared during the study is summarized in Table 1 and discussed in the following.

3.1 Size characterization of nanoparticles

3.1.1 DLS analyses. The average hydrodynamic diameter measured by DLS on the freshly made particles deviates by less than ±20% from the target size, with the exception of three batches (Nat-AgNP1-May12-F, 107-AgNP3-May12-F, and

Published on 27 March 2014. Downloaded on 27/04/2014 23:45:40.

107-AgNP3-Oct12-F), where the average diameter was 40 to 70% larger than the target size (Table 1).

In the following, we present and discuss the results of a statistical evaluation that interrogates whether isotopic labeling or other factors (*e.g.*, date or laboratory of synthesis) had a significant impact on the size of the prepared AgNPs. In order to incorporate all particle suspensions in this evaluation, including batches with different target sizes, we adopted the following procedure:

(i) All particle suspensions were split into one of three groups depending on their target particle size (17, 20 and 30 nm). For each individual batch, the proportional difference from the mean size (PDMS) of the group was calculated. This was achieved by finding the mean particle size (MS), as determined by DLS, for each group. The particle size determined for an individual suspension (SamS) was then subtracted from the mean value, to calculate the absolute difference between the individual and mean particle sizes. The proportional difference was then determined by dividing the absolute difference by the mean particle size (eqn (1), see ESI†).

$$\mathrm{PDMS} = (\mathrm{MS} - \mathrm{SamS})/\mathrm{MS} \quad (1)$$

This normalization procedure was validated by *t*-tests that, where possible, were carried out using both measured absolute size data and the calculated relative size differences. Specifically, this was possible when the DLS sizes of Nat-AgNPs were compared with 107-AgNPs for each of the three target sizes (30 nm, 20 nm, 17 nm; see ESI†) Notably, these three *t*-tests yielded exactly identical results when they were conducted with both the absolute and the normalized size data (see ESI†). This result validates the application of the normalized particles size data (obtained as detailed above) in further *t*-tests.

(ii) The PDMSs calculated for each individual particle suspension were pooled in different manners to produce populations that were evaluated using a student's *t*-test. These tests evaluated whether there are significant and systematic differences in size that can be assigned to a specific factor (see ESI†).

Based on two-tailed *t*-tests for populations of unequal variance, there was no significant difference at the 95% confidence level ($p = 0.05$) when the PDMSs were grouped into the following populations; (i) Nat-AgNPs and labeled 107-AgNPs ($p = 0.57$), (ii) synthesis at the FENAC and Imperial College laboratories ($p = 0.18$), (iii) synthesis date (*e.g.*, May12-F, May12-IC and Oct12-F; $p = 0.27$ to 0.73), (iv) NP preparation by operators AL and BS (particle synthesis in May and October 2012 respectively; $p = 0.45$), and (v) freshly prepared and aged particles after 6–12 months storage ($p = 0.98$). These results were obtained with the omission of batches 107-AgNP1-May12-F and 107-AgNP3-Oct12-F, which have particularly anomalous sizes of 41.6 nm (target size 30 nm) and 28.1 nm (target size 17 nm), respectively. These unusually large deviations from the target size may reflect experimental problems during synthesis. However, very similar results are produced when these data are included in the above *t*-test evaluations. A detailed summary of the *t*-test data and calculated *p*-values is presented in the ESI.†

Notably, the average particle diameters of the suspensions after storage deviated by less than 3.5 nm from the average diameters that were measured directly after preparation. The only exception is sample Nat-AgNP3-Oct-F, where the average diameter increased by about 90% (15.3 nm; Table 1). The PDIs determined by DLS were less than 0.45 for all AgNP suspensions and less than 0.3 for 16 of the 18 batches, indicating that the particle size distributions were fairly monodisperse (Table 1). A *t*-test demonstrated that there was no significant difference between the PDIs of (i) Nat-AgNPs and 107-AgNPs ($p = 0.59$) and (ii) pristine particles and particles after storage ($p = 0.65$) (see ESI†).

Whilst the *t*-tests discussed above indicate that there are no statistically significant differences in particles size and PDI that can be assigned to a single factor, the data of Table 1 nonetheless demonstrate small but resolvable differences in particle size for NP batches prepared with the same protocol. Given the results of the *t*-tests, these disparities most likely reflect 'normal' batch-to-batch variations that occur, if syntheses are carried out on different days, in different laboratories and by different operators. These results hence provide an indication of the particle size variability that can be expected if different scientists apply the protocols of Table 2 in their own laboratories. In contrast, Römer, *et al.*[26] previously demonstrated that, using similar protocols for the preparation of AgNPs, repeated synthesis by the same operator, in the same laboratory with the same equipment and reagents, can routinely provide particle batches with highly reproducible sizes. In summary, these results thus demonstrate that despite small batch-to-batch variations in particles size that reflect slight differences in experimental conditions, the protocols summarized in Table 2 are suitable for the robust and reliable synthesis of isotopically labelled AgNPs in different laboratories.

3.1.2 TEM analyses. Selected freshly prepared AgNP batches were imaged by TEM and evaluated by measuring the longest axis of discrete particles rather than their aggregates (Table 1, Fig. 2). The TEM micrographs show that the particles were spherical in shape and had a consistent size distribution, with the standard deviation of all batches being 40 to 45% of the average particle diameter, equivalent to coefficients of variance of 0.29–0.31 (Table 1).30 It is likely that the aggregation of particles seen in the micrographs occurred during drying of the samples on the TEM grids and is not due to the fusion of particles during synthesis. This conclusion is supported by the predominance of discrete particles in suspension, as indicated by the DLS results.

The average diameters determined from the TEM micrographs were typically 10 to 15% (about 3–4 nm) smaller than the average hydrodynamic diameters determined by DLS. This is a well-known phenomenon, which reflects that larger particles scatter proportionally more light, such that the average DLS particle diameters are biased towards larger values.[28] The exceptions to this are samples Nat-AgNP3-Oct12-F and

 This journal is © The Royal Society of Chemistry 2014

Published on 27 March 2014. Downloaded on 27/04/2014 23:45:40.

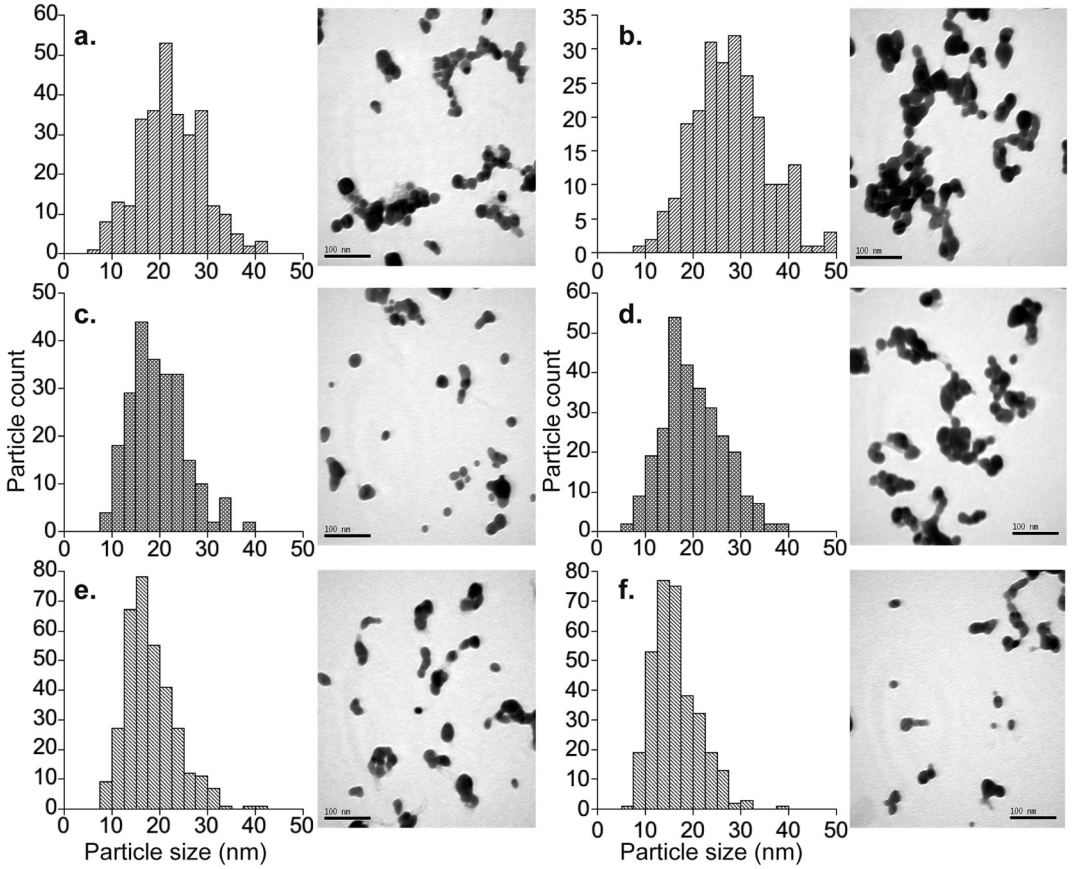


Fig. 2 TEM images and measured particle size distributions for particles batches synthesized in October 2012. all images are at a magnification of 300 000x; scale bars are 0.1 μm. (a) Nat-AgNP1-Oct12-F average particle size = 22.3 ± 6.7 nm (1sd) n = 290; (b) 107-AgNP1-Oct12-F average particle size = 28.2 ± 8.3 nm (1sd) n = 236; (c) Nat-AgNP2-Oct12-F average particle size = 19.5 ± 5.7 nm (1sd) n = 234; (d) 107-AgNP2-Oct12-F average particle size = 20.1 ± 6.3 nm (1sd) n = 283; (e) Nat-AgNP3-Oct12-F average particle size = 18.0 ± 5.3 nm (1sd) n = 337; (f) 107-AgNP3-Oct12-F average particle size = 16.3 ± 4.8 nm (1sd) n = 333.

107-AgNP3-Oct12-F. The Nat-AgNP3-Oct12-F particle batch shows an average TEM particle size that is very close to that determined by DLS, whereas there is a large discrepancy between the DLS (28.1 nm) and TEM (16.3 nm) size data for 107-AgNP3-Oct12-F. These observations are likely a consequence of the polydispersity of the respective samples. In particular, the particle size distribution histogram of Nat-AgNP3-Oct12-F shows the smallest size range (Fig. 2), suggesting it is highly monodisperse and therefore the DLS analysis shows very little size bias. In contrast, 107-AgNP3-Oct12-F is the most polydisperse sample (PDI = 0.44), and this may reflect a small number of larger particles in the suspension that heavily bias the DLS measurement.

3.1.3 FIFFF analyses. The FlFFF analysis[31,32] of selected AgNP samples provided full width at half maximum (FWHM) data for particle batches Nat-AgNP1-May12-F (24 nm), 107-AgNP1-May12-F (26 nm), Nat-AgNP2-May12-F (18 nm), ^{107}AgNP2-May12-F (17 nm) and Nat-AgNP3-May12-F (11 nm) (Fig. 3, Table 1). In addition, the FlFFF data were used to determine the number average hydrodynamic diameters (d_n), weighted average hydrodynamic diameters (d_w) and polydispersity (PD) using eqn (2)–(4), respectively, with results given in Table 1.

$$d_n = \sum_i C_i X_i / \sum_i C_i \quad (2)$$

$$d_w = \sum_i C_i X_i^2 / \sum_i C_i X_i \quad (3)$$

$$PD = d_w/d_n \quad (4)$$

Here, C_i is the UV-absorbance signal at a given hydrodynamic diameter, X_i. The d_n values were typically slightly smaller (up to 13%) whilst d_w was slightly larger (up to 32%) compared to the particle size determined by DLS. The d_n values for 107-AgNP2-May12-F (17 nm) and Nat-AgNP2-May12-F (18 nm) were only slightly larger than for Nat-AgNP3-May12-F (16 nm). The two former samples also showed a higher PD value than Nat-AgNP3-May12-F, with size distributions tailing towards larger diameters (Fig. 3). As a consequence, there is a slightly lager difference in d_w values between

Published on 27 March 2014. Downloaded on 27/04/2014 23:45:40.

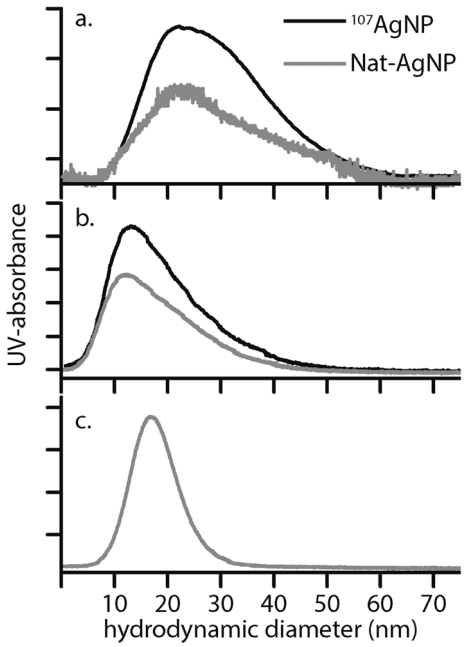


Fig. 3 Hydrodynamic diameter distributions determined by FIFFF for selected AgNP batches. (a): 107-AgNP1-May12-F and Nat-AgNP1-May12-F, (b) 107-AgNP2-May12-F, Nat-AgNP2-May12-F and (c) Nat-AgNP3-May12-F.

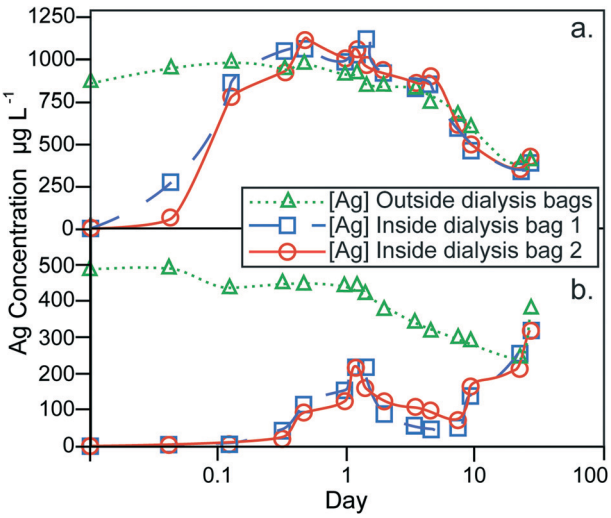


Fig. 4 Results for AgNP dissolution behavior in dilute-ASW, assessed by dialysis. (a) Control experiment, whereby aqueous $AgNO_3$ solution is added to the dilute asw outside of the dialysis bags to a concentration of 1 mg L^{-1}. (b) Experiment where ^{107}AgNPs, from particle batch 107-AgNP2-Oct12-F, were added to the dilute-asw outside of the dialysis bags to a concentration of 0.9 mg L^{-1}.

107-AgNP2-May12-F (22 nm) and Nat-AgNP2-May12-F (21 nm) *versus* Nat-AgNP3-May12-F (18 nm).

3.2 Synthesis yields

Reliable small-scale synthesis techniques with high yields are required for the production of isotopically labeled NPs, due to the expense of using enriched stable isotopes (*e.g.*, about $3.50 per mg for ^{107}Ag purchased from Isoflex USA in February 2012). The total Ag concentrations of 24 different particle suspensions, encompassing 16 batches of labeled ^{107}AgNPs and 8 batches of non-labeled AgNPs, were determined to assess the yield of the synthesis protocols (Table 1). Typically the yields were between 60% and 98%, with an average of 78% ± 23% (1sd). Considering that only small amounts of ^{107}Ag are required for a single synthesis (~2.7 mg) and due to the excellent yields achieved here, the preparation of ^{107}AgNPs is quite affordable, with a cost of approximately $4 to $5 per milligram.

3.3 Dissolution behavior

The results of the dialysis experiments are shown in Fig. 4. The particle stock suspension was added directly to the dilute-ASW without prior treatment or washing to remove excess sodium citrate. Although this effect was not investigated, the presence of sodium citrate at the expected concentration of ~4 mg L^{-1} is not anticipated to have a significant influence on the dissolution behavior. The Ag contents measured on the outside of the dialysis bags represent the total Ag concentration of the dilute-ASW, encompassing both particulate and dissolved forms of Ag. In contrast, the Ag measured inside the bags has crossed a 1 kDa MWCO dialysis membrane and therefore reflects the dissolved component only. The experimental setup therefore ensures that identical Ag concentrations for the dialysis bags and the container are only achieved, when all Ag in the latter reservoir is in dissolved form.

The dialysis control experiment, where 1.00 mg L^{-1} of aqueous Ag was introduced into the containers, can be used to assess the behavior of dissolved Ag in the absence of AgNPs. At the beginning of the control experiment, the Ag concentrations inside the dialysis bags increased rapidly and reached the same level (of about 0.8–1.1 mg L^{-1}) as on the outside after 8 hours, demonstrating the time required for equilibrium to establish over the dialysis membrane (Fig. 4a). During the remaining 27 days of the experiment, the Ag concentrations inside and outside the dialysis bags were always essentially identical, showing that the setup functioned well to provide a reliable monitor of dissolved Ag contents on the outside of the dialysis bags. However, the Ag concentration outside the bags decreased during most of the experiment to a value of about 0.4 mg L^{-1} after 22 days. This indicates that dissolved Ag was lost, presumably as a result of adsorption onto the container walls and the dialysis membrane. The small final increase in dissolved Ag concentration that is seen at day 27, is likely due to desorption of the Ag from the surfaces of the container and dialysis bags.

In the dialysis experiment of sample 107-AgNP2-Oct12-F, the Ag concentration outside the bags immediately after NP addition was 0.5 mg L^{-1}, a recovery of only 56% (Fig. 4b). The container was furthermore black in color after the addition of the ^{107}AgNPs, which indicates that AgNP adsorption to container surfaces was responsible for the loss of Ag. During the experiment, the Ag concentration outside of the bags

Published on 27 March 2014. Downloaded on 27/04/2014 23:45:40.

generally decreased until day 22. For the same time period, the Ag contents inside both dialysis bags initially showed an increase over the first 28 hours, followed by a decrease until day 8, with increasing concentrations observed thereafter (Fig. 4b). On day 22, the Ag concentrations outside and within both dialysis bags were identical and all three concentrations rose continuously during the final time period to day 27. This final increase in concentration is similar to that seen in the control experiment, which suggests that it is also most likely caused by desorption of Ag from surfaces that are in contact with the dilute-ASW.

Due to the adsorptive losses of both dissolved and nanoparticulate Ag during dialysis, it is difficult to quantify the dissolution behavior of the AgNPs. It may be assumed, however, that the dissolution of AgNPs will be similar, regardless of whether they are in suspension or adsorbed to container walls. With this assumption, our data can be applied to derive some general conclusions about the dissolution behavior of AgNPs. In particular, after an initial 8 hour equilibration time, the control experiment with dissolved Ag exhibited nearly identical Ag concentrations inside and outside of the dialysis bags (Fig. 4a). During the same time period, the dialysis experiment with NP sample 107-AgNP2-Oct12-F showed low Ag concentrations inside the dialysis bags (0.02–0.04 mg L^{-1}), which correspond to only 2–5% of the ^{107}AgNP concentration that was initially added to the container (Fig. 4b). These observations indicate that the ^{107}AgNP suspension in dilute-ASW produced only a very small fraction of dissolved Ag during the first few hours of the experiment. Over the following 27 days of the ^{107}AgNP dialysis experiment, the Ag concentrations inside the dialysis bags displayed an overall increase, demonstrating extensive ^{107}AgNP dissolution (Fig. 4b). This conclusion is supported by the observation that very similar Ag concentrations were observed for the inside and outside of the dialysis bags on day 27, with a final Ag concentrations of 0.32 mg L^{-1} for both bags (Fig. 4b). As some dissolved Ag was probably lost to adsorption onto the container walls, the value of 0.32 mg L^{-1} can be taken to represent a tentative minimum estimate for the solubility of the ^{107}AgNPs in dilute-ASW. Given the adsorption problems encountered here with the dialysis technique, future AgNP dissolution studies should consider using alternative methods, such as ultrafiltration, to obtain improved constraints on the dissolution behavior of AgNPs.

3.4 Reproducibility and reliability of synthesis method

The three synthesis protocols produced fairly monodisperse AgNP suspensions throughout, but suspensions prepared with the same protocol display small but significant batch-to-batch variations in size, regardless of the isotopic composition of the AgNPs (Table 1). A detailed evaluation of the results (Table 1) demonstrates, however, that the protocols for particle target sizes of 30 nm (AgNP1), 20 nm (AgNP2) and 17 nm (AgNP3) still offer acceptable control on particle size. Protocol AgNP1 produced the largest particles (26.5–31.2 nm, average = 30.7 ± 2.9 nm; 1sd, n = 5), whilst the particles from protocols AgNP2 (16.3–23.9 nm, average = 19.6 nm ± 3.0 nm; 1sd, n = 6) and AgNP3 (17.1–24.3 nm, average = 19.5 ± 2.7 nm; 1sd, n = 5) were smaller but similar. These quoted averages were calculated from all DLS data obtained for freshly prepared particles (Table 1), excluding the two most obvious outliers (Nat-AgNP1-May12-F and 107-AgNP3-Oct12-F), but very similar results are obtained when the complete dataset is considered (see ESI†).

These findings demonstrate that the methods provide a robust means of obtaining small batches of isotopically labeled AgNPs with diameters that closely match desired target sizes. However, due to the observed batch-to-batch variations in size, particle characterization will need to be carried out for applications, which require that particles diameters are known to a high degree of accuracy. Although only three synthesis protocols were utilized here, it is likely that the experimental conditions can be adjusted to target larger and smaller particle sizes. For example, slightly modified versions of the synthesis methods applied here were used in previous studies to produce AgNPs with diameters as small as 11.5 nm[33] and 7.2 nm[26] when measured by TEM.

3.5 Stability of particles

The particle suspensions in aqueous Na-citrate solutions were stored in the dark at 4 °C to help prevent ageing. To assess the stability of the particle suspensions under these conditions, a selection of particle batches were characterized by DLS periodically during 12 months of storage (Table 1). Batch Nat-AgNP3-Oct12-F showed the most significant signs of ageing, as after 6 months storage the average particle size and PDI increased from 17.2 to 32.5 nm and from 0.25 to 0.52, respectively. Whilst this is the type of change that would be expected as a result of particle aggregation, it was shown by Römer, *et al.*[26] that small citrate-capped Ag NPs generally have a greater stability and exhibit less agglomeration than larger particles. This indicates that the aggregation determined for sample Nat-AgNP3-Oct12-F may be an atypical result. All other particle batches exhibited no significant signs of ageing with all but one sample showing less than a 10% change in the average DLS particle size (Table 1). In addition, the PDI data also display only minor changes, indicating that the particle suspensions remained fairly monodisperse. The size and PDI results, furthermore, reveal no difference in aging behavior between natural and isotopically labeled AgNPs (Table 1). Any changes that might occur to the stock suspensions, such as agglomeration, may influence the particle behavior, but would have no effect on the isotope label or tracing capabilities.

3.6 Isotope label & detection capabilities

The motivation for synthesizing AgNPs from enriched ^{107}Ag is to produce a material with a distinct non-natural isotope signature, which can be used in experiments and exposures, so that changes induced in the ^{107}Ag/^{109}Ag isotope ratio of

Published on 27 March 2014. Downloaded on 27/04/2014 23:45:40.

relevant samples (*e.g.* biological materials, soil or water) can be used to trace and quantify the presence of the labeled material[17,18,22,23,27] (Fig. 1). The contribution of enriched ^{107}Ag to a sample is only detectable when the deviation induced in the ^{107}Ag/^{109}Ag ratio of the sample clearly exceeds (i) the precision of the isotopic measurement or (ii) any natural variations in the isotope composition of Ag. These factors are discussed below.

Isotopic analyses of Ag are generally carried out using ICP-MS instrumentation, as measurements by thermal ionization mass spectrometry (TIMS) are significantly more cumbersome.[34] Using standard quadrupole ICP-MS (Q-ICP-MS) instruments, ^{107}Ag/^{109}Ag ratios can typically be measured with a precision of about 1–5% (2sd). Improved data with a precision of ±0.2 to 1% (2sd) can be obtained with Q-ICP-MS at optimal analytical conditions (including separation of Ag from matrix elements) or by the application of single collector sector field ICP-MS (SF-ICP-MS).[35] Even more precise isotopic measurements are possible by multiple collector ICP-MS (MC-ICP-MS), which can achieve uncertainties of better than ±0.02% (2sd) for ^{107}Ag/^{109}Ag on purified solutions of Ag.[36,37]

Studies to investigate natural stable isotope fractionation of Ag are extremely limited in number and scope, with a primary focus on Ag ores (which are straightforward to analyze) and a few igneous rocks.[37–39] Data are also available from an archeological study on the provenance of coins[40] and an investigation into natural isotope fractionation based on a limited number of environmental samples.[41] These analyses revealed only minor differences of about ±0.05% in the ^{107}Ag/^{109}Ag ratios of the samples, relative to the NIST SRM 978a Ag isotope standard. Such small variations are only resolvable using MC-ICP-MS and hence have no impact on the sensitivity that can be achieved for the detection of isotopically labeled AgNPs by Q-ICP-MS and SF-ICP-MS. Given the published results, it is furthermore unlikely that samples, such as soils or sediments, from a single location will exhibit geological Ag isotope fractionations that exceed ±0.02% and hence impact the AgNP detection sensitivity of MC-ICP-MS. However, there are currently no studies that investigate whether changes in Ag isotope composition are generated by biological uptake and processing of this element. Based on data acquired for other elements, such Zn[42] and Cd,[43] it is conceivable that biotic reactions may induce Ag isotope effects in the range of 0.02% to 0.05% and such fractionations may be preserved in biological tissue and fluids, water samples or soils and sediments. It is unlikely, however, that biological isotope effects will normally exceed 0.1% to 0.2% and hence no serious impact on the detection sensitivity of MC-ICP-MS for isotopically labeled AgNPs is expected. Nonetheless, it will be important for future work to carefully characterize possible biological Ag isotope fractionations. If natural Ag isotope variations of ≥0.05% are found to be common and deemed to be obstructive, this problem can be readily circumvented by analyses of appropriate control samples. Such measurements can characterize the natural Ag isotope composition and variability of the background, and this permits appropriate corrections and/or uncertainties to be applied to the isotopic data collected for exposed samples.

Ecotoxicology studies typically generate and require analyses for a large number of samples (more than 100), making it important to consider the balance between optimal data quality and high sample throughput. Whilst MC-ICP-MS can provide unrivalled precision for the determination of ^{107}Ag/^{109}Ag, such analyses are also particularly laborious, because Ag must be separated from any sample matrix prior to analysis. In contrast, quadrupole and sector field ICP-MS can be employed for direct ^{107}Ag/^{109}Ag measurements without chemical separation. As sample preparation is much more straightforward, the latter instruments can achieve significantly higher sample throughput but at the cost of somewhat poorer precision for the data, which ultimately limits the tracing capabilities.

In the following, we discuss the tracing sensitivities that can be achieved using labeled ^{107}Ag (and thus ^{107}AgNPs) for two hypothetical cases with relevance to ecotoxicology, and where the endmember methods of Q-ICP-MS and MC-ICP-MS are evaluated for detection (Table 3). Case 1 involves analyses of 5 mg dry weight samples of biological tissue, as might be obtained from invertebrates following exposures, with a realistic Ag background of 100 ng g^{-1}.[5] Case 2 is for a 5 mL water sample (a realistic volume for removal and analysis from a laboratory exposure) that features a Ag background concentration of 200 ng L^{-1}, as would be appropriate for river, lake and estuarine waters.[5] Based on the concentrations quoted above, the case 1 and 2 samples would contain only 0.5 ng and 1 ng of Ag, respectively (Table 3), and these small amounts will limit the precision of the isotopic analyses by ICP-MS. Based on literature data and test measurements conducted at Imperial College (for MC-ICP-MS), it is estimated that the diagnostic ^{107}Ag/^{109}Ag isotope ratio can be determined in these samples with a precision of about ±5% for Q-ICP-MS and ±0.05% for MC-ICP-MS (an intermediate precision is expected for SF-ICP-MS).

The precision of mass spectrometric measurements is defined here as the 2sd calculated from replicate isotope analyses of samples or a standard reference material. The analytical precision is a key factor because it determines the smallest change in the ^{107}Ag/^{109}Ag isotope ratio (ΔR_{res}), as induced by addition of the ^{107}Ag tracer, which is analytically resolvable as a deviation from the natural ^{107}Ag/^{109}Ag ratio (R_{nat}), such that ΔR_{res} = 2sd.

The addition of an enriched ^{107}Ag tracer to a natural sample will increase the ^{107}Ag/^{109}Ag ratio of the system. In the following, we define R_{res}, as the ^{107}Ag/^{109}Ag ratio, which is associated with the smallest addition of ^{107}Ag tracer that is resolvable by measurement. R_{res} is therefore given by:

$$R_{res} = R_{nat} + \Delta R_{res} \quad (5)$$

Isotope mass balance can then be used to calculate the minimum molar amount of enriched ^{107}Ag (N_{res}-Ag_{en}), from

 This journal is © The Royal Society of Chemistry 2014

Published on 27 March 2014. Downloaded on 27/04/2014 23:45:40.

Table 3 Summary of data for the hypothetical cases that evaluate the detection sensitivities and quantification uncertainties achievable for tracing of highly enriched ^{107}Ag in environmental samples

	Case 1	Case 2
Sample	5 mg biological tissue	5 mL water
Background Ag concentration	100 ng g^{-1}	200 ng L^{-1}
Total natural Ag content of sample	0.5 ng	1 ng
Analysis by Q-ICP-MS, precision ±5% (2sd)		
Minimum concentration change detectable by ^{107}Ag/^{109}Ag analysis[a]	2.6 ng g^{-1}	5.2 ng L^{-1}
Uncertainty in quantification of label at:		
10× minimum concentration	126 ± 3.12 ng g^{-1}	252 ± 6.24 ng L^{-1}
100× minimum concentration	360 ± 4.37 ng g^{-1}	720 ± 8.76 ng L^{-1}
Analysis by MC-ICP-MS, precision ±0.05% (2sd)		
Minimum concentration change detectable by ^{107}Ag/^{109}Ag analysis[a]	0.026 ng g^{-1}	0.052 ng L^{-1}
Uncertainty in quantification of label at:		
10× minimum concentration	100.26 ± 0.026 ng g^{-1}	200.52 ± 0.053 ng L^{-1}
100× minimum concentration	102.6 ± 0.027 ng g^{-1}	205.2 ± 0.055 ng L^{-1}

[a] Smallest increase in the Ag concentration from the addition of highly enriched ^{107}Ag, which is resolvable by measurement of the ^{107}Ag/^{109}Ag isotope ratio using a given technique.

labeled ^{107}AgNPs, that must be added to a given molar amount of natural Ag (N-Ag_{nat}) in a system, to increase the ^{107}Ag/^{109}Ag ratio from R_{nat} to R_{res}:

$$N_{res}\text{-}Ag_{en} = N\text{-}Ag_{nat} \times ((R_{res} \times {}^{109}Ab_{nat}) - {}^{107}Ab_{nat})/({}^{107}Ab_{en} - (R_{res} \times {}^{109}Ab_{en})) \quad (6)$$

where the fractional (molar) isotope abundances of ^{107}Ag and ^{109}Ag in the enriched material ($^{107}Ab_{en}$ and $^{109}Ab_{en}$) and natural Ag ($^{107}Ab_{nat}$ and $^{109}Ab_{nat}$) are 99.2%, 0.8% and 51.8%, 48.2%, respectively. Eqn (6) can be readily revised to determine the minimum molar concentration [N_{res}-Ag_{en}] of enriched ^{107}Ag that must be added to obtain R_{res} – this requires only that N-Ag_{nat} is substituted with the molar concentration of natural Ag, [N-Ag_{nat}]. Given that the atomic weights of natural and enriched Ag differ by less than 1%, eqn (6) also provides a sufficiently accurate approximation for calculation of the minimum masses and mass concentrations of enriched ^{107}Ag, which must be added to the system, to achieve a detectable change in the final ^{107}Ag/^{109}Ag ratio.

The final ^{107}Ag/^{109}Ag isotope ratio of an exposed sample (R_{sam}), as measured by ICP-MS, is used to quantify the amount of enriched ^{107}Ag label present. This calculation is outlined in the following. The molar fraction of enriched ^{107}Ag to total Ag (fr_{en}) present in the sample is given by:

$$fr_{en} = N\text{-}Ag_{en}/(N\text{-}Ag_{nat} + N\text{-}Ag_{en}) \quad (7)$$

where N-Ag_{en} is the molar amount of enriched ^{107}Ag tracer present. Using R_{sam}, fr_{en} can be determined as:

$$fr_{en} = [({}^{107}Ab_{en} - (R_{sam} \times {}^{109}Ab_{en}))/((R_{sam} \times {}^{109}Ab_{nat}) - {}^{107}Ab_{nat}) + 1]^{-1} \quad (8)$$

The fractional molar abundance of ^{109}Ag in the exposed sample ($^{109}Ab_{sam}$) is then:

$${}^{109}Ab_{sam} = (fr_{en} \times {}^{109}Ab_{en}) + ((1 - fr_{en}) \times {}^{109}Ab_{nat}) \quad (9)$$

The molar abundance of total Ag (N-Ag) and enriched Ag (N-Ag_{en}) in the sample can be determined by quantifying N-^{109}Ag, the molar amount of ^{109}Ag present. This can be readily achieved using standard ICP-MS techniques, where a solution prepared from a known aliquot of the sample is analyzed, such that N-^{109}Ag can be determined relative to a suitable calibration curve. Following this, N-Ag and N-Ag_{en} can be calculated from:

$$N\text{-}Ag = (N\text{-}{}^{109}Ag/{}^{109}Ab_{sam}) \quad (10)$$

$$N\text{-}Ag_{en} = (N\text{-}{}^{109}Ag/{}^{109}Ab_{sam}) \times fr_{en} \quad (11)$$

The mass M-Ag_{en} and mass concentration [M-Ag_{en}] of enriched Ag in the sample can then be obtained as:

$$M\text{-}Ag_{en} = N\text{-}Ag_{en} \times AtW_{en} \quad (12)$$

$$[M\text{-}Ag_{en}] = (N\text{-}Ag_{en} \times AtW_{en})/M \quad (13)$$

where M is the sample mass. The atomic weight of the enriched Ag, AtW_{en}, can be determined from:

$$AtW_{en} = ({}^{107}Ab_{en} \times {}^{107}AtW) + ({}^{109}Ab_{en} \times {}^{109}AtW) \quad (14)$$

where ^{107}AtW and ^{109}AtW are the known atomic weights of ^{107}Ag and ^{109}Ag. Calculations analogous to those performed in eqn (12) to (14) can be used to derive the total mass of Ag in the sample (M-Ag) and the Ag mass concentration [M-Ag].

The results of these calculations for cases 1 and 2 are given in Table 3. In detail, they indicate that isotopic tracing with Q-ICP-MS requires that the addition of enriched ^{107}Ag raises the total Ag concentration by at least 2.6%, to 102.6 ng g^{-1} for the tissue (case 1) and 205.2 ng L^{-1} for the water sample

Published on 27 March 2014. Downloaded on 27/04/2014 23:45:40.

(case 2; Table 3). With MC-ICP-MS, measurements of the $^{107}Ag/^{109}Ag$ ratio are about 100-fold more precise and consequently the tracing sensitivity is also improved by two orders of magnitude. In this scenario the Ag sample concentration only needs to increase by 0.026% from the addition of ^{107}Ag, to generate analytically resolvable differences in the $^{107}Ag/^{109}Ag$ ratio. For the tissue and water samples, this means that increases in the Ag concentration to 100.026 ng g^{-1} (from 100 ng g^{-1}) and 200.052 g L^{-1} (from 200 g L^{-1}), respectively, are already traceable by isotopic analyses. Evaluation of the detection sensitivity for a given isotope label, analytical approach and natural background concentration in this manner, enables appropriate experimental plans and dosing levels to be prepared.

The uncertainties of the isotope ratio analyses can be propagated through the above equations to assess the impact of the measurement precision on the calculated mass of enriched tracer material present in a sample or its mass concentration. Importantly, the uncertainties do not scale in a linear manner and depend on the isotopic enrichment of the tracer and the proportion of enriched to natural Ag in the sample. To demonstrate this, the uncertainties for [M-Ag_{en}] of cases 1 and 2 (Table 3) were calculated for the addition of ^{107}Ag-enriched tracer at levels, which exceed the smallest detectable molar concentration N_{res}-Ag_{en} by a factor of 10× and 100×.

The results of these calculations are promising because they indicate that despite of the unfavorable natural isotope composition of Ag, stable isotope labeling of Ag can provide detection sensitivities and uncertainties of quantification that are far better than those achievable by concentration tracing. Considering that the latter methodology can only provide unequivocal results if the concentration anomalies generated by elemental uptake exceed the natural background levels by at least a factor of 2 (but preferably more), the application of stable isotope labeling enhances the tracing sensitivity by a least a factor of 40 (using Q-ICP-MS for detection) and possibly by up to a factor of ~4000 (with use of MC-ICP-MS). Furthermore, with the superior precision of MC-ICP-MS for isotopic analyses, the tracing sensitivities are likely to be sufficiently high, to enable experiments to be carried out at low and environmentally relevant exposure concentrations.

4. Conclusions

In this study, published methods were modified for small-scale synthesis of citrate-capped AgNPs from both natural Ag and enriched ^{107}Ag. Three different synthesis protocols were used on three occasions and in two laboratories to obtain AgNPs with target sizes of 17, 20 and 30 nm. All particles batches produced were thoroughly characterized and the results demonstrate that the new procedures provide reproducible, monodisperse particle suspensions at high yields of ~80% and with a long-term stability of up to 12 months. Whilst the measurements revealed small but significant batch-to-batch variations in size, the particles were generally found to have diameters that closely matched the desired target sizes. Detailed statistical tests furthermore argue against systematic differences in size between AgNPs prepared from enriched ^{107}Ag *versus* natural Ag. In summary, these results show that the new methods are ideally suited for the small-scale preparation of isotopically labeled AgNPs. Simple isotope mass balance calculations furthermore demonstrate that application of stable isotope labeling can increase the detection sensitivity of AgNPs in environmental samples by at least a factor of 40 and possibly by up to 4000×, in comparison to commonly employed bulk Ag concentration measurements. Use of the most precise isotopic measurement techniques should therefore, permit environmentally realistic exposure scenarios.

Acknowledgements

Katharina Kreissig and Barry Coles of the Imperial College MAGIC Laboratories are thanked for technical assistance. The research received funding from the NERC Facility for Environmental Nanoscience Analysis and Characterization (FENAC) at the University of Birmingham and was carried out as part of PROSPEcT, a public–private partnership between DEFRA, EPSRC, TSB and the Nanotechnology Industries Association (NIA Ltd.) and its members. Further funding was provided by a UK Research Council studentship to A.L. and the joint US-EPA and UK-NERC Research Program grant RD-834557501-0. The authors also thank three anonymous reviewers and editor Greg Lowry, for providing constructive comments and helpful suggestions.

References

1 T. W. Purcell and J. J. Peters, *Environ. Toxicol. Chem.*, 1998, **17**, 539–546.
2 S. W. P. Wijnhoven, W. J. G. M. Peijnenburg, C. A. Herberts, W. I. Hagens, A. G. Oomen, E. H. W. Heugens, B. Roszek, J. Bisschops, I. Gosens, D. Van de Meent, S. Dekkers, W. H. De Jong, M. Van Zijverden, A. J. A. M. Sips and R. E. Geertsma, *Nanotoxicology*, 2009, **3**, 109–138.
3 Woodrow Wilson consumer products inventory for products containing nano-silver, http://www.nanotechproject.org/cpi/browse/nanomaterials/silver-nanoparticle/, Accessed December 2013.
4 F. Gottschalk, T. Sun and B. Nowack, *Environ. Pollut.*, 2013, **181**, 287–300.
5 R. Eisler, *Silver hazards to fish, wildlife and invertebrates: A synoptic review*, U.S. Department of the Interior, 1996.
6 W. A. Shoults-Wilson, B. C. Reinsch, O. V. Tsyusko, P. M. Bertsch, G. V. Lowry and J. M. Unrine, *Soil Sci. Soc. Am. J.*, 2011, **75**, 365–377.
7 C. M. Zhao and W. X. Wang, *Environ. Toxicol. Chem.*, 2011, **30**, 885–892.
8 L. Maretti, P. S. Billone, Y. Liu and J. C. Scaiano, *J. Am. Chem. Soc.*, 2009, **131**, 13972–13980.

 This journal is © The Royal Society of Chemistry 2014

Published on 27 March 2014. Downloaded on 27/04/2014 23:45:40.

9 T. Xia, M. Kovochich, M. Liong, L. Madler, B. Gilbert, H. B. Shi, J. I. Yeh, J. I. Zink and A. E. Nel, *ACS Nano*, 2008, **2**, 2121–2134.
10 A. Chrastina and J. E. Schnitzer, *Int. J. Nanomed.*, 2010, **5**, 653–659.
11 C. Coutris, E. J. Joner and D. H. Oughton, *Sci. Total Environ.*, 2012, **420**, 327–333.
12 M. Zuykov, E. Pelletier and S. Demers, *Mar. Environ. Res.*, 2011, **71**, 17–21.
13 N. Lewinski, V. Colvin and R. Drezek, *Small*, 2008, **4**, 26–49.
14 T. Tenuta, M. P. Monopoli, J. Kim, A. Salvati, K. A. Dawson, P. Sandin and I. Lynch, *PLoS One*, 2011, 6.
15 N. Gibson, U. Holzwarth, K. Abbas, F. Simonelli, J. Kozempel, I. Cydzik, G. Cotogno, A. Bulgheroni, D. Gilliland, J. Ponti, F. Franchini, P. Marmorato, H. Stamm, W. Kreyling, A. Wenk, M. Semmler-Behnke, S. Buono, L. Maciocco and N. Burgio, *Arch. Toxicol.*, 2011, **85**, 751–773.
16 D. H. Oughton, T. Hertel-Aas, E. Pellicer, E. Mendoza and E. J. Joner, *Environ. Toxicol. Chem.*, 2008, **27**, 1883–1887.
17 F. R. Khan, A. Laycock, A. Dybowska, F. Larner, B. D. Smith, P. Rainbow, S. N. Luoma, M. Rehkämper and E. Valsami-Jones, *Environ. Sci. Technol.*, 2013, **47**, 8532–8439.
18 F. Larner, Y. Dogra, A. Dybowska, J. Fabrega, B. Stolpe, L. J. Bridgestock, R. Goodhead, D. J. Weiss, J. Moger, J. R. Lead, E. Valsami-Jones, C. R. Tyler, T. S. Galloway and M. Rehkämper, *Environ. Sci. Technol.*, 2012, **46**, 12137–12145.
19 N. A. Matwiyoff and D. G. Ott, *Science*, 1973, **181**, 1125–1133.
20 C. Sridar, I. Hanna and P. F. Hollenberg, *Xenobiotica*, 2013, **43**, 336–345.
21 S. K. Misra, A. Dybowska, D. Berhanu, M. N. Croteau, S. N. Luoma, A. R. Boccaccini and E. Valsami-Jones, *Environ. Sci. Technol.*, 2012, **46**, 1216–1222.
22 M. N. Croteau, A. D. Dybowska, S. N. Luoma and E. Valsami-Jones, *Nanotoxicology*, 2011, **5**, 79–90.
23 B. Gulson, M. McCall, M. Korsch, L. Gomez, P. Casey, Y. Oytam, A. Taylor, M. McCulloch, J. Trotter, L. Kinsley and G. Greenoak, *Toxicol. Sci.*, 2010, **118**, 140–149.
24 J. Gigault and V. A. Hackley, *Anal. Chim. Acta*, 2013, **763**, 57–66.
25 S. A. Cumberland and J. R. Lead, *J. Chromatogr. A*, 2009, **1216**, 9099–9105.
26 I. Römer, T. A. White, M. Baalousha, K. Chipman, M. R. Viant and J. R. Lead, *J. Chromatogr. A*, 2011, **1218**, 4226–4233.
27 F. Larner and M. Rehkämper, *Environ. Sci. Technol.*, 2012, **46**, 4149–4158.
28 M. Baalousha and J. R. Lead, *Environ. Sci. Technol.*, 2012, **46**, 6134–6142.
29 A. Litzen, *Anal. Chem.*, 1993, **65**, 461–470.
30 M. Baalousha and J. R. Lead, *Nat. Nanotechnol.*, 2013, **8**, 308–309.
31 M. Baalousha and J. R. Lead, *Environ. Sci. Technol.*, 2007, **41**, 1111–1117.
32 M. Baalousha, A. Manciulea, S. Cumberland, K. Kendall and J. R. Lead, *Environ. Toxicol. Chem.*, 2008, **27**, 1875–1882.
33 M. Tejamaya, I. Römer, R. C. Merrifield and J. R. Lead, *Environ. Sci. Technol.*, 2012, **46**, 7011–7017.
34 J. H. Chen and G. J. Wasserburg, *Geochim. Cosmochim. Acta*, 1990, **54**, 1729–1743.
35 K. G. Heumann, S. M. Gallus, G. Radlinger and J. Vogl, *J. Anal. At. Spectrom.*, 1998, **13**, 1001–1008.
36 M. Schönbächler, R. W. Carlson, M. E. Horan, T. D. Mock and E. H. Hauri, *Int. J. Mass Spectrom.*, 2007, **261**, 183–191.
37 S. J. Woodland, M. Rehkämper, A. N. Halliday, D. C. Lee, B. Hattendorf and D. Gunther, *Geochim. Cosmochim. Acta*, 2005, **69**, 2153–2163.
38 A. V. Chugaev and I. V. Chernyshev, *Geochem. Int.*, 2012, **50**, 899–910.
39 E. Hauri, R. Carlson and J. Bauer, presented in part at the 31st Lunar and Planetary Science Conference, Houston, March, 2000.
40 A. M. Desaulty, P. Telouk, E. Albalat and F. Albarede, *Proc. Natl. Acad. Sci. U. S. A.*, 2011, **108**, 9002–9007.
41 Y. Luo, E. Dabek-Zlotorzynska, V. Celo, D. C. G. Muir and L. Yang, *Anal. Chem.*, 2010, **82**, 3922–3928.
42 T. Arnold, M. Schönbächler, M. Rehkämper, S. Dong, F. J. Zhao, G. J. Kirk, B. J. Coles and D. J. Weiss, *Anal. Bioanal. Chem.*, 2010, **398**, 3115–3125.
43 S. Ripperger, M. Rehkämper, D. Porcelli and A. N. Halliday, *Earth Planet. Sci. Lett.*, 2007, **261**, 670–684.

Appendices iii)

Paper arising from the work of Chapter 4:

‘Stable isotope tracer to determine uptake and efflux dynamics of ZnO nano- and bulk particles and dissolved Zn to an estuarine snail’

Environmental Science & Technology

Article

pubs.acs.org/est

Stable Isotope Tracer To Determine Uptake and Efflux Dynamics of ZnO Nano- and Bulk Particles and Dissolved Zn to an Estuarine Snail

Farhan R. Khan,*[,‡,†] Adam Laycock,*[,§,∥] Agnieszka Dybowska,[∥] Fiona Larner,[§] Brian D. Smith,[‡] Philip S. Rainbow,[‡] Samuel N. Luoma,[⊥] Mark Rehkämper,[§,∥] and Eugenia Valsami-Jones[#,∥]

[‡]Life Sciences, Natural History Museum, Cromwell Road, London SW7 5BD, England

[§]Department of Earth Science & Engineering, Imperial College London, London SW7 2AZ, England

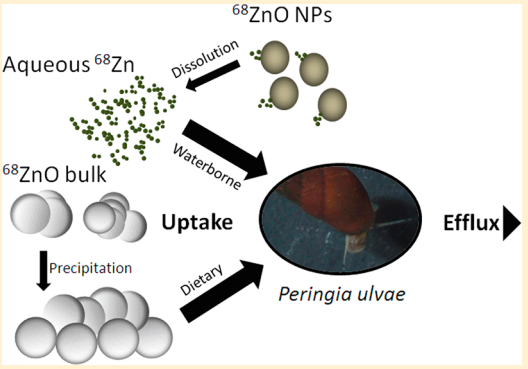
[∥]Earth Sciences, Natural History Museum, Cromwell Road, London SW7 5BD, England

[⊥]John Muir Institute of the Environment, University of California at Davis, Davis, California, United States

[#]School of Geography, Earth and Environmental Sciences, University of Birmingham, Edgbaston, Birmingham B15 2TT, England

Supporting Information

ABSTRACT: Zinc oxide nanoparticles (ZnO NPs) are among the most commercialized engineered nanomaterials. Their biological impact in aquatic organisms has been associated with dissolution, but there is also evidence of nanospecific effects. In this study the waterborne uptake and efflux kinetics of isotopically labeled ^{68}ZnO NPs (7.8 ± 1.2 nm), in comparison to aqueous ^{68}Zn and ^{68}ZnO bulk particles (up to 2 μm), were determined for the estuarine snail *Peringia ulvae* following a 7 d exposure (nominally 20 μg ^{68}Zn L^{-1}) and 28 d depuration. Detection of the ^{68}Zn label was achieved by high precision multiple-collector ICP-MS (MC-ICP-MS). Previous characterization in artificial estuarine water revealed that the NPs underwent initial aggregation and solubilized up to 60% within 1−2 days. Bulk and aqueous forms were significantly more bioavailable than ^{68}ZnO NPs ($p < 0.05$), but after correcting for dissolution, aqueous (0.074 L^{-1} g^{-1} d^{-1}) and NP (0.070 L^{-1} g^{-1} d^{-1}) uptake rate constants were highly comparable. The rate constant of loss for ^{68}Zn aqueous (0.012 ± 0.005 d^{-1}) and ^{68}ZnO NPs (0.012 ± 0.007 d^{-1}) were identical. These results strongly suggest that in this exposure scenario the bioaccumulation of Zn from ZnO NPs is primarily dependent upon solubility.



INTRODUCTION

Zinc oxide nanoparticles (ZnO NPs) are used in a number of commercial applications, including sunscreens, coatings, and paint.[1] Some are therefore expected to be released into the environment, particularly the aquatic environment. The biological impact of ZnO NPs is often attributed to their solubility and the release of labile Zn. ZnO NPs were shown to exhibit rapid dissolution kinetics in freshwater, resulting in ZnO NP exposure being equally as toxic to algae (*Pseudokirchneriella subcapitata*) as dissolved $ZnCl_2$.[2] However, complete dissolution is not always the case, and rarely is uptake by the organism and quantification of dissolution in the medium considered in the same study. This is perhaps why the presence of soluble Zn^{2+} within a ZnO NP exposure did not fully account for the adverse toxic effects induced in zebrafish embryos[3] or growth and survivorship inhibition in the amphipod *Corophium volutator*.[4] This would indicate that the particles themselves exert a nanospecific effect that is distinct from the aqueous Zn.

The aim of the present study was to determine if dissolution alone accounts for the bioavailability of Zn when ZnO NPs are dispersed in estuarine water and presented to the snail *Peringia ulvae* (Gastropoda; Hydrobiidae), a key estuarine species.[5] The bioavailability and *in vivo* fate of Zn in the ZnO NPs were assessed using the principles of biodynamic modeling,[6] specifically by quantifying the rates of influx (uptake) and efflux of Zn into and from the organism to provide a better understanding of the accumulation of ZnO NPs. Accumulation of a contaminant is generally regarded as a prerequisite to adverse biological effects.[7] Rates were also determined following exposure to similarly isotopically labeled aqueous Zn and ZnO bulk particles in comparison. If the bioavailability of the NP is dependent on solubility, then the uptake rate of Zn from the ZnO NP would be comparable to that of aqueous Zn. Moreover, loss dynamics would be identical regardless of the original form of Zn (i.e., aqueous vs nano).

Dissolution and aggregation were quantified in stock solution, freshwater, and the artificial estuarine water used as the exposure media. Although NP behaviors in artificial waters may not necessarily reflect those in natural waters largely owing to the absence of organic matter.[8] A number of factors have been shown to influence solubility of ZnO. Maio et al. (2010[9])

Received: March 15, 2013
Revised: June 21, 2013
Accepted: June 26, 2013
Published: June 26, 2013

ACS Publications © 2013 American Chemical Society

found that ZnO NP dissolution increased with decreases in pH and particle surface area, and dissolution was accelerated in seawater, which is relevant to the present study conducted in 17‰ water. As dissolution is a function of concentration, solubility is particularly relevant when working at environmentally realistic Zn concentrations.[2] Total Zn concentrations within aquatic environments vary with anthropogenic activity and natural geology. Dissolved Zn concentrations in the natural estuarine environments can be as high as 5 μg L^{-1}[10] and may reach 50 μg L^{-1} in contaminated hot spots.[11] In comparison, predicted environmental releases of ZnO NPs in European and U.S. surface water ranged from 1 to 10 ng L^{-1} and up to 430 ng L^{-1} in treated wastewater.[12] In biological tissue, a soft tissue concentration of 34.5 μg g^{-1} was estimated to fulfill metabolic Zn requirements,[13] while the measured Zn tissue burden of field collected *P. ulvae* used in this study was 148 ± 31 μg g^{-1} (mean value ± S.D., n = 30). Thus to differentiate Zn accumulated by organisms above their natural background it becomes necessary to use a label.[14] Stable isotopes have been suggested as a method trace engineered NPs containing multi-isotopic elements.[15,16]

The three forms of Zn (aqueous, nano, and bulk) investigated in this study were prepared using Zn composed of, and hence labeled with, >99% of the stable isotope ^{68}Zn. In comparison natural Zn has a ^{68}Zn isotope abundance of ∼19%, and Zn isotope compositions display only limited natural variability. For example, the ^{68}Zn/^{66}Zn ratio varies by only ∼0.25% in natural biological samples.[17] Our labeled Zn materials, therefore, possess a distinct and non-natural isotope signature. Once the ^{68}Zn label is introduced into the experimental system it is possible to track it by measuring the diagnostic ^{68}Zn/^{66}Zn isotope ratio in the various components of the system. Deviations from the natural ^{68}Zn/^{66}Zn isotope ratio indicate the presence of the isotopically enriched material. The magnitude of this perturbation can be used to quantify the relative and absolute amount of enriched material.

While distinct isotopes, and compounds made thereof, display very slight differences in their physical and chemical properties, these differences are not of consequence in tracer studies with enriched isotopes. It is therefore valid to assume that particles synthesized from enriched ^{68}Zn display the same environmental behavior as equivalent particles with a natural Zn isotope composition,[14] making them ideal for the purpose of tracing. Stable isotope labeling is not beset with the problems of alternative methods such as fluorescent dyes or radioactive isotope labeling,[18] where the label may be lost as a result of dissociation or radioactive decay. In the present study, stable isotope labeling is used in conjunction with multiple−collector−inductively−coupled−plasma−mass-spectrometry (MC-ICP-MS). This methodology offers very low detection limits as it provides high-precision data with minimal levels of uncertainty.[19] Isotopically enriched particles are increasingly utilized in ecotoxicological studies (e.g., refs 16, 18, and 20), but there remains a far greater potential for their use.

METHODS

Chemicals and Reagents. Isotopically enriched ^{68}Zn was purchased from Isoflex USA (CA, USA). ^{68}ZnO bulk particles and ^{68}Zn metal, used to prepare the aqueous and NP forms, were purchased as dry powders. For this study, a single 100 L batch of artificial estuarine water (17‰) was prepared from Tropic Marin Sea Salt (Dr Biener GmbH, Germany). Concentrated (14.5 M) HNO_3 and 6 M HCl were purified prior to use by sub-boiling distillation in a quartz still, and water of >18 MΩ cm quality (Millipore, UK) and 30% Suprapur H_2O_2 (VWR International Ltd., UK) were used throughout.

Experimental Organisms. *P. ulvae* were collected from the Blackwater Estuary, Essex, UK (51°46′05″N 00°50′13″E) at low tide and maintained in the laboratory in synthetic estuarine water at 10 ± 1 °C with an approximate 16 h light:8 h dark cycle as previously described.[20] Two days before the start of the exposures, adult snails (>2 mm) were randomly assigned into 90 groups of 25 individuals. Food (*Chlorella vulgaris*) was withheld during this period. *C. vulgaris* was cultured in 3N-BBM+V medium (Culture Collection of Algae and Protozoa, Scottish Marine Institute, UK) under artificial daylight (16 h light:8 h dark).

Preparation of Isotopically Enriched Forms of ^{68}Zn. The ^{68}ZnO NPs were synthesized by forced hydrolysis in diethylene glycol (DEG) as outlined by Dybowska et al. (2011[14]). Briefly, a ^{68}Zn acetate precursor was prepared by refluxing the ^{68}Zn metal in acetic acid (90 °C 72 h). The precursor (100 mg) was dissolved in 50 mL of DEG (60 °C 70 h), and the resulting mixture was heated (180 °C). When the mixture temperature stabilized, it was stirred (200 rpm), and 18 MΩ water (100 μL) was added to force hydrolysis and precipitate ^{68}ZnO NPs. The ^{68}Zn concentration of the NP stock suspension was measured as 743 mg L^{-1} (ICP-OES).

Stock suspensions of the ^{68}ZnO bulk particles in DEG and aqueous ^{68}Zn in 18 MΩ water were also prepared at 743 mg L^{-1} ^{68}Zn. The latter was prepared by dissolving ^{68}Zn metal powder in 6 M HCl. This solution was evaporated to produce $^{68}ZnCl_2$, which was dissolved in 18 MΩ water.

Characterization of ^{68}ZnO NP and Bulk Forms. To determine particle size, shape, and size distribution, ^{68}ZnO NPs and ^{68}ZnO bulk particles were imaged using TEM (Hitachi 7100, 100 kV) and SEM (Ultra plus FESEM, Carl Zeiss), respectively. The crystal structure of both the NP and bulk forms was verified by X-ray diffraction (XRD, Enraf Nonius coupled with INES CPS 120 position sensitive detector with Co Kα radiation) and compared to a ZnO standard (ICDD [36-1451]).[14] A Zetasizer Nano ZS (Malvern Instruments Ltd.) was used to determine the primary particle size, polydispersity, and zeta potential of the stock ^{68}ZnO NP and bulk particle DEG suspensions. Analysis of 1:10 (v/v) dilutions of the ^{68}ZnO NP stock suspensions with 17‰ water was also carried out by DLS over 11 h at 30 min intervals and was performed at 10 °C to reflect experimental conditions.

Waterborne Exposures. A number of precautions were made to eliminate the risk of background Zn entering the exposure system. Plastic laboratory-ware was used in preference to glass as the latter has been shown to leach Zn to a greater extent.[22] All plastic-ware was soaked in 1 M HCl and thoroughly rinsed in ultrapure water before use. Exposure chambers (50 mL plastic beakers) were presoaked at 20 μg L^{-1} ^{68}Zn, added as aqueous ^{68}Zn, ^{68}ZnO NPs, or ^{68}ZnO bulk particles, for 72 h to saturate surface binding sites. At the start of the exposure (i.e., t = 0 d) 3 of the 90 groups of snails were sampled for baseline measurements; *C. vulgaris* (both the stock culture and in 25 mL of 17‰ water as presented to the snails for food during efflux) and the 17‰ water were taken for background determinations of the ^{68}Zn/^{66}Zn ratio. The 100 L batch of 17‰ water was also sampled at the end of the experiment.

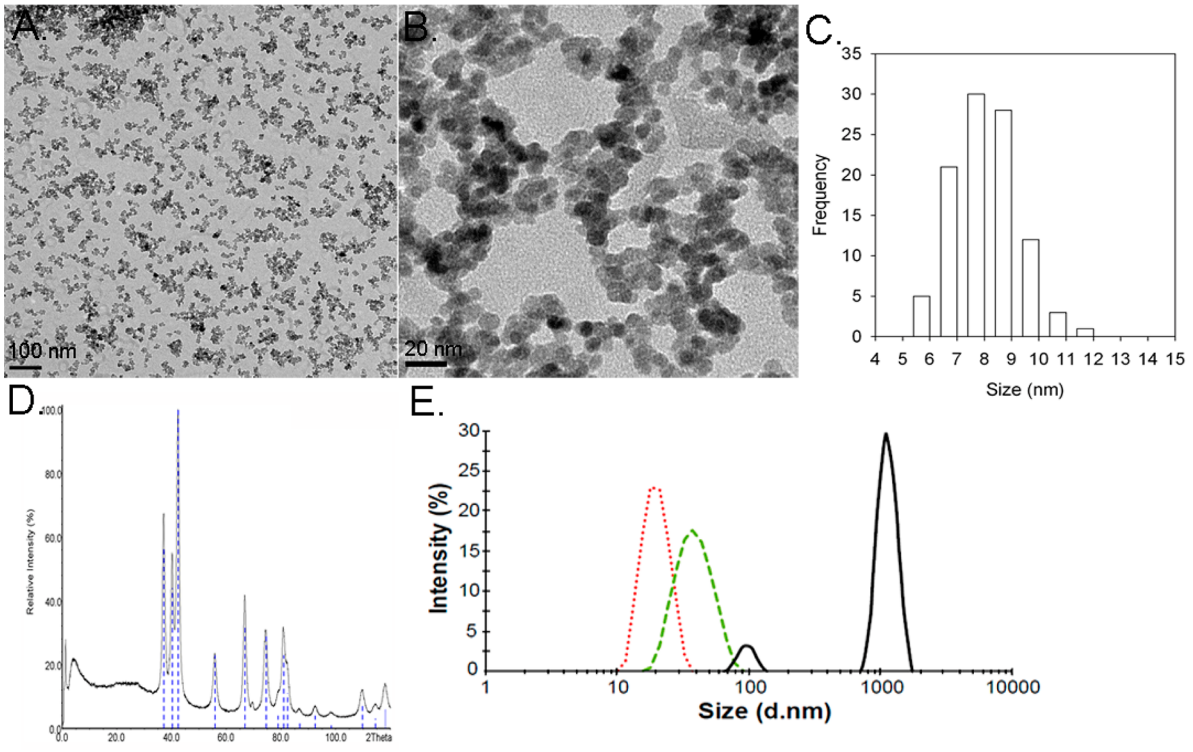


Figure 1. Characterization of ^{68}ZnO NPs after synthesis. Imaged particles (A and B) were determined to have an average size of 7.8 ± 1.2 nm (n = 100) with a size distribution close to the mean (C). The XRD pattern of the synthesized NPs (solid black line, is shown against the peak positions marked of the ZnO standard (ICDD [36-1451], dashed blue lines) which confirms the ZnO crystal structure (D). The hydrodynamic diameter size distribution of the ^{68}ZnO NPs expressed by intensity (%) in DEG (dotted red line), DI water (dashed green line), and after 3 h in 17‰ water (solid black line) was measured by DLS (E).

The remaining 87 groups of snails were randomly divided among the controls and exposures to aqueous ^{68}Zn, ^{68}ZnO NPs, or ^{68}ZnO bulk particles. For each ^{68}Zn form 27 groups of snails were exposed to 20 μg L^{-1} ^{68}Zn, and the 6 remaining groups were used as controls (no added ^{68}Zn). The 743 mg L^{-1} stocks of each ^{68}Zn form were diluted with 18 MΩ water to produce intermediate stocks with 20 mg L^{-1} ^{68}Zn. DEG was added to the aqueous ^{68}Zn intermediate stock to match the DEG concentration in the NP and bulk intermediate stocks. Each group of snails was placed in a presoaked exposure chamber with 25 mL of 17‰ water and 25 μL of the corresponding intermediate stock solution to achieve the exposure concentration (20 μg L^{-1}). Samples of the exposure solutions were taken to verify the concentration. The exposure was renewed each day for 7 days from freshly prepared intermediate stock solution, to minimize potential particle aging and dissolution. At each renewal, snails were removed from the exposure chamber, and both the chamber and snails were washed thoroughly with 18 MΩ water. Separate plastic-ware was used for each treatment and controls to prevent cross-contamination of the isotope label between treatments. Snails and exposure water from each treatment were sampled on Days 1, 4, and 7, with control snails also sampled on Day 7. Snails were not fed during the exposure phase of this study.

On Day 7 of the exposure, the remaining 57 groups of snails (18 of each ^{68}Zn treatment and 3 controls) were rinsed thoroughly in 17‰ water and transferred to new acid-washed plastic beakers containing 25 mL of 17‰ water to investigate the efflux rate of the different ^{68}Zn forms. During this depuration phase, snails and water were sampled on Days 1, 2, 4, 7, 14, and 28. The renewal of clean water was made at these time points, with an additional water change and sampling of water on Day 21. During efflux snails were fed with *C. vulgaris,* which was added to the water at the time of renewal. Postexposure snails sacrificed by freezing until analysis.

Sample Preparation and Analysis. A detailed description of the sample preparation and analysis is provided within the Supporting Information. All preparations were carried out in the class 1000 clean room. For MC-ICP-MS analysis a pure Zn solution was required from the water, tissue, and shell leachate samples. Five mL water samples were acidified with 1 mL of 6 M HCl. To remove *P. ulvae* soft tissue from the shell, each group (25 individuals) was left overnight in 10 mL of 0.06 M HCl to (a) soften the operculum allowing removal of the whole soft tissue[21] and (b) leach Zn from the shell surface. Soft tissue samples were dried and digested (microwave digestion). Soft tissue digestions and shell leachates were dissolved in 6 mL of 1 M HCl to match the water samples. All solutions were then processed via one-step anion exchange column chemistry[23] to isolate Zn from the sample matrix with an essentially quantitative yield. An appropriate standard was used during this step to ensure a Zn recovery of ∼100%. The purified Zn solutions were dried and subsequently reconstituted in 0.1 M HNO_3 for the isotopic analysis with a Nu Instruments Nu Plasma HR MC-ICP-MS, as outlined.[20]

Isotope Mass Balance Calculations. The diagnostic ^{68}Zn/^{66}Zn isotope ratio measured for samples is an expression of the relative contributions to the total Zn content from the two end member Zn sources of (i) natural Zn and (ii) isotopically enriched ^{68}Zn, which have contrasting isotope compositions. The measured ^{68}Zn/^{66}Zn of a sample can be expressed as (eq 1)

$$^{68}Zn/^{66}Zn_{meas} = (f^{68}Zn_{nat} \times MZn_{nat} + f^{68}Zn_{en} \times MZn_{en}) / (f^{66}Zn_{nat} \times MZn_{nat} + f^{66}Zn_{en} \times MZn_{en}) \quad (1)$$

where $^{68}Zn/^{66}Zn_{meas}$ is the ratio measured by MC-ICP-MS, $f^{xx}Zn_{nat}$ and $f^{xx}Zn_{en}$ denote the fractional molar abundance of the ^{xx}Zn isotope in the natural and isotopically enriched material, respectively, and MZn_{nat} and MZn_{en} are the molar quantities of the natural and enriched Zn present in the sample. The derivation of Zn concentrations in tissue and water samples from the $^{68}Zn/^{66}Zn$ isotope ratio is presented within the Supporting Information (eqs S1−S6).

Biodynamic Modeling. Biodynamic models quantify singular processes of uptake and loss from diet and food and growth (where appropriate) and then reconstruct bioaccumulation from the balance of these unidirectional fluxes.[6] This study presents uptake and loss rate constants calculated from a 7 day exposure and subsequent 28 day depuration of *P. ulvae* exposed to three forms of ^{68}Zn.

Efflux rate constants were calculated from the change in ^{68}Zn body burden during the 28 d period following exposure (eq 2), where $[C]_{snail}$ is the metal concentration ($\mu g\ g^{-1}$) at time points during efflux, $[C]^0_{snail}$ is the metal concentration ($\mu g\ g^{-1}$) at the start of the efflux period (i.e., t = 0 d), k is the rate constant of loss (d^{-1}), and t is depuration time (d). The slope formed by the points of $[C]_{snail}$ and $[C]^0_{snail}$ represents the rate constant for loss (k_e in d^{-1}).

$$[C]_{snail} = [C]^0_{snail} e^{-kt} \quad (2)$$

To calculate the unidirectional rate of ^{68}Zn influx (or uptake, U) for the exposure of *P. ulvae* to 20 $\mu g\ L^{-1}$ ^{68}Zn (uptake in μg $^{68}Zn\ g^{-1}$ dry tissue weight d^{-1}), the measured ^{68}Zn concentration in the snail tissue ($[C]_{snail}$), which reflects the accumulated concentration from exposure (i.e., a balance of uptake and loss), was corrected using the k_e to account for physiological loss during exposure time (t in d^{-1}) (eq 3). The uptake rate constant (k_u in $g^{-1}\ L^{-1}\ d^{-1}$) was calculated from the influx rate divided by the measured exposure concentration.[24]

$$U = [C]_{snail}/1 - (k_e \times t) \quad (3)$$

Statistical Analysis. Significant differences ($p \leq 0.05$) between uptake and efflux rates of snails exposed to different ^{68}Zn forms were determined by analysis of covariance (ANCOVA) with posthoc Tukey's test. Analyses were performed using STATISTICA software (StatSoft Ltd., Tulsa, OK, USA).

RESULTS AND DISCUSSION

Characterization of ^{68}ZnO Nano- and Bulk Particles. TEM analysis showed the ^{68}ZnO NPs to be spherical and homogeneous in size and shape, with a diameter of 7.8 ± 1.2 nm (n = 100, Figure 1 A−C). The crystal structure was verified as being ZnO by XRD analysis (Figure 1D). DLS analysis of the ^{68}ZnO NP stock diluted in 18 MΩ water (1:10) revealed a mean hydrodynamic diameter of 38.4 ± 0.7 nm (Figure 1E). These characteristics are consistent with those reported in other studies using NPs synthesized with the same method. The ^{67}ZnO NPs utilized by Buffet et al. (2012[25]) were determined to be <10 nm by TEM imaging and ∼40 nm in deionized water. Similarly synthesized ^{68}ZnO NPs had a hydrodynamic diameter of 33.0 ± 0.1 nm when suspended in deionized water and a primary particle size of <10 nm.[20] The discrepancy between particle size and hydrodynamic diameter is likely the result of the hydration sphere around the primary particles in solution and in the presence of DEG. The zeta potential of the ^{68}ZnO NPs in this study was +20.3 ± 0.8 mV, and the PDI (polydispersity index) was 0.175, which also compares favorably with those previously reported (zeta potential +17.2 ± 0.5 mV and PDI of 0.375).[20] The consistency of these comparisons demonstrates that the forced hydrolysis synthesis protocol[14] produces highly comparable batches of particles. The reproducibility of the synthesis enables meaningful comparisons between ecotoxicological studies and, in particular, allows the effect of specific variables to be tested, such as NP behavior in different environmental conditions (e.g., salinity) and among different species.

The SEM images shows that the ^{68}ZnO bulk particles are highly heterogeneous, with single particles and aggregates varying in shape and size from a few hundred nm to over 2 μm (Figure S1 A and B). The commercially available ^{68}ZnO bulk particles had an identical crystal structure to the ZnO standard (Figure S1 C). DLS analysis of the bulk particle stock, diluted in 18 MΩ water (1:10), also indicated heterogeneity with a hydrodynamic diameter of 556 ± 53 nm, a relatively high PDI of 0.563, and a surface charge of −23.8 ± 0.23 mV. Although DLS is recognized as being unsuitable for highly heterogeneous suspensions and where particles may sediment, it provides a useful comparison of the polydispersity and surface charge of the bulk particles in relation to the NP form.

Reactivity of ^{68}ZnO Nano- and Bulk Particles in Experimental Media. Seven hours after the dispersion of ^{68}ZnO NPs in estuarine water (at 1:10 (v/v) dilution) DLS analysis could not detect particles in solution, presumably owing to dissolution and/or aggregation and sedimentation (Figure S2). In determining the bioavailability of ^{68}ZnO NP and bulk particles to the estuarine amphipod *Corophium volutator*, the solubility and aggregation of both forms was assessed in artificial seawater (25 salinity, Tropic Marin Sea Salt).[20] The ^{68}ZnO NPs used in that study were synthesized with the same protocol and facilities and, as described, the characterization of the primary particles was highly comparable. The ^{68}ZnO bulk particles used in both studies were from the same commercially sourced batch. Thus the environmental characterizations previously performed[20] are applicable to the present exposure scenario.

Equilibrium dialysis experiments conducted with the ^{68}ZnO NPs in artificial seawater demonstrated both fast initial aggregation of the NPs and release of aqueous ^{68}Zn into the medium.[20] The former is confirmed by our DLS measurements in 17‰ water which show that the ^{68}ZnO NPs typically form aggregates of 2−4 μm in size that are not present in 18 MΩ water (Figure 1E). The dissolution of the ^{68}ZnO NPs occurs primarily within 24 h. Subsequent dissolution is less pronounced with near-equilibrium attained after 48 h. At equilibrium, 60% of the particles had dissolved.[20] This is in agreement with other studies which reported partial to complete dissolution of ZnO NPs.[2,26−28] Of the 48 ecotoxicology studies reviewed,[29] more than half demonstrated that partial dissolution of ZnO NPs contributed to the toxicity of the exposure.

The environmental stability of NPs is heavily influenced by pH, particle size, and surface area, although other factors (e.g., solution concentration and temperature) are also important.[9,30] Thus seawater which is slightly alkaline (pH range 7.4−8), has high ionic strength, and high concentrations of anions (Cl^- and

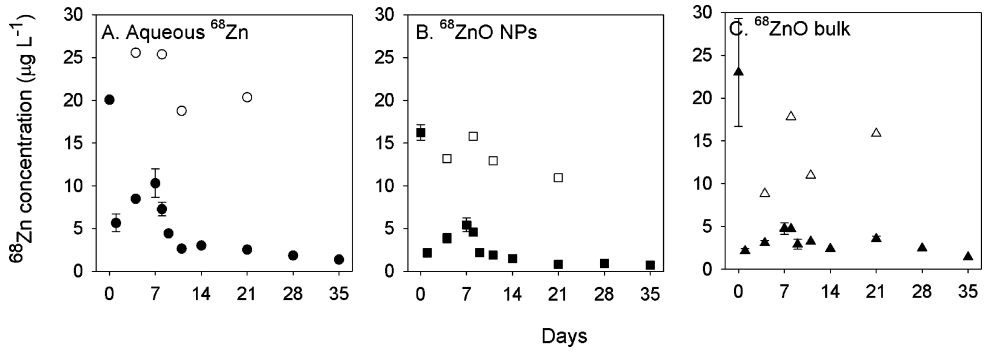


Figure 2. Total enriched ^{68}Zn concentrations (μg L^{-1}, error bars where present are the SD of duplicate or triplicate samples, else each symbol represents a single measure) in water samples (black symbols) and *P. ulvae* shell leachate (open symbols) for aqueous ^{68}Zn (A, circles), ^{68}ZnO NP (B, squares), and ^{68}ZnO bulk (C, triangles) treatments over the 35 d of the study, where the first 7 days were the exposure period followed by 28 d depuration. The day 0 point is the measured starting ^{68}Zn concentration in the exposure, nominally 20 μg L^{-1}.

SO_4^{2-}) that can serve as binding ligands, will promote aggregation of NPs to relatively small clusters, which readily dissolve.[9,28]

Dissolution kinetics vary among studies, likely resulting from the exact nature of the NPs used, concentrations and variations in experimental set-ups, but there is some consensus that ZnO NPs do dissolve, at least partially. Peng et al. (2012[28]) predicted that similarly synthesized ZnO NPs without surfactants (as used here, Buffet et al., 2012[25] and Larner et al., 2012[20]) would form similarly sized aggregates in spite of differences in concentrations and morphologies. Such aggregates will display a similar external surface, which is directly related to the diffusion efficiency of the solute (aqueous Zn), and hence comparable dissolution kinetics are expected for particles that have similar characteristics.[28,30]

In comparison, the ^{68}ZnO bulk particles did not reach equilibrium during dissolution studies (148 h) and <2% dissolution was observed.[20] Again, high ionic strength media promotes aggregation and, in the case of the larger bulk aggregates, results in rapid sedimentation. In keeping with the Gibbs-Thompson effect, the larger bulk aggregates would exhibit much lower solubility than the smaller ^{68}ZnO NPs aggregates.[4] The fate of the ^{68}ZnO bulk particles would be to settle out from solution as aggregates while remaining largely insoluble.

Analytical Precision. The control samples of water, snail tissue, and diatoms showed a total (natural) variability of ~0.1% for the diagnostic ^{68}Zn/^{66}Zn isotope ratio (0.663). A recent data compilation indicates that the total observed variability for ^{68}Zn/^{66}Zn in natural biological samples is ~0.25%.[17] In comparison, samples obtained from the exposure to enriched ^{68}Zn in the present study were found to deviate from the natural ^{68}Zn/^{66}Zn ratio by at least 2% and up to more than 800% (Table S1 presents a summary of the analyses and calculated ^{68}Zn concentrations). This demonstrates that natural isotopic variations have only a negligible impact on the isotopic data obtained for the exposed samples.

The use of MC-ICP-MS allows the rapid and routine determination of the ^{68}Zn/^{66}Zn isotope ratio to a precision of better than 0.05% in a single analysis requiring only 30 ng of Zn. As the isotopic composition of both natural and enriched ^{68}Zn are known, it is possible to quantify the amount of enriched ^{68}Zn required to alter the natural isotope ratio by 0.15%, thereby exceeding the natural background variability and precision of the analysis. Such a perturbation of the ^{68}Zn/^{66}Zn ratio can already be achieved by an increase of only 0.03% in the total Zn concentration from the enriched ^{68}Zn source. The strength of this method is demonstrated when considering the contribution of enriched ^{68}Zn in the samples was at least 2% and >60% of the total Zn, resulting in deviations in the isotope ratio 2−3 orders of magnitude above the required 0.15% (Figure S3). This method offers high resolution even at the relatively low, but environmentally realistic, exposure concentrations.

Measured Exposure Concentrations and the Influence of the Shell As a Binding Site. The waterborne exposure concentrations were verified by measuring the enriched ^{68}Zn concentration of freshly prepared media prior to exposure (Day 0). These were found to be 20.1 ± 0.3, 16.2 ± 0.9, and 23.6 ± 6.3 μg L^{-1} for aqueous ^{68}Zn, ^{68}ZnO NP, and ^{68}ZnO bulk exposures, respectively (n = 3, Figure 2). For each form this compared favorably with the expected nominal concentration (20 μg ^{68}Zn L^{-1}). The ^{68}ZnO NP concentration was lower than expected likely due to sample heterogeneity. Waterborne ^{68}Zn concentrations decreased in all treatments following 24 h exposure but rose steadily during the 7 d exposure period. After moving the snails to clean medium for efflux, ^{68}Zn concentrations in the water were not immediately reduced, but rather a steady decline was observed. Analysis of the shell leachate revealed that ^{68}Zn was recovered from the shell surface following exposures to each ^{68}Zn form (Figure 2). Shell leachate concentrations, represented as μg of enriched ^{68}Zn L^{-1} of efflux water, remained relatively consistent during the analyzed time points of both the exposure and efflux stage, approximately 20−25, 10−15, and 7−20 μg L^{-1} for aqueous ^{68}Zn, ^{68}ZnO NP, and ^{68}ZnO bulk exposures, respectively (n = 4). During the 7 day exposure period, and particularly within the first 24 h, it is likely that the shell provided binding sites for ^{68}Zn that reduced the bioavailable ^{68}Zn concentration within the water. The shells of marine gastropods were shown to accumulate (primarily by sorption) substantial concentrations of Zn during 30 h waterborne exposures, where up to 77% of the total Zn body burden was found on the shell.[24] The low concentrations of ^{68}Zn in the water samples analyzed from the efflux period likely result from the adsorption of ^{68}Zn to the shell's outer surface, rather than any significant elimination of accumulated ^{68}Zn by the snail. As discussed in the next section, the ^{68}Zn accumulated from all forms was eliminated extremely slowly.

Uptake and Efflux Dynamics of *P. ulvae* Exposed to Different Forms of ^{68}Zn. All three forms of ^{68}Zn were

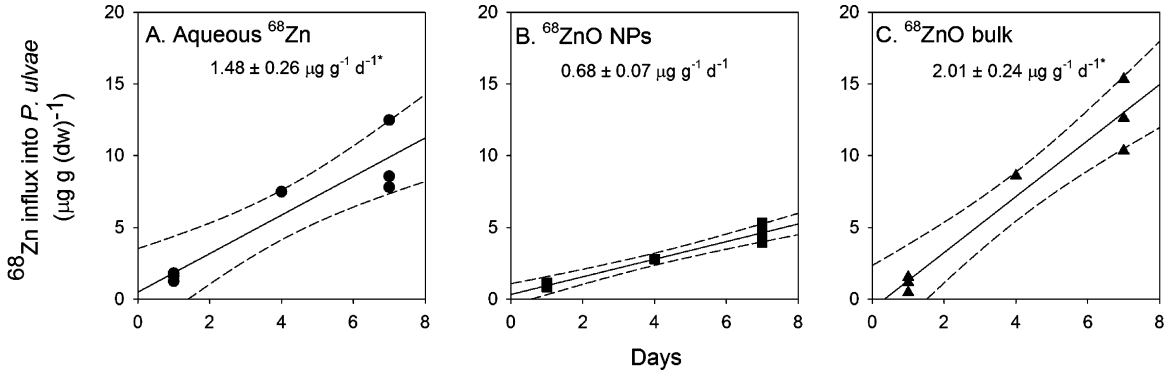


Figure 3. Unidirectional influx (i.e., uptake corrected for efflux) of aqueous ^{68}Zn (A, closed circles), ^{68}ZnO NPs (B, closed squares), and ^{68}ZnO bulk (C, closed triangles) into *P. ulvae* soft tissue during 7 d exposure at 20 μg ^{68}Zn L^{-1}. Each symbol represents one pooled sample of 25 individual snails. The linear regression (solid line) presented with 95% confidence limits (dashed lines) was used to determine an influx rate for each form at (nominal) 20 μg L^{-1} exposures (influx rates shown for each form ± S.D.). Differences between uptake rates were determined by analysis of covariance (ANCOVA) with a posthoc Tukey's test (*p < 0.05).

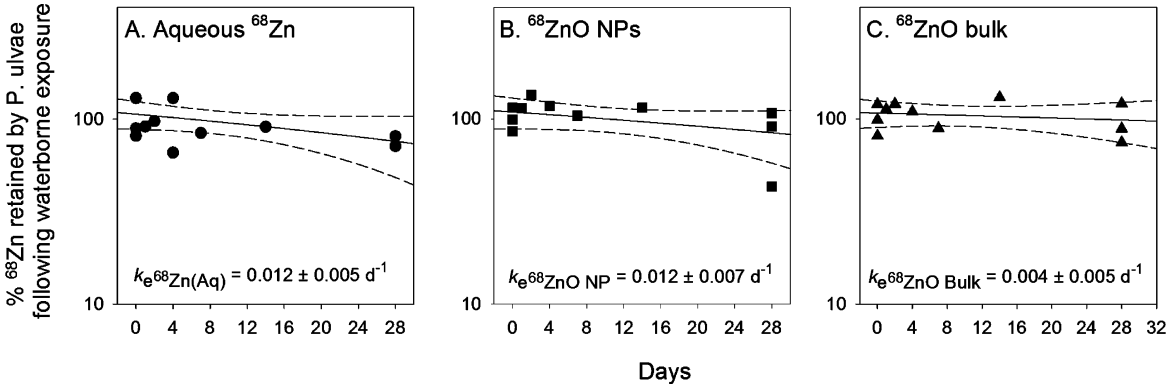


Figure 4. Proportional loss of enriched ^{68}Zn from *P. ulvae* soft tissue over time following waterborne exposure to aqueous ^{68}Zn (A, closed circles), ^{68}ZnO NPs (B, closed squares), and ^{68}ZnO bulk (C, closed triangles). Each symbol (pooled sample of 25 individual snails) represents the enriched ^{68}Zn concentration as a percentage of the total tissue concentration at day 0. For each form loss is described linearly (solid line) and is presented with 95% confidence limits (dashed lines). Efflux rate constants (k_e, shown for each form ± S.D.) are presented for each form.

available for uptake by *P. ulvae* during waterborne exposures at 20 μg ^{68}Zn L^{-1}. Unidirectional influx rates determined from the efflux-corrected tissue burdens revealed that ^{68}Zn presented as ^{68}ZnO NPs was the least available form with an influx rate approximately 2-fold lower than that of aqueous ^{68}Zn (Figure 3). ^{68}ZnO bulk particles were the most bioavailable form. The influx rates of both aqueous ^{68}Zn and ^{68}ZnO bulk particles were significantly greater compared to ^{68}ZnO NPs (p < 0.05, ANCOVA with posthoc tukey test, Figure 3). The relatively high rate of influx following ^{68}ZnO bulk particle exposure is likely related to their rapid precipitation and limited dissolution within the estuarine water as discussed. The sedimentation of the bulk particle aggregates would render them unavailable for waterborne uptake but highly available for ingestion. *P. ulvae* primarily feeds on particulate organic detritus and inorganic sediments by grazing over the sediment surface. Thus rather than a waterborne exposure, the uptake of the ^{68}ZnO bulk particles was presumably achieved primarily through diet. A similar finding was reported previously, where *C. volutator* was proposed to have fed on sedimented ZnO bulk particles leading to a reduction in growth that was not consistent with aqueous Zn exposures.[4] The relative importance of the dietary exposure route in comparison to waterborne exposures has been established in the literature for a number of metals for different aquatic species.[31−33] The efficiency of Zn assimilation from ZnO NP aggregates mixed with diatom food was 86% in studies with the snail *Lymnaea stagnalis*, and ingestion was likely to be the dominant uptake pathway.[16]

Using the measured ^{68}Zn exposure concentrations to normalize the influx rate of each form provides the uptake rate constants (k_u). For ^{68}ZnO NP k_u = 0.042 L^{-1} g^{-1} d^{-1}. This value was lower than that of aqueous ^{68}Zn (k_u = 0.074 L^{-1} g^{-1} d^{-1}) and ^{68}ZnO bulk (k_u = 0.085 L^{-1} g^{-1} d^{-1}). This would suggest that aqueous ^{68}Zn is more bioavailable than the ^{68}Zn in the NP. Comparable batches of ^{68}ZnO NPs were shown to undergo 60% dissolution (by weight) in estuarine water in 1−2 days.[20] Thus, with a total label concentration of 16.2 ± 0.9 μg ^{68}Zn L^{-1} in the ^{68}ZnO NP exposure, approximately 9.7 μg L^{-1} would be present as aqueous Zn. If this concentration is used to determine the k_u of the ^{68}Zn from the NP, the k_u = 0.070 L^{-1} g^{-1} d^{-1}, which is almost identical to the k_u derived from the aqueous ^{68}Zn exposures (0.074 L^{-1} g^{-1} d^{-1}). This strongly suggests that the bioavailability of ^{68}Zn in NP form is linked to solubility and ZnO NPs do not deliver Zn to the snail until they have undergone, at least partial, dissolution.

^{68}Zn accumulated from all sources was lost extremely slowly by *P. ulvae* during a 28 d depuration period. For all forms, efflux appeared to fit a one-component loss model, and there were no statistical differences between the efflux rate constants of each form (Figure 4, p < 0.05, ANCOVA). However, the k_e values

dx.doi.org/10.1021/es4011465 | Environ. Sci. Technol. 2013, 47, 8532−8539

for ^{68}Zn accumulated following exposure to aqueous ^{68}Zn and ^{68}ZnO NPs were identical, k_e = 0.012 ± 0.005 and 0.012 ± 0.007 d^{-1}, respectively, and are 3-fold higher than that of ^{68}ZnO bulk (k_e = 0.004 ± 0.005 d^{-1}). Effectively, ^{68}Zn accumulated via aqueous and NP exposures were eliminated at a rate of 1.2% d^{-1}, whereas ^{68}Zn accumulated via the bulk exposure was lost at a slower rate (0.4% d^{-1}). There are very few studies on the efflux of Zn from saltwater gastropods and fewer still that involve NPs and bulk particles. However, those studies that have reported k_e values show that elimination of ingested Zn generally occurs slowly. For *Babylonia formasae habei*, *Nassarius teretiusculus*, and *Rapana venosa* the Zn efflux rate constants were 0.0057, 0.0138, and 0.0105 d^{-1}, respectively.[24,34] Although these values were determined following dietary exposures, it has been demonstrated that neither exposure route (diet or water) nor form (ZnO NP or dissolved Zn) significantly altered the k_e in *Lymnaea stagnalis* which remained at approximately 0.08 d^{-1}.[16] The consistency of the *L. stagnalis* loss rate constants between NP and dissolved forms, particularly following the ingestion of the NPs, would suggest Zn from the ZnO NP undergoes a similar physiological fate as Zn taken up as the dissolved form.[16]

The identical uptake (when NP dissolution is accounted for) and loss rates constants of ^{68}Zn for *P. ulvae* exposed to aqueous and NP forms provides compelling evidence that ^{68}Zn from the ^{68}ZnO NP is both entering and eliminated from the snail as the aqueous form after the NPs have already undergone dissolution in the estuarine environment. Thus, the bioavailability of Zn from ZnO NPs when exposed via dispersion in water is primarily dependent upon their solubility. However, when particulate Zn forms are large enough to be ingested, uptake is accentuated even beyond that of exposure to aqueous Zn. Our study adds to the growing body of work which demonstrates that at environmentally realistic concentrations (a) both aggregation and dissolution of ZnO nanoparticles occurs in saline waters; (b) this aggregation does not prevent delivery of Zn from the NPs to aquatic organisms; (c) the environmental availability and toxicological impact of ZnO NPs is linked to their solubility when presented dispersed in estuarine water; and (d) Zn can also be delivered from very large aggregates with surprising efficiency probably via ingestion.

In summary, these results strongly suggest that solubility of ZnO NPs in exposure media is a key parameter that determines the availability of the Zn constituent. Our ability to conduct environmentally relevant exposures, especially for a metal as abundant as Zn, was made possible by employing stable isotope tracing combined with high-precision mass spectrometry. This methodology enabled the highly sensitive detection of newly accumulated Zn even in the presence of high and variable backgrounds concentrations. This methodology is highly applicable in determining the bioavailability of metal containing NPs when the constituent metal is multi-isotopic.

■ ASSOCIATED CONTENT

Supporting Information

Sample preparation and analysis. Isotope mass balance calculations. ^{68}ZnO bulk particle characterizations (Figure S1). DLS measurements of the ^{68}ZnO NPs in exposure media (Figure S2). Detection of ^{68}Zn against natural Zn background for MC-ICP-MS analysis (Figure S3). Summarized analytical results and calculated ^{68}Zn concentrations (Table S1). This material is available free of charge via the Internet at http://pubs.acs.org.

■ AUTHOR INFORMATION

Corresponding Author

*Phone: 0044-01314514562. E-mail: f.khan@hw.ac.uk; farhan.khan@gmx.com (F.R.K.). Phone: 0044-02075947140. E-mail: a.laycock10@imperial.ac.uk (A.L.).

Present Address

†School of Life Sciences, Heriot-Watt University, Edinburgh EH14 4AS, United Kingdom.

Author Contributions

F.R.K. and A.L. are joint first authors. E.V-J. and M.R. are joint senior authors. Study conception and funding (E.V-J., S.N.L., M.R.), study design (F.R.K.) with input (A.L., F.L., B.D.S., P.S.R., S.N.L., M.R.), nanoparticle synthesis (A.L., F.L., A.D.). Biological exposures were conducted at the Natural History Museum (F.R.K., A.L., B.D.S.), particle characterizations were performed at the NHM (A.D.), postexposure sample preparation and analyses were performed at Imperial College (A.L.). Mass balance calculations (A.L., M.R.), biodynamic modeling (F.R.K.).

Notes

The authors declare no competing financial interest.

■ ACKNOWLEDGMENTS

This research received funding from the European Union Seventh Framework Programme (FP7/2007-2013) under grant agreement no. 214478 (NanoReTox) (F.R.K.) and no. 262163 (QualityNano) (A.D.). This research was conducted as part of PROSPEcT. Work at Imperial College was supported by a STFC studentship to A.L., an EPSRC studentship to F.L., and grants from EPSRC and DEFRA. Katharina Kreissig and Barry Coles are thanked for their technical assistance at the MAGIC Laboratories, Imperial College.

■ REFERENCES

(1) Osmond, M. J.; McCall, M. J. Zinc oxide nanoparticles in modern sunscreens: an analysis of potential exposure and hazard. *Nanotoxicology* **2010**, *4*, 15−41.

(2) Franklin, N. M.; Rogers, N. J.; Apte, S. C.; Batley, G. E.; Gadd, G. E.; Casey, P. S. Comparative toxicity of nanoparticulate ZnO, bulk ZnO and ZnCl2 to a freshwater microalga (*Pseudokirchneriella subcapitata*): the importance of particle solubility. *Environ. Sci. Technol.* **2007**, *41*, 8484−8490.

(3) Zhu, X.; Wang, J.; Zhang, X.; Chang, Y.; Chen, T. The impact of ZnO nanoparticle aggregates on the embryonic development of zebrafish (*Danio rerio*). *Nanotechnology* **2009**, *20* (19), 195103.

(4) Fabrega, J.; Tantra, R.; Amer, A.; Stolpe, B.; Tomkins, J.; Fry, T.; Lead, J. R.; Tyler, C. R.; Galloway, T. S. Sequestration of zinc from zinc oxide nanoparticles and life cycle effects in the sediment dwelling amphipod *Corophium volutator*. *Environ. Sci. Technol.* **2012**, *46*, 1128−1135.

(5) Shipp, E.; Grant, A. *Hydrobia ulvae* feeding rates: A novel way to assess sediment toxicity. *Environ. Toxicol. Chem.* **2006**, *25*, 3246−3252.

(6) Luoma, S. N.; Rainbow, P. S. Why is metal bioaccumulation so variable? Biodynamics as a unifying concept. *Environ. Sci. Technol.* **2005**, *39*, 1921−1931.

(7) Campbell, P. G. C. Interactions between trace metals and aquatic organisms: A critique of the free-ion activity model. In *Metal speciation and bioavailability in aquatic systems*; Tessier, A., Turner, D. R., Eds.; Wiley: New York, USA, 1995; pp 45−102.

(8) Keller, A. A.; Wang, H. T.; Zhou, D. X.; Lenihan, H. S.; Cherr, G.; Cardinale, B. J.; Miller, R.; Ji, Z. X. Stability and aggregation of metal oxide nanoparticles in natural aqueous matrices. *Environ. Sci. Technol.* **2010**, *44* (6), 1962−1967.

(9) Miao, A.-J.; Zhang, X.-Y.; Luo, Z.; Chen, C.-S.; Chin, W.-C.; Santschi, P. H.; Quigg, A. Zinc oxide-engineered nanoparticles: dissolution and toxicity to marine phytoplankton. *Environ. Toxicol. Chem.* **2010**, *29*, 2814−2822.
(10) Luoma, S. N.; Rainbow, P. S. *Metal Contamination in Aquatic Environments: Science and Lateral Management*; Cambridge University Press: Cambridge, 2008.
(11) Hogstrand, C. Zinc. In *Fish Physiology*; Wood, C. M., Farrell, A. P., Brauner, C. J., Eds.; Academic Press: 2011; pp 135−200.
(12) Gottschalk, F.; Sonderer, T.; Scholz, R. W.; Nowack, B. Modeled environmental concentrations of engineered nanomaterials (TiO_2, ZnO, Ag, CNT, fullerenes) for different regions. *Environ. Sci. Technol.* **2009**, *43*, 9216−9222.
(13) White, S. L.; Rainbow, P. S. On the metabolic requirements for copper and zinc in molluscs and crustaceans. *Mar. Environ. Res.* **1985**, *16*, 215−29.
(14) Dybowska, A.; Croteau, M. N.; Misra, S. K.; Berhanu, D.; Luoma, S. N.; Christian, P.; O′Brien, P.; Valsami-Jones, E. Synthesis of isotopically modified ZnO nanoparticles and their potential as nanotoxicity tracer. *Environ. Pollut.* **2011**, *159*, 266.
(15) Gulson, B.; Wong, H. Stable isotopic tracing- A way forward for nanotechnology. *Environ. Health Perspect.* **2006**, *114*, 1486.
(16) Croteau, M.-N.; Dybowska, A. D.; Luoma, S. N.; Valsami-Jones, E. A novel approach reveals that zinc oxide nanoparticles are bioavailable and toxic after dietary exposures. *Nanotoxicology* **2011**, *5*, 79−90.
(17) Larner, F.; Rehkämper, M. Evaluation of stable isotope tracing for ZnO nanomaterials − new constraints from high precision isotope analyses and modelling. *Environ. Sci. Technol.* **2012**, *46*, 4149−4158.
(18) Misra, S. K.; Dybowska, A.; Berhanu, D.; Croteau, M. N.; Luoma, S. N.; Boccaccini, A. R.; Valsami-Jones, E. Isotopically modified nanoparticles for enhanced detection in bioaccumulation studies. *Environ. Sci. Technol.* **2012**, *46*, 1216−1222.
(19) Rehkämper, M.; Schönbächler, M.; Stirling, C. H. Multiple collector ICP-MS: Introduction to instrumentation, measurement techniques and analytical capabilities. *Geostand. Newsl.* **2001**, *25* (1), 23−40.
(20) Larner, F.; Dogra, Y.; Dybowska, A.; Fabrega, J.; Stolpe, B.; Bridgestock, L. J.; Goodhead, R.; Weiss, D. J.; Moger, J.; Lead, J. R.; Valsami-Jones, E.; Tyler, C. R.; Galloway, T. S.; Rehkämper, M. Tracing bioavailability of ZnO nanoparticles using stable isotope labelling. *Environ. Sci. Technol.* **2012**, *46*, 12137−12145.
(21) Khan, F. R.; Misra, S. K.; García-Alonso, J.; Smith, B. D.; Strekopytov, S.; Rainbow, P. S.; Luoma, S. N.; Valsami-Jones, E. Bioaccumulation dynamics and modeling in an estuarine invertebrate following aqueous exposure to nanosized and dissolved silver. *Environ. Sci. Technol.* **2012**, *46*, 7621−7628.
(22) Kay, A. R. Detecting and minimizing zinc contamination in physiological solutions. *BMC Physiol.* **2004**, *4*, 4.
(23) Arnold, T.; Schönbächler, M.; Rehkämper, M.; Dong, S.; Zhao, F.-J.; Kirk, G. J. D.; Coles, B. J.; Weiss, D. J. Measurement of zinc stable isotope ratios in biogeochemical matrices by double-spike MC-ICPMS and determination of the isotope ratio pool available for plants from soil. *Anal. Bioanal. Chem.* **2010**, *398*, 3115−3125.
(24) Wang, W.-X.; Ke, C. Dominance of dietary intake of cadmium and zinc by two marine predatory gastropods. *Aquat. Toxicol.* **2002**, *56*, 153−165.
(25) Buffet, P.-E.; Amiard-Triquet, C.; Dybowska, A.; Risso-de Faverney, C.; Guibbolini, M.; Valsami-Jones, E.; Mouneyrac, C. Fate of isotopically labeled zinc oxide nanoparticles in sediment and effects on two endobenthic species, theclam *Scrobicularia plana* and the ragworm *Hediste diversicolor*. *Ecotox. Environ. Saf.* **2012**, *84*, 191−198.
(26) Miller, R. J.; Lenihan, H. S.; Muller, E. B.; Tseng, N.; Hanna, S. K.; Keller, A. A. Impacts of metal oxide nanoparticles on marine phytoplankton. *Environ. Sci. Technol.* **2010**, *44*, 7329−7334.
(27) Li, M.; Pokhrel, S.; Jin, X.; Mädler, L.; Damoiseaux, R.; Hoek, E. M. V. Stability, bioavailabilty and bacterial toxicity of ZnO and iron-doped ZnO nanoparticles in aquatic media. *Environ. Sci. Technol.* **2011**, *45*, 755−761.
(28) Peng, X.; Palma, S.; Fischer, N. S.; Wong, S. S. Effect of morphology of ZnO nanostructures on their toxicity to marine algae. *Aquat. Toxicol.* **2011**, *102*, 186−196.
(29) Ma, H.; Williams, P. L.; Diamond, S. A. Ecotoxicity of manufactured ZnO nanoparticles - a review. *Environ. Pollut.* **2013**, *172*, 78−85.
(30) Borm, P.; Klaessig, F. C.; Landry, T. D.; Moudgil, B.; Pauluhn, J.; Thomas, K.; Trottier, R.; Wood, S. Research strategies for safety evaluation of nanomaterials, Part V: role of dissolution in biological fate and effects of nanoscale particles. *Toxicol. Sci.* **2006**, *90*, 23−32.
(31) Luoma, S. N.; Johns, C.; Fisher, N. S.; Steinberg, N. A.; Oremland, R. S.; Reinfelder, J. Determination of selenium bioavaialbility to a benthic bivalve from particlulate and solute pathways. *Environ. Sci. Technol.* **1992**, *26*, 485−491.
(32) Griscom, S. B.; Fischer, N. S.; Luoma, S. N. Kinetic modeling of Ag, Cd and Co bioaccumulation in the clam *Macoma balthica*: quantifying dietary and dissolved sources. *Mar. Ecol.: Prog. Ser.* **2002**, *240*, 127−141.
(33) Casado-Martinez, M. C.; Smith, B. D.; DelValls, T. A.; Rainbow, P. S. Pathways of trace metal uptake in the lugworm Arenicola marina. *Aquat. Toxicol.* **2009**, *92*, 9−17.
(34) Onat, B.; Topcuoglu, S. A laboratory study of Zn and ^{134}Cs depuration by the sea snail (*Rapana venosa*). *J. Environ. Radioact.* **1999**, *46*, 201−206.